Structural Determinants of Protein Tyrosine Phosphatase 1B Inhibition

Jacqueline Montalibet

A Thesis

In

The Department

of

Chemistry and Biochemistry

Presented in Partial Fulfilment of the Requirements
For the Degree of Doctor of Philosophy at
Concordia University
Montréal, Québec, Canada

February 2005

Your file Votre référence
ISBN: 978-0-494-34793-5
Our file Notre référence
ISBN: 978-0-494-34793-5

Abstract

Structural Determinants of Protein Tyrosine Phosphatase 1B Inhibition

Jacqueline Montalibet, Ph.D.

Concordia University, 2005

Inhibition of Protein Tyrosine Phosphatase 1B (PTP1B) has been proposed as a novel therapy to treat type 2 diabetes by sensitising the patients to the effect of insulin while protecting them against diet-induced obesity. A mutant screen in yeast was devised to facilitate the identification of residues involved in inhibitor binding. The screen was based on the observation that overexpression of v-Src, a tyrosine kinase, in yeast leads to lethality through mitotic dysfunction. This was reversed by co-expression of PTP1B whereas co-expression of the catalytically inactive enzyme failed to rescue the v-Src phenotype. Treatment with specific PTP1B inhibitors reversed, in a dose-dependent manner, the rescue effect of the phosphatase and indicated that this screen could be used to identify inhibitors with enhanced bioavailability properties. A library of PTP1B mutants was co-expressed with v-Src in yeast. The clones obtained were tested for their ability to grow in the presence of inhibitor: only PTP1B mutants that had conserved their catalytic activity and were resistant to inhibition grew. This screen revealed resistant mutations absent from the active site loops to concentrate on the α7 helix and its surrounding region. This region was further characterized using a mutation of serine 295 to phenylalanine resulting in resistance to a panel of structurally diverse inhibitors.

Inhibitor determinants previously identified using X-ray crystallography and site-directed mutagenesis have all been located to the active site. This is the first report that an active-site distal region can modulate inhibition of PTP1B. This novel approach to identify structural determinants of inhibition can be applied to other tyrosine phosphatases and has the advantage of not being biased towards primary shell residues.

Acknowledgments

I would like to take this opportunity to thank my thesis supervisor Dr. Brian Kennedy for his vision and unwavering faith in me and my academic supervisor Dr. Ann English, who made sure I took advantage of all the possible opportunities available to me and provided an additional forum to discuss perplexing data. I also want to thank Merck Frosst for welcoming me and offering physical resources I could only have dreamt of in an academic setting.

Although I cannot thank everyone by name, rest assured I do remember you and am forever grateful you took the time to show me how you get it to work or to sit down and talk science.

None of this could have been possible without financial support from NSERC (Industrial Postgraduate Scholarship), FCAR-MRST (Bourse de recherche en milieu pratique), Merck Frosst (contributions to the NSERC and FCAR-MRST scholarships) and Concordia University (External Grant Holder Doctoral Scholarship).

Thank You.

Table of Contents

List of Figures

List of Tables

List of Abbreviations

4E-BP1: 4E-Binding Protein 1

ATCC: American Type Culture Collection

ASO: Anti-Sense Oligonucleotide

ABC-MDR: ATP-Binding Cassette MultiDrug Resistant

BRET: Bioluminescence Resonance Energy Transfer

BzN-EJJ-amide: N-benzoyl-L-glutamyl- [4-phosphono(difluoromethyl)]-L-phenylalanyl-[4-phosphono(difluoromethyl)]-L-phenylalanineamide

CRK1: Cdc2-Related Kinase 1

CSK: Carboxy-terminal Src Kinase

DiFMUP: DiFluoroMethylUmbelliferyl Phosphate

DHFR: Dihydrofolate Reductase

DTT: Dithiothreitol

EC_{50}: median Effective Concentration

EGF: Epidermal Growth Factor

EGFR: Epidermal Growth Factor Receptor

Erk: Extracellular-signal-Regulated Kinase

FAK: Focal Adhesion Kinase

FDP: 3,6-Fluorescein DiPhosphate

FRET: Fluorescence Resonance Energy Transfer

GS: Glycogen Synthase

GSK3: Glycogen Synthase Kinase 3

GRB2: Growth-factor-Receptor-Binding protein 2

HDL: High Density Lipoproteins

IC_{50}: median Inhibitory Concentration

IGF-1: Insulin-like Growth Factor I

IGF1R: Insulin-like Growth Factor I Receptor

IR: Insulin Receptor

IRS: Insulin Receptor Substrates

LAR: Leukocyte Antigen-Related

mTor: mammalian Target of rapamycin

MEK: MAPK/Erk Kinase

MOPS: 3-(N-Morpholino)PropaneSulfonic acid

p70S6K: p70 ribosomal S6 Kinase

PDGFR: Platelet-Derived Growth Factor Receptor

PI3K: Phosphatidyl Inositol 3-Kinase

PDK1/2: Phosphoinositide-Dependent Kinase 1 or 2

pNPP: p-NitroPhenyl Phosphate

PVDF: PolyVinyliDene Fluoride

PTP1B: Protein Tyrosine Phosphatase 1B

PTP: Protein Tyrosine Phosphatase

RPTP: Receptor-Type Phosphatase

SHP2: SH2 domain-containing protein tyrosine Phosphatase-2

SNP: Single Nucleotide Polymorphism

SOS: Son-Of-Sevenless

T2DM: Type 2 Diabetes Mellitus

TCPTP: T-Cell Protein Tyrosine Phosphatase

UAS: Upstream Activation Sequence

1. Introduction

1.1. The Biology of Protein Tyrosine Phosphatase 1B

1.1.1. Diabetes [1]

In 2003, 194 million people worldwide were diagnosed with diabetes with a projected increase to 333 million by 2025[2]. Ninety percent of these patients suffer from Type 2 Diabetes Mellitus (T2DM) which is characterized by a resistance to insulin in contrast to type 1 diabetes which results from a lack of insulin production.

This resistance to insulin is developed years before frank observable hyperglycemia which dictates the diagnosis of T2DM. The preservation of glycemic control relies on the pancreas's ability to overcome tissue resistance by simply increasing its production of insulin. However, the increased stress on the insulin-secreting pancreatic β-cell due in part to glucotoxicity, lipotoxicity, inflammatory cytokines and genetic sensitivities leads to their failure.

The micro- and macrovascular morbidities associated with T2DM are directly correlated with the magnitude and duration of the hyperglycemia putting emphasis in the clinic on tight glycemic control.

There is a gap in the available therapies to address the underlying biochemical defect of T2DM: insulin resistance. Among the current therapies for T2DM, tiazolidinediones address the problem of peripheral insulin resistance but have weight

gain as a secondary side effect. This is worrisome in that 90% of T2DM patients are overweight or obese. In addition, onset of diabetes is preceded with the association of Syndrome X which is characterized by any three of the five following characteristics increased: abdominal obesity, fasting glucose, blood pressure, triglycerides and decreased High Density Lipoproteins (HDL).

Inhibition of Protein Tyrosine Phosphatase 1B (PTP1B) results in sensitization to insulin signalling and protection against diet-induced obesity. This dual effect of PTP1B makes it a promising target in the treatment of T2DM by addressing key issues not filled by current treatment modalities.

1.1.2. PTP1B and Insulin Signalling

Glucose stimulates the pancreas to secrete insulin. This is exacerbated in T2DM from the prolonged glucose stimulation due to its lack of uptake and clearance by the tissues in response to insulin. Insulin binds the α-chain of the Insulin Receptor (IR) to cause a conformational change activating the kinase activity of the β-chain and auto-phosphorylating its activation loop. This auto-phosphorylation further activates the kinase to phosphorylate other sites on the β-subunit recruiting and phosphorylating different substrates including Insulin Receptor Substrates (IRS). Mutations of the IR itself cause an extreme insulin resistance phenotype but are rare in humans. Aberrant insulin signalling observed in obese and T2DM patients is due to signalling events downstream from the receptor[3]. The phosphorylated IRSs recruit Phosphatidyl Inositol 3-Kinase (PI3K) to convert phosphatidyl inositol into 3,4-bisphosphate and 3,4,5-trisphosphate which stimulate the activity of Phosphoinositide-Dependent Kinase 1 or 2 (PDK1/2) itself

activating Akt (also called PKB). Akt is involved in the translocation of GLUT4 transporter to the cell surface for glucose uptake. The exact mechanism of this transporter recruitment is not completely understood and also involves a PI3K-independent pathway. Akt also phosphorylates and inactivates Glycogen Synthase Kinase 3 (GSK3) to release the repression on Glycogen Synthase (GS) and promote glycogen synthesis.[3]

The signalling pathway is turned off by dephosphorylation of the tyrosine residues on the activation loop of the IR abolishing its kinase activity. Several protein tyrosine phosphatases (PTP) have been proposed for that role: PTPα, Leukocyte Antigen-Related (LAR), CD45, PTPε, SH2 domain-containing protein tyrosine Phosphatase-2 (SHP2), T-Cell Protein Tyrosine Phosphatase (TCPTP) and PTP1B. These PTPs have all been observed to control insulin signalling *in vitro* or when overexpressed in cell lines but knockout mice studies showed obvious insulin signalling defects only for PTP1B. This dichotomy emphasizes the exquisite substrate selectivity of the phosphatases in the whole organism as opposed to artificial systems. [4]

The effect on the insulin signalling pathway seen in cultured cells by PTP1B up- or down-regulation is thought to be mediated upstream of PI3K[5,6] and to involve mostly dephosphorylation of the IR and IRS1[5-15]. The downstream effects on glucose uptake or glycogen synthesis have not been very robust in these systems and vary depending on the cell type used[5,6,10-13,16].

PTP1B which is located to the endoplasmic reticulum has been shown to interact directly with the IR in Fluorescence Resonance Energy Transfer (FRET)[17,18] and Bioluminescence Resonance Energy Transfer (BRET)[19] experiments where energy transfer was observed from the close association (<100Å) between the two enzymes. This

association was observed to occur without insulin stimulation indicating that PTP1B could dephosphorylate the IR during its biosynthesis in the ER. Stimulation with insulin resulted in a rapid increase of this association localizing to perinuclear spots. This insulin-stimulated interaction between PTP1B and the IR requires internalization of the receptor and can be prevented with the use of a PTP1B inhibitor.

The interaction between PTP1B and the IRS1 protein demonstrated in immunoprecipitation experiments is stabilized by the participation of the SH2 and SH3 domain-containing adaptor protein Growth-factor-Receptor-Binding protein 2 (GRB2)[20].

Inhibitor studies in cell lines have confirmed the effect of PTP1B on the insulin signalling pathway but have also proven to act as insulin mimetic enhancing basal phosphorylation and/or activity of IR, IRS1, PI3K and Akt along with glucose uptake[5,6]. This observation was intriguing in that no such effect was seen in PTP1B knockout animals and Anti-Sense Oligonucleotide (ASO) treated animals.

In addition to the effects of insulin on glucose metabolism, the insulin signalling pathway also stimulates transcriptional events through the MAPK kinase pathway. Phosphorylated IRS1 and Shc interact with GRB2 adaptor protein to recruit Son-Of-Sevenless (SOS) which participates in Ras activation. Activated Ras engages a serine phosphorylation cascade through Raf, MAPK/Erk Kinase (MEK) and Extracellular-signal-Regulated Kinase (Erk) which translocates to the nucleus and activates transcription. Akt also participates in translational events by modulating the mammalian Target of rapamycin (mTor) activity, which in turns regulates p70 ribosomal S6 Kinase (p70S6K) and 4E-Binding Protein 1 (4E-BP1).[3,21]

Modulation of PTP1B has been shown to affect the MAPK pathway in cultured cell lines[11,12,16,22] by interacting upstream from MEK[6]. PTP1B has been shown to directly dephosphorylate Shc thereby destabilizing its interaction with IRS1 and GRB2[16]. Similarly to the metabolic pathway, reports on downstream effects such as Erk activation have not been robust in cultured cell lines[6,13,15]. Nonetheless, the observation of blunted insulin-stimulated p70S6K activation with PTP1B microinjection in Xenopous oocytes[7] was the first indication that PTP1B had a role in the insulin signalling pathway.

1.1.3. PTP1B and Diabetes

1.1.3.1. PTP1B Knockout Phenotype

Ablation of PTP1B in the mouse resulted in enhanced insulin sensitivity as measured by improved glucose clearance in glucose and insulin tolerance tests[23,24]. In effect, the PTP1B knockout mice showed 13% decrease in blood glucose achieved with 50% lower circulating insulin levels than the wild-type animal[23]. Whole body glucose disposal was increased mainly via a 75% increase in glucose uptake by muscle cells with no difference in glucose uptake observed for adipose tissue[24]. The PTP1B heterozygous mice displayed a similar but attenuated phenotype[23,24].

The difference in insulin sensitization between the wild type and knock out was even more apparent when the animals were placed on a high fat diet[23]. Interestingly, on this diet the knock out mice were resistant to weight gain[23,24] and had lowered circulating triglyceride levels than the wild-type animal[23,24]. This resistance to diet-induced obesity resulted from a decrease in adiposity with a reduction in the volume of adipocytes but no change in their numbers[24]. This resistance was not due to a change in food consumption

but some debate exists as to whether there is a change in their metabolic rate, either unchanged or increased, depending on calculations using a 'per mouse' or 'per gram' correction factor[23,24].

PTP1B depletion not only protects against fat-feeding-induced insulin resistance dyslipidemia but also that of carbohydrate feeding: on a high fructose diet, the knock out mice exhibited resistance to increased total plasma triglycerides and cholesterol levels[25]. Increase in circulating ApoB has been identified as a risk factor for artherosclerosis and contribute to the dyslipidemia of the metabolic syndrome[26,27]. High fructose fed hamsters showed an overproduction of hepatic apolipoprotein B which is associated with an increased PTP1B protein amounts and activity in the liver[28]; high fructose feeding of the PTP1B knockout mice show decreased total circulating apolipoprotein B[25].

The PTP1B knockout obesity resistance phenotype was surprising in that an increase insulin sensitivity in adipose tissue should have led to an increase in fat storage and therefore weight gain. The fat-specific IR knockout mice were found to be resistant to obesity and obesity-related insulin resistance suggesting that insulin signalling in fat is critical for the development of obesity[29]. The tyrosine phosphorylation of the IR is enhanced in skeletal muscle tissues, prolonged in liver but not affected in adipose tissue of the PTP1B knock out mouse[23]. This would indicate that PTP1B has different functions in different tissues to enhance signalling from the IR in muscle and liver but not in fat.

Advanced diabetes is associated with a progressive loss of β-cells and a reduction in the size of pancreatic islets. This is reproduced in the IRS2 knockout mice which develop diabetes at 6-8 weeks of age and die at 14-17 weeks due to β-cell failure and uncompensated insulin resistance. Crossing this mouse with the PTP1B knockout results

in an improved glucose tolerance from peripheral insulin sensitisation, improved islet function and delays diabetes onset to prolong survival up to nine months.[30]

In the same way multiple phosphatases have been observed to affect insulin signalling in artificial systems, many different pathways have been shown to be affected by PTP1B including the Epidermal Growth Factor Receptor (EGFR)[31], Platelet-Derived Growth Factor Receptor (PDGFR)[31,32], Insulin-like Growth Factor I Receptor (IGF1R)[10] and integrin[33]. PTP1B has also been shown to modulate transformation by Src[34]. However, the knockout shows a very specific phenotype with a normal lifespan, no gross or histological abnormalities and no increase in tumorigenicity resulting from modification of growth factor pathways[23,24]. Treatment of the knockout with Insulin-like Growth Factor I (IGF-1) resulted in an increase in receptor phosphorylation but with no difference in the response between the wild-type and the knockout animal[4]. This indicate that in the organism, the involvement of PTP1B in these other pathways is not rate limiting. Corollary, the IR is dephosphorylated at some point in the knockout mouse indicating that other phosphatases can compensate but that PTP1B is the rate limiting phosphatase in this pathway[35].

1.1.3.2. PTP1B in the Leptin Pathway

Weight gain regulation by PTP1B is thought to be mediated through both a leptin-dependent and independent pathway[36,37]. Leptin is secreted from adipocytes and functions to signal the brain of a positive energy balance and so to reduce food intake. It also has a peripheral effect to prevent lipid accumulation in non-adipose tissue thereby preventing lipotoxicity from fatty acid derivatives such as ceramide[38]. Most forms of

obesity are associated with a resistance to leptin: excess circulating leptin but normal leptin and leptin receptor genes. Ablation of the leptin (ob/ob) or leptin receptor (db/db) gene in mice results in an obese phenotype including dyslipidimia, hyperglycemia and hyperinsulinemia.

Circulating leptin levels are directly proportional to fat mass and so are lowered in the PTP1B knockout mouse; these levels are maintained even on the high fat diet[24]. Interestingly, peripheral leptin administration in the knockout animal induces a greater anorexigenic effect and weight loss than the wild type indicating increased leptin sensitivity in the knockout[36].

Crossing the ob/ob mouse with the PTP1B knockout resulted in a reduced weight gain due to a reduction in adiposity, an increase in insulin sensitivity as measured by reduced fasting glucose levels and improved glucose tolerance compared to the ob/ob mouse and a modest sensitization to leptin as seen from the ability of the double knockout to lose weight in response to lower doses of leptin[36]. Ablation of the leptin-responsive hypothalamic neurons with gold thioglucose had only a modest effect on the obesity resistance of the PTP1B knockout[39].

Although PTP1B has been involved in the leptin pathway to dephosphorylate JAK2[36], ablation of the leptin pathway in two different animal models had only a mild effect on the PTP1B obesity resistance phenotype. This would indicate that only some of the obesity resistance of the PTP1B knockout is leptin-dependent, the greater part of it involving another mechanism. Since the insulin and leptin pathways are tightly coupled, the enhanced leptin sensitivity seen in the PTP1B knockout may be the result of the insulin sensitivity. Interestingly, leptin treatment of ob/ob mice has been found to

decrease PTP1B protein expression back to wild-type levels in liver but not in muscle or fat[40]; leptin treatment of the HepG2 liver cell line resulted in an increase in PTP1B expression[40] thereby further emphasizing the dichotomy between mammalian cell culture systems and animal models.

1.1.3.3. In vivo *Modulation of PTP1B Expression*

PTP1B ASOs have been developed by ISIS and shown to decrease PTP1B protein levels by ~50% in liver and adipose tissue[41,42]. The distribution of the ASO shows selectivity for liver, kidney and fat with a lower distribution in bone marrow and spleen. It is completely absent from muscle and the central nervous system. Treatment with the ASO causes insulin sensitization and normalization of blood glucose and insulin in obese and insulin resistant diabetic mice (ob/ob and db/db mice).

It also causes a reduction in adiposity associated with a reduction of the genes involved in fat homeostasis and SREBP-1 and its targets[42]. Since the ASO does not penetrate the brain, this reduction in weight gain is not centrally mediated. Reduction of PTP1B expression in liver and fat with no effect on muscle is enough to achieve glucose normalization in this model. Indeed, re-expression of PTP1B in the liver of the knockout mouse returned the animal to normal glucose metabolism levels[43].

Although this might underemphasize the role of PTP1B in muscle, 75% of the 80% increased in glucose uptake in the knockout mouse was found to be mediated by skeletal muscle[24]. PTP1B overexpression in that tissue[44] results in 37% less glucose required to maintain euglycemia in a hyperinsulinemic-euglycemic clamp due to 40-50% impaired glucose uptake with normal hepatic glucose production and insulin-stimulated

suppression. This overexpression reduced tyrosine phosphorylation of IR, IRS1, IRS2 and PI3K activation in muscle. PI3K activation was also decreased in liver although IR, IRS1 and IRS2 phosphorylation were unaffected in this tissue as well as glucose homeostasis indicating a possible indirect effect across tissues.

Repetition of the phenotype seen in the knock out mice with the ASO indicates that the effects seen in the knockout are not due to developmental defects or compensatory mechanisms. Along with the lack of serious side effects of PTP1B removal, it confirms the validity of PTP1B inhibition as a target for insulin resistance and obesity in diabetes.

1.1.3.4. PTP1B Levels in Diabetes

Human PTP1B is located in the 13q region of chromosome 20 which has been associated with diabetes and obesity[45]. A recent overview[46,47] of the 161-kb PTP1B-coding region reveals a total of 35 Single Nucleotide Polymorphisms (SNP). A block of eight non-coding SNPs (rs941798, rs3787345, rs754118, rs2282147, rs718049, rs718050, rs3787348 and 1484insG) spanning exons four to ten, form haplotypes that are most consistently associated with a protection (GTCCTGT∅) or susceptibility (ACTTCAG∅) to T2DM. Previously identified polymorphisms such as the silent 981T/C in the Oji Cree conferring 42% less likelihood of suffering from impaired glucose tolerance or T2DM[48] and P387L impairing serine phosphorylation of PTP1B and associated with a 3.7-fold increase in the risk of developing T2DM in Danish Caucasians[49] were found to be rare or missing in these recent studies. In addition, haplotypes containing the 1484insG which alone had been previously observed to increase PTP1B mRNA stability and to be

associated with insulin resistance[50] were not more strongly associated with T2DM. P387L and 1484insG were also found to lack association with T2DM depending on the population studied[51,52]. This indicated that non-coding polymorphisms in PTP1B were significant contributors to T2DM. However, there is evidence that other genes than PTP1B located in the chromosome region 20q12-13 also contribute to the pathology.

Correlations between muscle and adipose tissue PTP1B levels and obesity/diabetes in human have been explored by different groups showing no consistent correlation[53-58]. A similar lack of clear trends was observed in animal models[59-61]. It is now thought that protein levels are not representative of the activity of the phosphatase in cells and that current activity assays do not take into account the regulated state of PTP1B in the cell.

It has been found that the active site cysteine nucleophile of PTP1B can be oxidized leading to inactivation of the phosphatase[62]. Insulin stimulation generates a burst of reactive oxygen species which leads to the inactivation of 60% of cellular PTP and 88% of PTP1B[63]. It has been observed that the sulfenic acid could react with neighboring serine 216 to form a reversible sulfenyl-amide bond and protect the enzyme from irreversible oxidation and facilitate thiol-mediated reactivation[64,65]. Since activity assays contain a high amount of dithiothreitol (DTT), any oxidation-inactivated PTP1B in the cell would be reactivated thereby masking the true level of active phosphatase in the observed tissue.

1.1.4. PTP1B and Treatments

Knock out and ASO studies have confirmed PTP1B to be an interesting target in the treatment of T2DM. Total ablation of the gene or partial reduction in the level of the protein does not lead to adverse off-target effects such as tumor formation, nor does it predispose the mice to hypoglycaemia.

Prompted by these promising results, a flurry of activity to develop an inhibitor as a drug was initiated[66,67]. However, it has quickly become apparent that this is not an easy target to obtain inhibitors with the appropriate *in vivo* properties.

PTP1B displays a substrate preference for phosphotyrosine flanked on the N-terminus by acidic residues[68,69]. This is due to the positive nature of the active site which attracts these negatively charged substrates while they are repulsed from the rest of the otherwise negative surface of the phosphatase.

The phosphotyrosine moiety which penetrates the catalytic 9Å-deep cleft has been successfully mimicked by three different negatively charged chemical groups: difluorophosphonomethyls, oxalaminobenzoic acids and carboxymethoxy groups. Difluorophosphonomethyls are the most potent of the three with the fluorine atoms increasing potency 1000-fold.

These mimetics are affixed to different scaffolds designed to maximize interactions with the residues forming the active site. Selectivity for PTP1B is necessary since inhibition of other phosphatases can lead to serious side effects as suggested by the distinctive phenotypes of the different phosphatase knockouts. TCPTP is the closest relative of PTP1B with 72% identity which is raised to 94% when only considering the active site residues. The consequence of hitting TCPTP is not clear: the homozygous TCPTP knock out is embryonic lethal but the heterozyote displays only a mild

phenotype[70] yet TCPTP has been involved in the regulation of the insulin signalling pathway in a non-redundant function coordinated with PTP1B in cellular cultures[15].

In the quest to achieve greater affinity and selectivity, the molecules increase in size and in charge to engage a greater number of positively charged active site residues. However, with this expansion comes a deterioration of their physical properties. Charged molecules have difficulty crossing cell membranes and are less favourable to trans-cellular intestinal absorption. Para-cellular absorption is possible for molecules with molecular mass lower than 300Da fitting through pores at the junction of intestinal cells[71].

In effect, molecular mass, polar surface area and molecular flexibility are the three physical properties that need to be maximised for adequate oral availability. Statistically, there are very few orally bioavailable molecules with molecular mass greater than 500Da: increased mass is associated with issues of permeability, aqueous solubility and metabolism. Polar surface area is the sum of the polar atom (such as oxygen and nitrogen) surfaces in a molecule. For adequate bioavailability, it is desired to be less than 140Å whereas most PTP1B inhibitors are around 200Å. Finally, the most potent PT1B inhibitors to date are peptidomimetic and, where acceptable molecular flexibility is set at less than ten rotable bonds, these inhibitors are very flexible.[71]

The properties necessary for oral bioavailability are not compatible with the requirements for targeting the active site of PTP1B. The use of pro-drugs to decrease the number of negative charges has had only limited success[72]. A few lipophilic compounds have been identified to inhibit PTP1B and to normalize glucose and insulin levels in

animal models but were later identified to have a more complex mechanism *in vivo* hitting PPARγ, the target of thiazolidinediones[73].

As alternatives to competitive inhibition at the active site, allosteric inhibitors or modulation of a PTP1B regulatory protein may be more amenable to the development of orally bioavailable compounds. An allosteric site has been identified and targeted by a compound with micromolar affinity for PTP1B, fivefold selectivity for TCPTP and cellular activity[74]. On the other hand, the PTP1B ASO treatment which was successful in animals, is now undergoing Phase II clinical trials: ISIS 113715[75].

1.2. The Biochemistry of PTP1B

1.2.1. Structure

PTP1B is a 435 amino acid, 50kDa protein belonging to the non-transmembrane PTP family. The conserved core PTP catalytic domain is coded by residues 1-280 and contains the consensus tyrosine phosphatase signature motif: (I/V)HCxAGxGR(S/T)G which in PTP1B corresponds to VHC^{215}SAGIGRSG. The PTP loop contains the active site cysteine 215, which is responsible for the catalytic activity of the phosphatase. The last C-terminal 35 residues are necessary and sufficient to anchor the phosphatase to the endoplasmic reticulum with the catalytic domain oriented towards the cytosol[76]. Alternative splicing of the mRNA, upon stimulation with growth factors including insulin, replaces the last seven residues (FLFNSNT) for a shorter four amino acid tail (VCFH)[77,78]. The intervening 122 residues between the PTP domain and the ER anchor have been involved in protein-protein interaction, substrate binding and regulation.

The first crystal structure of PTP1B showed residues 5 to 282 forming a single domain of eight α-helices and 12 β-strands, ten of which formed a twisted β-sheet spanning the entire length of the molecule[79]. The lack of electron densities for the residues 283-321 was assumed to be due to disorder of that segment of the protein. However, in later crystals, where residues 1 to 298 were visible, the α1 helix was found disordered and residues 286-294 formed a helix[80]. This last helix was numbered α7 to follow the numbering of the original paper (the first two helices were named α1' and α2'

due to their location outside the then consensus catalytic PTP core). Although α1 is rarely seen in most of the available structures[81], α7 is sometimes found disordered[79,82,83].

There are very little sequence similarities between the members of the PTP family but all share the same overall tertiary structure[81]. The conserved PTP catalytic domain is contained within 280 amino acids, 22 of which are invariant amongst mammalian PTPs[81]. In the structure of PTP1B, most of these invariant residues are located on loops connecting structural elements that converge around the active site. Invariant residues which are further away from the active site are buried and appear to play a role in stabilizing the protein fold: R257 participates in hydrogen bonding with N44, Y66 and N68; Y124 and H214 are held within a hydrophobic pocket formed by residues F95, W96, C121 and W126.

The PTP loop contains the signature motif and connects the α4 helix to the β12 strand. The orientation of the PTP loop is maintained by interactions between the main-chain carbonyl group of residues forming the loop and the side chain of H214 (for C215), the main-chain nitrogen of G86 (for S216), the side chain NH1 of R257 (for A217) and the side-chain hydroxyl of S222 (for G218). H214 is also involved in a hydrogen bond with the hydroxyl group of Y124. The conformation of G218 gives the PTP loop a sharp turn that is essential for catalytic activity. Furthermore, the glycine-rich motif of the PTP loop (GxGxxG) allows close packing of the loop with neighbouring residues and the phosphate groups of the substrate. This arrangement makes the PTP loop rigid such that it shows little fluctuations when substrate binds[84].

Residues 179-185 form the WPD loop: WPD[181]FGVP. This loop closes over the active site when substrate binds to bring the aspartate 181 5.5Å closer to the PTP loop to

participate in catalysis. Tryptophan 179 is invariant and, along with P185 and G183, is critical for loop closure. In the free phosphatase, the WPD loop oscillates between the closed and open conformations, existing in a delicate electrostatic balance with the active site[85]. When the active site cysteine is replaced by a serine residue, effectively replacing the negative charge of the thiolate with a neutral polar alcohol, the PTP loop extrudes from the active site, limits the flexibility of the WPD loop and effectively locks it in an open conformation[82]. On the other hand, when the cysteine is mutated to an aspartate, which slightly enhances the negativity of the active site (lower pK_a), the WPD loop has a higher propensity to be in the closed conformation than the wild-type enzyme[86].

Overall, molecular dynamic modelling reveals that the flexibility of the side chains at the surface of the free phosphatase is similar to the peptide substrate-bound complex[87]. The most pronounced structural change associated with the binding of the substrate was found to originate from the movement of the WPD loop and affect mostly the loop hanging below the active site linking the α3 helix to the β12 strand: V198-G209. In addition, substrate binding was found to reduce the motions of P31-N40 (contains the α2' helix), E97-V108 (the loop connecting, and part of, the α2 helix and β4 strand), K128-141 (this includes K128 and K131 on the βsheet), P179-G182 (part of the WPD loop), L192-S204 (α3 helix) and to increase the motion of L88-H94 (loop between the β3 strand and α2 helix), D235-D240 (C-terminal end, PTP loop-distal, of α4 helix) along with the α7 helix.

The substrate recognition loop (or North loop), KNRYRD[48], is positioned above the active site and is responsible for substrate selectivity. Aspartate 48 is positioned at the rim of the loop and dictates the depth of the active site: 9Å. This creates specificity for

phosphotyrosine residues because phosphoserine and phosphothreonine cannot reach the base of the active site to interact with the PTP loop.

In effect, the active site is delineated by the PTP loop at the bottom and on top by both the WPD loop on one side and the substrate recognition loop on the other. In addition, the active site is bordered on one side by the West loop, residues 115-120, and on the East by a secondary binding site[88] that is catalytically inactive but that can bind phosphotyrosine with a decreased affinity compared to that of the active site. The two sites are separated by the loop formed by residues 257-262: RMGLIQ (East loop), and essentially gated by residue G259. A larger residue at this position prevents access and binding to the secondary binding site[89]. R24 (on the α2' helix) and R254 (on the α5 helix) are located at the distal end of the secondary binding site to engage the phosphate group. The residues on the East loop have also been found to have a critical role in catalysis. (See Figure 1.1)

Figure 1.1: 3-Dimensional structure of the PTP1B inactive mutant C215A crystallized with the autophosphorylation loop of the IR (residues 1160-1166) entry 1G1H from the RCSB Protein Data Bank. A) view from above, B) view from the side, C) only the active site loops of A are shown, D) only the active site loops of B are shown. The two phosphotyrosines of the substrate are shown located in the active site: one in the active site pocket interacting with the PTP loop and the other in the secondary binding site; for B) the backbone of the peptide is also shown in orange. Pink: PTP loop with residue 215 shown in darker pink, Blue: North loop, Yellow: West loop, Green: WPD loop, Purple: East loop with the Arginine 24 also shown in purple as the far limit of the secondary site.

1.2.2. Phosphorylation and Residues C-terminal to the Catalytic Domain

PTP1B was first demonstrated to be serine phosphorylated in unsynchronised HeLa cells[76,90]. More specifically, PTP1B was found to be phosphorylated on serine 352 and 386 in mitosis-dependent events[91,92] and as a result of osmotic shock[93]. This phosphorylation was reported to either have no effect of the activity of the phosphatase[91] or to decrease it by 30%[92] and mutation of the neighbouring proline 387 to leucine was observed to decrease serine phosphorylation to 28% of the wild-type levels[49]. The kinase responsible for the phosphorylation of S352 has not been identified but p34cdc 2 has been observed to phosphorylate S386. PKC has been shown to phosphorylate serine 378 both *in vivo* and *in vitro* without an effect on activity[92]. Both these kinases were found to phosphorylate less than 20% of total PTP1B.

Located within the catalytic domain, serine 50 has been found to be phosphorylated by Akt, via an insulin-stimulated pathway, resulting in decreased activity of the phosphatase by 25% against phosphorylated peptides[94]. In addition, mutation of serine 50 to an alanine severely repressed the activity of PTP1B. CLK1 and CLK2 have also been observed to phosphorylate S50 with a three- to fivefold increase in activity against p-nitrophenyl phosphate (pNPP). While S50 was the principle target of CLK1/2, S242 and S243 are also phosphorylated by these kinases[95].

The IR and the EGFR can associate with PTP1B only when they are auto-phosphorylated and in turn phosphorylate PTP1B on the conserved tyrosine 66, located somewhat below the substrate recognition loop[96,97]. In unstimulated cells, 5.8% of PTP1B is found serine phosphorylated and only 0.2% phosphorylated on tyrosine residues. Stimulation with Epidermal Growth Factor (EGF) to activate the EGFR results in a

dramatic increase in phosphorylation: 21.9% of PTP1B is phosphorylated on serine and 12% on tyrosine[97]. Other than phosphorylation, PTP1B shows no other post-translational modification beyond N-acetylation of the N-terminal methionine[98].

There are discrepancies in the literature about the effect of serine phosphorylation on PTP1B activity. The effects of tyrosine phosphorylation, however, seem to all indicate an increase in activity[97,99] except for one study[100] in mouse treated with insulin where the activity of PTP1B was found to be diminished correlating with an increase in its tyrosine phosphorylation and a decrease in its serine phosphorylation. This was supported by an increase in activity following activation of adenylate cyclase associated with an increase in serine and a decrease in tyrosine phosphorylation.

Broad-specificity kinases (e.g. Elk in the TKB1 bacterial strain) can phosphorylate PTP1B on only three tyrosine residues: 66, 152 and 153[101] to suggest that post-translational modifications by tyrosine phosphorylation in the cell is limited to these three locations. Although, the PTP1B-IR complex includes other proteins[102], the activated IR is the most probable kinase that phosphorylates PTP1B on tyrosine 66[99]; tyrosines 152 and 153 are not phosphorylated by the IR or the EGFR.

Cadherin is involved in morphogenesis and interacts with different catenins which in turn bind to actin and modulate the cytoskeleton. PTP1B binds to cadherin and de-phosphorylates β-catenin enabling it to couple cadherin to the actin cytoskeleton. In this complex, the phosphorylation of PTP1B is regulated: only phosphorylated PTP1B interacts with cadherin and de-phosphorylates β-catenin. Tyrosine 152 is critical for binding to cadherin.[101]. The kinase responsible for this required phosphorylation of PTP1B is not known[103].

In addition to sites for serine phosphorylation, the C-terminal region of PTP1B contains two proline-rich sequences: residues 301-315 and 386-397. Proline rich sequences are ligands for SH3 domain-containing proteins. Mutation of prolines 309 and 310 to alanines abolished binding of PTP1B to p130cas[33,104] and to the SH3 domains of GRB2 and Cdc2-Related Kinase 1 (CRK1)[33]. The ability of PTP1B to down-regulate the insulin signalling system is sensitive to residues 152 and 153, which mediate IR binding, but not to these proline residues although interactions with SH3-containing proteins are necessary for the insulin signalling pathway (GRB2 and CRK1 are adaptor proteins which bind to IRS1)[33].

Although the 122 residues between the catalytic domain and the site of interaction with the ER are often overlooked, they are active participants in substrate recognition, protein-protein interactions and activity of PTP1B. Residues 301-313 form a proline rich region which might play a role in binding protein containing SH3 domains and the following residues, up to M364 are highly charged and presumably exposed as they are susceptible to protease degradation and serine phosphorylation[90].Cleavage in this region by calpain yields a 42kDa fragment with increased activity suggesting it might have been released from inhibitory C-terminal residues[105].

1.2.3. Catalytic Mechanism[106-109]

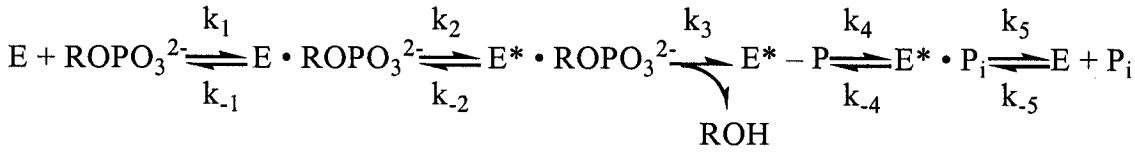

Figure 1.2: PTP reaction mechanism[107]. $ROPO_3^{2-}$ represents the phosphorylated aryl substrate, E* represents the enzyme with a closed WPD loop, P_i represents inorganic phosphate.

The PTP catalyzed hydrolysis of phosphate monoesters proceeds through the formation of a phosphoryl cysteine intermediate (see Figure 1.2). The uni-bi reaction occurs in two chemical steps: formation and breakdown of the E-P intermediate. The first step includes binding of the substrate (k_1) and closure of the WPD loop (k_2). These two events are rapidly reversible and do not constitute a commitment to catalysis[107]. The phosphate is coordinated in the active site through interactions between its equatorial oxygens and the guanidium groups of R221 as well as a network of hydrogen bonds to the backbone amides of the PTP-loop. Formation of the E-P intermediate (k_3) occurs from attack of the phosphate phosphorous atom by the thiolate anion of C215. This is accompanied by a proton transfer from D181 to the leaving group to facilitate departure by neutralizing the charge on the first product. D181 then activates a water molecule, coordinated by Q262, for hydrolysis of the E-P intermediate (k_4) and regeneration of the enzyme accompanied by release of inorganic phosphate (k_5). See Figure 1.3.

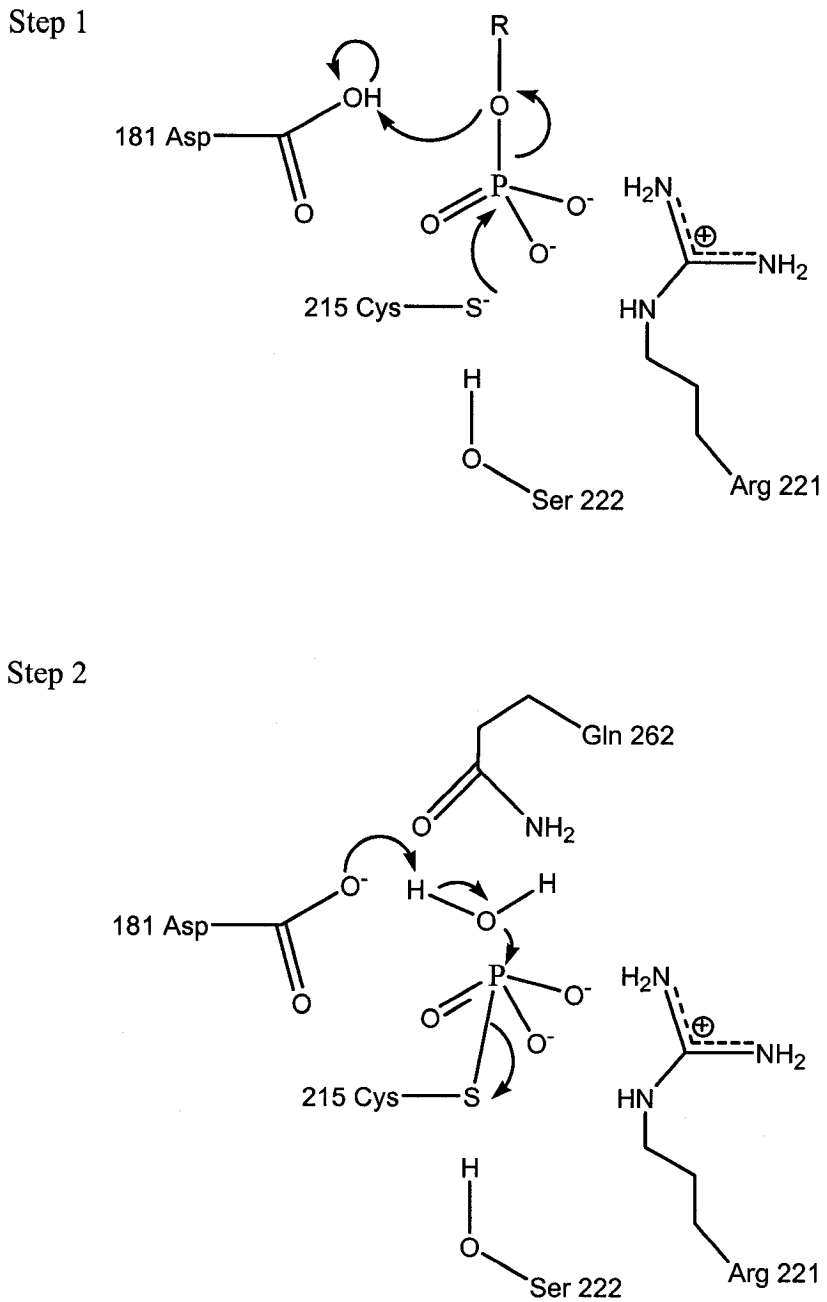

Figure 1.3: Schematic representation of the PTP chemical reaction. Step 1 shows nucleophilic attack by cysteine 215 and cleavage of the product. Step 2 show hydrolysis of the phosphoryl cysteine intermediate and regeneration of the enzyme.

G259 has been found to orient Q262 in the proper conformation for its interaction with the water molecule. Mutations at position 259 can affect the turnover of the enzyme through interactions with Q262 preventing its motion to participate in catalysis[89].

Mutation of aspartate 181 to an alanine results in a phosphatase that binds the substrate with high affinity but is unable to catalyze the reaction thereby essentially trapping the substrate[110]. The absence of the general acid/base suppresses cleavage of the P-O bond. Higher binding affinity, compared to the wild-type enzyme, results from the loss of the charged aspartate residue which reduces the electrostatic repulsion with the active site thiolate and the negatively charged substrate to favour closure of the WPD loop and to increase binding enthalpy[111].

The pK_a of the active site cysteine residue is calculated to be relatively low compared to free cysteine (~5[112,113] compared to 8.3). This low value can be attributable to the environment of this residue susceptible to the dipoles created by the N-terminus of the α4 helix and the vicinal histidine 214 residue, however the accumulations of the backbone microdipoles generated by the spacial orientation of the residues forming the PTP loop is thought to have the largest impact on the pKa of the cysteine[113]. Mutation of serine 222 slightly increases the pK_a of the cysteine but is mostly seen to have a greater impact on the second step of the reaction rather than the first one. Its hydroxyl group is thought to engage the thiolate in an H-bond and thereby stabilizes the leaving group thiolate of the second step[114]. This stabilization could further lower the pK_a of the cysteine residue. Additionally, S222 could be positioning the S-P bond for in-line attack by the water molecule[109]. D181 and R221 strongly interact with the cysteine: the arginine

to stabilize the thiolate and the aspartate to destabilize it, in effect neatly cancelling each other out[113].

Phenylalanine 182, on the WPD loop, is found to contribute substantially to substrate binding by interacting with the phenyl ring of the phosphotyrosine substrate. This interaction is driven by the closure of the WPD loop that moves the phenylalanine residues 12Å towards the active site[80]. However, amongst the 37 known human full-length PTPs, only four have a phenylalanine in that position with the majority, 25 of them, having a histidine residue instead. Mutational studies[115] revealed that replacement of the phenylalanine with histidine lowered the turnover of the enzyme while slightly increasing its affinity for the substrate. The histidine was found to interact with Q262 and D181 and to bind the phenolic oxygen of the substrate via a water molecule. The lowered K_M implied that this interaction was more than able to compensate for the loss of aromatic-aromatic interactions. The decreased turnover was found to be due to a deficiency in hydrolysis of the phosphoryl cysteine intermediate resulting from loss of aspartate 181 positioning by F182.

In addition to bringing D181 and F182 towards the active site and so participate in substrate binding and/or catalysis, closure of the WPD loop also functions to cap the active site. This sequesters the intermediate and the water molecule and prevents the transfer of the phosphate to another acceptor molecule[114].

The mechanism of the first step is thought to have a highly dissociative character (S_N1-like) in which the P-O bond of the transition state, stabilized by R221[116], is mostly broken, the proton transfer to the leaving group well advanced and the central phosphoryl in a trigonal bipyramidal conformation. The second step is also highly dissociative.

There is some disagreement as to the rate limiting step of the tyrosine phosphatase reaction. However, there is little dependence of the catalytic activity on the nature of the leaving group and when burst kinetics are observed, the rate of formation of the phosphoenzyme intermediate is only a few fold higher than its breakdown. This slight difference may contribute to the diverging conclusions when the reaction is performed under varying conditions.[107]

The traditional binding of the substrate as a dianion (fully deprotonated) to the thiolate has been pointed out to be unfavourable[112]. Instead, a model has been proposed where the substrate binds as a monoanion or that the protonated nucleophile cysteine is activated by transferring the hydrogen to the substrate.

1.2.4. Substrate Binding Determinants

Since the identity of the cellular substrate for PTP1B has long been unknown, its substrate specificity has been extensively defined using short phosphorylated peptides. Of the least intuitive experiment conducted was a reverse-alanine scan screening of a library of peptides where each position on the AAAApYAAAA scaffold was changed for one of the 20 naturally occurring amino acids to identify the substrate with highest affinity for PTP1B to be: ELEFpYMDYE-NH_2 (k_{cat}/K_M 2.22 x 10^7)[117].

This observation was however preceded by experiments based on the observed affinity of *Yersinia* phosphatase for a short peptide modeled on the auto-phosphorylation site of the Epidermal Growth Factor Receptor (EGFR): DADEpYLIPQQG[118]. Selective deletions and mutations of this peptide were tested on rat PTP1 (rat homologue of PTP1B) as a mammalian counterpart to compare and contrast the selectivity of the

Yersinia phosphatase[106,119]. This identified broad selectivity criteria namely that the phosphotyrosine was not sufficient by itself for high affinity binding, that the residue lying N-terminal to the phosphotyrosine were the major contributors to the binding compared to residues located C-terminal and that they were preferred to be acidic, that the minimal size of the peptide was six residues: four N-terminal and one C-terminal and finally that the most efficient substrate was: DADEpYL-NH2 (k_{cat}/K_M 1.57 x 10^7). Longer peptides were found to add nothing to the efficiency of this consensus sequence. These experiments were then repeated using PTP1B with similar conclusions[120,121].

This peptide was co-crystallized with PTP1B to finally reveal substrates determinants[80]. The active site cysteine 215 residue, which was mutated to serine in order to observe the phosphorylated substrate in the active site, was co-linear with the phenolic oxygen atom of the phosphotyrosine residue, placing it in an optimum position for attack. D181, directly or through a buried water molecule, also interacted with the phenolic oxygen atom. The other phosphate oxygen atoms where coordinated by hydrogen bonding to the backbone nitrogen groups of the residues forming the PTP loop: S216, A217, G218, I219, G220 along with the side chain of R221 which was found to be precisely positioned through interactions with the side chain of E115.

Binding of the peptide induced closure of the WPD loop. The closed loop was stabilized through interactions between F182 and the phenyl ring of the phosphotyrosine residue, hydrogen bonding between backbone nitrogen of F182 and the buried water molecule and interactions of F182 with Q262 and T263. In addition to interactions with F182, the closed loop was stabilized by a salt bridge between the side chains of D181 and K120; in the unliganded state, D181 engaged R112 in a salt bridge.

The phenyl ring of the phosphotyrosine residue nestled in a hydrophobic pocket formed by residues A216, I219, Y46, F182 and Q262. The aromatic ring of Y46 which, along with F182, participated in pi-pi interactions with the phenyl ring, was maintained in a favourable orientation through a hydrogen bond with the side chain hydroxyl group of S216.

D48 was the primary determinant of the bound peptide conformation and its orientation in the active site. With two hydrogen bonds, it engaged the backbone nitrogen of the phosphotyrosine residue and the first C-terminal residue (+1). The guanidium group of R47 formed salt bridges with the side chain of residues -1 (first residue N-terminal to the phosphotyrosine) and -2 and a long hydrogen bond with -4. Its backbone nitrogen group formed a hydrogen bond with the backbone carbonyl of -2. Interestingly, when the same complex was probed by NMR, the interaction of the side chain of -2 with R47 was lost in favour of K41, suggesting this might have been a crystal packing artefact[122]. Nonetheless, the crystal structure did show a leaning of K41 towards -2 and -3.

The single C-terminal residue (+1) engaged in Van der Waals interactions with V49, I219 and Q262, its backbone nitrogen involved in a water-mediated hydrogen bond with Q262. Although nothing more is noted in the crystal structure for residue +1, the NMR structure shows additional interactions of the backbone carbonyl with R24 and R254 and increased the hydrophobic collapse patch to include residues Y46, A217 and M258.

An additional interaction was seen between a fluorine atom and the main-chain nitrogen of F182 in the NMR structure which used a difluorophosphonomethyl group

instead of phosphate as tyrosine modifier. They also noted a cation-pi interaction between the side chain of K120 and the phenyl ring of the tyrosine residue resulting from a rotation of K120 away from its favourable packing position found the apo-structure.

Further refinements on DADEpYL were investigated by systematically mutating each position to yield a library from which EEDE(F2PMP)YL was identified as the highest affinity peptide for PTP1B (k_{cat}/K_M 2.78 x 10^7)[121]. In addition, the screen recognized that the -1 position could also be accommodated by an aromatic residue. This was supported by the reverse-alanine scan which observed the greatest increase in affinity when phenylalanine was used in position -1[117].

Since the acidic nature of -1 was well accepted as a determinant of binding affinity and that the X-ray structure showed strong electrostatic interactions with R47, a new structure needed to be resolved to identify the newly found plasticity of the -1 position. The crystal structure of PTP1B and ELEFpYMDYE[123] showed most of the interactions seen in the structure with DADEpYL except for R47. The side chain of R47 was seen to be rotated 120°, shifting the guanidium group by 7Å such that its side chain now created a hydrophobic patch with D48 for the large hydrophobic residue at -1, and also now participated in Van der Waals interaction with -3.

In essence, the orientation of R47 in PTP1B could accommodate either an acidic residue at -1, in which case it dictated an acidic residue for -2 also, or a large hydrophobic group on -1 such that it now participated in hydrophobic interactions with -1 and -3.

Although these peptides showed high affinity for PTP1B, they were not the cellular substrate of the phosphatase which had been observed to bind and de-

phosphorylate different cell-surface receptors including the IR and the EGFR. These interactions could only be observed when substrate-trapping mutants of PTP1B were used indicating their transient and unstable nature. The PTP1B-IR interaction occurred on the auto-phosphorylation site of the IR and required the presence of phosphorylated Y1162 > Y1163 > Y1158[99,102] with PTP1B preferentially de-phosphorylating the Y1162 residue. Depending on the technique used, one[124] or two[96] binding sites have been counted on the IR and complete competition with the appropriate peptide could be seen[96] or not[124]. The inability of a short peptide to completely abolish the binding of the IR and PTP1B can be expected when modelling of the complex reveal 5000 $Å^2$ of buried surface that needs to be disrupted[125]. The EGFR contained two sites of interaction with the PTP1B: the high affinity site displaying a K_d of 100nM[119]; the IR high affinity site had a K_d of 75nM[96] or a single site with a K_d of 108nM[124]. For comparison, high affinity phosphorylated peptides displayed K_M values in the low micromolar range.

The auto-phosphorylation site and activation segment of the IR contains three tyrosine residues which become phosphorylated when the receptor binds insulin: RDIYETDY[1162]YRKGGKGLL. The crystal structure with this bis-phosphorylated peptide showed pY1162 bound in the active site of PTP1B and pY1163 located in the secondary binding site[126]. The active site phosphotyrosine engaged in similar interactions as seen in previous crystal structure: the phosphate oxygen atoms were involved in hydrogen bonds with the main-chain nitrogen groups of S216, A217, G218, I219, G220 and R221 along with the side chain group of R221. Y46 and F182 sandwiched the phenyl ring.

The phosphate group of pY1163 was coordinated in the secondary binding site by direct and water-mediated interactions with R24 and R254. Its phenyl ring was not very ordered but showed some interactions with Q262 and M258. Amongst tyrosine phosphatases, PTP1B has selectivity for vicinal phosphorylated di-tyrosine. This is due to the small size of the glycine residue at position 259 which allows interaction with the bulky pY1163 residue and also the interaction with R24 and R254 which phosphoserine of phosphothreonine cannot reach. In mutational studies, R24 is seen to participate solely in peptide binding whereas G259 and R254 seem to also have a role in hydrolysis[126].

Residues D48 still directed peptide orientation through its two hydrogen bonds to pY1162 and pY1163. The side chain of R47 participated in a hydrogen bond with the side chain of aspartate located at -1 and its backbone nitrogen in a long hydrogen bond with the side chain of threonine at -2. F182 was seen in a pi-cation interaction with the guanidium group of arginine at position +2. Q262 coordinated the main chain nitrogen of +2 while R24 interacted with the main chain nitrogen of +4.

The structure of the tri-phosphorylated peptide showed similar interactions as the bis-phosphorylated structure due to the lack of order of residues beyond -2 thereby indicating the absence of a specific binding pocket for pY1158.

Most of the interaction energy of PTP1B with peptide substrates can be accounted for by the binding of the phosphotyrosine residue along with four residues on its N-terminal side and one residue on its C-terminal side. The phosphate group on the tyrosine interacts with the PTP loop: C215, S216, A217, G218, I219, G220 and R221. The WPD loop (F182, D181) also interacts with the phosphotyrosine. K41, Y46, R47, D48 and V49 are located on the substrate recognition loop named after the strong contribution of D48

and R47 to the specificity for the substrate and its orientation in the active site. Q262, T263, R254, M258 and G259 are all located on the East loop and dictate interactions in the secondary binding site along with R24. R112, E115 and K120, located on the West loop, do not directly interact with the substrate but are involved in the precise positioning of other residues which are critical for substrate binding.

Binding energies between PTP1B and peptide substrates contain both enthalpic and entropic contributions[111]. The favourable entropy comes from the release of the tight water network that surrounds the active site[84] and the enthalpy comes from the network of interactions listed above. Interestingly, when the active site cysteine is mutated to a serine, the phosphatase is inactive but its affinity for the peptide does not change. The respective contributions to the binding energy are however different from the wild type with the enthalpic contribution increasing and the entropy becoming unfavourable. The removal of the negative charge of the thiolate and replacement with a neutral polar residue increased the enthalpy of binding by removing the electrostatic repulsion between the PTP loop and the substrate. For the same reasons, the D181A mutant shows higher binding enthalpy and a higher affinity for the substrate. The loss of the entropy component was thought to be due to an increased flexibility of the PTP loop when the thiolate was removed, thereby resulting in restricted flexibility once substrate binds.[111]

The structures obtained with the various peptides have been useful to thoroughly define the binding of substrates in and around the active site of PTP1B. However, no structures have been resolved with the phosphatase in complex with macro molecules such as the receptors it has been seen to interact with. This interaction has however been modelled *in silico*[125].

The model of the complex between PTP1B and the IR showed good surface complementarity between the two enzymes with no significant cavities and an interface composed mainly of uncharged residues and some identically matched charged residues. The charged interactions occurred mostly over the active site, as described for the crystal structure with the bis-phosphorylated IR peptide, and an important hydrophobic patch was observed between residues 133-140 on PTP1B, forming the β7 and β8 strands and their connecting loop, and residues 1059-1066 on the IR.

Tyrosines 152 and 153, sandwiched between the β-sheet and the α3 helix, have also been implicated in binding of the IR where mutations of these residues to phenylalanine did not affect catalytic activity of the phosphatase but resulted in a loss of receptor binding[33,102,127]. These mutations did not affect EGFR binding[97].

Truncation studies have identified residues 100-193 of PTP1B, forming most of the β-sheet along with the West and the WPD loops, to be important for IR binding. Mutation of tyrosines 152 and 153 strongly repressed receptor binding in a 1-193 PTP1B construct. Interestingly, when the same mutation is made in the context of the full-length (minus ER targeting domain) 1-400 phosphatase, some residual IR binding can still be observed[33,127]. In addition, residues 193 to 403 can mediate binding to the IR on their own[127], suggesting that residues beyond the catalytic domain could play a role in substrate binding.

In addition to the interactions defined by short model peptides, binding cellular substrates also implicates residues distant from the active site including the two tyrosines 152 and 153, a hydrophobic patch formed by residues 133-140 and possibly other residues outside the catalytic domain.

1.2.5. Inhibitor Binding Determinants

Inhibitors developed for PTP1B mimic the phosphorylated tyrosine residue of the substrate. The minimum unit of the inhibitors is a non-hydrolysable phosphate mimetic war head attached to an aromatic ring. Naphthalene, phenyl or biphenyl have been used amongst others for this war head aromatic ring with the observation that biphenyl rings are more potent than naphthalene rings which are themselves more potent than phenyl rings.

The war head bearing aromatic ring of the inhibitor is sandwiched between the aromatic rings of Y46 and F182. Closure of the WPD loop brings the F182 residue in close enough proximity for the interaction but some inhibitors can still bind with the WPD loop open[83,128]. Additional hydrophobic interactions are provided by the side chains of V49, A217, I219 and Q262[83,128-134]. Depending on the conformation of the inhibitor used, other residues can participate in the hydrophobic pocket: G220[133] and L119[134]. The potency of the inhibitors has been shown to increase when the aromatic scaffold can make Van der Waals interactions with the side chains of E115, K116 and K120[133].

The ability of a naphthalene ring to maximise interactions with the hydrophobic pocket in the active site is responsible for its increased potency versus single-phenyl inhibitors[130,131]. Further improvement with bi-phenyl systems are due to additional interactions with E115, E116 and K120[133]. Although potency of the inhibitors can be increased by taking advantage of the hydrophobic elements of the active site, ~93% of the total protein-inhibitor interaction energy is provided by electrostatic terms[129].

The interactions of the war head with the active site are similar to the substrate's phosphate moiety: hydrogen bonding with backbone nitrogen of residues S216, A217,

R221, G218 and G220. Most of these interactions are maintained with the inhibitor but depending on the nature of the war head some bonding is lost while new interactions are formed. Most mimetics maintain bonding with the R221 residue along with S216, A217 and G220; G218 is often missing but I219 sometimes participates. In addition to hydrogen bonding with backbone nitrogen, salt bridges can be found with the side chain of R221. For some of the war heads which do not completely penetrate into the active site, most of these interactions are still maintained, mediated by a network of water molecules[128]. Inhibitors missing most of these interactions with the PTP loop often display stronger hydrophobic interactions to compensate[132]. The two fluorine atoms included in the difluorophosphonomethyl war head interact with residue F182 through Van der Waals interactions and/or are hydrogen bonded to a water molecule which also interacts with the backbone nitrogen of F182 and sometimes the side chain nitrogen of Q266[129,134-136]. K120 has been mentioned in the context of interactions with aromatic rings but its side chain nitrogen group can interact with carboxylic groups attached as substituent to the war head proximal aromatic ring[128,131,137] and is sometimes accompanied by D181 in this interaction[128,137].

V49, I219, M258 and Q262 form the curtain separating the active site from the secondary binding site. These residues form a hydrophobic patch for the inhibitors. In some structures where the inhibitor occupies the secondary binding site, the side chain nitrogen of Q262 is found to engage carbonyl or ester groups[138-141]. R24, R254 and F52 are responsible for binding inhibitors that reach deeper into that secondary site[134,138-141]; occasionally, Y20 and H25 (through a water network) also participate in this binding[134,141].

TCPTP and PTP1B share 72% overall amino acid identity which is raised to 94% when only the residues forming the active site are considered. In effect, the only difference in the active site residues between the two enzymes lies at position 52 and 27 (F and A for PTP1B and Y and S for TCPTP). Selectivity between the two enzymes has been observed for inhibitors that were capable of reaching deep enough in the secondary binding site to engage position 52.[134]

R47 is found to interact with carboxylic[128,130,136], sulphate[132], phosphate[136]or nitro[132] groups positioned on the end of inhibitors that are long enough to reach up, and/or through a water molecule[135,142] and D48 mostly with nitrogen atoms as part of peptide chains[128,130,136,139,143] or aromatic rings[134,144]. The aliphatic part of their side chain can also participate in Van der Waals interactions with extended ring systems[132,134,145]. For inhibitors capable of reaching further than R47 or D48, the position K41 has been found to be able to interact with appropriate groups[146,147]. However, K41 had been previously shown to interact with the -2 position on a peptide inhibitor[148] and its involvement in small-molecule inhibitor binding becomes rare and more appropriately assigned to binding bigger substrates.

Increase in binding of the inhibitor can be obtained by introducing modifications in the structure that will replace tightly bound water molecules[128]. For example, addition of a hydroxyl group positioned to replace an active site water molecule and so hydrogen bond with K120 has been shown to increase inhibitor potency[129]. The increased binding results from an increased entropy obtained from the release of the tightly bound water molecule[129]. Higher affinity can also be obtained by using rigid molecules which do not suffer the loss in entropy seen when a flexible inhibitor molecule becomes constrained in

the active site. For example, replacing linear with cyclic peptides results in more potent inhibitors[83]. The corollary is also true for the enzyme: constraining the motion of a flexible residue will result in an unfavourable loss of entropy. The side chain of R47 shows considerate flexibility and motion in the X-ray structures; involving this residue in binding the inhibitor may not lead to increased affinity although in terms of enthalpy the extra interaction with the inhibitor molecule might be thought advantageous[131].

To summarize, the active site is surrounded by five loops: the PTP loop (pink) at the bottom, the WPD loop (green) nearest the viewer, the substrate-recognition loop (blue)to the North, the East loop (yellow) gating the secondary binding site and the West loop (purple). Residues that are shown to interact with the inhibitor on the PTP loop are: S216, A217, G218, I219, G220 and R221, on the WPD loop: D181 and F182, North: K41, Y46, R47, D48 and V49, West: E115, K116, L119 and K120 and East: Q262, M258; in addition, Y20, R24, H25, F52 and R254 which are found in the secondary binding site and Q266. (See Figure 1.4)

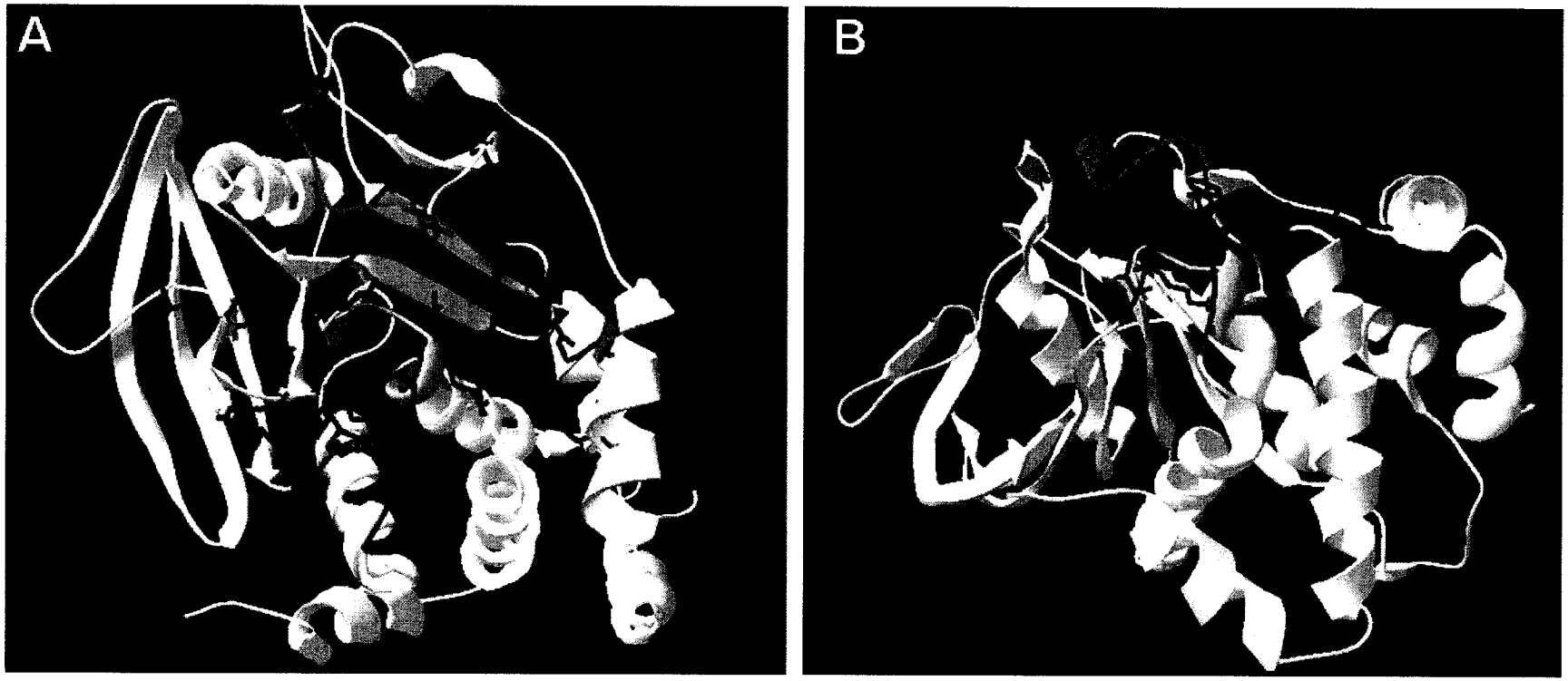

Figure 1.4: Projection of PTP1B inhibitor determinants identified from the literature on the structure of PTP1B as modeled from the crystal structure of entry 1G1H in the RCSB Protein Data Bank. Active site loops are coloured as in Figure 1.1. Pink: PTP loop, Blue: North loop, Yellow: West loop, Green: WPD loop, Purple: East loop with the Arginine 24 also shown in purple as the far limit of the secondary site.. Only the side chains of the determinants are shown coloured in red. A) view from above, B) view from the side.

1.3. PTP1B and Yeast

1.3.1. Yeast Screens

1.3.1.1. Phosphodiesterase in Yeast

Phosphodiesterases, such as PDE4 which hydrolyses the intracellular messenger cAMP, are targets for a wide range of pathologies from asthma to erectile dysfunction. Ablation of the yeast *S. cerevisiae pde1* and *pde2* results in an increase in cAMP levels which prevents the cell from undergoing the necessary biochemical changes to maintain quiescence. This defect leads to a wide range of phenotypes including sensitivity to heat shock. Human PDE4 can complement this defect and restore growth. Treatment with specific PDE4 inhibitors, such as rolipram, abolishes this complementation and reverts the yeast to heat shock sensitivity. This phenotype has been exploited to screen libraries of PDE4 mutants and identify the structural requirements of inhibitor binding.[149,150]

Libraries of mutants can be generated by transforming the target in an *E. coli* strain with a defect in DNA repair or editing, or treating the bacteria with hydroxylamine or simply by submitting the target to error-prone PCR amplification[151]. To identify the determinants required for inhibitor binding but not for enzyme activity, the library obtained for PDE4 was transformed into yeast, treated with rolipram, heat shocked and assayed for growth[149,150]. The only viable colonies were those expressing a PDE4 mutation that was still active, to confer heat-shock resistance, but that had lost sensitivity to the PDE4 inhibitor[149,150].

Two general types of determinants were obtained from the yeast PDE4 screen: those that affected only inhibitor binding and those that also altered substrate binding.

These latter were rare: T405A[149] and I408N[152] showed dramatic increase in yeast survival with 330- and 909-fold increases respectively in the rolipram median Inhibitory Concentration (IC_{50}) measured on the purified enzymes but also increased the K_M of the phosphodiesterases 17.8- and 585-fold. All of the other mutations identified shifted the IC_{50} while preserving near-native K_M. In one study[149] all resistant clones were found to contain only single-point mutations whereas the second study[152] also identified double mutants. When these mutations were evaluated separately, one clone was revealed to carry a spurious mutation (K439R) whereas the others where found to be additive, synergetic or antagonistic[152]. Of the ten resistant mutations identified using yeast, six were found to cluster within a sequence of 30 residues involved in substrate specificity[152].

Alternatively, this same system was used to identify specificity determinants in PDE4 and PDE3. PDE3 is resistant to rolipram and by using chimeras of the two phosphodiesterases, the specific residues involved in this selectivity were identified[152].

1.3.1.2. Dihydrofolate Reductase in Yeast

In addition to identifying binding determinants, the PDE4 heat shock yeast system has also been proposed to be useful for PDE4 inhibitor screening[150]. Compound screening in yeast has been effective in identifying Dihydrofolate Reductase (DHFR) inhibitors[153]. Inhibition of DHFR is an efficient strategy to fight apicomplexan parasite infections such as *C. parvum*. These parasites colonize the lining of the small intestine to cause diarrheal diseases in a wide range of mammals including humans[153]. A healthy individual can easily overcome this infection but it can be deadly for weaker patients with a compromised immune system.

Screening inhibitors of *C. parvum* has been complicated by the small window offered in mammalian cell culture and the prohibitive cost of animal testing necessitating the use of neonates or immunocompromised animals. Enzymological screening was also hampered by the restricted numbers of parasites obtainable for purification and the undeveloped molecular biology approach. The use of yeast has been critical to engage inhibitor discovery by circumventing the obstacles of existing techniques.[153]

Deletion of the yeast DHFR causes growth arrest from depletion of intracellular folate pools[153]. This can be complemented by the *C. parvum* DHFR but also human and other parasite's DHFR. The ability to measure both parasite and human DHFR inhibition in yeast permits the evaluation of inhibitor selectivity. Specificity is especially desirable for an inhibitor used to treat a human infection where a potent parasite DHFR inhibitor would not affect the host's folate biosynthesis.

Insensitivity to the inhibitor in yeast has been observed with high intracellular concentrations of DHFR: the use of high-copy plasmid can necessitate the use of 100-fold more inhibitor to get sensitivity[151]. To obtain a response to the DHFR inhibitors, the enzyme had to be placed on a low-copy plasmid, under an attenuated promoter and the cells further treated with sulphonamide which is known to synergize clinical DHFR inhibitors[153].

Modulating target expression is crucial to obtain a system that functions efficiently in inhibition assays. A delicate balance must be obtained between expression that is high enough to observe a robust phenotype but low enough that inhibition of the target has a directly proportional effect on the phenotype[151].

Yeast provides a multitude of strategies to achieve this careful modulation[151]. The target may be expressed from plasmid with a 2μ origin of replication resulting in 30 to 100 copies per cell or limited to only one copy per cell from a centromere based plasmid or integrated in the genome. The promoter used to drive expression can be selected from a series of well defined sequences, inducible or constitutive, and of varying strength. Alternatively, as has been done for the DHFR inhibitor screen, the promoter itself can be randomly mutagenised to obtain the required strength[153].

1.3.1.3. Inhibitor Screening in Yeast

The advantage of cell-based inhibitor screening is mostly due to the relevant biological context in which the compounds are evaluated. Although mammalian cells are closest to clinical relevance, they lack the ease and cost-effectiveness of propagation and the simplicity of genetic manipulation of yeast. The use of cells also provides a permeability barrier that needs to be overcome by the inhibitor thereby providing some insight about bioavailability.[151,154]

Compound permeability or efflux affects median Effective Concentration (EC_{50}) values measured in the yeast. *C. parvum* DHFR inhibitors designed to mimic a charged folate species display a 200-fold higher EC_{50} value in yeast than on the purified enzyme; in comparison, lipophilic compounds essentially display the same inhibitory values in both systems[153]. The EC_{50} value in yeast combines intrinsic inhibition, expression level of the target and penetration of the compound in the cell such that it should not be directly compared with the intrinsic inhibition measured on the purified enzyme but is useful to compare different inhibitors against to same target[151,155].

In PDE4 inhibitor screening, survival requires only a small amount of PDE activity such that an IC_{50} change of only fourfold can lead to a 10 000-fold increase in survival[149]. However, even with such a sensitive system, drug concentrations significantly above IC_{50} values were required for efficient inhibition: rolipram displays an IC_{50} in the low micromolar range on purified wild-type PDE4 but was used at a concentration of 2mM to identify resistant mutations in yeast[150].

Certain genetic modifications of yeast strains can improve the penetration and accumulation of compounds. The yeast strain used in the PDE4 studies contained a *cam* mutation for cAMP permeability but seemed to also affect rolipram uptake because the use of a wild-type strain led to a 100-fold reduction in rolipram sensitivity[149]. Mutations that alter the function of ABC transporters have also been found to be useful to obtain the necessary intracellular accumulation[151,156].

1.3.1.4. Yeast Growth Arrest

Growth arrest is the most common phenotype obtained in yeast complementation assays. Growth can be measured on agar plates by monitoring the appearance of colonies or the thickening of a patch. These methods are useful when a large number of clones need to be assayed as in a library screen however the measure of turbidity in liquid culture is the only method that will generate a quantitative inhibitory value. Liquid cultures used for this purpose have been modified to make them higher throughput by performing them in 96-well plates rather than the traditional Erlenmeyer or test-tube culture vessel[151,155-157]. This reduced the handling required from having to remove an aliquot from the culture to measure its optical density in a spectrophotometer cuvette. Liquid cultures are also

considered to be more sensitive to growth changes which might be dismissed as insignificant in agar plate assays[156]. The absorbance of the culture is directly proportional to the biomass concentration as long as the optical density at 600nm stays below 1; over this value, it is not linear with most spectrophotometers and is completely out of range with higher biomasses[157].

The small volumes associated with the use of 96-plate wells and the long incubation periods make evaporation a concern. This has been circumvented by overlaying the well with mineral oil. The only drawback observed has been the lack of gaseous exchange with the environment which, when the oxygen dissolved in the media is used up, creates an anaerobic environment. This technique was used in a topoisomerase II complementation system and resulted in an inflection in the growth curve when the yeast switched respiration modes but did not affect overall growth, complementation or inhibitor response. The 96-well growth curves yielded results comparable to viable counts but with an improvement in accuracy resulting from the ease of increasing the number of replicates[155]. Viable counts were found to suffer from higher variance than the liquid cultures and to be more time consuming and labor intensive[155].

A genetic functional screen has identified growth interference to be a common effect of the overexpression of heterologous cDNA from libraries. The ability to affect growth differed between enzyme families: 50% of kinases were found to be able to reduce growth by 55% or more while only 9% of nuclear receptors were successful hits. This toxicity was found to be due to the biochemical activity of the target and not their overexpression because it could be reversed by inhibitors or mutations. This generalized behaviour in yeast provides a system to study unknown ORF identified from genomic

sequencing. In yeast, mutations that affect the activity of the novel enzyme can be used to map active sites and compound libraries can be screened for inhibitor leads to further define the function of the target in different systems. In addition, since inhibitors restore growth in this system, using it to screen compounds has the advantage of not being subjected to false positive toxic compounds.[156]

1.3.2. The Lethality of v-Src and the PTP1B Phenotype in Yeast

1.3.2.1. Src Lethality in Yeast

v-Src is a 60kDa tyrosine kinase that confers tumorigenicity to the Rous Sarcoma virus[158] and is lethal when expressed in the yeast *S. cerevisiae*[159-166]. Starting from the N-terminus, the enzyme contains a myristylation site which is required for membrane attachment[167,168], an SH3 and an SH2 domain which bind to proline-rich sequences and phosphotyrosines respectively and the kinase domain at the C-terminal end[158]. The enzyme is auto-phosphorylated on tyrosine 416 in the active site by intermolecular interactions[158].

The lethality of v-Src in yeast is completely dependent on kinase activity but binding to phospho-tyrosine residues and myristylation are required to obtain a complete effect[164,166]. Mutations that abolish binding to phospho-tyrosine residues, such as in the conserved arginine in the consensus FLVR[175]ES motif of the SH2 domain[169], abolishes the lethality of v-Src[166]. On the other hand, removal of the entire SH3 domain does not rescue yeast growth[166]. Interestingly, the same SH2 and myristylation mutations that decrease the lethality of v-Src in yeast are also found to reduce its ability to transform mammalian cells[161,166,169,170].

The SH2 domain has been proposed to participate in growth arrest by protecting phosphotyrosine residues from de-phosphorylation, by recruiting substrates for phosphorylation at a second site and/or by directing v-Src to a specific location in the cell[166]. Interestingly, although residues 1-14 are required for myristylation, association with the membrane also requires the presence of residues 169-264 which span most of the SH2 domain (residues 147-245)[170].

The proto-oncogene c-Src is the cellular homologue of v-Src, differing only by a few point mutations and a C-terminal substitution[158]. These modifications of the c-Src enzyme make it less active than the v-Src kinase[158] leading to a decrease in its transformation potential in mammalian cells but also a decreased lethality in *S. cerevisiae*[160,171].

As opposed to v-Src, c-Src is strongly regulated by phosphorylation. The C-terminal substitution in c-Src includes a regulatory tyrosine residue at position 527 that inactivates the kinase when phosphorylated by Carboxy-terminal Src Kinase (CSK)[172]. This phosphorylated residue is bound intramolecularly by the SH2 domain and the interaction is further stabilised by the SH3 domain[172].

The reduced lethality of c-Src in *S. cerevisiae* requires treatment of the yeast with 1mM orthovanadate to obtain a robust lethal phenotype (this level of orthovanadate did not affect the growth of wild-type yeast)[171]. In this system, the extent of growth inhibition is proportional to gene dosage. However, even the highest dosage obtained by using a high copy vector yields a lower response than v-Src on a low copy vector. In contrast, c-Src is lethal in *S. pombe* and this lethality can be rescued by co-expression of CSK provided the SH2 and SH3 domains are intact[173].

1.3.2.2. Phenotype of v-Src Expression

Yeast expressing v-Src were seen to display a massive increase in their total tyrosine phosphorylation levels: from 0.01-0.02% in wild-type yeast up 4% of the total protein content[159,162]. This broad specificity increase was correlated with the activity of the kinase but not with toxicity[164,166]. High phosphorylation levels were seen with non-lethal SH2 mutations[166] and very low levels have been detected with the lethal SRX5 mutant (Tyr 416 replaced by Ser-Arg-Asp)[164]. This indicated that only a small subset of phosphorylated proteins mediated the growth arrest[164]. Although SRX5 showed very low levels of phosphorylation, it specifically phosphorylated three proteins (210, 185 and 150kDa) which could interact with an SH2-SH3 construct and were subsequently found to be exclusively associated with lethal mutations of v-Src and absent from the lysates of non-lethal mutations[166].

The broad phosphorylation phenotype has been exploited in yeast-two-hybrid screens where the prey required its bait to be phosphorylated. In that system, c-Src was used preferentially over v-Src and was modified to remove myristylation and regulation by tyrosines 416 and 527[174,175]. Only one group has used v-Src in *S. cerevisiae* for a yeast-two-hybrid screen reporting increased phosphorylation levels but stable cell growth[176]. This data-less observation is the only non-lethal report in the literature and may stem from their use of the weaker Met25 promoter instead of the GAL10 or GAL1 promoter used in all other studies[159-166].

v-Src expression induced a mitotic stop during the G_1, S or G_2 phases of the yeast cell cycle to produce a phenotype whose lack of uniformity was not due to varying v-Src expression levels[162-164]. The cells were abnormally large unbudded or budded[163] with a

nucleus located at the bud, anucleated or multinucleated[164]. They displayed multiple spindles which were detached from their nuclear anchor and disoriented in relation to the daughter cell[164]. This microtubule disruption was mirrored by the increased sensitivity of v-Src-expressing yeast to Benomyl which inhibits tubulin dimerization[164].

These aberrant morphologies were correlated with toxicity: mutations that inactivated the kinase activity of v-Src, like K295M, did not induce these changes[162] and strains which were slower to die were equally delayed in the appearance of large budded cells[163]. However, gross increase in tyrosine phosphorylation was not responsible for these changes since the lethal SRX5 mutant was able to induce this phenotype[164].

The biochemical mechanism of v-Src lethality is not known but wild-type v-Src has been observed to increase the activity of CDC28[163,164,166]. CDC28 is a 34kDa cyclin-dependent kinase involved in the G_1/S and G_2/M transition of the cell cycle[163]. Although it is negatively regulated by phosphorylation of tyrosine 19, mutation of this residue to a phenylalanine did not rescue the yeast and the mutant was still activated by v-Src[164]. The increased activity of CDC28 was delayed in yeast strains which were slower to die from v-Src expression[163], and seemed to be correlated with toxicity and not overall phosphorylation levels: the lethal SRX5 mutation could activate the kinase but the non-lethal myristylation and SH2-domain mutations could not[164,166]. However, some v-Src constructs which showed decreased toxicity were still able to activate CDC28 suggesting that the elevation of CDC28 activity may be necessary for v-Src toxicity but is not sufficient[164,166].

1.3.2.3. Modulation of v-Src Lethality

The first report of the lethality of v-Src in *S. cerevisiae* was accompanied by the observation of spontaneous recovery suggesting that the cells either became desensitised or acquired suppressor mutations[159]. The rapidity with which the resistant cells were able to take over suggested that a large number of loci could confer resistance or that the expression of the kinase was leaky allowing the resistant mutations to accumulate over time[159].

Two separate mutations in the chaperone *Ydj1* gene were identified in spontaneous resistant colonies[165]. One mutation was able to abolish the lethality of v-Src by repressing its translation leading to lower amounts of v-Src proteins and the second mutation prevented the release of v-Src from chaperone proteins thereby decreasing its catalytic activity[165]. A point mutation in Ydj1 (C315D) has also been identified to reduce the accumulation and activity of v-Src in yeast and to permit growth[177].

Hsp90 has been identified as a chaperone protein that stabilizes v-Src during its synthesis and keeps it in an inactive unphosphorylated form in the cytosol. At the plasma membrane, v-Src releases from Hsp90 to become fully active[162]. Disruption of the yeast Hsp90 gene resulted in a decrease of the v-Src activity and protein levels, a decrease in the total phosphorylation levels and a concomitant rescue of yeast growth[162,177]. The Ydj chaperone is known to participate in the function of Hsp90[177].

Tyrosine phosphatases have been found to modulate the biological effects of v-Src. Co-expression of PTP1B can decrease the transformation phenotype of v-Src in mammalian cells without altering the phosphorylation pattern of v-Src itself[178] and was shown to de-phosphorylate the Focal Adhesion Kinase (FAK) thereby breaking its

interaction with v-Src[179]. In yeast, PTP1B expression rescued the growth inhibition of v-Src and reduced the tyrosine phosphorylation levels of yeast proteins[164]. The lethality of SRX5 was also rescued by PTP1B supporting the view that this mutation arrested growth by phosphorylating its few proteins targets[164]: the three phospho-proteins associated with lethality were also de-phosphorylated by the phosphatase[166].

PTP1B by itself did not affect the growth of wild-type yeast nor did it affect the levels of the v-Src protein[166]. Its rescue effect required the continuous presence of the phosphatase and was not absolutely complete in the same way that the phosphotyrosine levels did not completely return to baseline[164].

The role of endogenous yeast tyrosine phosphatases on v-Src toxicity was subtle and required mild conditions to reveal them. Deletion of the yeast PTP1 conferred toxicity to the non-lethal SH2-domain mutations of v-Src and to the c-Src mutation Y527F[166]. This effect was however specific to PTP1 because deletion of PTP2 did not render these mutations lethal[166].

Phosphatases have also been identified from a library screen to confer resistance to c-Src lethality in *S. pombe*. TCPTP and PTPBas were identified to de-phosphorylate cellular substrates while PTP-PEST, which was a more potent antagonizer, directly reduced the phosphorylation of c-Src. Of the 39 resistant clones identified in the screen, 23 showed reduced or absent c-Src levels and 11 coded for CSK which had already been identified to inactivate c-Src and so reduce its lethality. The last five clones contained two incidences of PTP-PEST, two of TCPTP and one of PTPBas. The bias of the library for these specific phosphatases may however not be correlated to their substrate specificity but to their abundance in the library.[180]

1.4. Research Overview and Outline of the Thesis

PTP1B is an interesting target in the treatment of T2DM. A drug inhibiting this phosphatase would improve insulin sensitivity in patients and at the same time protect against diet-induced obesity which leads to and accompanies T2DM.

Affinity and selectivity for PTP1B has been acquired by maximizing interactions between the inhibitor and residues in the active site. These have been identified through X-ray crystallography and site-directed mutagenesis but these techniques are very time consuming and sometimes narrowed by a biased selection of residues in the active site.

Yeast have been used to identify inhibitor determinants of PDE4. A screen that selects for mutations that do not affect activity yet confer inhibitor resistance to the enzyme has been obtained from yeast dependent of the activity of PDE4, transformed with a mutated PDE4 library, treated with an inhibitor and assayed for growth.

A similar system was established using the growth phenotype of PTP1B in v-Src expressing yeast to identify PTP1B inhibitor determinants. By screening all the amino acids comprising the PTP1B protein, this screen would provide a more comprehensive coverage of the sequence than traditional techniques and might identify novel determinants.

A library of PTP1B mutants was generated using degenerate PCR conditions and co-expressed with v-Src in yeast. Mutants that grew were identified as still catalytically active and were treated with a specific PTP1B inhibitor. Ability to grow in the presence of the inhibitor identified resistant mutations.

Optimization of this yeast system as a determinant screen also functioned in establishing a PTP1B inhibitor screen. The use of yeast proved insightful in that it did not select compounds based on their potency, as was expected, but first required them to satisfy basic physical properties for oral bioavailabilty.

The PDE4 screen identified resistant mutations within a region associated with substrate recognition. The location of these mutations did not affect binding of small substrates but prevented interactions with larger inhibitors. Established PTP1B substrate binding determinants are focused on the five active site loops. Known PTP1B inhibitors, which mimic the substrate, localize to the active site and generally used these same interactions. Incorporating a need for conserved catalytic activity in the screen should discriminate between determinants common to both the substrate and the inhibitor and unique determinants.

As opposed to the expected findings similar to those for the PDE4 screens, the determinants identified for PTP1B completely avoided the five active site loops and concentrated on a region distal from the active site. Mutations in this region conferred cross resistance to inhibitors other than the one used for the screen. This was reminiscent of HIV protease mutations which, by not localising to the active site, potentiated the resistance of active site mutations and conferred broad spectrum inhibitor resistance to the enzyme[181,182].

The first chapter: "PTP1B Rescues yeast from v-Src Lethality" explores the phenotype of the PTP1B rescue and the conditions necessary to obtain a robust window by modifying the amounts of v-Src and PTP1B expressed. Reduction of this rescue by an inhibitor is also shown in this chapter along with the effect of using yeast strains

containing cell wall mutations for increased permeability. This chapter ends with the creation and characterization of a yeast strain in which v-Src is integrated in the genome.

This strain is used in the second chapter: "Screening for PTP1B Inhibitor Determinants Using an Integrated v-Src Yeast Strain" for screens I, II and III using libraries generated using different strategies and transformed in the yeast using either electroporation or the lithium acetate protocol. This chapter also describes some of the kinetic properties of the S295F resistant mutant identified in screen I and of selected point mutants identified from screen III.

The weakness of the third screen resided in the high proportion of false positives obtained. The last chapter: "Screening for PTP1B Inhibitor Determinants Using a Wild-Type Yeast Strain and a Potent Inhibitor" addresses this problem by using v-Src on a plasmid and not integrated in the genome and using an inhibitor with increased potency. Testing for this inhibitor also leads to the identification of the necessary physical characteristics required for compounds to have an effect on yeast rescue. Two screens are preformed with this inhibitor. The last screen reveals adequate coverage of the PTP1B protein sequence with a low incidence of false positives.

1.5. Publications and Contribution of Colleagues

All inhibitors, except those commercially available, were synthesized by Merck Frosst chemists. The IC_{50} values shown in Table 4.1 were generated by Merck Frosst PTP1B screening facilities. Figure 2.7 and 2.8 (selected data), Figure 2.12, Figure 4.2 and 4.3 (selected data and modified presentation) and Figure 4.4 were published in *Biochemical Pharmacology* (2004) **68**, 1807-1814: "Using yeast to screen for inhibitors of protein tyrosine phosphatase 1B" by J. Montalibet and B. Kennedy. I wrote this paper to describe the yeast system developed here as a screen for PTP1B inhibitors.

Kinetic assays were published in *Methods* (2005) **35**, 2-8: "Protein tyrosine phosphatase: enzymatic assays" by J. Montalibet, K. Skorey and B. Kennedy. I wrote the paper using knowledge gathered in part from biochemists at Merck Frosst including Dr. E. Asante-Appiah, Dr. Z. Huang and K. Skorey. K. Skorey developed the Difluoromethylumbelliferyl Phosphate (DiFMUP) assay, generated the data for Table 1 (of the publication) and the data for the peptide substrate in Table 2 (of the publication).

The analysis of the PTP1B promoter (Appendix 3) was initiated by Yves Boie who generated the expression vectors containing the promoter deletions construct from 8kb to 2kb. Rosiglitazone was synthesized by Merck Frosst Chemists. Figure A.1 and A.2 (selected data) were published in *Gene* **260**, 145-153: "Genomic characterization of the human and mouse protein tyrosine phosphatase-1B genes." by P. Forsell, Y. Boie, J. Montalibet, S. Collins and B. Kennedy.

2. PTP1B Rescues Yeast from v-Src Lethality.

2.1. Introduction

Our goal was to establish a system in yeast where a library of PTP1B mutants could be screened for their sensitivity to a specific inhibitor. A clear phenotype for PTP1B activity in yeast has been reported where PTP1B rescues the yeast from v-Src lethality thereby promoting growth. The measure of PTP1B activity in yeast required a sensitive growth assay and in our case this assay should be compatible with screening of a large number of clones.

The relative expression of the two exogenous proteins needed to be regulated to obtain the largest rescue window; the larger the window, the easier it would be to observe the effect of the PTP1B inhibitor in reducing it. The GAL promoter system and plasmids or genomic location were used to modulate the expression of both v-Src and PTP1B.

Although the PTP1B phenotype in yeast needed only to be confirmed from the literature and maximized, the effect of the inhibitor on this rescue had not been measured before. This required testing a few inhibitors to find the right amount needed to obtain a strong growth reduction. Again, the largest inhibitor effect obtainable would facilitate the identification of resistant mutants: the use of designer yeast strains was explored to maximise this window.

2.1.1. Growth Assays

Expression of v-Src abolishes growth of yeast through mitotic dysfunctions. The activity of PTP1B can be measured in yeast by its ability to revert the v-Src lethality thus allowing growth. Measurement of yeast growth can be done in many ways. A drop-test involves plating a liquid suspension of yeast on agar and counting the resulting number of colonies. This number is equal to the number of viable yeast cells in the liquid suspension. A streak test involves picking a colony from an agar plate and painting it on a second plate. Growth can be seen by a thickening and enlargement of the painted material. Growth of yeast in liquid media leads to an increase in turbidity which can be followed by the increase in absorbance at 600nm. The typical curve that results from plotting the absorbance at different time points has an initial lag phase, an exponential phase where the yeast divides most actively and a plateau where the yeast stops dividing. During the exponential phase, due to rapid division rate, the cell wall is weak and the yeast is at its most permeable.

2.1.2. Yeast Strains

The cell wall of *S. cerevisiae* is composed mostly of polysaccharides (chitin and glucans) and glycoproteins (mannoproteins)[183]. It is involved in morphogenesis and in protection by preventing entry of large molecules and by resisting turgor pressure[183]. However, a sieve-like vision of the cell wall would be flawed from the lack of correlation between size of molecules and permeability in yeast[184]. Nonetheless, mutations that remove components of the cell do increase its permeability.

For example, Mnn9p is a glycosyltranferase involved in the elongation of the mannose polymer[185,186]. Yeast carrying a mutation in this gene show an osmotic fragility, requiring addition of 10% sorbitol in the liquid culture media[187], but most interestingly show an increased cell wall porosity[184,187,188]. The *ERG6* gene encodes for Δ^{24}-sterol-C-methyltransferase which methylates zymosterol at C-24 in the biosynthetic pathway of ergosterol. Ergosterol, similar to cholesterol, functions in membrane fluidity. Deletion of this gene in yeast results in impaired ergosterol biosynthesis and increased passive diffusion of drugs across the membrane[189-196].

The use of yeast to identify inhibitor determinants requires the compound to cross the cell wall and plasma membrane to enter the intracellular space. Inhibition of PTP1B may not be feasible if the inhibitor is not able to accumulate in the yeast cell. The use of mutated yeast strains that facilitate this process could increase loading of the PTP1B inhibitor in the cell.

2.1.3 GAL Promoter

The GAL1 promoter contains three Upstream Activation Sequences (UAS) to which Gal4p is bound. In the absence of galactose, Gal80 binds to Gal4p and represses its transcriptional activity. When galactose is provided, Galp4 is released from repression and transcription proceeds. Glucose is a strong repressor of the GAL1 promoter lowering expression by 1000-fold. Glucose represses transcription of the GAL2 gene which codes for the galactose transporter, the GAL3 genes which produce the inducer that will release Gal4p from Gal80 repression and the GAL4 gene to directly reduce the level of the Gal4p protein. In addition, independently from the Gal4p pathway, glucose directly represses

transcription from the GAL1 promoter through an upstream repressor site and assorted DNA-binding proteins.[197]

The strength of expression from the GAL1 promoter can be modulated by deletion of UAS. GALL and GALS are mutations of the promoter that lack either one or one and a half UAS, thereby resulting in a lower amount of expression[198].

This promoter system can be used to express an exogenous protein in yeast. Expression driven from this promoter is strongly induced by addition of galactose to the growth media yet can be completely suppressed by the presence of glucose. In addition, the mutated promoters can be used to fine-tune the amount of protein expression desired.

2.1.4. Genomic Integration

The DNA encoding for v-Src and PTP1B in the yeast can be sustained on a plasmid or integrated in the yeast genome. The most efficient technique for integrating foreign DNA in the yeast genome is by homologous recombination.

Recombination between DNA sequences is mostly driven by their homology but introduction of double stranded breaks in their homologous region can stimulate recombination up to 3000-fold. This increase is significant enough that DNA containing multiple sites of homology with the genome will be entirely targeted to recombine with the homologous segment which contains the double-strand breaks. [199-201] The minimum length of homologous sequence required for recombination is about 50 base pairs with longer sequences increasing the efficiency of recombination[202-204].

DNA can be integrated in the yeast genome or a plasmid by cloning the foreign DNA in the middle of segments which are homologous to the region where integration is

desired. In effect, for genomic integration, digestion of any plasmid by a restriction enzyme that cleaves the plasmid in the middle of its selectable gene marker and transforming the resulting linear DNA in yeast will result in integration of the plasmid, and its foreign DNA, in the genomic locus for the auxotrophic gene[200].

However, this method generates homologous repeats on either end of the integration. These can recombine with each other and expel the DNA in between them. A more stable recombination product can be obtained by γ transformation[205] which does not generate these repeats: the homologous sequences that target the integration are cloned in the plasmid in reverse tandem order (putting the fragment coding for the "right" side of the target integration locus 5' to the "left" side fragment).

Selection of positive recombinants can be made by either selecting for a gain in auxotrophy, where integration at the target locus disrupts a marker gene or a gain of prototrophy, where the integrating plasmid carries an intact marker gene. For example, if the plasmid used is cleaved in the middle of *TRP1*, which confers growth in the absence of exogenous tryptophan, targeted integration in the genome will make the yeast auxotrophic for tryptophan. In this case, the resulting clones must be replica plated on tryptophan drop out to verify their lack of growth. This process is time consuming but can be avoided if the genetic disruption has a viable easily scoreable phenotype like color such as for disruption of *MET15* and *ADE2* marker genes[206-208]. *Ade2* yeast accumulate p-ribosylaminoimidazole in the biosynthetic pathway towards adenine, this intermediate becomes red upon oxidation and give the yeast a pink colour.

2.1.5. Inhibitors

The phenotype of the PTP1B knockout in mouse generated great interest to develop PTP1B inhibitors resulting in a great variety of inhibitors with different structures, affinity and selectivity. Vanadate was the first tyrosine phosphatase inhibitor identified. It is a general tyrosine phosphatase inhibitor with no specificity for the different members of this family but that can be used to differentiate them from serine/threonine phosphatases[209]. Vanadate is a small molecule which inactivates the enzyme by mimicking the transition state of the reaction and thus blocking the active site[210-213].

One of the most potent and specific PTP1B inhibitors identify to date is N-benzoyl-L-glutamyl- [4-phosphono(difluoromethyl)]-L-phenylalanyl- [4-phosphono(difluoromethyl)]-L-phenylalanineamide, or BzN-EJJ-amide[214]: It is a short peptide-like molecule which inhibits PTP1B with low nanomolar affinity[214,215]. The crystal structure of the inhibited complex has been resolved and the binding determinants defined[136]. Since these determinants are already known, using this molecule in the yeast system developed here would be a useful tool to validate the screen.

2.2. Methods

See Appendix 1 for inhibitor structures and Appendix 2 for primer sequences.

2.2.1. Yeast Strains

BwG1-7a: MATa *leu2-3 leu2-112 his4-519 ade1-100 ura3-52* (Courtesy Dr. R. Storms)

mnn9 (LB 3003-4B): MATα *mnn9 ura3 leu2 his4* (American Type Culture Collection (ATCC) 96872)

erg6 for curves (568): *leu2 his3 ura3 erg6* (Courtesy Dr. M. El Sherbeini)

erg6 for integration (R2563): MATα *his4-15 lys9 ura3-52 erg6Δ* (Courtesy Dr. R. Gaber)

YPH 499: MATa *ura3-52 lys2-801^{amber} ade2-101^{ocher} trp1Δ63 his3Δ200 leu2Δ1* (Stratagene)

2.2.2. Media Formulation

Most media were formulated from Clontech's pre-prepared powders: YPD medium (8600-1), YPD agar medium (8601-1), minimal SD base (8602-1), minimal SD agar base (8603-1), minimal SD base/Gal/Raf (8611-1), minimal SD agar base/Gal/Raf (8612-1). Since these media contain glucose or galactose/raffinose, drop out media containing only raffinose as the carbon source were made with: 2% raffinose (Sigma R-7630), 0.67% yeast nitrogen base without amino acids (Sigma Y-0626), appropriate drop out supplement: leucine dropout (8605-1), uracil dropout (8607-1), leucine and uracil double

dropout (using His/Leu/Ura triple dropout (8614-1) with 20mg/L histidine), tryptophan dropout (8604-1), and the pH was adjusted to 5.8. Media for growth curves was prepared from raffinose dropout media to which is added 2-4% galactose (Fluka 48260) or glucose (Anachemia AC-2857).

2.2.3. Plasmid Construction

*Eco*R I and *Sal* I were used to cut out the catalytic domain (amino acids 1-320) of human PTP1B previously cloned in a pFLAG vector[216]. The resulting fragment was gel purified and ligated to p416GAL1 (ATCC 87332) or p426GAL1 (ATCC 87333) previously digested with *Eco*R I and *Sal* I and de-phosphorylated. The plasmids p416GAL1-PTP1B and p426GAL1-PTP1B were sequenced to confirm the correct construction. PTP1B mutants C215S (amino acids 1-320) and D181A (amino acids 1-298) were cloned into p416GAL1 in a similar manner. The plasmid p416GAL1 is a low-copy vector containing the *URA3* marker for growth in uracil-deficient media, p426GAL1 is the corresponding high-copy plasmid. Sequencing primers were: ptp6, ptp7, ptp8, ptp9, ptp10, ptpin1 and ptpin2.

v-Src was amplified by PCR using the pEcoRIB clone obtained from ATCC (41005) as a template and the srcfwd and srcrvrs primers. The amplified DNA was inserted into pCR2.1-TOPO (Invitrogen) to give the TA-v-Src plasmid. The fragment obtained by restriction digestion of TA-v-Src with *Xba* I and *Sal* I was gel purified (Qiagen) and ligated to p415GAL1 (ATCC 87326), p415GALL (ATCC 87338) or p415GALS (ATCC 87346)[198] previously digested with *Xba* I and *Sal* I and de-phosphorylated. The resulting constructs were sequenced. All three plasmids are low-

copy vectors containing the *LEU2* marker for growth in leucine-deficient media. The primers used for sequencing were: v1, v2, v3, v4, v5, v6, v7 and v8.

2.2.4. Sequencing

Sequencing was performed on a 373 DNA sequencer (Applied Biosystems) or on a 3100 Genetic Analyzer ABI Prism (Applied Biosystems) using the manufacturer reagents and protocols.

2.2.5. Transformations

Yeast were transformed either by electroporation or using the lithium acetate method[217]. For electroporation, a saturated 50mL overnight culture was pelleted at 3000 RPM for five minutes at 4°C. Resuspended in 40mL water (4°C), spun down at 2500 RPM for five minutes, resuspended in 20mL cold water, spun down at 2500 RPM for five minutes, resuspended in 5mL cold 10% sorbitol, pelleted at 2000 RPM for five minutes and finally resuspended in 150μL 10% sorbitol. 40μL of this paste along with the DNA to be transfected was transferred to a 0.2cm gap electroporation cuvette. The suspension was tapped to settle at the bottom of the cuvette and make good contact between the two electrodes and pulsed with 2kV, 25μF, 200Ω (Gene Pulser™, BioRad). One milliliter of 10% cold sorbitol was added to the cuvette and transferred to an eppendorf. The quantity of DNA used and the amount of transfected suspension plated on appropriate dropout plates depends on the yeast strain used. For example, 100μL of the transfection of YPH 499 with 0.1μg of pGALL-v-Src yields a good density of transformed colonies on a 7mm petri dish, double transformations were routinely done with 2μg of each plasmid and

plating 500μL of the resulting suspension. During the whole electroporation procedure, the yeast is maintained at 4°C in a refrigerated centrifuge or on ice, as well as the electroporation cuvette, eppendorf and all solutions used. This protocol has been modified from the protocol previously described by Z. Nelson[218].

2.2.6. Protein Extraction and Western Blotting

For Figure 2.3, yeast cultures were pelleted, washed once with 0.5mL water, resuspended in loading buffer (50mM tris pH 6.8, 2% β-mercaptoethanol, 2% SDS, 0.1% bromophenol blue, 10% glycerol) and sonicated four times on ice. Amounts of protein were estimated from the OD 600nm of the overnight culture. This absorbance is proportional to the number of yeast cell in the culture, itself proportional to protein content. The samples were run on three parallel 10-20% tris-glycine gels. One of the gels was stained with Coomassie to control for the amounts of protein loaded and two other gels were transferred to a polyvinylidene fluoride (PVDF) membrane. For detection of PTP1B, the membrane was blocked with 5% milk in TTBS (0.1% Tween 20, 10mM tris pH 7.5, 0.1mM NaCl), probed with an in-house polyclonal antibody (P3) against PTP1B raised in rabbit, washed in TBS (10mM tris pH 7.5, 0.1mM NaCl), probed with a secondary anti-rabbit peroxidase-linked antibody (Amersham Biosciences) and detected by chemiluminescence (NEN Life Sciences). For detection of tyrosine phosphorylated proteins, the membrane was blocked with 5% BSA in TTBS, probed with an anti-phosphotyrosine HRP-conjugated antibody (4G10 from Upstate) in TTBS containing 1% BSA, washed and detected by chemiluminescence. The blots were visualized using a CCD camera (Fujifilm) or BioMAX imaging film (Kodak).

For Figure 2.7B and 2.17, yeast proteins were extracted using Y-PER Yeast Protein Extraction Reagent (Pierce) and the protein content was quantified using Coomassie Plus Reagent (Pierce). The extract was run (15μg per lane) on a 4-12% NuPage® BisTris gel (Invitrogen) in in 3-(N-morpholino) propanesulfonic acid (MOPS) buffer and transferred to a PVDF membrane. The blot was probed with anti-phosphotyrosine antibodies as described.

For Figure 2.9 and 2.12 total yeast protein was extracted using the glass bead method[219] and run on two tris-glycine 10-20% SDS-PAGE. One of the gels was stained with Coomassie to estimate the amounts of protein loaded and the other gel was transfer to a PVDF membrane and probed with anti-phosphotyrosine antibodies as described.

The P3 PTP1B in-house polyclonal antibody was purified by affinity chromatography from the serum of a rabbit immunized with the peptide H-NRNRYRDVSPFDHSR-OH, which corresponds to the N-terminus of human PTP1B (Courtesy P. Payette).

2.2.7. 96-well Growth Curves

Yeast were transformed with the various plasmids and the colonies that formed three days later were transferred to dropout media containing raffinose as the sole carbon source and grown overnight. The 96-well plates (Nunclon™ Surface TC microwell 96 with lid) containing dropout media with 4% galactose (with or without inhibitor) were inoculated with the overnight yeast cultures at a final concentration of 10^6 cells per ml[155] and a final volume of 200μL. The wells were overlaid with mineral oil, incubated at 30°C and read periodically at 600nm for four days. The number of cells used was calculated

from the correlation between OD 600nm of a culture and its cell number. This correlation was obtained from an average of multiple hemacytometer countings and the corresponding absorbance at 600nm: 1 OD 600nm $\approx$ 1.5 x 10^7 cells/ml.

While determining the conditions to obtain the greatest growth in the presence of v-Src it was observed that the age of the transformed yeast influenced the degree of rescue by PTP1B. For example, yeast co-transformed with PTP1B and v-Src were unable to grow on galactose when scraped from a stock of the transformed yeast stored as a streak at 4°C whereas yeast co-transformed with the corresponding empty vectors, p415GAL1 and p416GAL1, were still able to grow on dropout media. If the transformed cells were kept as a glycerol stock at -80°C, only yeast cultures starting from a large amount of the glycerol stock (high cell number) and cultured for very short amounts of time (less than two days) before being assayed could show PTP1B-mediated rescue. It was found that the best rescue was obtained from an overnight yeast culture inoculated with freshly transformed material (three or four day-old colonies).

2.2.8. v-Src Integration

To integrate in the *TRP1* locus, the fragment of p415GAL1-v-Src containing the GAL1 promoter, v-Src and the CYC terminator was retrieved from the plasmid using *Sac* I and *Eag* I and cloned into pRS404 (Stratagene). pRS404 is a yeast integrating plasmid containing the *TRP1* selectable marker. The resulting construct was digested with *Mfe* I which cuts the *TRP1* gene to generate 141 and 538 base pairs tails of homologous sequence to the *TRP1* locus and transformed in *mnn9*. The resulting colonies were replica plated on tryptophan drop out agar to test for tryptophan auxotrophy.

This method did not generate any integrated clones and was very time consuming, as the clones needed to be picked and streaked on tryptophan dropout media to be identified.

To facilitate the identification of positive clones, the same fragment was integrated in the *ADE2* locus by subcloning it from pRS404 into pRS402 (ATCC 87477). pRS402 is a yeast integrating plasmid containing the *ADE2* selection marker. The resulting construct was digested with *Hpa* I which cleaves the *ADE2* marker on the plasmid to generate two homologous tails of 600 and 1115 base pairs, transformed in *mnn9* yeast and plated on adenine drop out media. The resulting colonies were inspected for a pink color. This method also failed to generate integrated clones.

For gamma integration, the fragment containing the GAL1 promoter with the v-Src coding sequence and the CYC terminator was amplified by PCR from the p415GAL1-v-Src clone using the primers gammafwd and gammarvrs. The fragment obtained was subcloned into a pCR2.1 vector (Invitrogen), digested with *Eco*R I and subcloned into pRS303Leu2-γ to give the pRS303Leu2-v-Src. pRS303Leu2-γ (Courtesy Dr. P. Hieter) is a vector containing two fragments of the *LEU2* locus (650 and 500 base pairs) that drive a γ-type transplacement and a selection marker for histidine. This vector generates stabler integrated constructs that are less prone to reversion than using traditional vectors linearized in the gene targeted for insertion. The pRS303Leu2-vSrc clone was digested with *Not* I, gel cleaned, ethanol precipitated, de-phosphorylated and re-ethanol precipitated. The resulting fragment was electroporated in the yeast and plated on histidine-dropout plates. This failed to generate integrated clones for the *erg6* yeast but was successful for YPH499.

All construct were sequenced using the v1 through v8 oligos along with seq303 for the pRS303 construct.

2.2.9. Vanadate and Pervanadate

Vanadate was dissolved in 2.1 equivalents of 1N NaOH. The initial yellow solution was stirred until the color disappeared and then diluted with water to 100mM. To make 50mL of 100mM stock: 456mg of vanadium (V) oxide was added to 5.25mL of 1.0N NaOH (fresh or recently standardized) in a 50mL volumetric flask. The flask was capped and the solution was stirred with a small stir bar for one to three days until the yellow color became faint. The volume was adjusted to 50mL with distilled water. Pervanadate was prepared by reacting 5mM H_2O_2 (from a 100mM stock buffered in 20mM Hepes) with 1mM vanadate.

2.2.10. Colony PCR

The colony PCR[219] protocol is a PCR reaction in which the template DNA is obtained from the crude heat lysis of yeast cells during the denaturation step of the cycling program. 0.25μL of yeast was scraped from a yeast colony growing on agar using a pipet tip and mixed with 1.2μL 25mM $MgCl_2$, 1μL of each primers at a concentration of 10pM, 0.4μL of all four dNTPs at a concentration of 10mM, 0.2μL of Taq enzyme (5units/mL) in a final volume of 20μL. The program used was 94°C four min., 35 cycles of 94°C one min., 55°C one min. and 72°C 2.5 min. followed by ten min. at 72°C. The primers used were: S8, Y2, Y3 and Y4.

2.3 Results

2.3.1. Growth Assays

The readout for the biological activity of PTP1B in the yeast was growth. Different assays were used to measure growth: streaking, drop-test on agar plates and liquid cultures.

BwG1-7a yeast were transformed with either v-Src, PTP1B or co-transformed with v-Src and PTP1B. The resulting colonies formed after three days of growth using glucose as the carbon source were streaked on agar plates of the appropriate dropout media containing galactose as the carbon source: leucine dropout for the yeast transformed with v-Src or the empty vector control (p415GAL1), uracil dropout for PTP1B (empty control p416GAL1)-transformed yeast or leucine and uracil double dropout for co-transformants.

After two days of incubation at 30°C, yeast expressing v-Src did not grow whereas yeast expressing the empty plasmid were able to grow (Fig. 2.1A). In comparison, yeast co-expressing v-Src and PTP1B were able to grow (Fig. 2.1C). Expression of PTP1B alone did not affect the growth of the yeast as it grew just as well as its empty plasmid control (Fig. 2.1B).

In addition, to see if a potent and specific PTP1B inhibitor could abolish the rescue of PTP1B and thereby prevent growth of the yeast, 100μM of BzN-EJJ-amide was included in the leucine and uracil double dropout media. However, as seen in Figure 2.1D the inhibitor was not able to abolish the rescue mediated by PTP1B and thereby prevent growth.

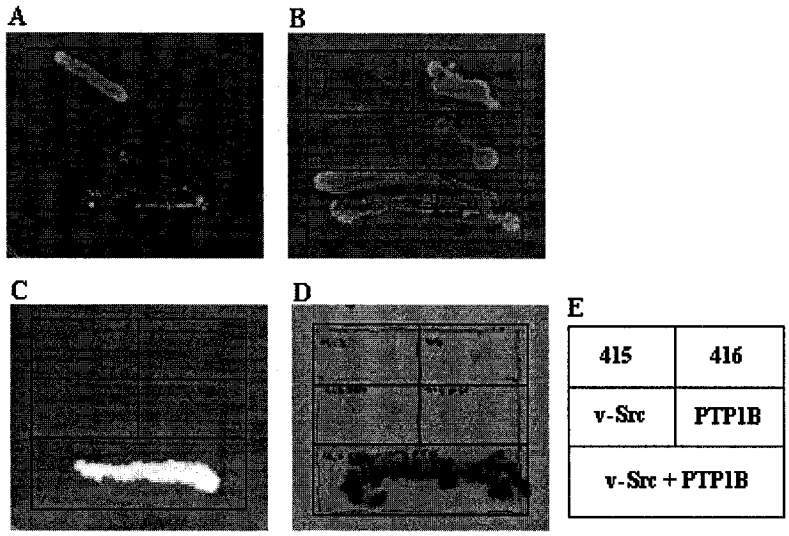

Figure 2.1: Expression of v-Src prevents growth of yeast streaked on agar, but co-expression of PTP1B rescues the yeast BwG1-7a. A) Leucine dropout selects for p415 vectors. B) Uracil dropout selects for p416 vectors. C) Uracil and leucine double dropout selects for both p415 and p416. D) Uracil and leucine dropout with 100μM BzN-EJJ-amide. E) Road map for plasmid transformed in the yeast: p415GAL1 (415), p416GAL1 (416), p415GAL1-v-Src (v-Src), p416GAL1-PTP1B (PTP1B), or co-transformed with p415GAL1-v-Src and p416GAL1-PTP1B (v-Src + PTP1P). The picture in D was taken as phase contrast and the yeast appears black instead of white.

Alternatively for drop-tests, the same yeast used for the streak assay were inoculated in liquid culture of the appropriate dropout medium, grown overnight and a known dilution was plated on solid media with glucose or galactose as the sole carbon source. After five days of growth on galactose, 141, 172 and 152 colonies were counted on the plates inoculated with yeast transformed with the empty vectors (p415GAL1 or p416Gal1) or with PTP1B respectively. Even after 15 days, yeast transformed with v-Src or co-transformed with v-Src and PTP1B had not grown. For comparison, all permutations grew on glucose with an average of 150 colonies.

For growth assays in liquid culture, the seven days-old colonies that grew on the glucose control of the drop-test were inoculated in the appropriate dropout media containing glucose for an overnight growth. The cultures were then diluted to a fixed concentration in 50mL of appropriate dropout media and grown at 30°C with constant shaking. Aliquots of the cultures were removed periodically and their absorbance read at 600nm. The results are plotted in Figure 2.2. Yeast transformed with v-Src did not grow as opposed to yeast transformed with the empty control vector p415GAL1. An increase in the growth of yeast expressing v-Src was observed with co-expression of PTP1B.

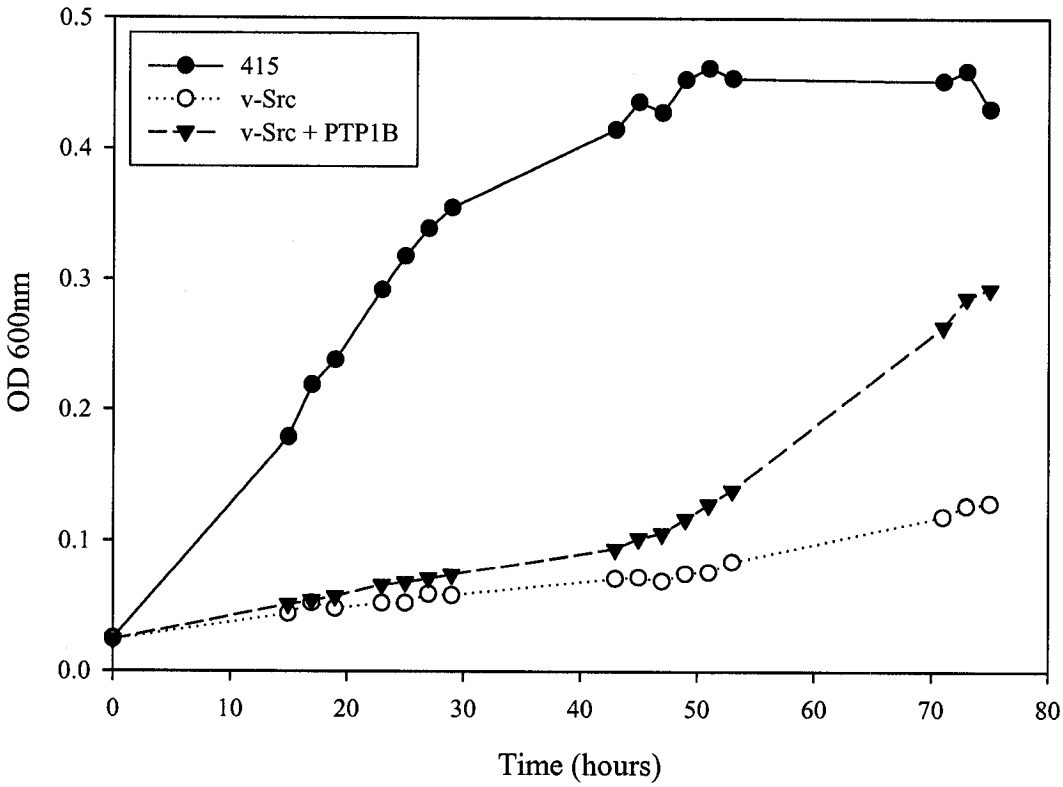

Figure 2.2: Expression of v-Src prevents the growth of yeast in liquid culture; this is reversed by co-expression of PTP1B. Growth curves of BwG1-7a yeast transformed with p415GAL1 (415), p415GAL1-v-Src (v-Src) or co-transformed with p415GAL1-v-Src and p416GAL1-PTP1B (PTP1B).

In parallel, some of the cells from the overnight culture used for the growth curve were induced in galactose for four or 24 hours. The proteins from these induced cultures were extracted and analyzed by western blotting (Fig. 2.3). Probing with an antibody against phosphorylated tyrosine residues revealed that yeast expressing v-Src have a massive increase in total protein tyrosine phosphorylation and co-expression of PTP1B reduced this increase in phosphorylation (Fig. 2.3A lanes "v-Src" compared to "v-Src + PTP1B"). The corresponding blot probed with an antibody against PTP1B (Fig. 2.3B) confirmed expression of the enzyme in the yeast. Figure 2.3C reveals by Coomassie stain that unequal amounts of protein were loaded on the gel although similar quantities were expected based on the culture's OD 600nm. This prevented identification of the phosphatase in certain lanes but did not affect the conclusions of the anti-phosphotyrosine blot. Although the lack of a good v-Src antibody prevented direct identification of the expressed enzyme, the results from the anti-phosphotyrosine blot indicated that a tyrosine kinase was over-expressed and active in the yeast transformed with v-Src.

Growth assays in liquid culture gave the most quantitative results. However, the format of this assay using 200mL Erlenmeyer flask was very cumbersome. A different method using 96-well plates was developed. Instead of a 50mL culture, the yeast grew in a 200μL volume and absorbance at 600nm could be continuously monitored without removal of a sample aliquot. Continuous growth curves measured using this method are shown in Figure 2.4 for varying starting concentration of yeast. Decreasing the number of cells added to the wells did not affect final saturating absorbance.

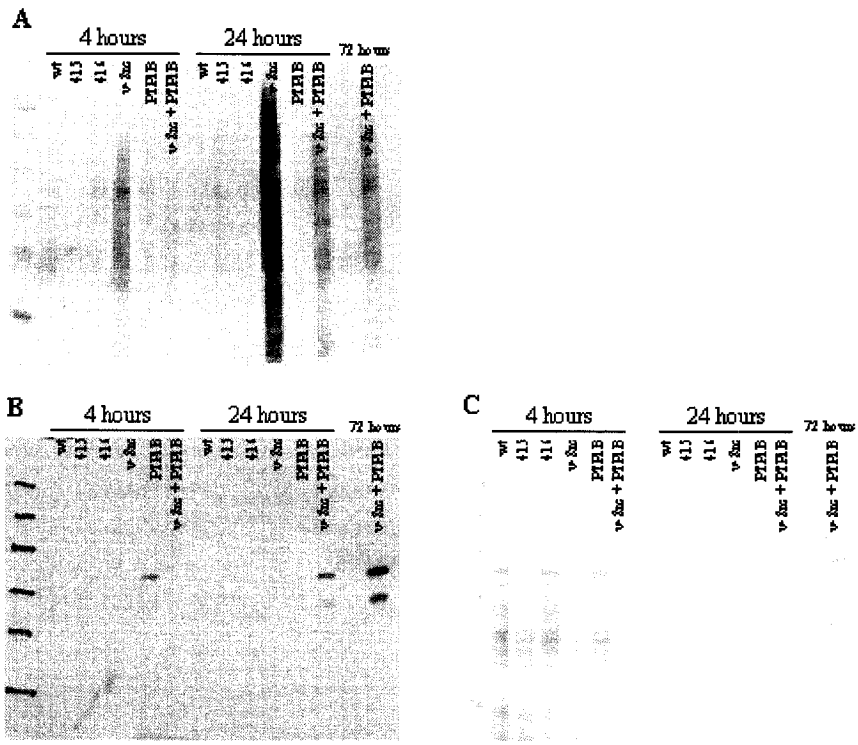

Figure 2.3: Western blotting reveals that expression of v-Src in yeast increases the level of protein tyrosine phosphorylation and co-expression of PTP1B can reverse it. Human PTP1B can be expressed in yeast and cleanly detected by western blotting. Total protein extracted four or 24 hours following galactose induction from BwG1-7a yeast transformed with p415GAL1 (415), p416GAL1 (416), p415GAL1-v-Src (v-Src), p416GAL1-PTP1B (PTP1B) or co-transformed with p415GAL1-v-Src and p416GAL1-PTP1B (v-Src + PTP1B) were separated by SDS-PAGE and analysed by: A) western blotting with anti-phosphotyrosine antibodies, B) western blotting with anti-PTP1B antibodies, C) Coomassie stain. The last lane shows proteins extracted following 72 hours of galactose induction from yeast co-transformed with v-Src and PTP1B.

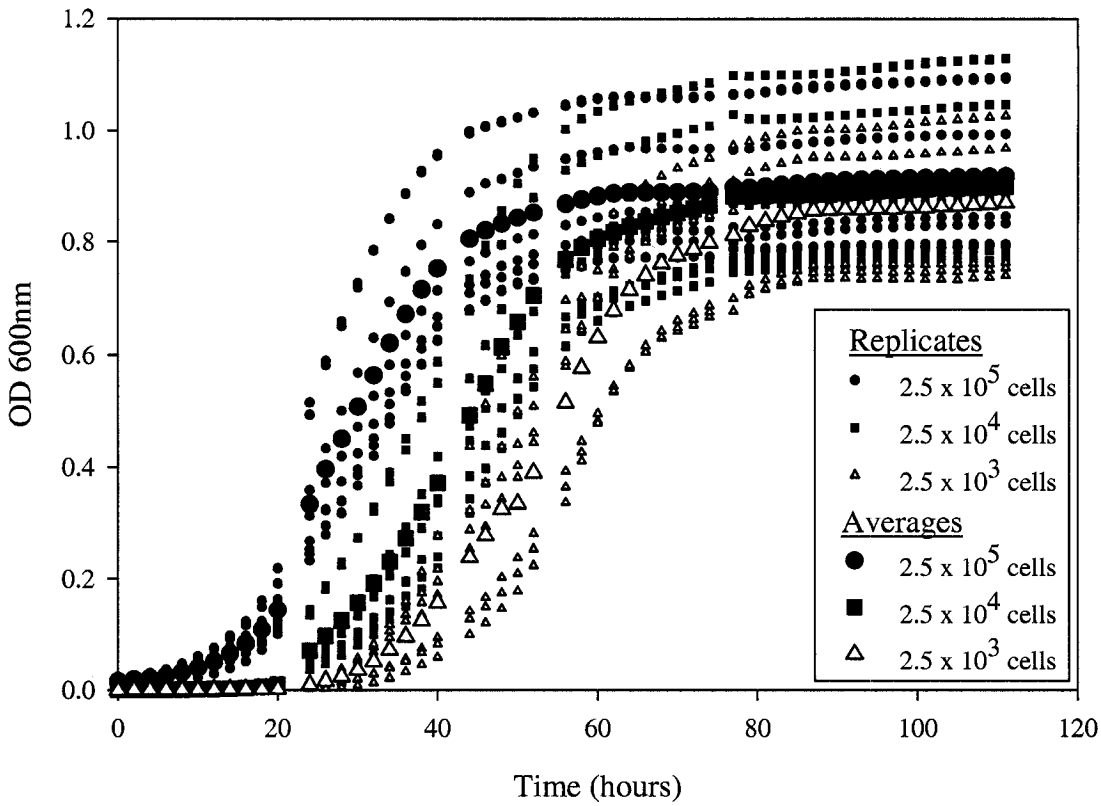

Figure 2.4: Growth curve in 96-well plate of *mnn9* yeast seeded at different concentrations in complete media with galactose. The number of cells from an overnight culture was counted in a hemacytometer and diluted to distribute 2.5 $x10^{5, 4 \text{ or } 3}$ cells to eight wells of a 96 -well plate. The absorbances of the resulting octuplicates were plotted against time along with their averages.

2.3.2. Titration of PTP1B and v-Src Expression in mnn9 Yeast

When an inhibitor was included in the streaking growth assay, it was unable to repress the growth induced by PTP1B expression (Fig. 2.1D). This was thought to be due to the inability of the inhibitor to cross the yeast cell wall. To facilitate inhibitor loading of the yeast, a yeast strain with a mutation in the *MNN9* locus was used. Also, to increase the window of PTP1B rescue, attenuated GAL promoters were used to lower the amount of v-Src expression and a high-copy vector carrying PTP1B was used to increase the level of PTP1B protein in the yeast.

mnn9 yeast co-transformed with PTP1B and v-Src expressed from various GAL promoters were assayed for growth in liquid culture. PTP1B was able to rescue the yeast when v-Src was expressed from the mutated GALL promoter (Fig. 2.5B) but not from the wild-type GAL1 promoter (Fig. 2.5A). Fifty nanomolar of BzN-EJJ-amide was also included in the assay but did not prevent rescue by PTP1B. The level of v-Src expression from the GALL promoter was also found to be optimal when compared with the GALS promoter which was not rescuable by PTP1B (Fig. 2.6A and B).

PTP1B was transferred to a high copy-vector to further increase the ratio between PTP1B and v-Src thereby increasing the rescue window. Here also, PTP1B was able to rescue yeast expressing v-Src from the GALL promoter (Fig. 2.6C) but the amounts of v-Src generated from a low copy vector and driven by the GALS promoter still overwhelmed the capacity of PTP1B even when carried on a high-copy vector (Fig. 2.6D). Interestingly, treatment with 10μM of Inhibitor L-A slightly decreased the rescue ability of a low-copy PTP1B but not of the high-copy one (Fig. 2.6A and C).

The use of a high-copy vector to carry PTP1B did not dramatically increase the rescue window and seemed to create an inhibitor resistance. Therefore, the best condition to get the greatest rescue sensitive to inhibition was with PTP1B on a low-copy vector and v-Src, also on a low-copy vector, driven by the GALL promoter.

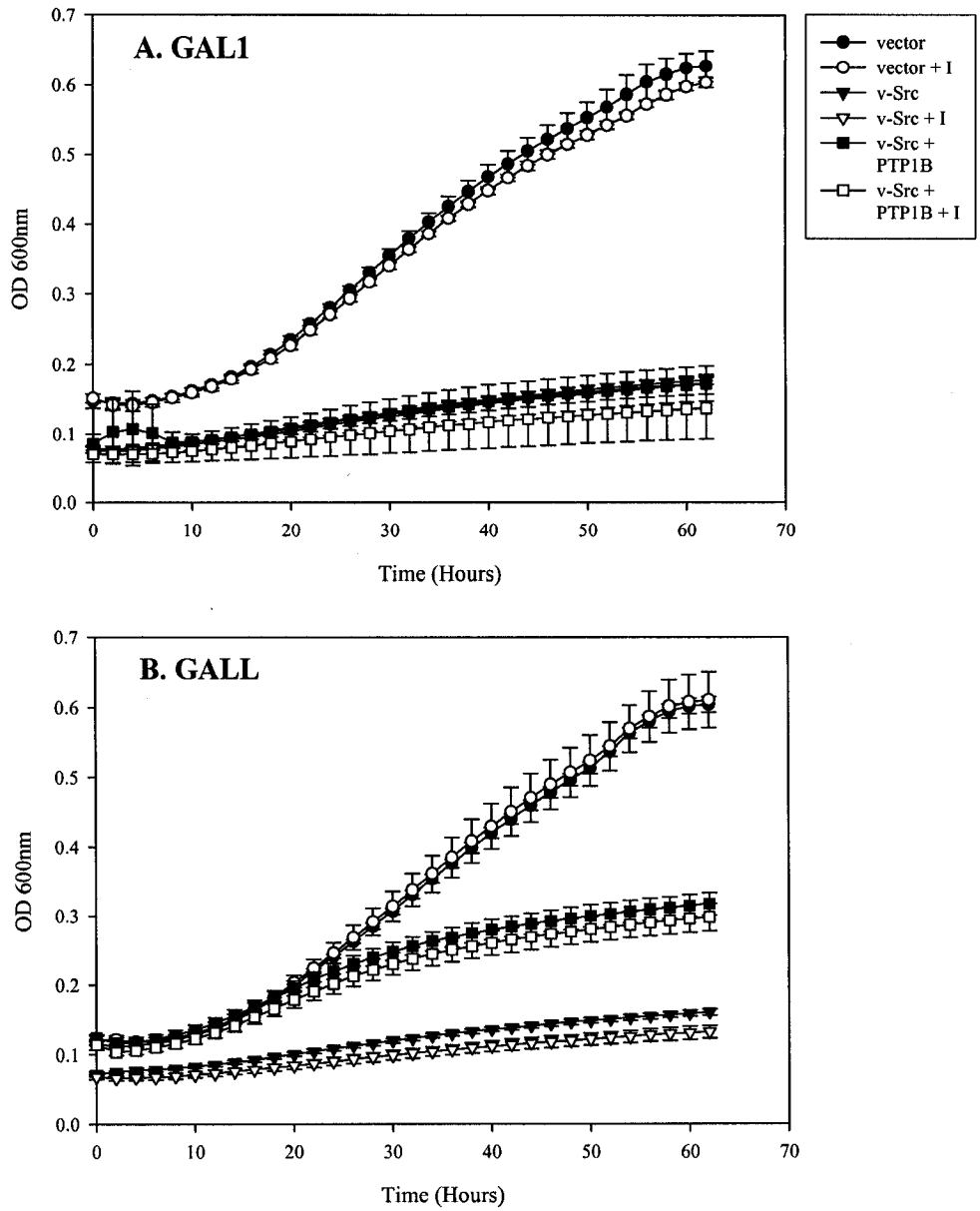

Figure 2.5: Expression of PTP1B can rescue *mnn9* yeast from the lethality of v-Src expressed from the mutant GALL promoter but not from the GAL1 promoter, and addition of 50μM inhibitor did not affect the efficiency of this rescue. A) Growth curves of yeast co-transformed with p415GAL1 and p416GAL1 (vector), p415GAL1-v-Src and p416GAL1-PTP1B (v-Src + PTP1B) or p415GAL1-v-Src and p416GAL1 (v-Src) in the presence or absence of 50nM of the inhibitor BzN-EJJ-amide (+I). B) Growth curves of yeast co-transformed with p415GALL and p416GAL1 (vector), p415GALL-v-Src and p416GAL1-PTP1B (v-Src + PTP1B) or p415GALL-v-Src and p416GAL1 (v-Src) in the presence or absence of 50nM of the inhibitor BzN-EJJ-amide. Error bars are standard deviation n = 3.

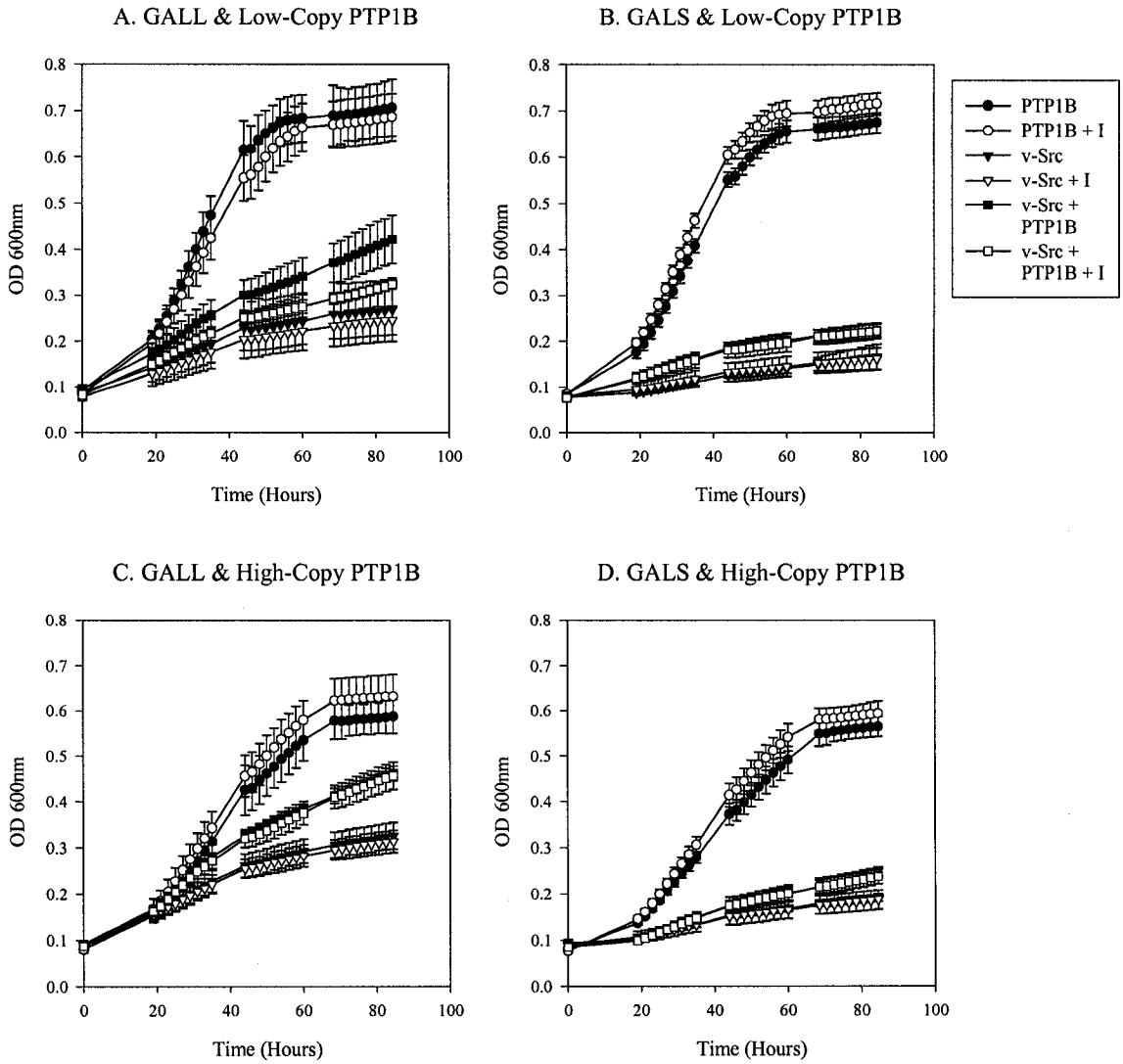

Figure 2.6: PTP1B expressed from a high- or low-copy vector allows the growth of *mnn9* yeast expressing v-Src from the GALL promoter but not the GALS promoter. Treatment with 10μM of the PTP1B inhibitor L-A is not toxic to the yeast and showed only a slight trend in preventing the low-copy PTP1B rescue. A) Growth curves of yeast co-transformed with p415GALL and p416GAL1-PTP1B (PTP1B), p415GALLv-Src and p416GAL1 (v-Src) or p415GALL-v-Src and p416GAL1-PTP1B (v-Src + PTP1B) with or without inhibitor (I). B) Growth curves of yeast co-transformed with p415GALS and p416GAL1-PTP1B (PTP1B), p415GALSv-Src and p416GAL1 (v-Src) or p415GALS-v-Src and p416GAL1-PTP1B (v-Src + PTP1B) with or without inhibitor (I). C) Growth curves of yeast co-transformed with p415GALL and p426GAL1-PTP1B (PTP1B), p415GALLv-Src and p426GAL1 (v-Src) or p415GALL-v-Src and p426GAL1-PTP1B (v-Src + PTP1B) with or without inhibitor (I). D) Growth curves of yeast co-transformed with p415GALS and p426GAL1-PTP1B (PTP1B), p415GALSv-Src and p426GAL1 (v-Src) or p415GALS-v-Src and p426GAL1-PTP1B (v-Src + PTP1B) with or without inhibitor (I). Error bars are standard deviation n=3.

2.3.3. Inactive PTP1B Mutants

Catalytically inactive PTP1B mutants were co-transformed with v-Src to verify that the rescue effect of PTP1B on v-Src lethality was due to its enzymatic activity. Two mutants were assayed: C215S where the active site cysteine was mutated to a serine and D181A where the general acid/base involved in the phosphatase enzymatic reaction was replaced by an alanine. The results in Figure 2.7A show that only wild-type PTP1B can rescue yeast from v-Src lethality whereas the C215S or D181A mutants were ineffective. Western blots of total phosphotyrosine (Fig. 2.7B) revealed that only the catalytically active PTP1B and not the mutants attenuated the increase in tyrosine phosphorylation due to v-Src expression. These results indicated that PTP1B mediated its effect through enzymatic dephosphorylation of the targets of v-Src.

2.3.4. The erg6 Yeast Strains

Some inhibitor effect could be seen in liquid culture using the *mnn9* yeast strain (Fig. 2.6A) but the magnitude of this effect was very small. Although this mutation has been described as increasing yeast permeability, the literature was relatively poor in its use as a drug-permeable strain. In comparison, the literature revealed many groups had successfully used the *erg6* yeast as a drug-sensitive strain. The popularity of this strain was further supported by discussions with Dr. M. El Sherbeini, working in the metabolic disorders group at Merck & Co., who selected this specific strain to develop a screen for caspase inhibitors. Since the integration process was proving to be non-trivial, it was thought that changing strain at an early stage might be strategic if the end product proved to be more permeable to inhibitors.

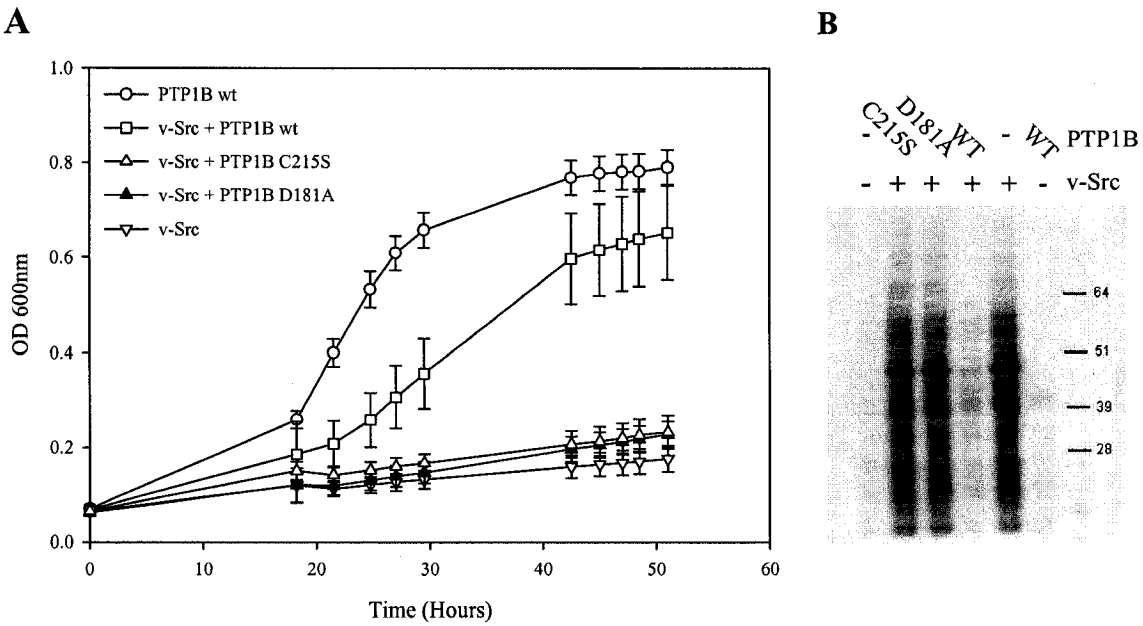

Figure 2.7: The catalytic activity of PTP1B is required for the growth of yeast expressing v-Src and to decrease the total tyrosine phosphorylation levels induced by v-Src expression. A) Growth curves of yeast co-transformed with p415GALL and p416GAL1-PTP1B (PTP1B), p415GALL-v-Src and p416GAL1 (v-Src) or p415GALL-v-Src and p416GAL1-PTP1B (wild-type or mutant). Wild-type is denoted wt, catalytically inactive PTP1B mutants are D181A and c215S. Error bars are standard deviation n=3. B) Western blot of total yeast protein extracted from yeast transformed as in A, induced in galactose for 51 hours and probed with anti-phosphotyrosine antibody.

PTP1B was able to rescue the growth of yeast expressing v-Src under the GAL1 promoter in the BwG1-7a but not in the *mnn9* strain where v-Src had to be expressed under the GALL promoter. To confirm that the *erg6* yeast strain behaved similarly to *mnn9*, growth curves comparing the rescue by PTP1B of the lethality of v-Src under the attenuated or wild-type promoters were repeated. In *erg6* as in *mnn9*, v-Src expressed from any of the three promoters abolished yeast growth to the same extent and PTP1B was able to rescue the lethality of v-Src only if expressed from the GALL promoter (Fig. 2.8). Western blots of total protein extracted from yeast grown from the same overnight culture as the one used for the growth curves in Figure 2.8 and induced 63 hours in galactose were probed with an antibody against phosphorylated tyrosine residues (Fig.

2.9). v-Src driven by either the GAL1 or GALS promoters resulted in a higher level of protein tyrosine phosphorylation than v-Src under the GALL promoter. Co-transformation with PTP1B effectively reduced the total tyrosine phosphorylation level for all the permutations of the GAL promoters driving v-Src.

Once the lethality of v-Src and the rescue ability of PTP1B were confirmed in the *erg6* strain, a few PTP1B inhibitors were tested in the system: L-A, L-B, L-C, L-D, vanadate and pervanadate. At 50μM, none of these compounds were toxic to the yeast, as seen from the lack of effect on the PTP1B control curves, but none reduced the growth of yeast co-expressing v-Src and PTP1B (Fig. 2.10).

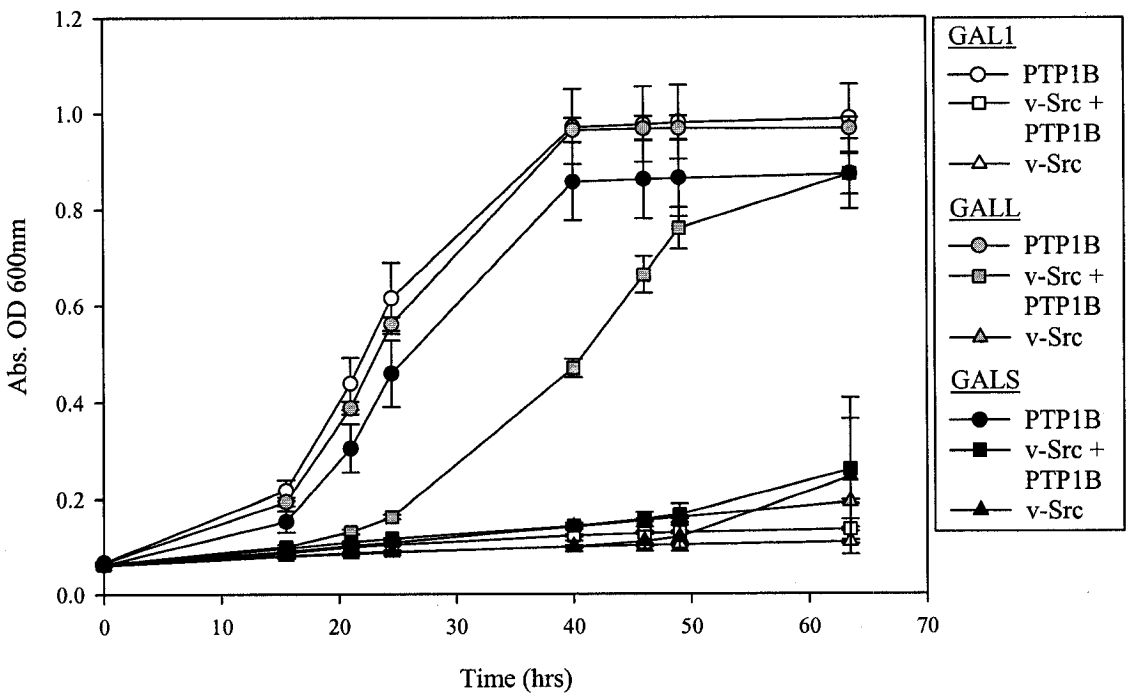

Figure 2.8: Co-expression of PTP1B allows the growth of *erg6* yeast expressing v-Src from the GALL (grey) but not from the GAL1 (white) or GALS (black) promoters. Growth curves of yeast co-transformed with p415GAL1 or L or S and p416GAL1-PTP1B (PTP1B), p415GAL1- or L- or S-v-Src and p416GAL1-PTP1B (v-Src + PTP1B) or p415GAL1- or L- or S-v-Src and p416GAL1 (v-Src). Error bars are standard deviation n=3.

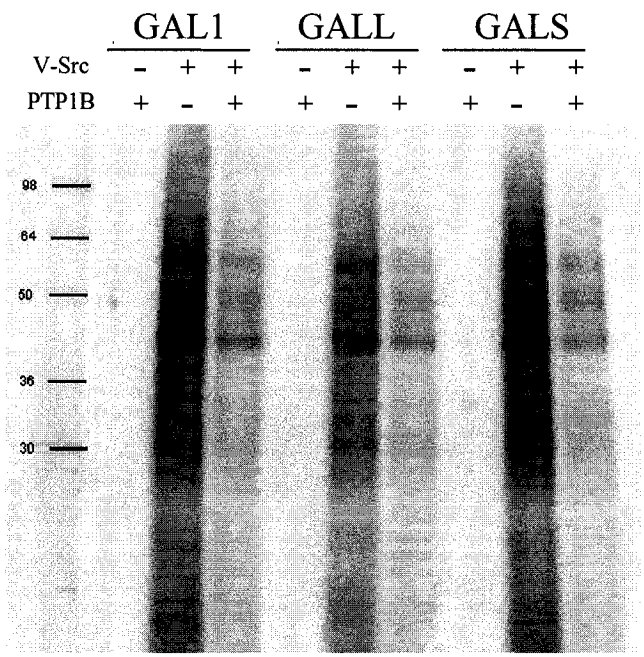

Figure 2.9: PTP1B expression reduces the level of tyrosine phosphorylation in *erg6* yeast expressing v-Src from the GAL1, GALL or GALS promoter. Western blot of total protein extracted from yeast transformed as in Figure 2.8, induced in galactose for 63 hours and probed with anti-phosphotyrosine antibody. GAL1, GALL and GALS refer to the promoter driving v-Src or the identity of the empty vector co-transformed with PTP1B.

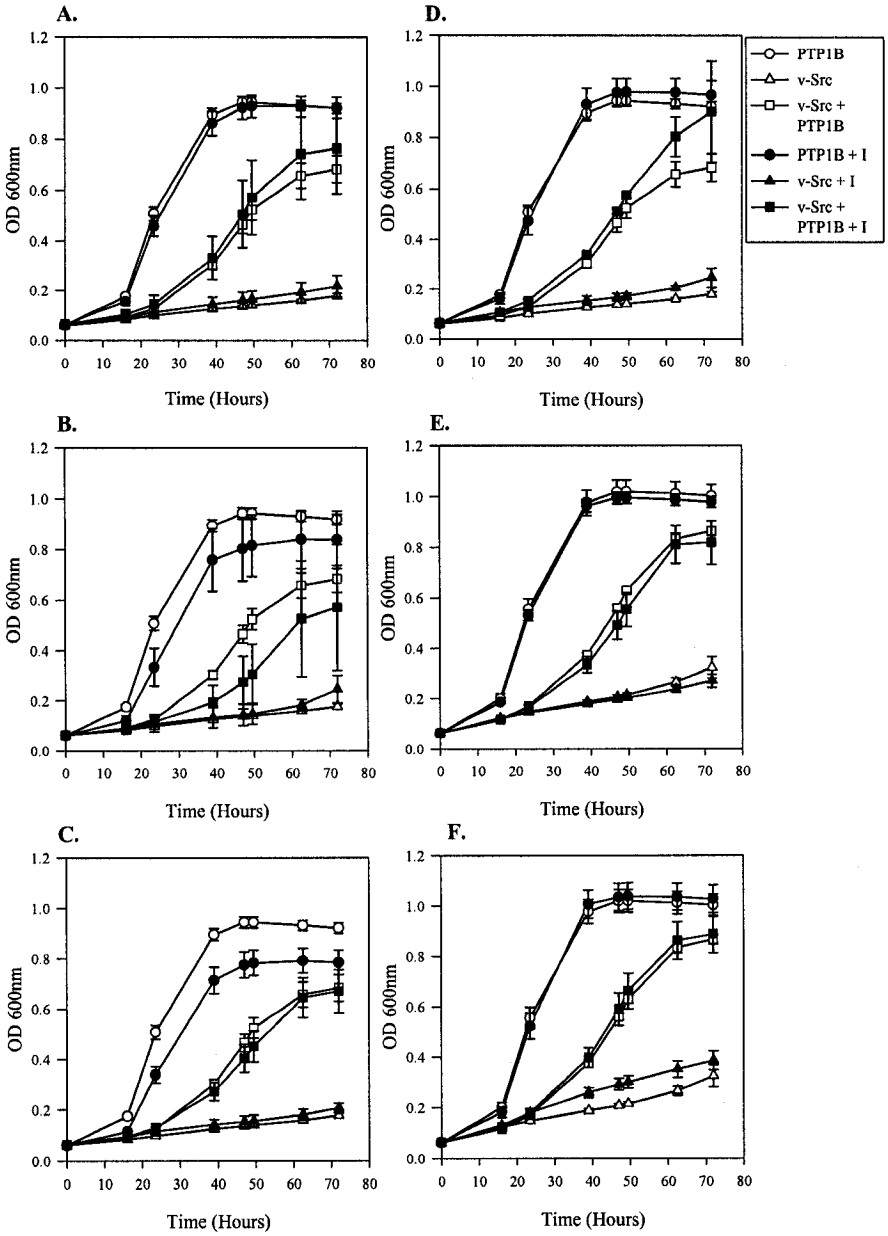

Figure 2.10: The rescue from v-Src lethality mediated by PTP1B in *erg6* yeast is not sensitive to 50μM of PTP1B inhibitors. Yeast were co-transformed with p415GALL and p416GAL1-PTP1B (PTP1B), p415GALL-v-Src and p416GAL1 (v-Src) or p415GALL-v-Src and p416GAL1-PTP1B (v-Src + PTP1B) and grown in the presence (+I) or absence of the inhibitors A) L-B, B) L-C, C) L-D, D) L-A, E) vanadate and F) pervanadate. To compare with the compounds prepared from DMSO stocks, control curves for A) to D) contain 0.2% DMSO. Error bars are standard deviation n=3.

Due to the small-scale synthesis of the inhibitors, only limited amounts were available for use in the growth curves. Faced with the lack of reaction of the yeast to these quantities, a few inhibitors were discovered in large enough supply to directly go up to one or two millimolar: grossly exaggerated quantities compared to the sub-micromolar efficiency of these inhibitor on the purified recombinant enzyme. Figure 2.11 shows the ability of 1mM L-B to decrease the PTP1B-dependent growth while not being toxic to the yeast itself as seen by the lack of effect of L-B on yeast expressing only PTP1B. Boosting the concentration of L-B to 2mM after 24 hours of growth totally abolished the ability of PTP1B to rescue the yeast from v-Src lethality while still remaining non-toxic to yeast expressing only PTP1B. Similar results were obtained for vanadate. L-C was toxic to the yeast when its concentration was increased to 0.5mM. Dose-response curves were generated yielding an EC_{50} of 1.0 ± 0.2mM for L-B and 0.72 ± 0.09mM for vanadate (Fig. 2.12).

L-B was also able to reduce the activity of PTP1B in the yeast as measured by phosphotyrosine content. Figure 2.13 shows the increase in phosphotyrosine levels in yeast expressing of v-Src and the concomitant reduction by co-expression of PTP1B. Treatment with the inhibitor did not affect the phosphotyrosine levels in yeast expressing only v-Src but did raise those of yeast co-expressing v-Src and PTP1B.

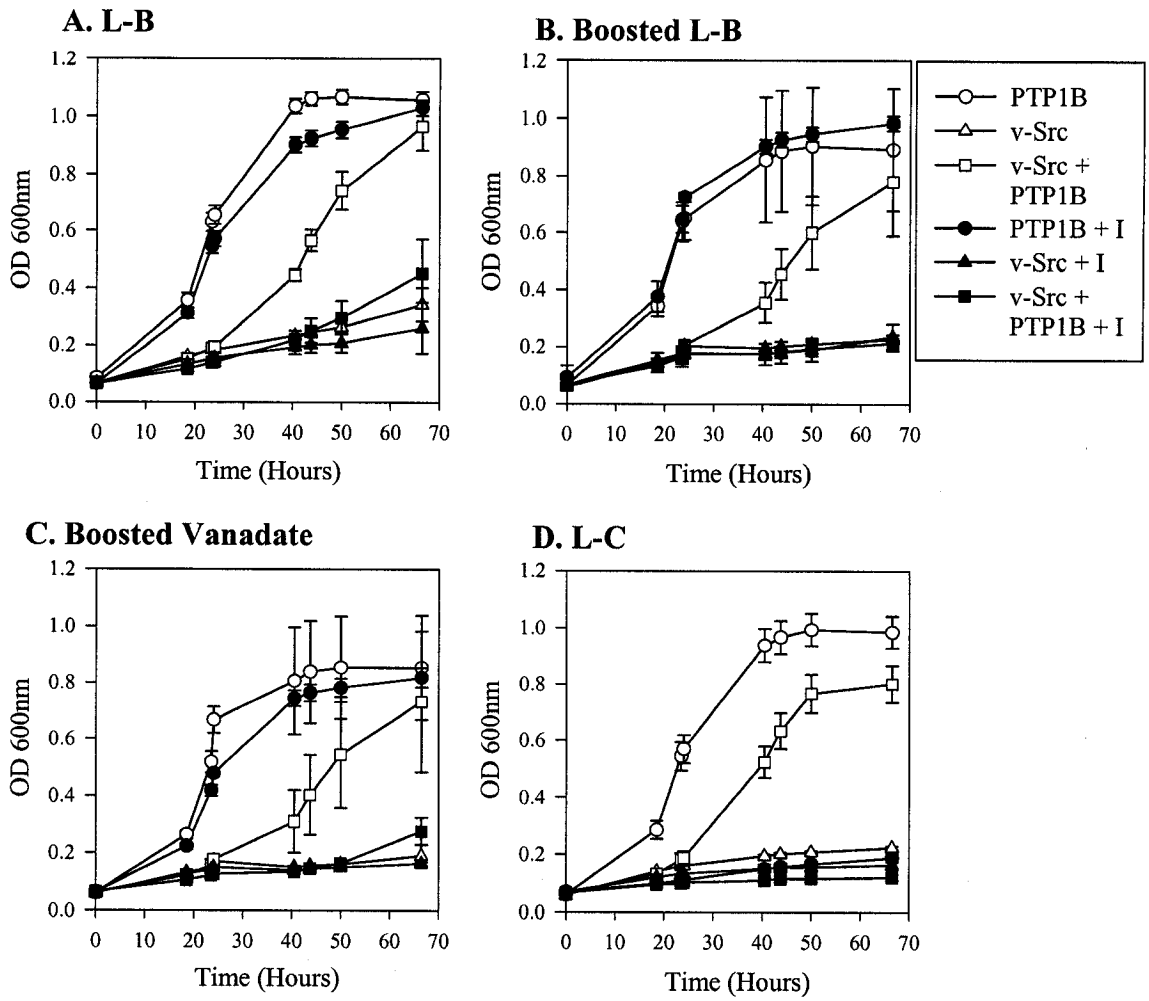

Figure 2.11: Millimolar quantities of PTP1B inhibitors abolish the growth of yeast dependent on PTP1B activity for growth. Yeast were transformed as in Figure 2.10 and grown in the presence (+I) or absence of A) 1mM L-B, B) 1mM L-B boosted up to 2mM after 24 hours of growth, C) 1mM vanadate boosted up to 2mM after 24 hours of growth and D) 0.5mM L-C. The control curves for L-C contain 2% DMSO to reflect the DMSO content of the compound. Error bars are standard deviation n=3.

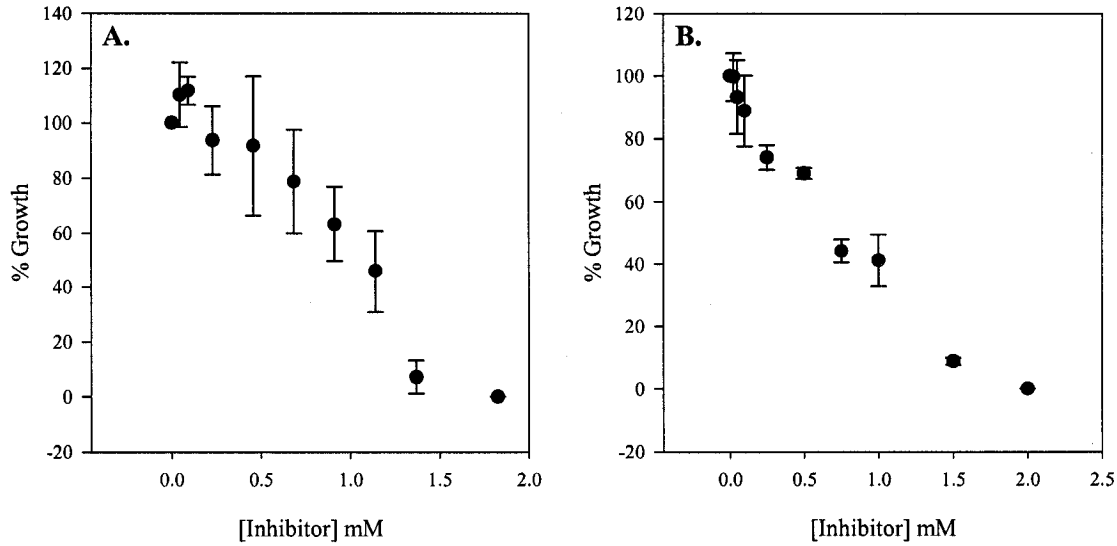

Figure 2.12: PTP1B inhibitors dose-dependently reduce the ability of *erg6* yeast co-expressing v-Src and PTP1B to grow. Dose response curves were generated by growing yeast transformed as in Figure 2.10 in the presence of galactose and increasing amounts of A) L-B and B) Vanadate. % Growth refers to the OD 600nm after 65 hours of growth normalized to reflect 100 % growth at 0mM inhibitor and 0% growth at 2mM. Data represent two experiments done in triplicate, error bars are standard error n=2.

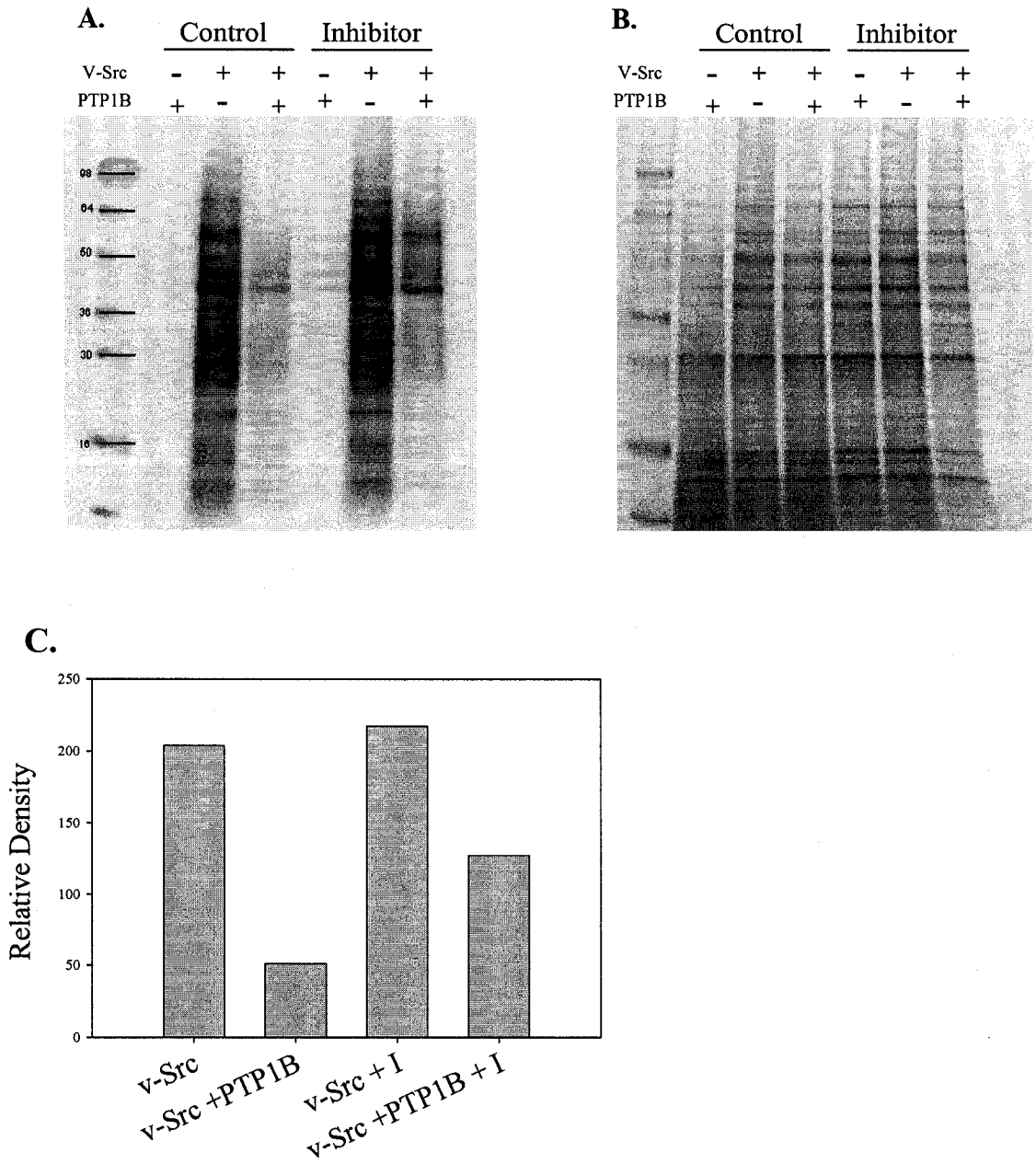

Figure 2.13: Treatment with a PTP1B inhibitor prevents PTP1B from dephosphorylating the protein targets of v-Src in yeast. Yeast were transformed as in Figure 2.10 and induced in galactose for 42 hours in the presence or absence of 2mM L-B. A) Western blot of total yeast protein probed with an anti-phosphotyrosine antibody. B) Coomassie stained gel to control for amount of total protein loaded in A. C) Quantification of phosphotyrosine content from A normalized on total protein content from B.

2.3.5. Integration and the YPH499 Yeast Strain

Integration of v-Src in the genome was thought advantageous in part to increase the rescue window by decreasing the expression of v-Src from the low copy vector to a single genomic locus but mostly to bypass the necessity for co-transformation of the v-Src plasmid at the same time as the library. The need to co-transform v-Src along with the library was a concern because it decreased the efficiency of the transformation protocol which needed to be excellent to ensure that the complete library was introduced in yeast. Integrating v-Src in the genome would allow the library to be transformed alone.

All integration attempts in either *mnn9* or *erg6* yeast failed. The consistent failure to generate integrated clones regardless of the strategy used was thought to be due to these strains reduced transfection efficiency[190,220,221]. If this weakness was an obstacle to obtain an integrated clone it would also be an obstacle for complete transformation of a library. To verify that a compromised cell wall was truly necessary for the inhibitors to get in the cell, response curves were generated in the millimolar range concentration for L-B in the wild-type yeast YPH499. Figure 2.14 shows that with an EC_{50} of 1.2 ± 0.2mM, yeast with an intact cell wall are just as sensitive to these levels of inhibitor as *erg6* yeast. Since the wild-type yeast has normal transformation efficiency and took up the inhibitor just as well as the mutant strain, they were transformed with the integrating construct. This yielded many positives clones which were further characterized to obtain the desired phenotypic window.

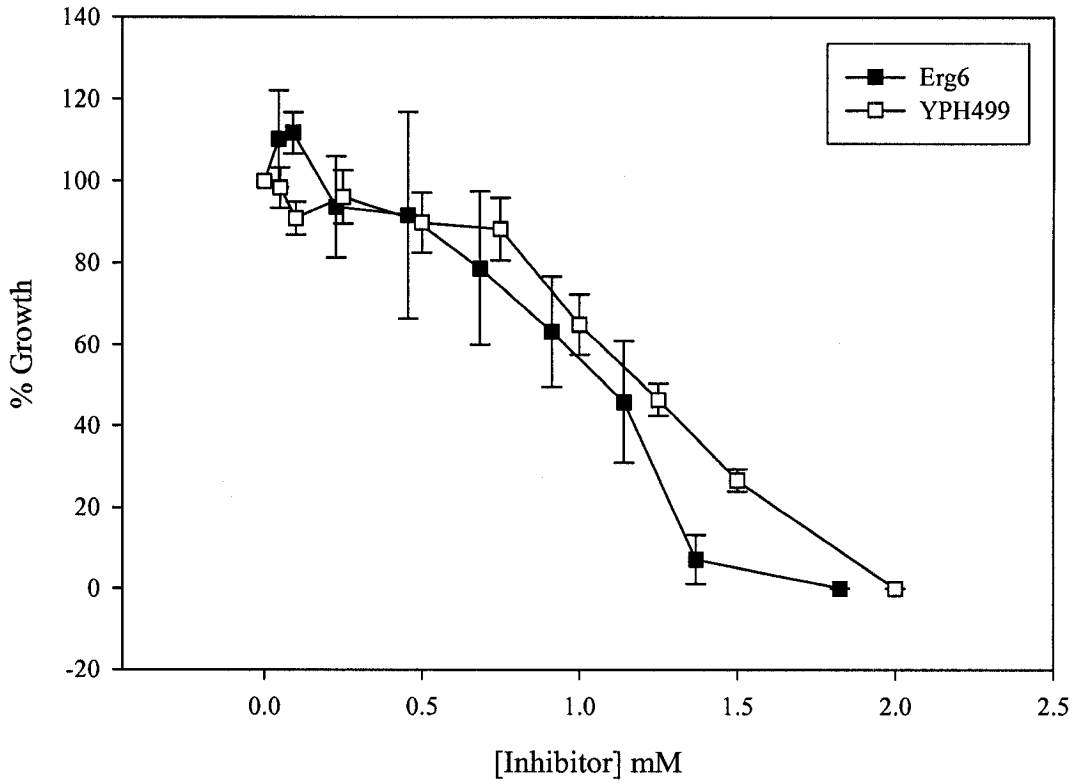

Figure 2.14: The compromised cell wall of *erg6* yeast does not make it more permeable to PTP1B inhibitor compare to the wild-type strain YPH499. Dose response curves for *erg6* and YPH499 were generated with L-B as in Figure 2.12. Data for *erg6* transcribed from Figure 2.12. Data from YPH499 represents 14 experiments each done in triplicate, error bars are standard error n=14.

2.3.6. Characterization of Integrated Clones

The integrated clones that grew on histidine selection plates from the transformation with the integrating fragment were picked and grown in liquid culture with galactose or glucose as the sole carbon source. Using galactose as the sole carbon source would induce expression of v-Src if properly integrated and prevent growth compared to glucose. Clones A2, H2, B4, E6, A8 and F8 were selected because they gave robust growth on glucose and did not grow on galactose (Fig. 2.15). Since lack of growth on galactose should be phenotypical of v-Src expression, the clones were transformed with PTP1B on a high or low copy vector and their growth on galactose was again measured;

Figure 2.16 shows that expression of PTP1B is able to reverse the phenotype and allow growth. Clones transformed with a high copy PTP1B grew better on galactose than those transformed with a low copy PTP1B. However, the integrated clones transformed with the empty high copy vector, as a control for growth on media lacking uracil which is selected by the vector, showed some growth on galactose sometimes even greater than the clones expressing PTP1B from the low copy vector. In comparison, clones transformed with the empty low copy vector displayed a very clean lethality.

Phosphotyrosine blots revealed that the integrated clones had a massive level of tyrosine phosphorylation compared to the mother strain YPH499 (Fig. 2.17). In addition, transformation of these clones with PTP1B reduced the total level of tyrosine phosphorylation. These results suggested that v-Src was expressed and active in these cells. Although the difference was minor, clones transformed with the empty high copy vector seemed to display a lower level of total phosphorylation than clones transformed with the low copy vector agreeing with the perplexing growth curve data.

Colony PCRs were performed to verify that the foreign DNA transformed in the yeast had been introduced in the predicted region of the genome. A PCR product was obtained using a primer coding in the 3' end of v-Src (S8) and a primer coding in the genomic sequence of the yeast directly 3' to the region targeted for disruption (Y4). As a control, primers on either sides of the integration target, Y3 and Y2, yielded a 2kb fragment only for the mother strain, YPH499, and not for the integrated clone using a 2.5 minutes extension time for the PCR reaction. As additional control, no fragments were amplified in the absence of genomic DNA template. Figure 2.18 shows the data obtained for clone H2 along with a location schematic of the primers used.

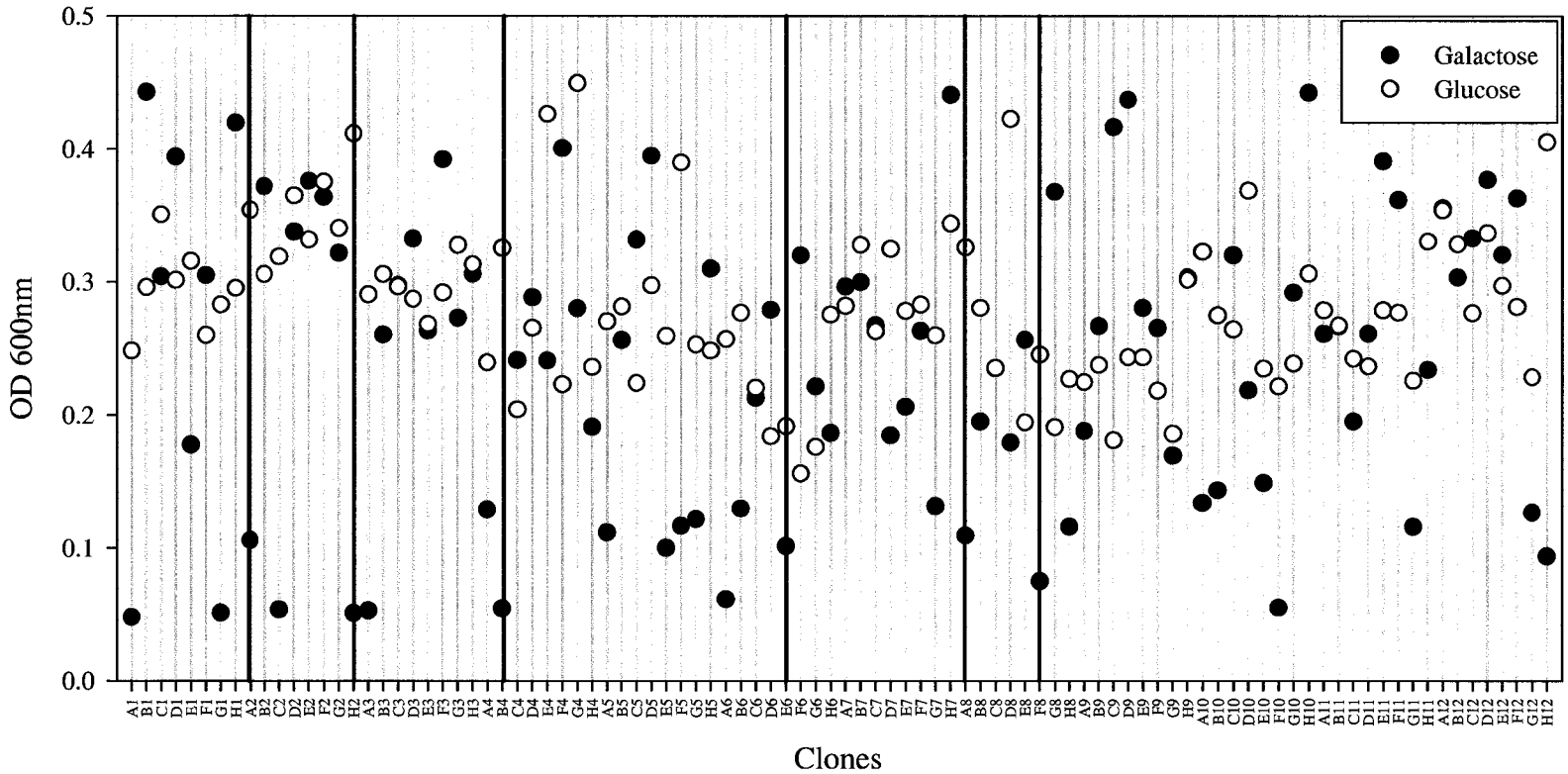

Figure 2.15: Clones that have integrated a functional copy of v-Src do not grow on galactose but have normal growth on glucose. The absorbance after 70 hours of growth on glucose or galactose was measured for 96 clones picked from the transformation of YPH499 with the GAL1-v-Src-CYC integrating fragment. Red lines highlight the clones that were selected for further characterization.

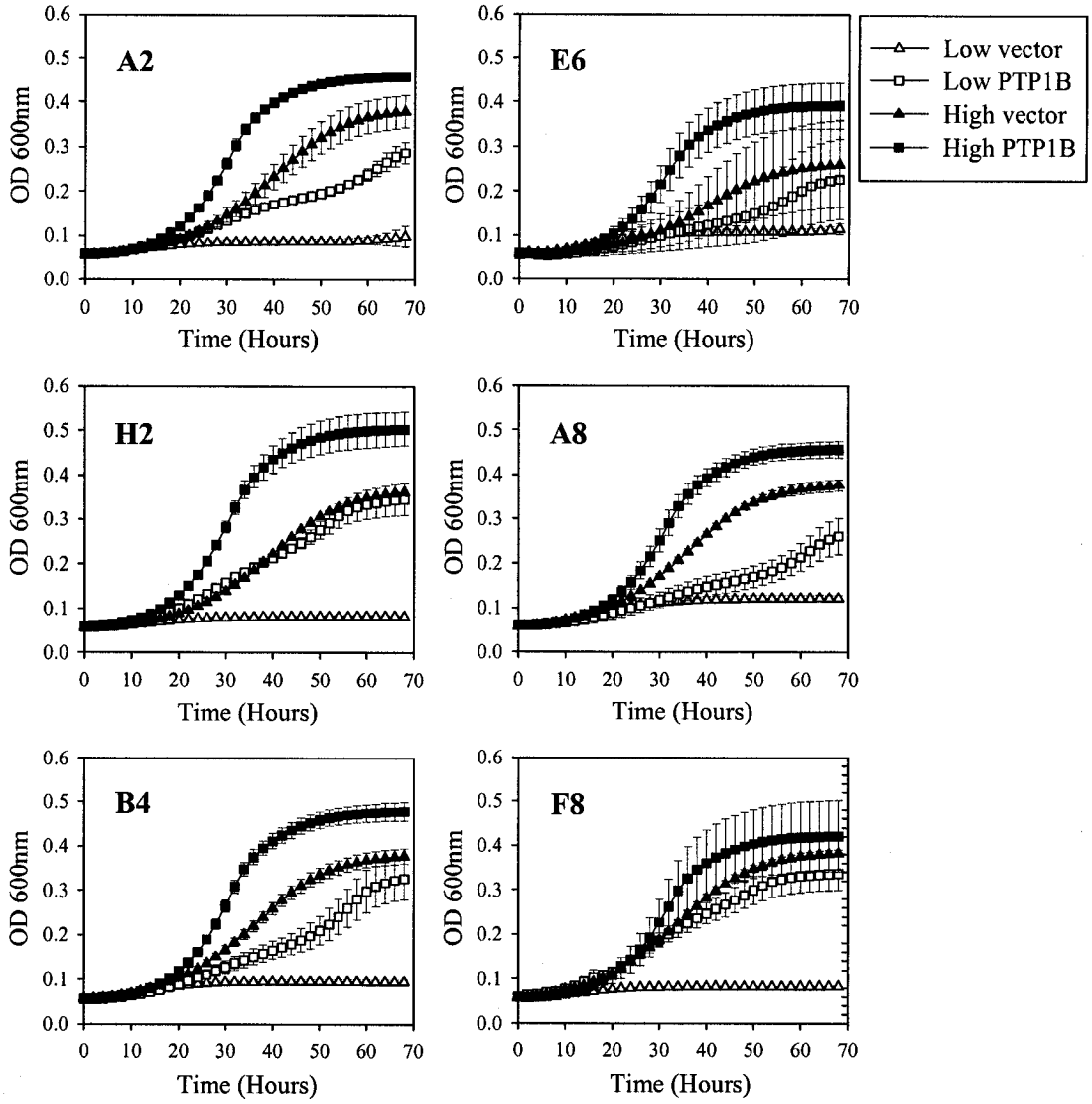

Figure 2.16: Transformation of v-Src integration-positive clones with PTP1B allows growth on galactose. Positives clones selected from the galactose screen in Figure 2.15 were transformed with either p416GAL1 (Low vector), p416GAL1-PTP1B (Low PTP1B), p426GAL1 (High vector) or p426GAL1-PTP1B (High PTP1B) and grown in galactose. Error bars are standard deviation n=3.

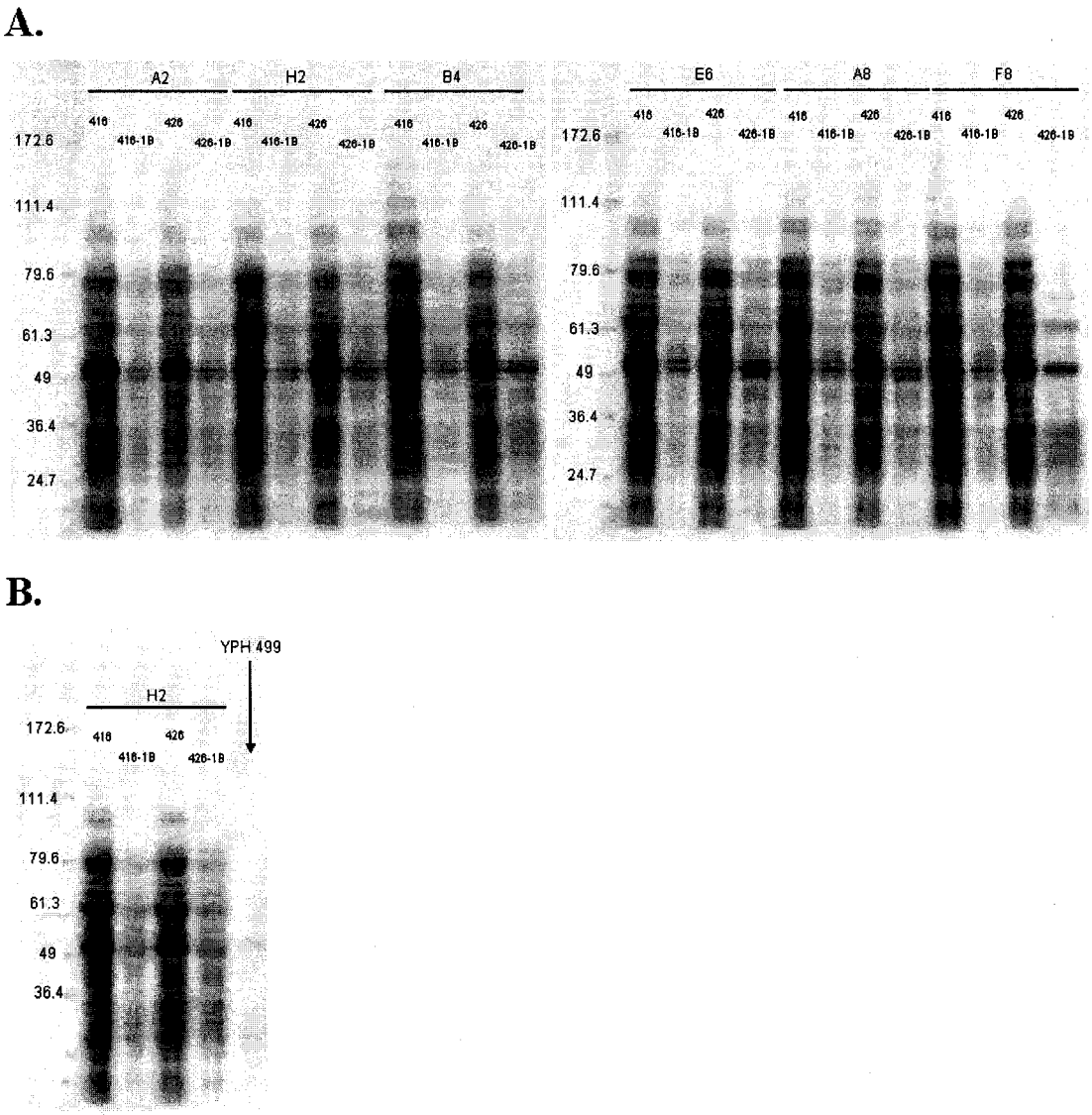

Figure 2.17: Elevated phosphotyrosine levels in integrated clones indicate expression of v-Src; expression of PTP1B in these clones reduces phosphotyrosine levels. Integrated clones were transformed as for Figure 2.16 and grown in the presence of galactose for 62 hours. Total protein was extracted and analyzed by Western blotting with anti-phosphotyrosine antibodies. A) Phosphotyrosine levels for all six selected clones. B) Phosphotyrosine levels for clone H2 probed again in parallel with the mother strain YPH 499.

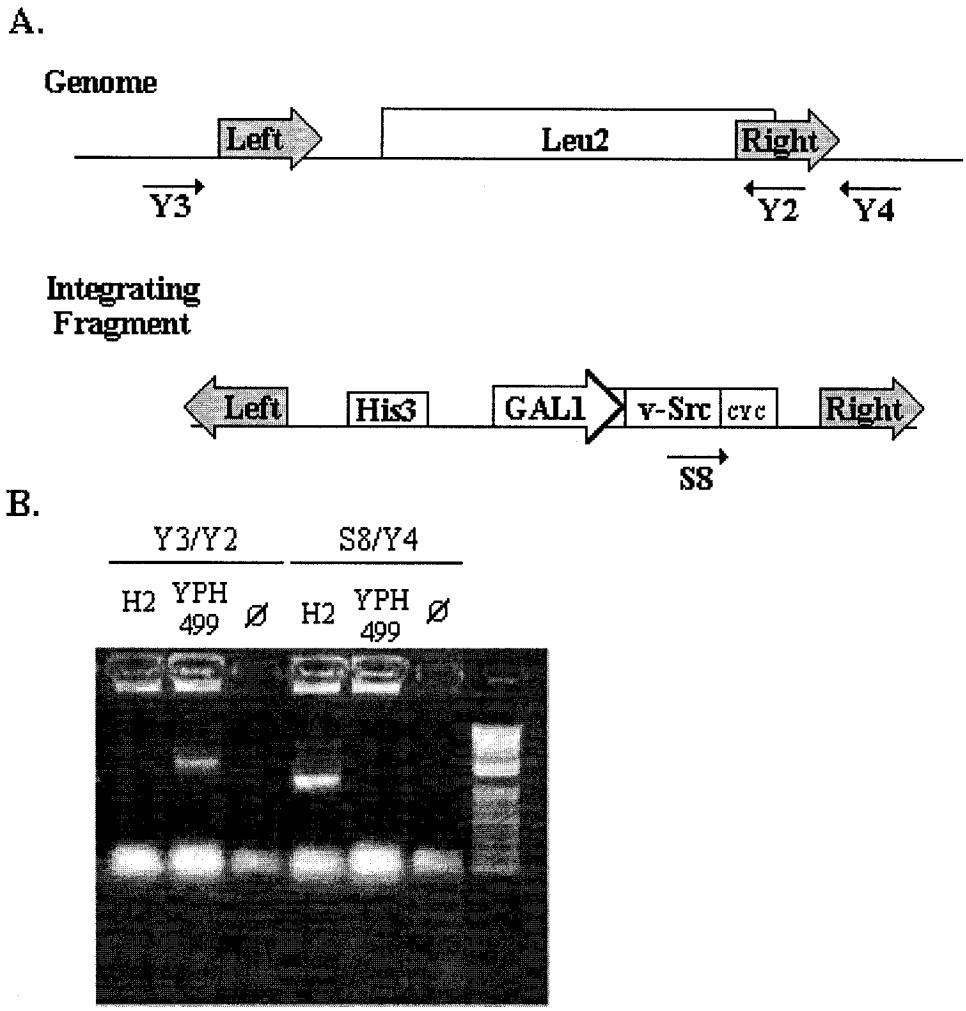

Figure 2.18: A) Schematic representation of the integration partners along with locations of primers used in the colony PCR reaction. Grey box are left and right fragment of the *LEU2* locus used for homologous recombination. Drawing not to scale: genomic locus ≈1.8kb, integrating fragment ≈ 6kb. B) TBE gel of the colony PCR reaction using genomic DNA from either H2 or the YPH499 strains as template or no template DNA as control (∅) using two primer pairs: Y3 and Y2 or S8 and Y4.

2.3.7. The H2 v-Src Integrated Yeast Strain

All six clones gave similar positive functional integration results: lack of growth on galactose despite robust growth on glucose reversed by expression of PTP1B and high phosphorylation levels also reversed by expression of PTP1B. Since the characterization

results of all the clones were similar, the H2 clone was chosen at random to determine the sensitivity of this strain to PTP1B inhibitors and then be used in the yeast library screen.

The activity of PTP1B to rescue the v-Src lethality had been measured as its ability to show robust growth in liquid culture with these growth curves initiating from a suspension of cells obtained after an overnight growth. Overnight growth with concomitant absorbance measurements to normalize starting culture concentration were thought to be incompatible with processing of a large number of clone like those generated from a library. Directly inoculating the 96-well plates with the colonies picked from the transformation plates would streamline the assay. Figure 2.19 compares the two techniques. Similar to the results previously obtained (Figure 2.16), the empty high copy vector seemed to allow H2 to grow on galactose whereas the empty low copy vector maintained a very low background growth (Fig. 2.19B). For the curves started directly from the colonies on the transformation plates, transforming H2 with the empty high copy vector maintained the clean lethality of H2 grown on galactose similar to the empty low copy vector (Fig. 2.19A). In addition, the greater window of rescue obtained when PTP1B was carried on a high copy rather than a low copy vector became obvious in the direct curve where both controls behaved similarly. This indicated that the best condition to obtain the greatest rescue window in H2 was using PTP1B on a high copy vector and using colonies directly from the transformation plate for the growth curves. The response of H2 to the inhibitor was then measured using these conditions. Figure 2.20 shows that treatment with 0.75mM L-B only delays the growth of yeast co-expressing v-Src and PTP1B but boosting the inhibitor levels up to 1.25mM results in a reduced viability.

A. Direct from the plate

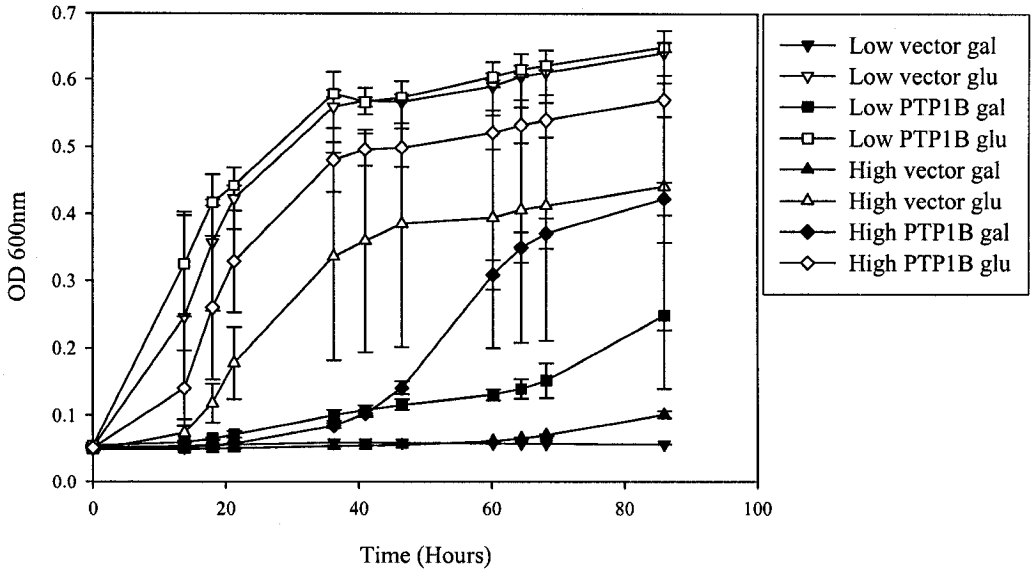

B. From overnight culture

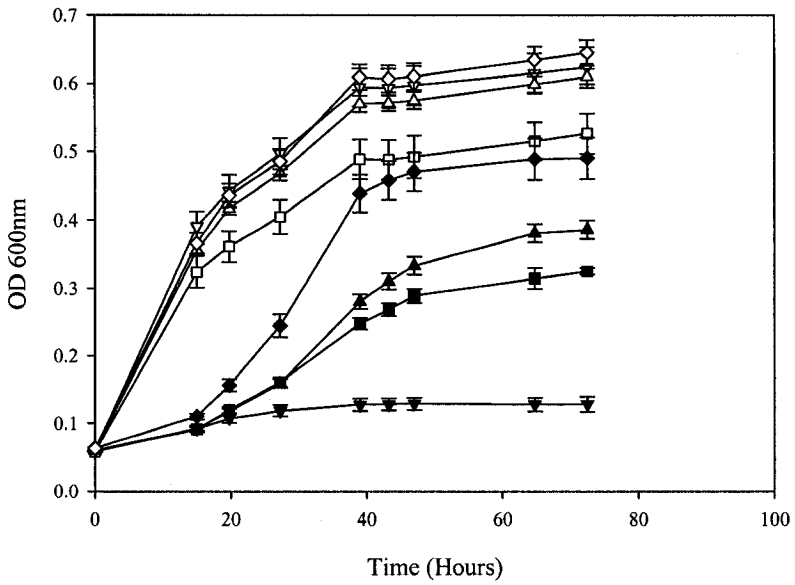

Figure 2.19: Expression of PTP1B in H2 allows growth on galactose when measured by growth curves started from an overnight culture or directly from a suspension of the colonies obtained on the transformation plate. H2 yeast was transformed as in Figure 2.16 and a suspension of the resulting colonies was used for growth curves in dropout media containing galactose (gal) or glucose (glu). A) Growth curves started from 20µL of a suspension of single colonies in 200uL raffinose dropout media. B) Growth curves initiated from 20µL of an overnight culture in raffinose dropout media. Error bars are standard deviation n=3.

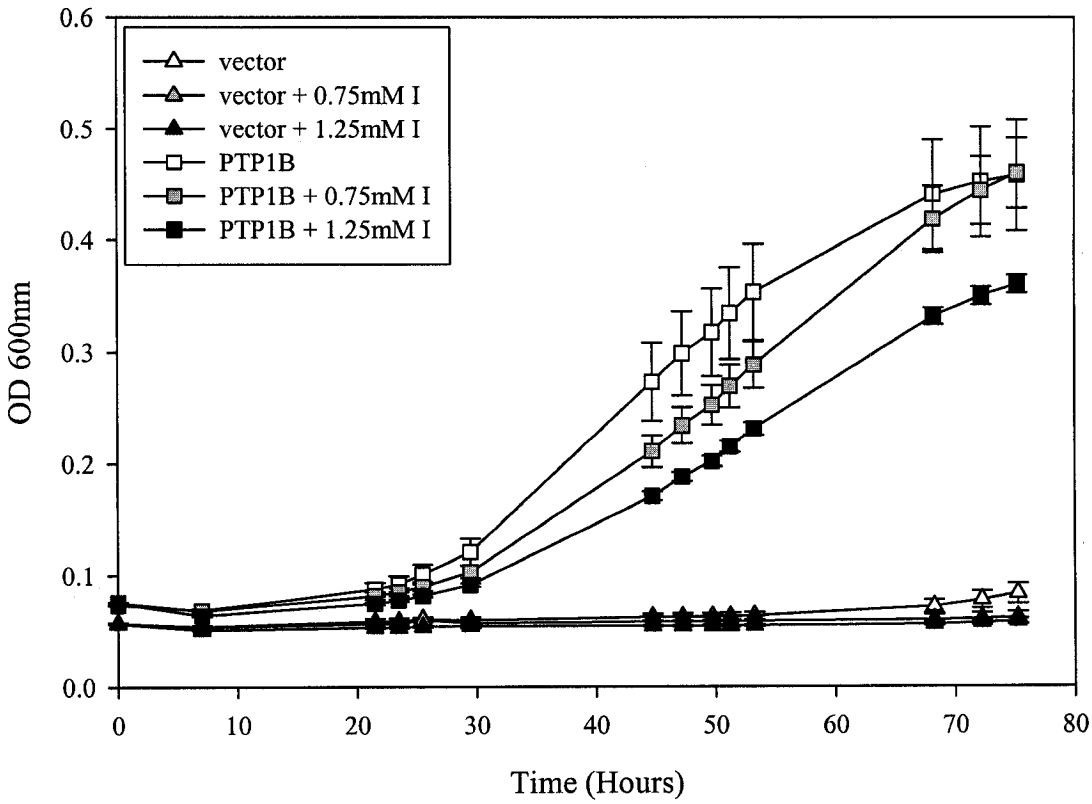

Figure 2.20: The ability of PTP1B to permit H2 yeast, containing an integrated copy of v-Src under the GAL promoter, to grow on galactose is sensitive to treatment with a PTP1B inhibitor. H2 yeast were transformed with p46GAL1 (vector) or p426GAL1-PTP1 (PTP1B) and grown in the presence of galactose with or without 0.75mM L-B and/or boosted to 1.25mM after 24 hours of growth.

2.4. Conclusions

Based on the previous observation that co-expression of PTP1B can rescue yeast from v-Src lethality, we optimized the expression levels of PTP1B and v-Src such that inhibition of PTP1B activity results in growth interference. PTP1B catalytic activity was absolutely required for yeast growth since the catalytically inactive PTP1B mutants C215S and D181A failed to overcome the lethality of v-Src. There was a certain stoichiometry between PTP1B and v-Src expression that was required to obtain a robust growth phenotype and at the same time be sensitive to inhibitors. For example, it has been shown that expression from a high copy vector can result in inhibitor resistant phenotypes due to high levels of protein expression[151]. Previous reports[164,166] had utilized the GAL1 promoter to express PTP1B from high copy vectors. Therefore it was necessary to reduce the expression levels of PTP1B from the high copy vectors to a low copy vector. However, diminishing the levels of PTP1B compromises its ability to rescue the yeast; thus v-Src was also expressed from a low copy vector and expression was further decreased with the use of the attenuated GALL promoter. This combination yielded the greatest rescue growth while being sensitive to PTP1B inhibitors.

When the system was modified to integrate v-Src in the genome, it was found that the high copy PTP1B gave a much greater window of rescue than the low copy PTP1B. This window was thought to be more critical for the success of the screen than a possible inhibitor resistance resulting from the use of high-copy vectors. Interestingly, streamlining the assay in preparation for the library screen by modifying the growth curves starting material from overnight cultures to direct suspensions of the colonies from

the transformations further increased the rescue window through a reduction in the background growth.

2.4.1 Cell Wall

Mutant yeast strains with deficiencies in cell-wall synthesis were explored to obtain a greater sensitivity to the inhibitors. Using these strains, the optimum quantities of inhibitors that needed to be used to obtain a good effect were determined to be much greater than those required in assays using purified recombinant PTP1B. Although these yeast strains were thought to be advantageous for inhibitor penetrance, their compromised transformation efficiency proved to be a serious obstacle in the establishment of a yeast screen that involved transformation of a library of PTP1B mutants. Since the initial negative assays with the inhibitors in the wild-type yeast were done at low concentrations, a question remained as to the actual contribution of the modified cell wall versus the concentration range used for the inhibitor effect. When the higher concentrations of inhibitors were used in the wild-type yeast they were found to mediate a comparable effect on PTP1B rescue as in the strains with a modified cell wall. Since these mutant yeast strains did not provide an advantageous inhibitor effect and actually presented an obstacle for efficient transformation, they were discarded in favor of a wild-type yeast strain.

The lack of advantage of a porous cell wall was intriguing but trivial since the goal to obtain a robust inhibitor effect for the screen was attained anyway. Nonetheless, upon perusal of literature published later on it seemed that the consensus for loading of small molecules in the yeast had changed from limited entry to active expulsion[222]. In

other words, entry of molecules was still thought to be limited by the cell wall. This characteristic has been stated as an advantage to using yeast for inhibitor screens because it introduced a permeability component in the screen: if the compound can enter the yeast cell then it should enter a mammalian cell[154]. What was later discovered was the major contribution of efflux pumps for compound loading in the cell. Yeast ATP-Binding Cassette MultiDrug Resistant (ABC-MDR) transporters, including *PDR5, SNQ2* and *YOR1,* are broad-substrate specificity pumps that expel xenobiotics from the cell. Mutations in these transporters or in their regulators, *PDR1 and PDR3*, result in increased sensitivity of yeast to a broad range of small molecule drugs[223]. Of interest, the activity of the Pdr5p pump has been found to be modulated by membrane composition[224]. In yeast with a defective ergosterol synthetic pathway, like the *erg6* yeast, the activity of the pump is decreased. In effect, it is thought that the ability of the *erg6* yeast to accumulate drugs may not be solely due to an increase in permeability to the compound but mostly due to a decrease efflux of the compound. So although current suggestion to increase compound loading in the yeast run toward the use of efflux pump mutants, the use of ergosterol mutants is still valid.

In the system described here, the use of *erg6* yeast did not improve inhibitor sensitivity. If the mechanism of hypersensitivity of this mutant is dominated by a reduced activity of an efflux pump, changing the yeast strain to ones currently in fashion might not be useful. Nonetheless, all the members of the MDR pathways have not yet been completely identified and characterized. As such it is possible that a different mutation might be more potent at sensitizing the yeast to PTP1B inhibitors. This would be useful

to bring the dose-response of the inhibitor in the yeast in closer agreement with the data obtained using purified phosphatases.

3. Screening for PTP1B Inhibitor Determinants Using an Integrated v-Src Yeast Strain

3.1. Introduction

The use of designer yeast strain with a modified cell wall was found to reduce transformation efficiencies and did not improve inhibitor loading. v-Src under the control of the GAL promoter was integrated in the LEU2 locus of YPH499 yeast, which has a normal cell wall and good transformation efficiencies. This generated the H2 strain which was dependent on PTP1B for growth on galactose: treating this strain with a PTP1B inhibitor reduced its growth.

A library of PTP1B mutants generated by degenerate PCR conditions was transformed in the H2 strain and assayed for growth on galactose in the presence of a PTP1B inhibitor. The resistant clones were isolated and sequenced to reveal PTP1B inhibitor determinants.

These determinants were expressed and purified for *in vitro* kinetic characterization to confirm the results from the screen. This included determination of their catalytic activity against synthetic substrates and inhibition by a panel of structurally diverse PTP1Binhibitors.

3.1.1. Library Generation

A library of PTP1B mutations was generated by low fidelity PCR. Fidelity of the reaction was lowered using two different approaches: skewed dNTP ratio or a low fidelity polymerase. The rate of mismatch introduction in the sequence was controlled in the first instance through the amount of dGTP, manganese and template used; for the second method, mutation rates were varied only by modulating the amounts of template used. The components, protocols and starting conditions were obtained from commercially available kits: Clontech's Diversify PCR Random Mutagenesis kit or Stratagene's Genemorph Kit.

3.1.2. Vitality [225,226]

HIV proteases have been a target of choice in the design of inhibitors to stop the replication of the HIV virus. In dividing virus populations, inhibitor-resistant protease mutations emerge permitting the virus to still replicate in the presence of the inhibitor. Interestingly, these mutations are not specific for the inhibitor and can also confer resistance to other structurally different inhibitors.

For a mutation to allow viral replication in the presence of the inhibitor it must both prevent inhibitor binding and conserve the enzymatic activity of the protease. This duality is interesting when studying mutations on the bench where the efficiency of the protease and its affinity for the inhibitor can be separately determined by measurement of k_{cat}/K_M and K_i values.

It was found that K_i values alone were not sufficient to predict survival of the mutated virus treated with an inhibitor: a mutation that preserves the catalytic efficiency

of the protease has a selective advantage even though its affinity for the inhibitor is greater than another mutation with a compromised efficiency. The ability to predict how well a mutation will allow the virus to replicate in the presence of the inhibitor therefore depends on both k_{cat}/K_M and K_i values. To reflect this concept, a term called vitality was proposed which combined both the catalytic efficiency of the protease and its affinity for the inhibitor in the equation:

$$\text{Vitality} = (K_i\ k_{cat}/K_M)_{\text{mutant}} / (K_i\ k_{cat}/K_M)_{\text{wild type}}$$

A value of one suggests that the mutation does not affect the ability of the inhibitor to reduce replication of the virus, a value greater than one identifies a mutation that confers inhibitor resistance to the virus.

This concept comfortably translates into the yeast system established here for PTP1B. The screen first identifies mutations in PTP1B that allow the yeast to grow in the presence of v-Src, i.e. mutations that leave the catalytic activity of the phosphatase intact. As a second selection, the screen identifies PTP1B mutations that allow the yeast expressing v-Src to grow in the presence of a PTP1B inhibitor. Like the HIV protease drug-resistant mutants, to obtain growth of yeast, PTP1B mutants must be both catalytically active and have a lowered affinity for the inhibitor.

As an added twist, if an inhibitor is targeted to the active site, as are the PTP1B inhibitors used here, mutations that lower the affinity of the enzyme for that compound are most often located in the active site and therefore are more prone to affect catalytic activity. The design of the screen with the requirement of catalytic activity focuses on

mutations that are either not in the active site or that can differentially affect inhibitor affinity over substrate affinity while leaving the turn-over of the enzyme intact. Vitality values are therefore especially useful in the context of this yeast screen to be able to integrate the two effects of the mutation for comparison with the wild-type enzyme.

3.2. Methods

See Appendix 1 for inhibitor structures and Appendix 2 for primer sequences.

3.2.1. Library Generation

The first library was generated using Clontech's Diversify PCR Random Mutagenesis kit, the primers "mutfwd" and "mutrvrs" and pGAL1416-PTP1B was used as template. The final reaction contained 200μM of each dNTPs with an additional 40μM of dGTP, no manganese, 40mM tricine-KOH pH 8.0, 16mM KCl, 3.5mM $MgCl_2$, 3.75μg/mL BSA and the AdvanTaq Plus™ DNA polymerase. The program and amounts of template and primer used are discussed in the Results section. The product obtained from the PCR reaction was cloned in pCR®2.1 (Invitrogen) which has been engineered with Topoisomerase I covalently bound to the linearized plasmid allowing cloning without the use of ligase or restriction sites. The resulting clones were sequenced with the forward and reverse primers along with ptp6.

The second library was generated using the GeneMorph™ PCR Mutagenesis Kit (Stratagene). This kit relies on a proprietary low fidelity polymerase and variations in the amount of template to introduce random mutation in the PCR product. The final reaction contained 250μg/μL each of the same primer as the first library and the amount of p416GAL1-PTP1B used as template was varied as described in the results. The program of amplification was: 94°C four min, 30 or 25 cycles of 94°C 30 sec, 60°C 30 sec and 72°C one min, and 72°C ten min. An aliquot of the product obtained was cloned in

pCR®2.1 (Invitrogen) and the resulting clones were sequenced with the forward and reverse primers along with ptp6 or ptp8.

In the third library, the primers were modified to permit homologous recombination with the plasmid. The 58-mer "fwdhom" and the 55-mer "rvrshom" were used initially as primers but failed to generate a product. New ~20-mer oligos were designed to align 83 base pairs upstream from the ATG-start codon ("libfout") and 79 base pairs downstream from the TGA-stop codon ("librout"). The degenerate PCR conditions were the same as the second library (100ng template, 25 cycles) with a program of amplification slightly modified to increase the extension time (72°C) from one minute to 1.5 minutes.

3.2.2. Screen I

The colonies obtained from the electroporation of the library (gel cleaned in Fig. 3.1D) along with 1μg of vector in H2 yeast were picked three days later and resuspended in 50μL of 15% glycerol. Duplicate 10μL aliquots of this suspension were used for growth curves with or without inhibitor L-B as previously described.

3.2.3. Screen II

Rapid ligations were performed with the Rapid DNA Ligation Kit from Roche which yields circulized products within five minutes. The reaction was allowed to proceed with 2μg of *Eco*R I/*Sal* I-digested and dephosphorylated plasmid along with a third of the final

library product (see results) for 1.5 hours and directly electroporated into the H2 yeast strain.

Traditional ligation was performed with 200 units of T4 DNA ligase (Invitrogen) in 60mM Tris-HCl pH 7.5, 60mM $MgCl_2$, 50mM NaCl, 1mg/mL BSA, 70mM β-mercaptoethanol, 1mM ATP, 20mM DTT and 10mM spermidine at 14°C overnight using 2μg digested/dephosphorylated plasmid and a third of the final library product (see results). The reaction mixture was directly electroporated in H2 yeast. The colonies obtained from the transformation were assayed for growth and resistance as for screen I but not in duplicate.

3.2.4. Screen III

One hundred nanograms of library generated with homologous tails was transformed using the lithium acetate method along with 1μg of *Eco*R I/*Sal* I-digested and dephosphorylated p426GAL1 vector in H2 yeast. The resulting colonies were resuspended in 40μL of 15% glycerol and aliquoted in 96-well plates containing uracil dropout media supplemented with 4% galactose containing or not 0.75mM inhibitor L-B boosted to 1.25mM after 24 hours. The growth of the clones was monitored by absorbance at 600nm.

3.2.5. Plasmid Retrieval

The plasmid was retrieved from the library clones using the YEASTMAKER™ Yeast Plasmid Isolation Kit (Clontech) in which the cell wall was digested with lyticase and the yeast was lysed with SDS and freeze-thaw cycles. The resulting crude cell extract was

passed through a size exclusion chromatography column (CHROM-SPIN™-1000 DEPC-H_2O) and the resulting low-concentration plasmid solution was used to transform MAX Efficiency® DH5α™ (GibcoBRL 18258-012) chemically competent *E. coli* cells. The plasmid was re-isolated from the bacteria using Qiagen Minipreps. The resulting material was digested with *Eco*R I and *Sal* I to verify the presence of library insert and sequenced using the forward and reverse primers used to generate the library along with the ptp6 oligo.

3.2.6. Subcloning of Identified Clones

The PTP1B mutants were subcloned from the p426GAL1 vector used in the library screen into p416GAL1 or pFLAG2 using *Eco*R I and *Sal* I. The resulting constructs were sequenced using ptp6, ptp7, ptp8 and ptp9 oligos. Clones identified from screen III were sequenced with the additional primers: PA, PB2, PC and PD.

The 1-298 constructs were generated by PCR using 298fwd and 298rvrs as primers, the mutant's respective pFLAG constructs as templates and the program 94°C 2min, 25 cycles of 94°C 30sec, 50°C 30sec, 72°C 1min followed by 72°C 10min. The resulting product was inserted in pCR®2.1 by TA cloning and sequenced. The fragment was retrieved using *Eco*R I and *Sal* I, cloned into digested and dephosphorylated pFLAG vector and sequenced using PA, PB2, PC, PD and PC2.

3.2.7. In vitro *Expression and Characterization of PTP1B* [227]

BL21 *E. coli* bacteria were transformed with a pFLAG2 construct containing the appropriate PTP1B species and expression was induced with IPTG for 3hrs at 27°C. The

cells were harvested by centrifugation, frozen and stored at -80°C. For purification, the pellet was thawed on ice and resuspended in binding buffer (20mM Tris-HCL 7.5, 0.1mM EDTA, 5mM DTT) supplemented with a Complete Protease Inhibitor Cocktail Tablet (Roche) and 10μM phenylmethylsulfonyl fluoride. The cells were lysed using a French press at 18000psi for three passages and centrifugated at 31000g. The lysate was first purified on a HiTrap™ Blue column (Amersham Pharmacia Biotech). This column contains Cibacron blue F3G-A covalently linked to an agarose matrix. PTP1B binds the column by affinity to the Cibacron ligand whose sulfate groups may mimic the phosphate groups of the PTP1B substrate. The enzyme was gradually eluted from the column with high salt buffer (20mM Tris-HCL 7.5, 0.1mM EDTA, 5mM DTT, 2M NaCl). The eluate fractions containing the enzyme were run through a HiTrap™ Q column (Amersham Pharmacia Biotech). This column is an anion exchanger with $N^{+}(CH_3)_3$ covalently linked to the agarose matrix which will bind the negatively charged PTP1B. The eluate fraction containing the enzyme was dialyzed in storage buffer (20% glycerol, 20mM Tris-HCl 7.5, 150mM NaCl, 5mM DTT, 0.1mM EDTA) overnight at 4°C, aliquoted and stored at -80°C.

3.2.8. Kinetics[228]

Purified enzymes were reacted with pNPP, 3,6-Fluorescein DiPhosphate (FDP) or DiFluoroMethylUmbelliferyl Phosphate (DiFMUP) in 50mM Bis-Tris, 2mM EDTA, 2% glycerol, 0.01% triton, 5mM N,N'-dimethyl-bis(mercaptoacetyl)hydrazine, pH 6.3[227]. Product formation was monitored spectroscopically at 405nm for pNPP, 450nm for FDP and by fluorescence at 450nm from 360nm excitation for DiFMUP using a Spectramax

190 (Molecualr devices) or a SpectraMax Gemini (Molecular Devices). Michaelis-Menten parameters and turnover number were obtained by fitting initial rates to the Michaelis-Menten equation using the non-linear regression analysis package Grafit 4.0.10 (Eraticus Software Inc.).

IC_{50} values were obtained from initial rates of the reaction of wild-type or mutant PTP1B with FDP or DiFMUP at concentrations corresponding to the K_M of the respective phosphatase mutant in the presence of inhibitor, fitted to a four-parameter inhibition curve.

K_i values were obtained for L-B and BzN-EJJ-amide using pNPP by fitting the data to the equation: $v_i = [S]\ V_{max} / (K_M(1 + I/K_i) + [S])$ using Grafit (Eraticus Software).

Vitality values were calculated using the equation presented in the Introduction. K_i values were obtained from IC_{50} values which are equal to twice the K_i when measured at K_M.

3.3. Results

3.3.1. Generating the Library

Random mutations were introduced in PTP1B using a degenerate PCR reaction to create a library of PTP1B mutants. The composition and the components for this PCR reaction were provided by the Diversify™ PCR Random Mutagenesis Kit which uses high dGTP levels to lower the fidelity of the Taq polymerase. The primers used introduced *Sal* I and *EcoR* I restriction sites in the PCR fragment to facilitate eventual cloning.

The conditions for the reaction were optimized to obtain a mutation rate closest to one mutation in the coding sequence of PTP1B (960bp for amino acids 1 to 320). The starting recommended conditions resulted in a very low yield (Fig. 3.1A). To increase the yield, the concentration of primers was increased from 10μM to 50μM and template concentration was also increased from 1ng to 25ng. In addition, the program of amplification was changed from the recommended 94°C 30 sec, 25 cycles of 94°C 15 sec and 68°C one min, and 68°C one min to a program previously used successfully to amplify PTP1B: 94°C four min, 25 cycles of 94°C 15 sec, 55°C 15 sec and 72°C one min, and 72°C seven min. Modifying the primer and template content did not alter the yield much but the modified program did bring the yield up to the control levels provided by the kit (Fig. 3.1B). The library generated with the recommended primer and template concentration but with the modified program was cloned in pCR®2.1 and sequenced to determine the mutation rate. Out of the 15 clones sequenced, eight were wild types, two had only one mutation in the coding sequence, three clones had two and one clone had three mutations.

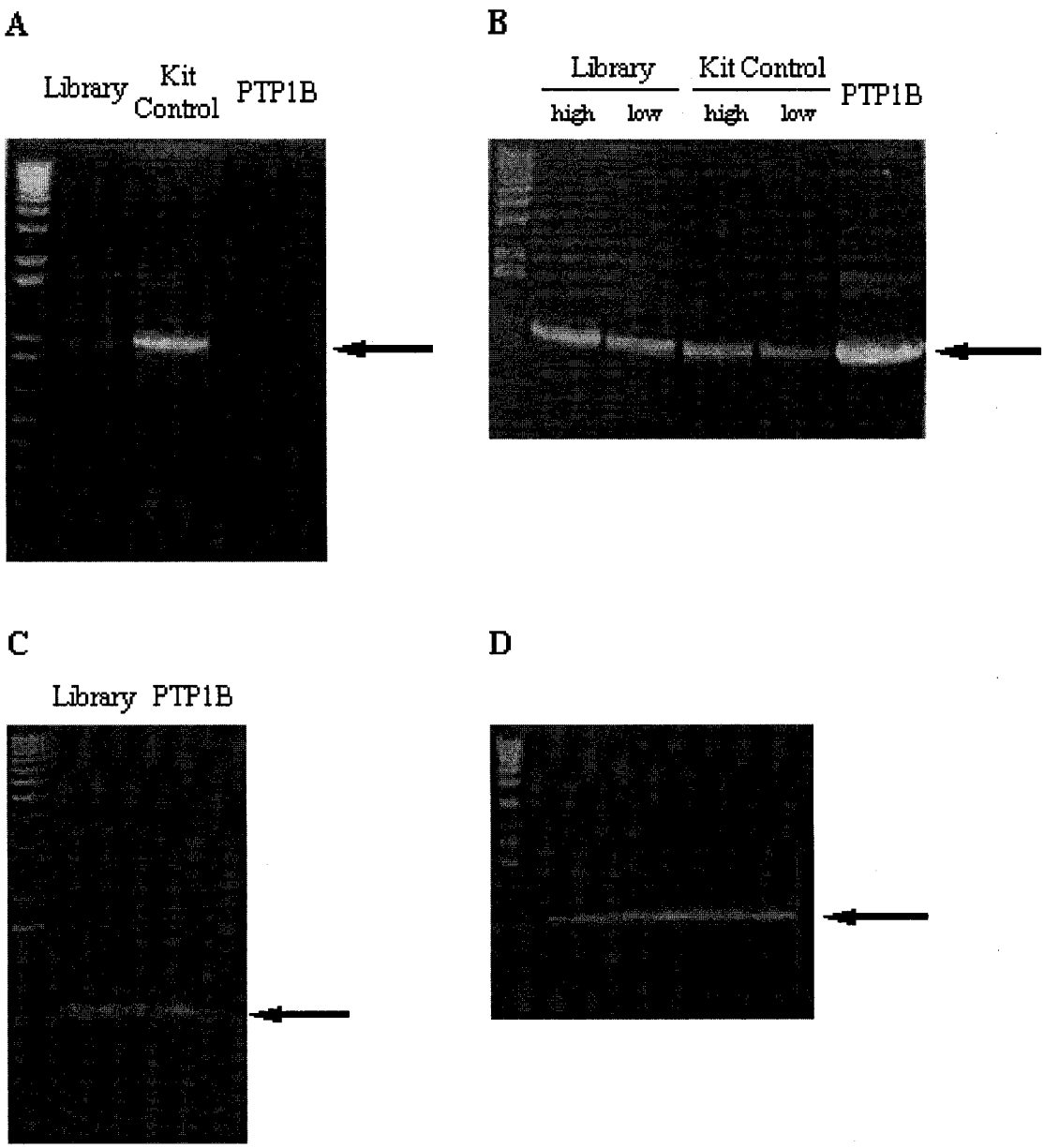

Figure 3.1: Initial conditions for generations of the library using the Diversify™ kit needed to be modified to obtain good yields. TBE gels of PCR reactions using different conditions: A) suggested by manufacturer, B) using a program previously successful for PTP1B amplification and either "high" (50μM primers and 25ng template) or "low" (10μM primers and 1ng template which is suggested by the manufacturer) amounts of reaction components, C) as per manufacturer but a program of amplification closer to the one used for PTP1B, D) same as C but with 100ng of template. "Library" refers to a reaction performed with skewed dGTP content, "Kit Control" is a reaction performed with primers and template provided by the manufacturer and skewed dGTP amounts, "PTP1B" refers to a reaction performed under the same conditions as the library but using normal amounts of dGTP.

Although the modified program increased the yield of the reaction, to reconcile with the manufacturer's recommendations, another reaction was performed using a program closer to the suggested conditions: 94°C four min, 25 cycles of 94°C 30 sec, 68°C two min, and 68°C seven min. This gave adequate yields (Fig. 3.1C) and a mutation distribution of three wild types, one single, five double, one triple and one quintuple. To reduce the mutation rate, a fourth permutation using 100ng of template instead of 1ng gave a library with a mutation distribution of 16 wild types, nine singles, four doubles and one quintuple. A large quantity of library was generated using this final condition, gel cleaned (Fig. 3.1D) and digested with *Sal* I and *Eco*R I. The mutational data for the different conditions is displayed in graph form in Figure 4.7.

3.3.2. Screen I

Ligation of complementary ends generated by restriction digest was used to insert the library in the expression vector. The expression vector, p426GAL1, was digested with *Sal* I and *Eco*R I and de-phosphorylated. The resulting linear vector was co-transformed with the digested library in the H2 strain. Ligation of the library fragment and the expression vector relied on the yeast's own repair machinery.

H2 yeast transformed by electroporation with 2.5μg of the linearized vector alone yielded 32 colonies. The number of colonies obtained was increased tenfold (348 colonies) when 0.5μg of wild-type PTP1B PCR product was digested and included in the transformation, 320 colonies were obtained when the amount of linearized vector was reduced to 1μg and 24 colonies for 0.25μg. For comparison, 1μg of uncut vector yielded 390 colonies.

The digested library (0.5μg) was electroporated into the H2 yeast along with 1μg of linearized vector. This resulted in only 21 colonies whereas yeast transformed with the linearized vector alone resulted in two colonies. Although the yield was very poor, the 21 colonies were picked and their growth on galactose assayed in the presence or absence of 0.75mM of L-B boosted to 1.25mM after 24 hours. The inhibitor treatment was not toxic to the yeast as shown in Figure 3.2 where yeast grew equally well with or without L-B when glucose was provided as the non-inducible carbon source. None of the clones grew on galactose except clone #7 which was also resistant to the effect of the inhibitor (Fig. 3.3). The lack of growth on galactose indicated that the clones had either recirculized the plasmid without incorporating a library fragment or that the mutation abolished the activity of PTP1B. Clone #7 did integrate a library fragment (Fig. 3.4A) and sequencing revealed one mutation: C884T, which translated to a change at position 295 from a serine to a phenylalanine (Fig. 3.4B).

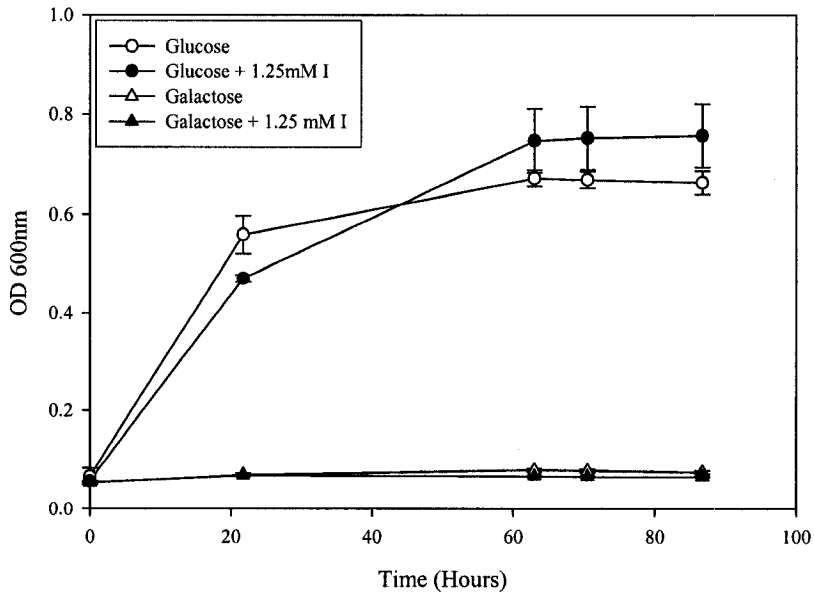

Figure 3.2: Treatment of yeast with the inhibitor is not toxic to the yeast. H2 yeast were grown in glucose or galactose and treated with or without 0.75mM L-B boosted to 1.25mM after 24 hours. Error bars are standard deviation n=3.

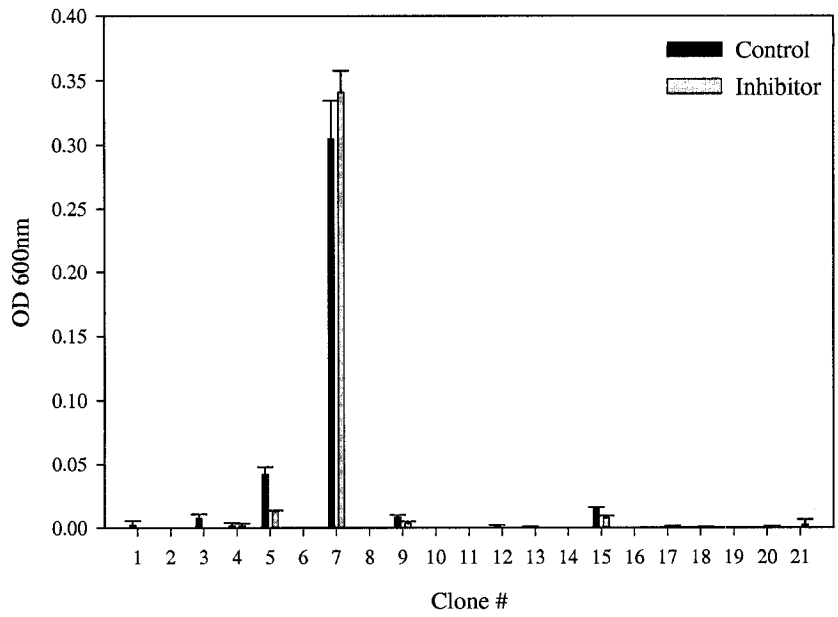

Figure 3.3: Clone #7 is resistant to the effect of the L-B inhibitor. The absorbance after 86 hours of growth was measured for the 21 clones obtained from screen I. Black bars indicate control growth in the absence of the inhibitor; grey bars are the growth in the presence of 0.75mM L-B boosted to 1.25mM after 24 hours. Error bars are standard deviation n=2.

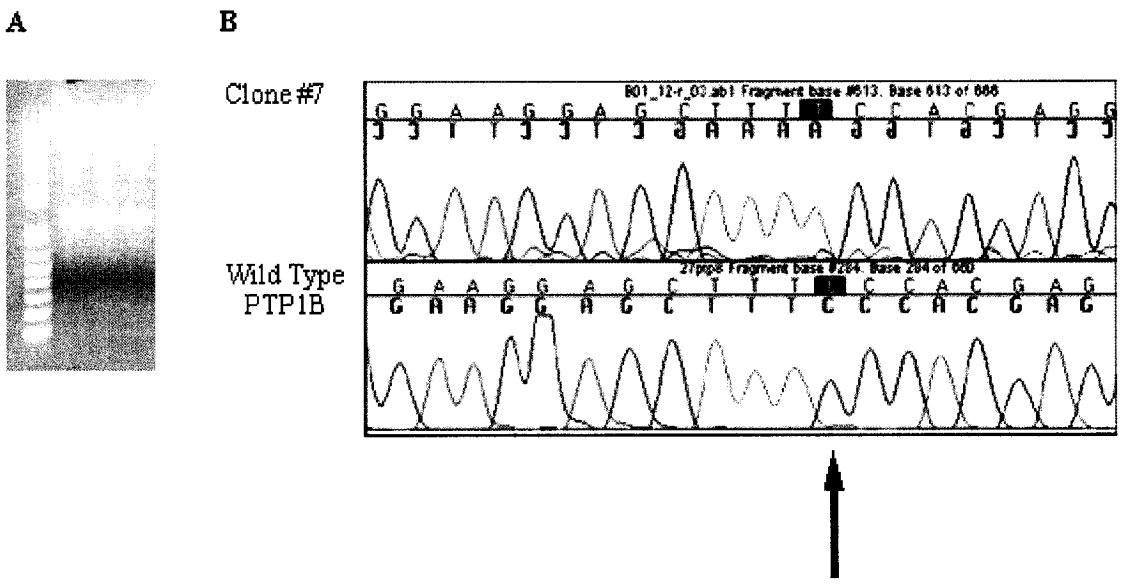

Figure 3.4: The plasmid retrieved from the resistant clone #7 contained a library fragment with a mutation at position 884. A) TBE gel of the retrieved plasmid (in triplicate) digested with *Eco*R I and *Sal* I to release the library fragment. B) Chromatogram of the sequencing reaction for clone #7 (top) versus the wild-type PTP1B (bottom).

3.3.3. S295F

To confirm resistance, the S295F mutant was reintroduced in the H2 strain. The mutant had the same efficiency of rescue as the wild-type enzyme but treatment with the inhibitor did not reduce the rescue as it did for the wild-type enzyme (Fig. 3.5).

Although primary characterization of the H2 strains was positive, further work using this strain revealed an inherent instability in its behavior. For example, the H2 strain should not grow on galactose but five out of a total of 28 growth curves measured over time displayed growth on galactose. More worrisome was the unreliability of the rescue mediated by PTP1B: 16 of the 28 curves measured displayed a very low rescue or very delayed. This variation in the rescue complicated the interpretation of inhibitor effects or PTP1B activity.

S295F could show resistance to inhibition in the H2 strain but the inherent variability of that strain warranted confirmation with a more stable system. The mutant was subcloned into the low copy vector p416GAL1 and growth curves were generated in the YPH499 wild-type strain. Here again S295F was as good as the wild-type PTP1B to rescue yeast from v-Src lethality and treatment with an inhibitor attenuated the rescue mediated by the wild-type PTP1B but not the mutant (Fig. 3.6).

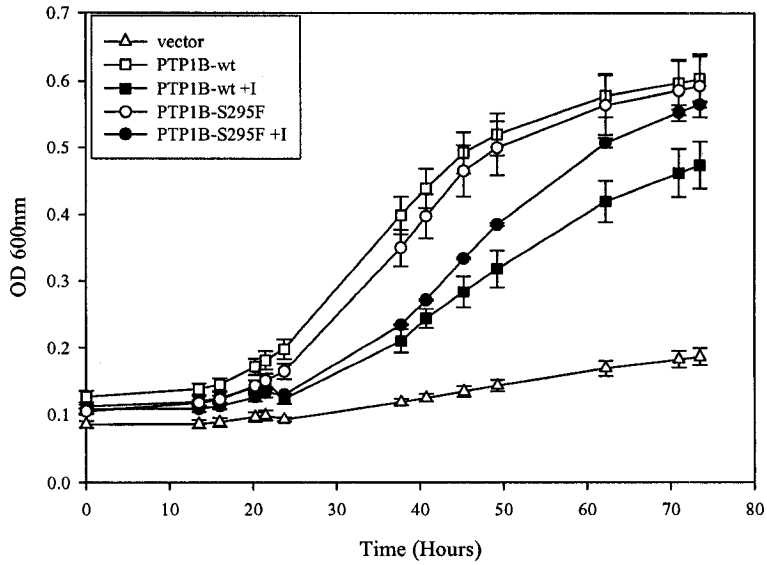

Figure 3.5: The PTP1B inhibitor-resistant mutant S295F allows the H2 yeast to grow on galactose in the presence of inhibitor. H2 yeast were transformed with p426GAL1 (vector), p426GAL1-PTP1B (PTP1B-wt) or with the retrieved plasmid from clone #7 (PTP1B-S295F). The resulting transformants were resuspended in 15% glycerol and their growth on galactose was measured in the presence of 0.75mM L-B boosted to 1.25mM after 24 hours.

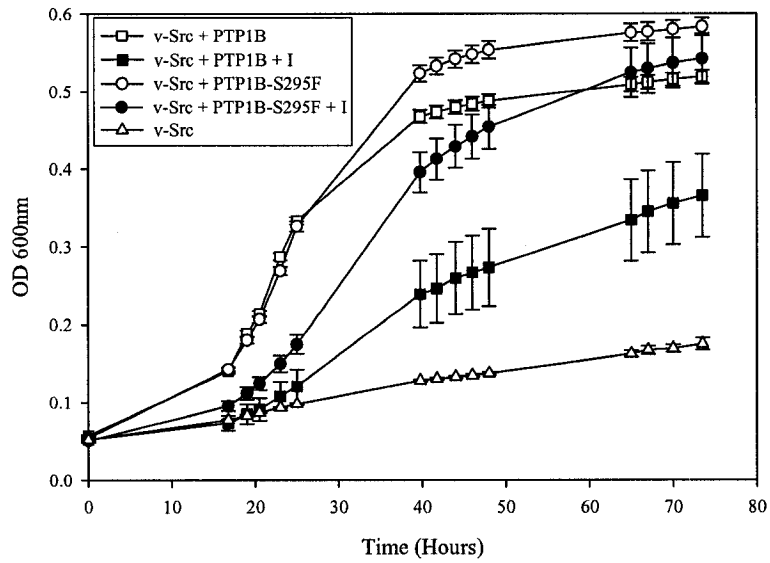

Figure 3.6: The PTP1B inhibitor-resistant mutant S295F allows YPH499 yeast expressing v-Src to grow in the presence of a PTP1B inhibitor. YPH499 yeast were co-transformed with p415GALL-v-Src and p416GAL1-PTP1B (v-Src + PTP1B) or p415GALL-v-Src and p416GAL1-PTP1B-S295F (v-Src + PTP1B-S295F) or p415GALL-v-Src and p416GAL1 (v-Src). Growth curves were measured in the presence (+I) or absence of 0.75mM L-B.

To further characterize its inhibitor resistance, the S295F mutant was subcloned in the pFLAG2 bacterial expression vector, expressed in bacteria and purified to >90% purity (Figure 3.7). This purification method yielded 6 to 15mg of purified protein starting from a one liter bacterial culture.

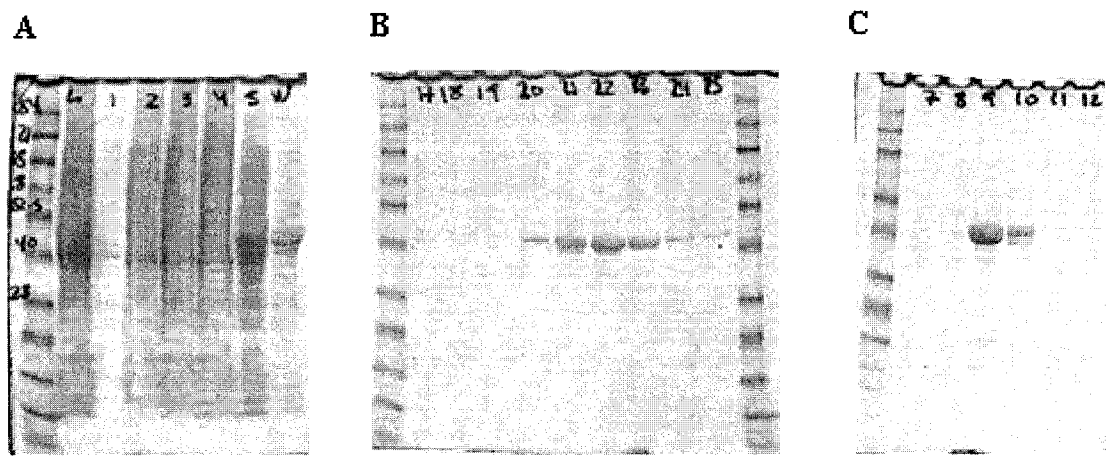

Figure 3.7: PTP1B purified from a crude bacterial extract. PTP1B-S295F mutant was expressed in *E. coli* and purified using both an affinity and an ion exchange column. Aliquots of the fractions eluting from the purification columns where analysed by SDS-PAGE and Coomassie stain: A) the lysate (L) loaded on the column along with the first fractions containing the flow through for the HiTrap™ Blue column, B) the specific fractions from the affinity-selection HiTrap™ Blue column that contained PTP1B and C) the final purified fraction obtained from the anion exchange HiTrap™ Q column.

The catalytic constants of the mutant were measured for the hydrolysis of two substrates: pNPP and FDP. Results shown in Table 3.1 reveal that compared to the wild-type enzyme, the mutant had a lower affinity for pNPP and a lower turnover number for both pNPP and FDP. The inhibitor resistance of the mutant was tested by measuring IC_{50} values for a panel of structurally diverse PTP1B inhibitor (Table 3.2). When assayed on the mutant, all the inhibitor profiles were found to be right shifted resulting in a threefold increase in IC_{50} values. Furthermore, K_i values were measured for the two inhibitors L-B

and BzN-EJJ-amide using pNPP as substrate; Lineweaver-Burke plots in Figure 3.8 demonstrate the competitive nature of these two inhibitors. L-B was found to have a K_i of $0.10 \pm 0.02\mu M$ on wild-type PTP1B and $0.69 \pm 0.09\mu M$ on the mutant. A similar shift was observed for BzN-EJJ-amide from $3.4 \pm 0.2nM$ on the wild-type to $20.2 \pm 0.6nM$ on the mutant.

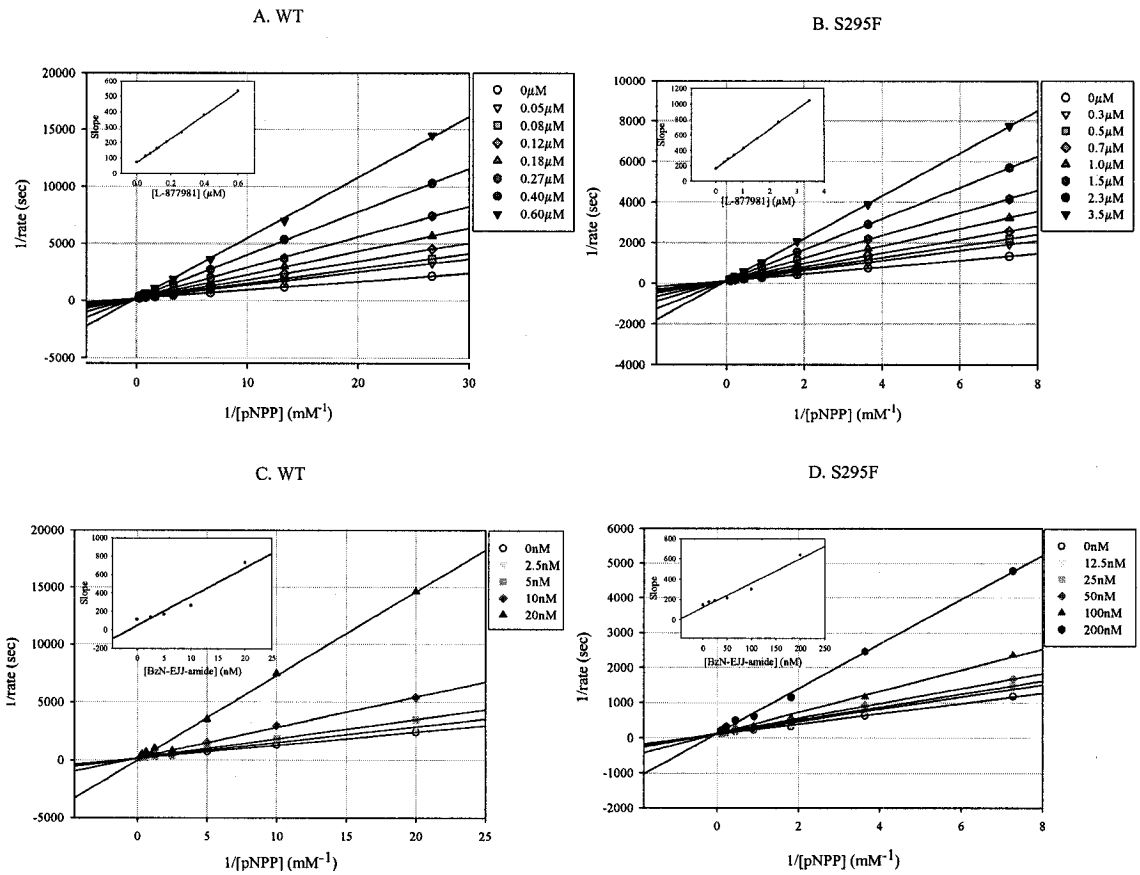

Figure 3.8: L-B and BzN-EJJ-amide are competitive inhibitors on both the wild-type and the S295F mutant PTP1B. Lineweaver-Burke plot for the inhibition of the wild-type PTP1B (WT) and the S295F mutant by L-B (A. and B.) and BzN-EJJ-amide (C. and D.). All lines pass through the origin and the secondary plots are linear indicating a competitive mechanism.

Table 3.1: Kinetics properties of purified wild-type and mutant S295F PTP1B for the hydrolysis of pNPP and FDP.

	pNPP			FDP		
	k_{cat} (sec^{-1})	K_M (mM)	k_{cat} / K_M	k_{cat} (sec^{-1})	K_M (μM)	k_{cat} / K_M
Wild Type	45 ± 3	0.38 ± 0.02	1.2×10^5	2.0 ± 0.3	19 ± 3	1.1×10^5
S295F	18 ± 1	1.1 ± 0.1	1.6×10^4	0.41 ± 0.04	15 ± 2	2.7×10^4

Error is standard error n = three to seven.

Table 3.2: IC_{50} values (nM) of a panel of seven competitive inhibitors for purified wild-type or mutant S295F PTP1B using FDP as substrate.

	Wild Type	S295F	Wild Type / S295F
L-F	79 ± 11	270 ± 12	3.6 ± 1.3
L-G	114 ± 25	367 ± 47	3.5 ± 1.1
L-H	235 ± 36	918 ± 93	4.1 ± 1.2
L-B	431 ± 71	1614 ± 186	4.0 ± 1.5
L-I	137 ± 20	488 ± 64	3.8 ± 1.5
L-J	9 ± 1	29 ± 2	3.6 ± 1.4
BzN-EJJ-amide	14 ± 2	43 ± 3	3.4 ± 1.1

Error is standard error n=3 for the IC_{50} values and standard deviation n=3 for the ratio.

3.3.4. Improved Library Generation

To improve the yields of the PCR that generates the insert library, a low fidelity polymerase was used to drive the mutation instead of skewed dNTP ratios. In this instance, the mutation rate is controlled by the amounts of template included in the reaction. This method is commercialized by Stratagene in their "Genemorph PCR mutagenesis" kit.

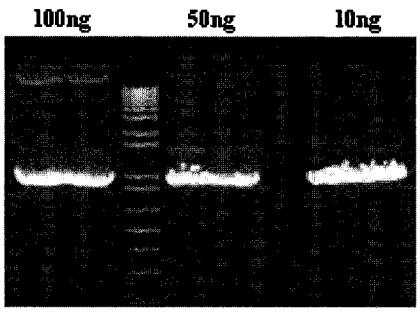

Figure 3.9: Using a low fidelity polymerase to generate the library gives good yield for all template amounts used. TBE gel of the PCR product generated using 100, 50 or 10ng of template with the Genemorph conditions.

Mutation rates were obtained for 30 cycles of amplification using ten, 50 and 100ng of template. All three conditions resulted in a very high yield compared to the Diversify™ kit (Fig. 3.9). The mutation rates obtained were ten nanograms: one triple, two quadruples and one quintuple; 50ng: two wild types, three singles, two doubles, one triple and one quadruple; 100ng: one single, three doubles, two triples, one quadruple, one quintuple. To lower the mutation rate, the number of amplification cycles was reduced to 25; 100ng of template yielded a mutation rate of five wild types, eight singles, two doubles, one triple, one quadruple and two quintuples. See Figure 4.7 for a diagram of the mutational rate data.

Three separate reactions using these final conditions were pooled, gel cleaned, digested with *Eco*R I and *Sal* I and used as the library material to transform the H2 strain for the screen.

3.3.5. Screen II

Since the previous library transformation had generated so few colonies, it was thought that prior ligation of the library to the vector might increase the yield of the

transformation. Rapid ligation was performed on the new library with the digested de-phosphorylated vector. The resulting reaction mix was then electroporated in the H2 strain: only one colony was obtained. Thinking the rapid ligation protocol might not have been sufficient, a new reaction was run overnight using fresh ligase and electroporated in H2 resulting in 47 colonies.

These colonies were picked, resuspended in glycerol and aliquoted in 96-well plates containing media with or without 0.75mM of L-B. The inhibitor treatment was boosted to 1.25mM 24 hours later. Only six clones were able to grow on galactose: 41, 20, 14, 16, 21 and 38 (Fig. 3.10). The inhibitor was able to reduce the growth of these clones but since a wild-type control was not included in the screen, a reduced sensitivity to the inhibitor could not be established right away. The clones were re-introduced in H2 but proved to lack resistance compared to the wild-type and S295F PTP1B (Fig. 3.11). The plasmids were retrieved from the six clones and sequenced revealing only two mutants: P302S (clone 41) and I307T (clone 21).

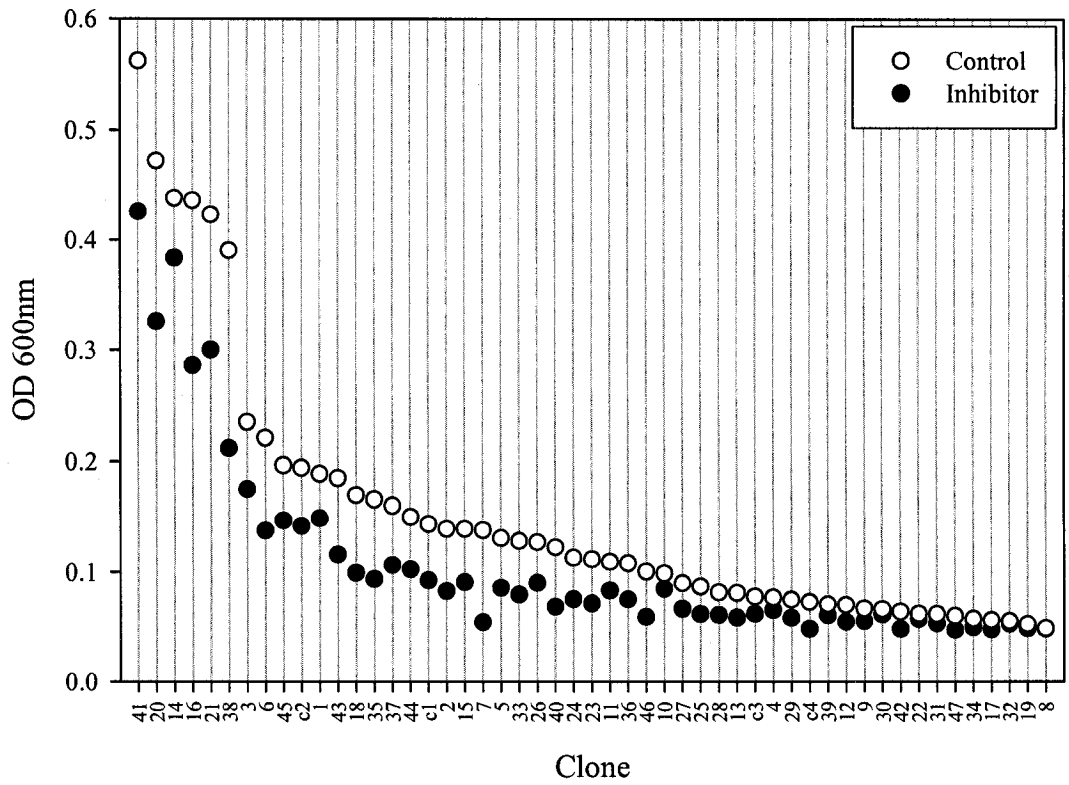

Figure 3.10: Screen II yielded six clones able to rescue yeast from v-Src lethality. Growth of the 47 clones obtained from the library transformation in H2 yeast after 51 hours in the presence or absence of 0.75mM L-B boosted to 1.25mM after 24 hours. Clones c1, c2, c3 and c4 are H2 yeast transformed with the vector alone as library controls.

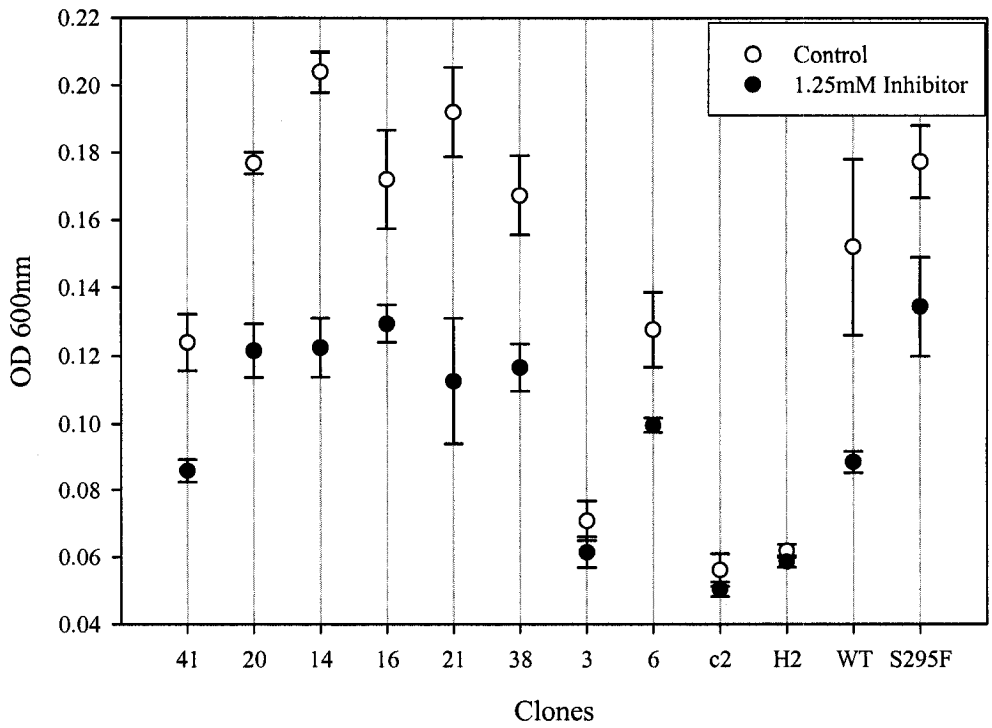

Figure 3.11: The clones that showed catalytic activity in screen II proved to lack frank inhibitor resistance when compared to the wild-type and the S295F mutant PTP1B. H2 yeast were electroporated with the plasmids retrieved from the library clones of screen II, p426GAL1 (H2), p426GAL1-PTP1B (WT) or p426GAL1-PTP1B-S295F (S295F) and the absorbance at 600nm was measured after 49 hours of growth in the presence or absence of 0.75mM inhibitor boosted to 1.25mM after 24 hours. Error bars are standard deviation n=3.

3.3.6. Screen III

It was realized that an overlooked advantage of working with yeast was the possibility of using homologous recombination to join the library to the expression vector. A new library was generated replacing the restriction site used for complementary ligation with a stretch of 55 base pairs homologous to the vector sequence where the library needed to be inserted. A degenerate PCR reaction using p416GAL1-PTP1B as template and 58mers primers coding in the vector sequence yielded no products. The primers were replaced with standard 24mers designed to initiate amplification 60 base pairs from the start and

end of the PTP1B coding sequence. This yielded a library of mutant PTP1B with 5' and 3' tails of sequence homologous to the yeast expression vector. Using the same degenerate conditions as optimized for screen II yielded a mutation rate of five wild types, one single, four doubles and two quadruples.

The persisting low yield of the library transformation was identified to also be caused by the transformation protocol itself and not only the material being transformed. Electroporation and the lithium acetate methods were first compared in Egr6 yeast. A double transformation of *erg6* yeast with 4μg of each plasmid yielded more colonies by electroporation (511 colonies) than the same using lithium acetate (113 colonies). Although this experiment did give an indication of the most efficient method to prepare yeast dependent on PTP1B activity, it was not an exhaustive comparison of the two methods. This was done in the H2 yeast strain, using a gradient of DNA concentration and varying the voltage of the electroporation or the length of the 42°C lithium acetate incubation. By exploring the extended parameters of the two methods, it was found that for H2 yeast, electroporation yielded 100 times less colonies than the lithium acetate method (Table 3.3).

H2 yeast were transformed with the new homologous library using the lithium acetate protocol with a 45 minutes incubation at 42°C instead of the 15 minutes used previously. One thousand four hundred and forty-two colonies were picked from the ~150 000 transformants obtained and grown in galactose media with or without 0.75mM L-B, boosted to 1.25mM after 24 hours.

Table 3.3: Transformation efficiency of H2 yeast using electroporation *versus* the lithium acetate method.

	Voltage (kV)	# transformants / μg DNA
Electroporation	1	∅
	1.5	4×10^2
	2	4.9×10^3
	Incubation Time at 42°C (minutes)	# transformants / μg DNA
Lithium Acetate	15	1.9×10^4
	30	9.96×10^4
	45	4.37×10^5

A "hit" was defined as a clone that grew on galactose and that displayed at least 77% of the control growth in the presence of the inhibitor. To compare, wild-type PTP1B included in the screen as a control was able to grow on galactose and that growth was reduced to 43% of the control in the presence of the inhibitor. Plasmids were retrieved from the 88 hits along with seven clones that appeared hypersensitive to the inhibitor. Table 3.4 shows the sequencing results for 77 of the selected clones. Interestingly, none of the mutations were located in catalytic loops, some clustered together such as P31R, S55R and H54Q, Q127R, M133I, E136K, N139I, L163H, L163R, Q166E and T168I as well as Q290L, Q290R and L294H. Most striking was the high incidence of false positives, clones with either silent mutations or none at all: 30 out of 77 clones.

Table 3.4: Nucleotide mutations and associated amino acid change in 71 resistant and *six hypersensitive* clones identified in screen III.

Clone	Nucleotide	Amino Acid	% of control growth
6-514	G22A (C949T)	E8K	86
4-5	A67T	I10F	172
5-144	T58A	Y20N	88
5-357	G76A	E26K	91
6-213	C92G (C720T)	P31R	79
6-65	T162A	H54Q	83
6-171	T165A	S55R	261
5-505	A182T (T540A)	Q61L	90
6-157	C260A	P87H	86
6-24	A313T	R105W	753
5-268	C328T (G870A)	L110F	77
4-28	T356C (C813T)	L119S	136
5-156	A380G (C525T)	Q127R	91
5-292	C251T G406A	T84I E136K	112
6-352	T221C G399A C929G	M74T M133I P310R	86
5-149	(G264A) C272T A416T A743G	T91I N139I K248R	106
4-17	C503T	T168I	83
6-350	(G15A) C126A C496G	N42K Q166E	95
6-348	C461G	T154R	86
6-253	A578G	N193S	104
5-198	T593G	V198G	88
5-533	C791T (C921T)	A264V	88
5-2	A869T	Q290L	82
6-204	(A453G) A869G	Q290R	93
6-52	T881A	L294H	97
6-267	(G750A) C926T	P309L	1112
5-673	A78T A250G (C783A)	E26D T84A	85
6-538	A107T (C252T) A837C	K36M K279N	81

	(A924G)		
5-261	C113A T551C	P38H V184A	90
6-212	A334G (C543T) C562T (C909T)	R112G P188S	91
6-19	C683T A717T	A228V K239N	84
5-588	(T171A) C665T G847T	S226F G283W	90
6-260	G306T A309T C566A A869G	Q102H K103N A189D Q290R	84
5-249	G22A (G51A) G193A T221A G817A A899G (C918T)	E8K D65N M74K A273T E300G	123
5-422	55_56insT (A197T C720T)	Y20L then PGYPT stop	106
5-158	A121del	N42K then TEIGTETSVPLTIVGLNYIKK IMTISTLV stop	100
5-160	C304T (A511T)	Q102stop	88
6-147	G300T C372G	W100C Y124Stop	85
5-529	C353T A359T T431A	S118L K120I L140stop	86
5-241	G508T (C531A C559A C948T C956T)	E170stop	103
5-235	T546del (C624del T758C)	F182L then ESLNHQPHS stop	84
5-205	C595T	R199Stop	98
5-437	T488A G741del	L163H, V249C L250C L251stop	99
5-321	T917del	I306T then PHLPGHPNESWSHTENStop	78
6-492	(C138T A590G)		92
5-291	(G396A)		182
6-542	(C657T C960T)		90
6-258	(T751C)		79
4-57	(G777A)		81
5-737	(C783T)		97
5-41	Wt		92
5-99	Wt		126
5-101	Wt		112
5-102	Wt		105
5-245	Wt		92
5-535	Wt		79

5-571	Wt		94
5-722	Wt		94
6-2	Wt		90
6-41	Wt		228
6-42	Wt		337
6-60	Wt		85
6-163	Wt		90
6-244	Wt		116
6-252	Wt		85
6-342	Wt		120
6-392	Wt		97
6-394	Wt		94
6-486	Wt		95
6-496	Wt		102
6-540	Wt		90
5-272	*C232G*	*Q78R*	*24*
6-194	*(C372T) T488G*	*L163R*	*9*
5-313	*(C402T) C862T*	*Q288Stop*	*25*
5-675	*(G747A)*		*7*
5-634	*(C795T)*		*26*
6-530	*Wt*		*7*

% of control growth refers to absorbance at 600nm after 67 hours in the presence of inhibitor *versus* control growth. Nucleotide mutations in parentheses are non-coding, Wt = wild type.

3.3.7. Characterization of Resistant Clones

The resistant clones were reintroduced in H2 to confirm their resistance. Again, H2 proved extremely unpredictable: for ten out of the twelve attempts, the control grew too weakly on galactose to permit a clear inhibitor effect easily quantifiable for comparison.

Since the validity of the hits could not be confirmed, a few clones were selected based on the sequencing data to be subcloned in a low copy vector for testing in the

YPH499 yeast and also subcloned in pFLAG2 for bacterial expression. The chosen clones contained single coding mutations: P31R, H54Q and S55R because of their spacial clustering, Q290L, Q290R and L294H because of their location on the same helix as S295F, L119S because of previous unpublished data from Dr. E. Asante-Appiah and P309L because it is part of the proline-rich region involved in SH3-domains binding. Kinetic constants along with inhibition profiles were measured for the purified enzymes using DiFMUP. Table 3.5 shows that the activity of the mutants are similar to the wild type with Q290R being slightly higher. The affinity of the mutants for the substrate was however more varied: P31R and S55R had the least affinity along with H54Q and S295F. These affinity values agreed with the purification data where S55R, with the highest K_M, required an extra purification step through a heparin column, in addition to the Cibacron Blue and the Q columns, to reach adequate purity whereas P31R did not. P309L had such a lowered affinity for substrate that it did not bind the column during purification by affinity selection with Cibacron blue or heparin.

Inhibitor profiles for a panel of seven inhibitors (Table 3.6) were also right shifted for these same mutants: S55R followed by S295F and P31R. H54Q and L294H had somewhat raised IC_{50} values two- and 1.7-fold respectively above the IC_{50} values obtained for the wild type. Q290R and Q290L were not significantly shifted. Interestingly, L119S had an increased IC_{50} value only for L-E and L-F. It was found that only these two contained a ketone group positioned to interact with residue 119 resulting in repulsion from the hydroxyl group of the serine residue of the mutant. This specificity of resistance was not seen in the other mutants which displayed the same magnitude of reduced inhibition by all of the seven structurally different inhibitors.

Table 3.5: Kinetics properties for the hydrolysis of DiFMUP by purified wild-type and mutants PTP1B in the context of the amino acids 1-320 or truncated to 1-298.

		k_{cat} (sec^{-1})	K_M (μM)	k_{cat} / K_M ($\times 10^6$)
1-320	Wt (14)	29 ± 1	5.2 ± 0.2	5.6
	P31R (2)	25 ± 1	18.0 ± 0.7	1.4
	H54Q (6)	23 ± 1	7.7 ± 0.3	2.9
	S55R (6)	26 ± 2	24.3 ± 1.7	1.1
	L119S (3)	27 ± 2	3.9 ± 0.2	7.0
	Q290R (3)	38 ± 1	5.9 ± 0.2	6.4
	Q290L (2)	33 ± 0.6	4.7 ± 0.4	7.0
	L294H (6)	26 ± 2	5.9 ± 0.2	4.5
	S295F (10)	34 ± 2	11.1 ± 0.4	3.1
1-298	Wt (5)	31 ± 0.6	6.1 ± 0.1	5.0
	H54Q (3)	26 ± 2	8.1 ± 0.2	3.2
	S55R (3)	25 ± 0.2	26.8 ± 0.8	0.9
	L294H (3)	26 ± 3	6.2 ± 0.2	4.1
	S295F (3)	22 ± 1	9.3 ± 0.2	2.3

Wt = wild type. Error is standard error, n number indicated in parentheses.

Table 3.6: IC_{50} values (nM) of a panel of seven competitive inhibitors for purified wild-type or mutant PTP1B using DiFMUP as substrate.

	L-E	L-F	L-H	L-B	L-I	L-J	BzN-EJJ-amide
Wt	82 ± 5	321 ± 16	232 ± 11	285 ± 13	157 ± 13	2.2 ± 0.1	3.7 ± 0.2
P31R	339 ± 63	1060 ± 59	1008 ± 39	1333 ± 145	677 ± 45	14 ± 2	20 ± 2
H54Q	185 ± 16	664 ± 29	454 ± 11	565 ± 57	315 ± 19	4.5 ± 0.2	6.8 ± 0.8
S55R	685 ± 171	2219 ± 87	1397 ± 218	2260 ± 59	1201 ± 8	13 ± 2	33 ± 6
L119S	117 ± 19	683 ± 96	166 ± 32	189 ± 19	105 ± 7	1.50 ± 0.03	3.0 ± 0.4
Q290R	85 ± 9	329 ± 6	247 ± 10	297 ± 35	155 ± 29	2.3 ± 0.5	3.7 ± 0.1
Q290L	65 ± 6	305 ± 22	156 ± 8	230 ± 38	122 ± 7	2.1 ± 0.2	3.0 ± 0.2
L294H	138 ± 3	471 ± 35	472 ± 53	517 ± 17	266 ± 7	3.6 ± 0.2	5.9 ± 0.4
S295F	399 ± 32	1266 ± 133	1285 ± 134	1644 ± 125	779 ± 71	11 ± 2	18 ± 1
Wt 1-298	128 ± 8	411 ± 24	364 ± 1	455 ± 11	233 ± 9	3.1 ± 0.2	5.9 ± 0.2
L294H 1-298	130 ± 2	423 ± 4	408 ± 8	427 ± 9	246 ± 3	3.2 ± 0.1	5 ± 1
S295F 1-298	342 ± 14	1086 ± 44	1067 ± 28	1400 ± 16	673 ± 4	8.6 ± 0.2	15.7 ± 0.1

Wt = wild type, 1-298 denotes truncation from 1-320. Error is standard error n = 2, except Wt n = 7, S295F and L294H n = 4. Q290L standard deviation n = 3.

The mutants that were found to be resistant to the inhibitor were also the same mutants with a shifted K_M. Since the inhibitors were substrate mimetics targeted to the active site, it was thought that the observed resistance was a non-specific lowered affinity of the mutants for active site ligands in general. Vitalities were calculated and only S295F along with L119S for the ketone inhibitors showed a clear increased vitality (Table 3.7). S55R, which showed the most shifted IC_{50} values, gave low vitalities indicating that its resistance to the inhibitor was probably due to a general disturbance of

the enzyme affecting its catalytic efficiency. This was also the case for P31R which had displayed comparative IC_{50} values to the S295F mutant.

Table 3.7: Vitality values of mutant PTP1B using wild-type PTP1B 1-320 as reference (vitality =1) for a panel of seven inhibitors and DiFMUP as substrate.

	L-E	L-F	L-H	L-B	L-I	L-J	BzN-EJJ-amide
P31R	1.0	0.8	1.1	1.2	1.1	1.6	1.4
H54Q	1.2	1.1	1.0	1.0	1.1	1.1	1.0
S55R	1.8	1.3	1.1	1.5	1.5	1.2	1.7
L119S	1.8	2.7	0.9	0.8	0.8	0.9	1.0
Q290R	1.2	1.2	1.2	1.2	1.1	1.2	1.2
Q290L	1.0	1.2	0.8	1.0	1.0	1.2	1.0
L294H	1.3	1.2	1.6	1.5	1.4	1.3	1.3
S295F	2.7	2.2	3.1	3.2	2.7	2.8	2.7
Wt 1-298	1.4	1.2	1.4	1.4	1.3	1.3	1.5
L294H 1-298	1.2	1.0	1.3	1.1	1.2	1.1	1.1
S295F 1-298	1.7	1.4	1.9	2.1	1.8	1.7	1.8

When the mutants were reintroduced in YPH499 yeast, their ability to rescue the v-Src phenotype was correlated with their measured catalytic efficiency (Table 3.8). The ability of the inhibitor to reduce the rescue by the clones identified in screen III was variable from experiment to experiment (Table 3.9) and did not agree with the vitality data. In comparison, the S295F mutant, included in these experiments as a control, was consistently more resistant than respective wild-type controls. Since the S295F mutant gave the highest vitalities it might be concluded that to get robust inhibitor resistance in the yeast requires a certain vitality threshold which the other mutants had not reached.

Table 3.8: Ability of mutant PTP1B to rescue the growth of YPH499 yeast expressing v-Src correlated with catalytic efficiency.

	k_{cat} / K_M ($\times 10^6$)	% Normal Growth	% Wild-Type Rescue
S55R	1.1	53	73
P31R	1.4	68	88
H54Q	2.9	71	89
P309L	ND*	83	93
S295F	3.1	90	106
L294H	4.5	94	101
Wt	5.6	92	100
Q290R	6.4	117	107
Q290L	7.0	114	104
L119S	7.0	147	153

*Not Determined: P309L does not bind the Cibacron blue or heparin affinity purification columns.

% Normal Growth is absorbance at 600nm after 80 hours of growth setting growth of yeast expressing only the PTP1B mutant at 100% and yeast expressing only v-Src at 0%.

% Wild-Type Rescue is absorbance at 600nm after 80 hours of growth setting the growth of yeast co-expressing v-Src and wild-type PTP1B at 100% and yeast expressing v-Src alone at 0%.

Table 3.9: Three separate experiments measuring the % growth of YPH499 yeast co-expressing v-Src and various PTP1B mutants after 80 hours in the presence of 1.5mM L-B.

	Sept 23rd 2002	Sept 30th 2002	Oct 21st 2002	Average
wt	43	77	29	49
L119S	27			27
L294H	53		26	40
S55R	64		32	48
H54Q	50		82	66
Q290L		57		57
Q290R		66		66
P309L		72		72
P31R		54	63	59
S295F		93	50	71

% growth was calculated by setting growth of yeast co-expressing v-Src and the PTP1B mutant in the absence of inhibitor as 100% and the growth of yeast expressing v-Src alone as 0%.

The mutants were truncated from 320 amino acids to 298 to further investigate the mechanism of resistance of the mutants by X-ray crystallography. This truncation was necessary for proper crystal formation. In addition for mutants S295F and L294H, conservation or loss of resistance upon truncation would narrow the possible mechanisms by eliminating or confirming participation of the amino acids C-terminal to the last X-ray-resolvable helix. Kinetic characterization revealed no drastic changes by truncation (Table 3.5). The right shift in IC_{50} values was conserved with the truncation of S295F and L294H (Table 3.6) but the vitality values were slightly decreased (Table 3.7). Interestingly, truncation of the wild type slightly raised its IC_{50} values while leaving the catalytic activity intact thereby resulting in a slight increase in vitality compared to the 1-320 wild-type enzyme.

3.4. Conclusions

Screen III was an improvement over the other screens because of the increased number of transformants obtained from the library but resulted in a high proportion of false positives. Nonetheless, some of the clones were chosen rationally to be expressed in bacteria and purified for kinetic studies.

L119S shifted the IC_{50} values of only two of the seven inhibitors tested. This was unique to this mutation as the others mutants studied shifted IC_{50} values non-specifically for all the inhibitors. This mutation also stood out because of its slightly lowered K_M value, again counter-current with all the other mutations studied. L119 has been shown to interact with some inhibitors by providing a hydrophobic patch for phenyl substituent[134]. K120, in addition to providing the aliphatic part of its side chain for Van der Waals interactions with naphthalene scaffolds, also uses its side-chain amino group to engage it in cation-pi interaction[133]. In different inhibitor structures, the side-chain nitrogen of K120 can also participate in hydrogen bonding with carboxylate groups[133]. Based on this information, L119 would be an expected inhibitor determinant for certain inhibitor structures. In effect, the inhibitors shifted by this mutation are the only ones to contain a ketone group oriented towards that residue. However, the potency of the inhibitor used in the screen (L-B) was not shifted by this mutation and therefore should not have been selected for by the screen. Therefore, L119S along with the other silent mutation was a false positive in the screen.

S55R, P31R and H54Q were selected because of their spatial clustering. Kinetic analyses revealed that, although distant from the active site and not in direct contact with

the substrate, these residues were able to affect the catalytic efficiency of the enzyme. In the yeast system, this lowered efficiency was clearly translated in a lowered ability to rescue the v-Src phenotype. These residues have not been identified in the literature as participating in the catalytic mechanism or in substrate recognition. However, serine 50, which is relatively close to that cluster, has been shown to decrease catalytic efficiency when mutated to an alanine or when phosphorylated[94]. The selected mutations were also able to shift the IC_{50} for all seven inhibitors tested, without any indication of a preference for one structure over another. As opposed to S295F, their vitalities were not high enough to allow a robust inhibitor-resistance phenotype when they were reintroduced in the yeast. Here again, although the mutations were revealed to be false positives they uncovered unexpected contributions to the activity of the PTP1B enzyme.

P309L displayed a much reduced affinity for active site ligands as seen from its inability to bind affinity purification columns and a correlated reduced ability to rescue the v-Src phenotype in yeast. The only mutations identified from screen II were also in the same region of the enzyme: P302S and I307T. The validity of these mutations in screen II were questioned based on their non-reproducibility and the high rate of false positives and again in screen III. Although this cast a valid doubt on their participation in inhibitor binding, from the behavior of the P309L mutant, this region of the enzyme might be involved in general catalysis or substrate recognition. Of interest, this proline-rich region has been implicated in binding of SH3-containing protein[33].

Although the number of transformants obtained was very low, screen I was successful in identifying one inhibitor determinant: Serine 295. Mutation of this position to phenylalanine allowed growth of the yeast in the presence of inhibitor, did not affect

enzyme efficiency and right-shifted the potency of a panel of structurally diverse inhibitors. This mutation was a useful comparison for the clones identified in screen III: its robust inhibitor resistance set the bar to eliminate false positives that might otherwise be subject to discussion.

L294H, Q290L and Q290R were chosen to be further studied based on their location on the same helix as S295F. L294H was not as resistant as the S295F mutation and the 290 position proved to be equivalent to the wild type. This indicated that location on the same helix was not enough to mediate inhibitor resistance. Upon examination of the crystal structure, it was found that the serine side chain at position 295 pointed inward to occupy a pocket formed by the α3 helix, α7 helix and the β9-β10 loop. The 295 side chain hydroxyl group formed one H-bond with Asn193 (on the α3 helix) itself forming H-bonds with Tyr152 (on the β9-β10 loop) and Glu297. L294H pointed upward from the α7 helix, its side chain not displaying any H-bonding but still within 4Å of Ala189 located on the α3 helix. The 290 position pointed further out from the enzyme interacting only with its neighbors on the α7 helix.

Truncation of the enzyme from 1-320 to 1-298, in effect terminating right after the α7 helix, did not abolish the resistance of the S295F mutation. This truncation ruled out propagation through the C-terminal residues. Propagation through the N-terminal residues would be unlikely given the lack of effect of mutation at positions 294 and 290: N-terminal and proximal to residue 295.

There is the possibility that the residue at position 295, 21Å away from the active site cysteine residue, by specifically disturbing the network of interaction in the α3-α7-

β9β10 pocket could affect the enzyme's inhibitor sensitivity. If this were the case, a successful screen was expected to identify more determinants in that region.

4. Screening for PTP1B Inhibitor Determinants Using a Wild-Type Yeast Strain and a Potent Inhibitor

4.1. Introduction

Screening for PTP1B inhibitor determinants using L-B and v-Src integrated in the genome revealed that determinants that could both preserve the activity of the enzyme yet protect against inhibition completely avoided the active site and its immediate region. Serine 295, which is located 21Å away from the active site, was the only inhibitor determinant identified from the screens.

Screen III addressed the poor transformation efficiencies of screen I and II but revealed a high proportion of false positives. Using a more potent inhibitor and changing the expression of v-Src could address these issues. Both commercial and internal inhibitors were assayed in the system to identify a more potent inhibitor than L-B used in the previous screens and a new transformation protocol was devised which preserved transformation efficiency while keeping v-Src on a plasmid.

In addition to these modifications, the library used was modified to include the last 80 C-terminal amino acids of PTP1B.

4.1.1. Commercially Available PTP1B Inhibitors

Suramin is a reversible competitive inhibitor of tyrosine phosphatases[229]. The compound binds to PTP1B with a 1:1 stoichiometry, locates to the active site and displays an IC_{50} of 5μM[215].

Phenyl arsine oxide is an oxidizing agent that reacts specifically with vicinal dithiols which has been shown to bind to PTP1B with an EC_{50} of 2μM; this binding can be abolished by mutating the active site cysteine to a serine residue[215]. It has been implicated in the IR signaling pathway as having a tyrosine phosphatase inhibitory effect[230-238].

Benzyl phosphonic acid is a non-hydrolysable structural mimetic of phosphotyrosine and has been used as a weak competitive inhibitor with a K_i of 4.6mM[239]. In the same fashion that vanadate inhibits tyrosine phosphatase, molybdate being also a transition metal ion can mimic the transition state of the reaction; the reported K_i value of molybdate on PTP1B is 3.7μM[212].

4.1.2. Screening PTP1B Amino Acids 1-320 versus 1-400

The extra 80 residues spanning the C-terminal region are mostly charged and contain sites for serine phosphorylation (S352, S386 and S378). Phosphorylation of these sites has been proposed to alter the activity of PTP1B. Cleavage by calpain in this region seems to release the catalytic domain from C-terminal inhibition and increases its activity. This C-terminal region also contains one of the two proline-rich regions found outside the catalytic domain of PTP1B (386-397), the first one (301-315) known to mediate the interaction with the SH3 domain of p130cas. These 80 residues are often

overlooked as the 1-320 and 1-298 constructs seem most popular in the literature; their inclusion in the screen might reveal them to play a role in inhibitor binding.

4.2 Methods

See Appendix 1 for inhibitor structures and Appendix 2 for primer sequences.

4.2.1. 1-400 Construct

PTP1B 1-400 was amplified from the full length (1-435) (Courtesy M. Reece) construct using the primers "400fwd" and "400rvrs" and the program 94°C 4min, 25 cycles of 94°C 30sec, 50°C 30sec and 72°C 1.5min followed by 72°C 10min. The resulting PCR product was inserted in the pCR®2.1 vector by TA cloning and sequenced with the primers used for the amplification along with oligos PA, PB2, PC2 and PD. The fragment was digested from the pCR®2.1 vector using *Eco*R I and *Sal* I, ligated with digested and dephosphorylated p416GAL1 and sequenced using oligos PA, PB2, PC, PD, libfout and librout. The full length sequence was found to contain the polymorphism G1112A (R371K).

4.2.2. Sequential Transformation

Yeast were electroporated with one plasmid and plated on single dropout plates. The same dropout media containing 4% glucose is inoculated with the resulting colonies for an overnight culture which is used to start the exponential cultured used for the lithium acetate transformation of the second plasmid.

For screen IV, p415GALL or p415GALL-v-Src was first electroporated in YPH499 yeast. After two days of growth, 50mL of leucine dropout medium was

inoculated with the resulting transformant for an overnight growth. The resulting culture of yeast transformed with p415GALLv-Src was re-transformed, using the lithium acetate method, with the library, along with 1ug of p416GAL1 vector linearized with *Eco*R I and *Sal* I and de-phosphorylated. In addition, an aliquot of that culture was also transformed with p416GAL1 and p416GAL1-PTP1B as controls. As additional controls, p416GAL1 and p416GAL1-PTP1B were electroporated in the yeast carrying the p415GALL plasmid. All permutations were plated on double dropout containing glucose.

For screen V, YPH499 yeast were also electroporated with p415GALL or p415GALLv-Src. After two days of growth, 50mL of leucine dropout medium was inoculated with the resulting transformant for an overnight growth. The resulting culture of yeast transformed with p415GALLv-Src was re-transformed, using the lithium acetate method, with the library, along with 1μg of p416GAL1 vector (linearized with *Eco*R I and *Sal* I and de-phosphorylated), and plated on leucine and uracil drop out plates with 2% galactose and 0.075% glucose. The addition of trace glucose increases the transformation efficiency[156] without repressing expression from the GAL promoters. An aliquot of the transformation was also plated on double drop out plates with 2% glucose to monitor the number of transformants obtained. As controls, yeast transformed with p415GALLv-Src were also re-transformed with p416GAL1PTP1B(1-400) or p416GAL1PTP1B(1-320) or p416GAL1PTP1BS295F(1-320) and plated on double drop out plates with galactose and trace glucose or with p416GAL1 and plated on double dropout plates with glucose. For additional controls, yeast transformed with p415GALL was electroporated with p416GAL1 or p416GAL1PTP1B(1-400) and plated on double drop out plates with 2% galactose and 0.075% glucose.

4.2.3. Resistance Assay

The resulting colonies from the double transformation were picked after three, four or five days of growth on the agar plates and suspended (~0.2μL) in 50μL of 15% glycerol in the 60 center wells of round bottom 96-well plates. 10μL of this suspension was transferred to the center wells of a flat bottom 96-well plate containing 190μL of leucine and uracil drop out media with 2% galactose and 0.75mM of inhibitor L-O. The wells were overlaid with mineral oil, incubated at 30°C and the absorbance at 600nm was read periodically. The leftover glycerol suspension was stored at -80°C.

4.2.4. Plasmid Retrieval

Plasmids were retrieved from a three-milliliter overnight culture inoculated with the glycerol stock, treated for one hour with 50 units of lyticase (Clontech) and purified with Qiaprep spin minipreps (Qiagen) with the additional step of five minutes of vortexing with 250μL of 400-500 micron glass beads after addition of the P1 buffer. Larger yields of DNA used for sequencing were obtained by transforming DH5α max *E. coli* cells with the material obtained from the yeast extraction and re-isolating the plasmid. These were digested with *Eco*R I and *Sal* I to confirm the presence of a library fragment and sequenced using PB2, PC2 and PE.

4.3 Results

4.3.1. A better Inhibitor

Screen III was a definitive improvement from the previous screens mainly because of the greater number of transformants obtained. However, the quality of the screen was poor as seen from the large number of false positives. This lack of stringency might have been the result of not using enough inhibitor. The concentration used in the screen was chosen to be effective in reducing wild-type growth but not too excessive to cause yeast toxicity or to miss subtle resistant clones. Tabulating all L-B response curves collected over two years revealed significant variability. Figure 4.1 shows the spread of the L-B inhibitor response obtained from 14 different experiments; in six experiments, not included in Figure 4.1, the inhibitor affected the controls or did not elicit a response. Given this variability, the concentration of inhibitor used in the screen might not have been high enough to select for true resistance. The source of this variability was thought to be due to the characteristics of the inhibitor molecule: IC_{50} values for this inhibitor are right shifted in the presence of BSA and affected by ionic strength.

The unpredictable behavior of L-B made it unreliable to screen for resistant mutants. A different inhibitor needed to be identified that was potent in this yeast system, that was not sensitive to the composition of the growth media and that showed low toxicity to be able to confidently use stringent concentrations without non-specific effects cropping up. The available synthesized amounts were still a limiting factor in the choice of inhibitors because of the large amount of inhibitor required for the screen: screen III

used 180mg of inhibitor not including previous characterization and following confirmation.

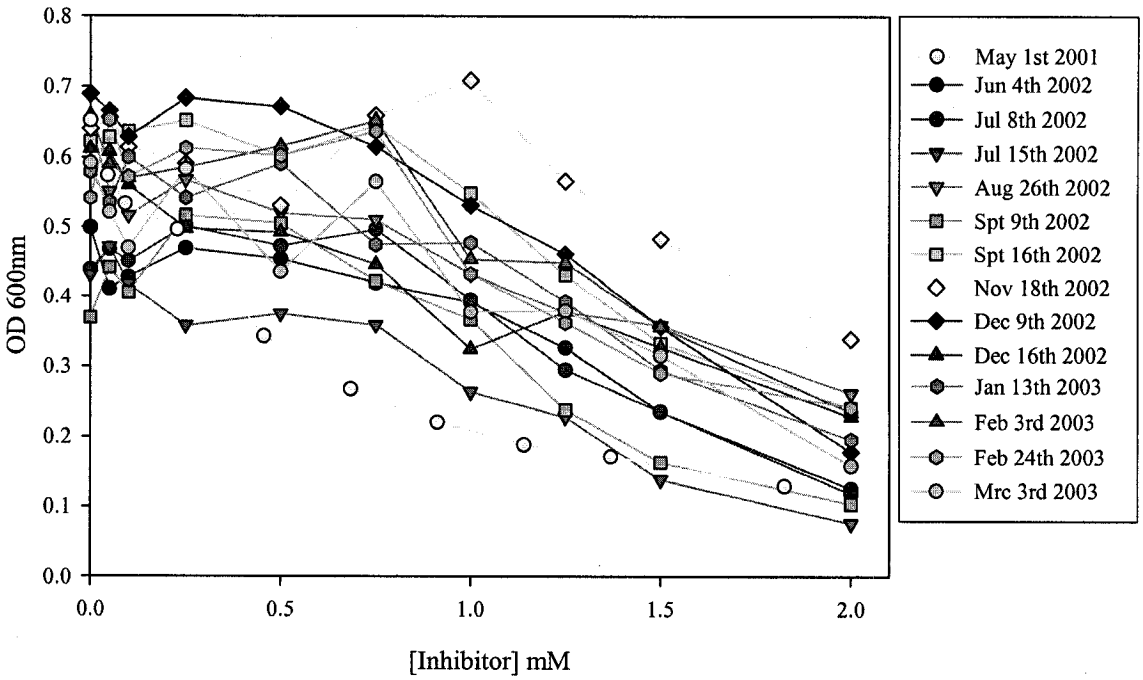

Figure 4.1: The rescue mediated by PTP1B in YPH499 yeast is sensitive to the L-B inhibitor but is subject to much variability. YPH 499 yeast were co-transformed with p415GALL-v-Src and p416GAL1-PTP1B and grown in the presence of varying concentrations of L-B and the absorbance at 600nm after 68 hours of growth was measured. Response curves are shown for 14 separate experiments.

Figure 4.2 and 4.3 show the results of all the inhibitors tested. The results are shown as three curves plotting absorbance of the yeast culture at one given time point over amount of inhibitor. The top curve is generated by the positive control: yeast expressing PTP1B alone. If the compound is toxic, this top curve will slope downwards with increased inhibitor concentration. The negative control, yeast expressing only v-Src, generates the bottom curve. This curve sets the lower limits and can give indication of non-specific actions of the inhibitor. The third curve, which should run between these

two controls, is generated by yeast co-expressing PTP1B and v-Src. If this rescue curve is sensitive to the inhibitor it will join the positive control curve in the absence of inhibitor and steadily decrease with increasing inhibitor concentrations to finally join with the negative control curve. The perfect inhibitor should give a graph looking like an inverted "Z": flat on top and bottom with a connecting curve.

Known phosphatase inhibitors, available in sufficient quantities from commercial sources, were assayed in the yeast system: suramin, phenylarsine oxide, molybdate, phenylphosphonic acid and benzylphosphonic acid (Fig. 4.2). None of these compounds had a specific effect on the rescue of yeast and all showed toxicity when concentrations were used above: 5μM for phenylarsine oxide, 4mM for both phenylphosphonic acid and benzylphosphonic acid and 1.25mM for molybdate. Although the response for suramin was variable, it too showed toxicity when assayed up to 12mM.

Ten inhibitors synthesized at Merck Frosst were selected to be assayed based on their abundance, inhibitory efficiency and water solubility: L-K, L-L, BzN-EJJ-amide (re-assayed at higher concentrations), L-I, L-M, L-N, L-O, L-P, L-F and L-Q. L-R and L-S were not active against the purified recombinant PTP1B and were included as controls. Figure 4.3 shows the three-curve graphs for these inhibitors along with L-B for comparison.

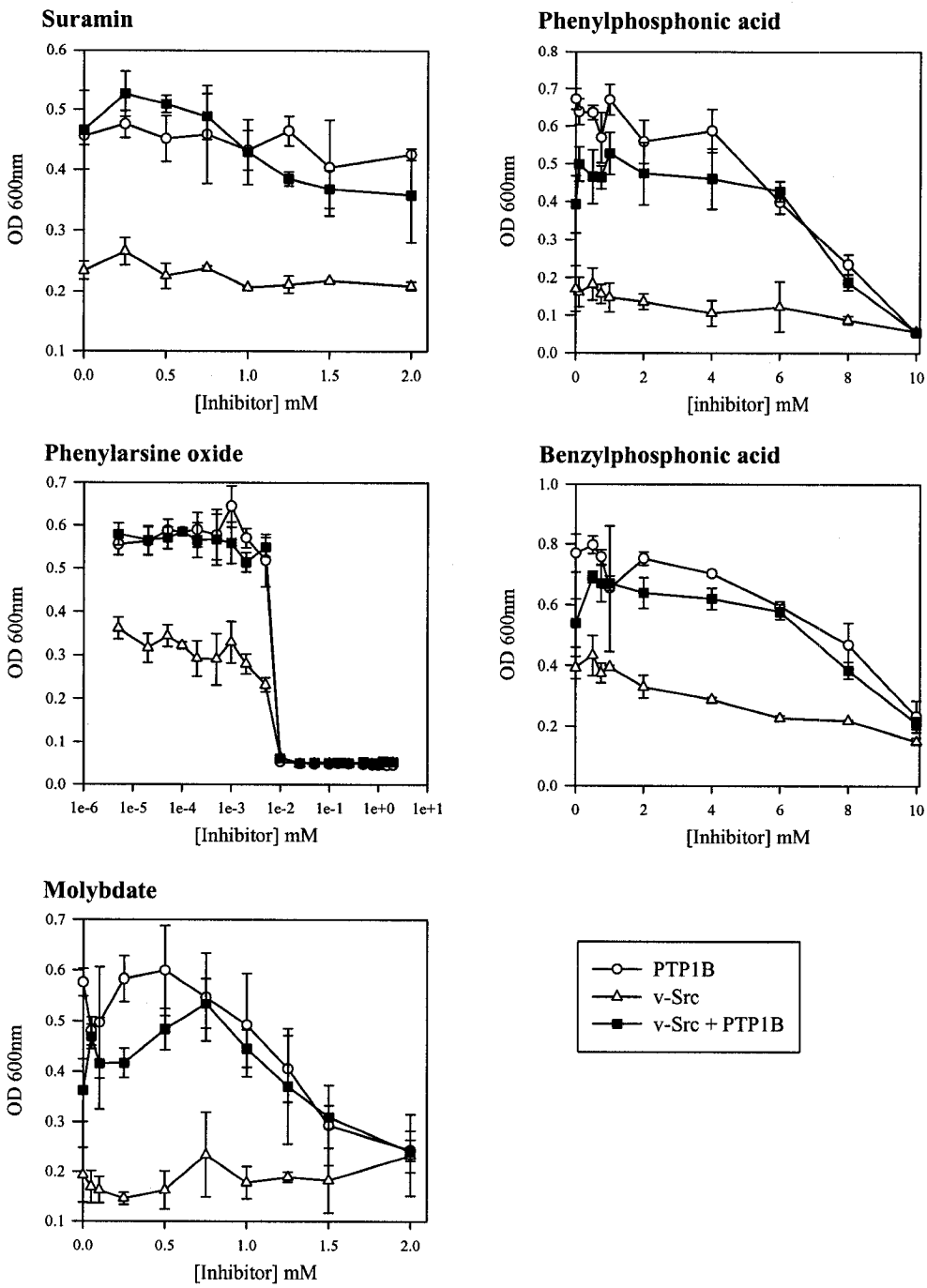

Figure 4.2: The few commercial PTP1B inhibitors tested did not affect the rescue of yeast co-expressing v-Src and PTP1B. YPH499 yeast were co-transformed with p415GALL and p416GAL1-PTP1B (PTP1B) or p415GALL-v-Src and p416GAL1 (v-Src) or p415GALL-v-Src and p416GAL1-PTP1B (v-Src + PTP1B) and grown for 68 hours in the presence of increasing concentrations of different inhibitors. Error bars are standard deviation n=3.

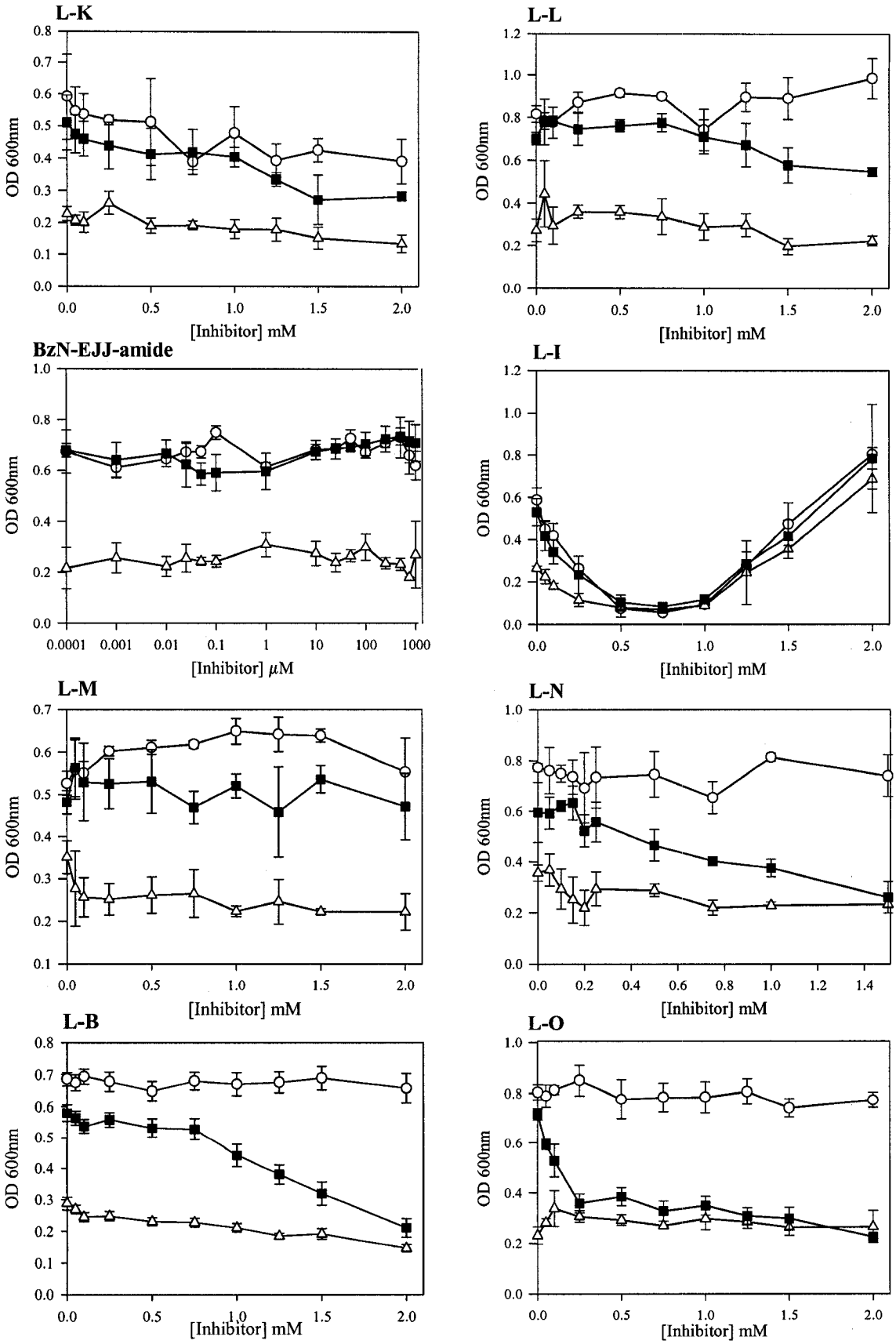

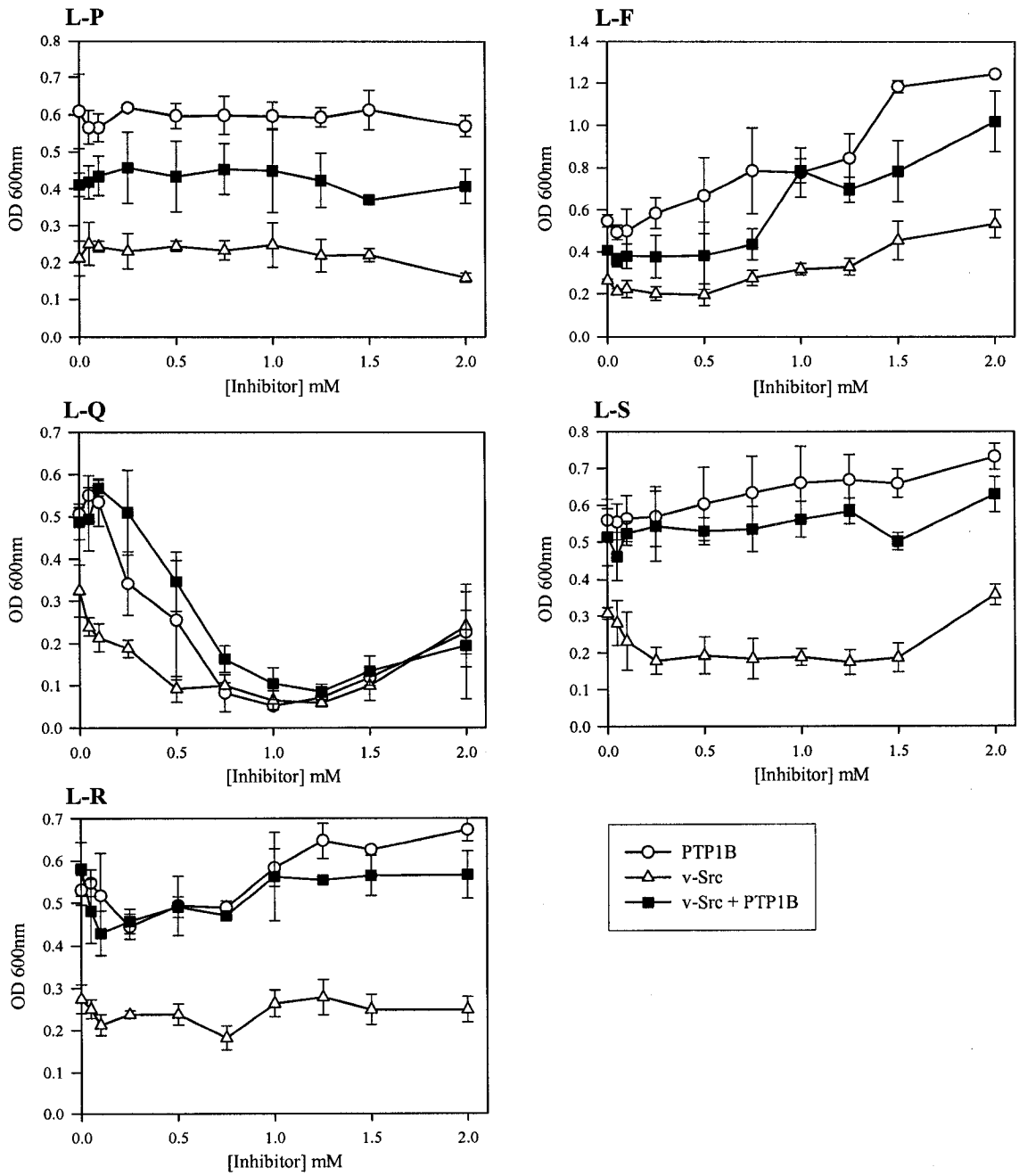

Figure 4.3: Only a few in-house PTP1B inhibitors can lower the rescue of yeast co-expressing v-Src and PTP1B while still remaining non-toxic and assay-friendly. YPH499 yeast were co-transformed and assayed as in Figure 4.2. Error bars are standard deviation n=3. The data for inhibitor L-B was included for ease of comparison and consists of the average of 14 different dose-response experiments with error bars standard error n=14.

Inhibitor L-F precipitated at high concentration therefore non-specifically increasing the turbidity of the cultures. L-Q was toxic to the yeast above 0.25mM. L-I showed both toxicity and precipitation of the compound at higher concentrations. The rest of the inhibitors displayed well-behaved controls with or without an effect on the rescue of the yeast. The control inactive inhibitors did not have an effect in the yeast, thereby confirming the specificity of the inhibitor effect; for example: removing the ortho bromine from L-B to give L-R abolished the potency of the inhibitor in the yeast system to agree with the data on purified recombinant enzyme.

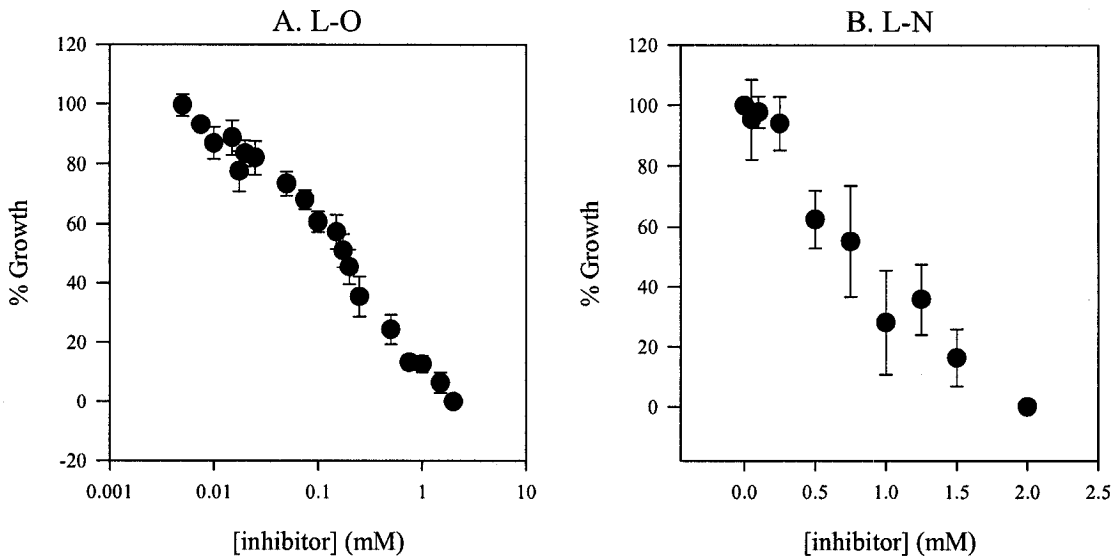

Figure 4.4: Two more PTP1B in-house inhibitors were found to dose-dependently lower the rescue of yeast co-expressing v-Src and PTP1B. YPH499 yeast were transformed as in Figure 4.2 and the growth in the presence of the inhibitor measured after 68 hours. % Growth refers to the resulting absorbance at 600nm normalized to 100% in the absence of inhibitor and 0% in the presence of 2mM inhibitor. Error bars are standard error n=6 for L-O and n=3 for L-N.

Surprisingly, inhibitors that were found to be most potent on purified recombinant PTP1B were not active in the yeast system: L-K, L-L and BzN-EJJ-amide. The only three inhibitors that were successful in the yeast (L-O, L-N and L-B) turned out to be the

smallest and least charged (EC_{50} curves shown in Figure 4.4): the results are summarized in Table 4.1 where the inhibitors have been ordered by increasing molecular weight. Of interest, these same inhibitors active in the yeast system are the only ones that have shown oral bioavailability in mice[240].

Table 4.1: Rank order potency of PTP1B inhibitors in yeast follows molecular weights and not IC_{50}s obtained for the purified enzyme.

	MW	Charge	IC_{50} (nM)	Yeast (EC_{50})
L-O	396.1	-2	133	0.17 ± 0.03mM
L-R	467.2	-2	13270	No effect
L-N	495.4	-2	123	0.9 ± 0.1mM
L-B	501.6	-2	129	1.2 ± 0.2mM
L-Q	543.2	-2	329.5	Toxic
L-S	551.2	-2	4105	No effect
L-I	557.3	-2	44	Precipitates
L-P	570.3	-2	186	No effect
L-M	619.2	-4	83	No effect
L-F	633.5	-2	209	Precipitates
L-K	667.2	-4	7	No effect
L-L	763.5	-4	8	No effect
BzN-EJJ-amide	804.6	-5	8	No effect

IC_{50} were measured using FDP as substrate.

L-O was found to be the most promising of all compounds tested. It displayed strong potency in the yeast system thereby lowering the quantities needed for screening. Total abolition of the rescue was achieved at concentrations that were not toxic to the yeast and that could even be exceeded while still being non-toxic. This allowed screening with high enough concentrations to ensure stringency.

4.3.2. Inhibitor L-O

The resistance profiles of the mutants identified from screen III reintroduced in yeast showed variability from experiment to experiment (Table 3.9). This might have been caused by the nature of the mutants tested, with S295F being the only stably resistant mutant, but this might also have been cause by the inhibitor used. The reintroduction experiment was repeated using the higher efficiency inhibitor L-O. The results were less variable than for L-B showing again the resistance of the S295F with L294H also displaying resistance (Table 4.2).

Although the S295F mutation showed broad inhibitor resistance when tested against a panel of structurally varied inhibitors, the K_i for L-O was nonetheless measured to insure that the S295F mutation was also resistant to that particular compound. Using DiFMUP as substrate, the S295F mutation induced a fivefold increase in the K_i values ($0.088 \pm 0.003\mu M$ for the wild-type and $0.44 \pm 0.05\mu M$ for the S295F mutant PTP1B) while maintaining the competitive nature of the inhibitor.

Table 4.2: Two separate experiments measuring the % growth of YPH499 yeast co-expressing v-Src and mutants PTP1B after 70 hours in the presence of 0.5mM L-O.

	Experiment #1	Experiment #2	Average
Wt	19	19	19
S55R	4	26	15
H54Q	-4	12	4
P31R	19	16	18
S295F	39	70	54
L294H	45	59	52
P309L	16	15	15

% growth was calculated by setting the growth of yeast co-expressing v-Src and the PTP1B mutant in the absence of inhibitor as 100% and the growth of yeast expressing v-Src alone as 0%.

4.3.3. 1-320 versus 1-400

The failure of the last screen was thought to be mainly due to the inhibitor used prompting the inhibitor to be changed for L-O. Having to repeat the screen with a new inhibitor provided the opportunity to include the last 80 C-terminal residues overlooked in previous screens which evaluated only residues 1-320. To include these amino acids in the screen, the 1 to 400 PTP1B construct first needed to be tested for its ability to rescue the yeast from v-Src lethality and for sensitivity to inhibitors. The conditions for generating the library also needed to be revisited to ensure that the mutation rate was optimal when using the longer template.

Yeast expressing 1-400 PTP1B rescued yeast from v-Src lethality as efficiently as yeast expressing 1-320 PTP1B (Fig. 4.5). The 1-400 construct also responded to the inhibitors as well as did the 1-320 constructs; inhibitor response curves are shown in Figure 4.6 with the curves for 1-320 transposed from Figure 2.14 and 4.4 for comparison. Libraries were generated using the Genemorph kit with 25 or 30 cycles of amplification and using 10, 50 or 100ng of template. Figure 4.7 shows that the same condition as for 1-320 gives the best mutation rate: 25 cycles, 100ng template.

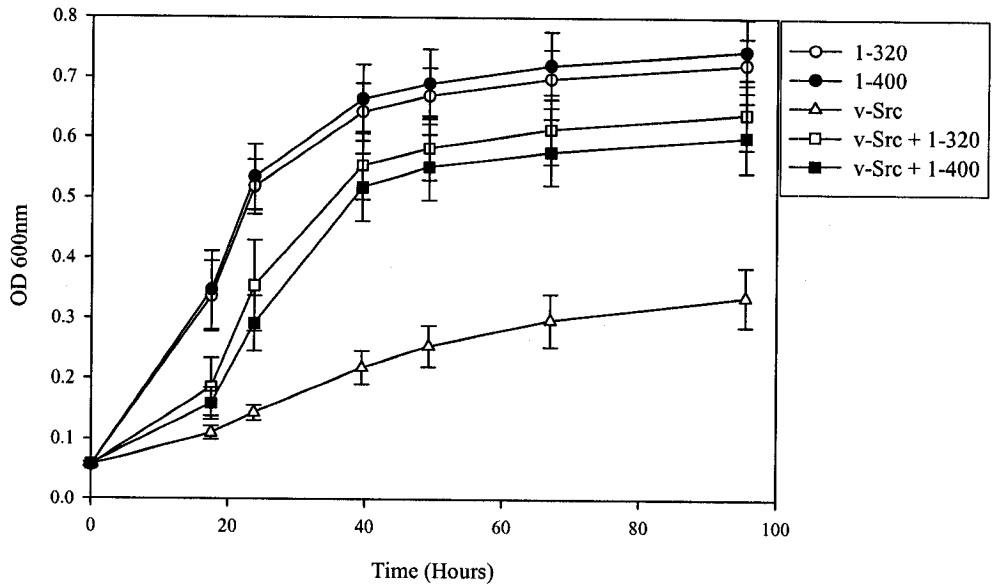

Figure 4.5: Adding the 80 amino acids C-terminal to the catalytic domain does not affect the ability of the PTP1B to rescue yeast from the v-Src lethality. YPH499 yeast were co-transformed with p415GALL and p416GAL1-PTP1B-1-320 (1-320) or p415GALL and p416GAL1-PTP1B-1-400 (1-400) or p415GALL-v-Src and p416GAL1 (v-Src) or p415GALL-v-Src and p416GAL1-PTP1B-1-320 (v-Src + 1-320) or p415GALL-v-Src and p416GAL1-PTP1B-1-400 (v-Src + 1-400). Error bars are standard deviation n=3.

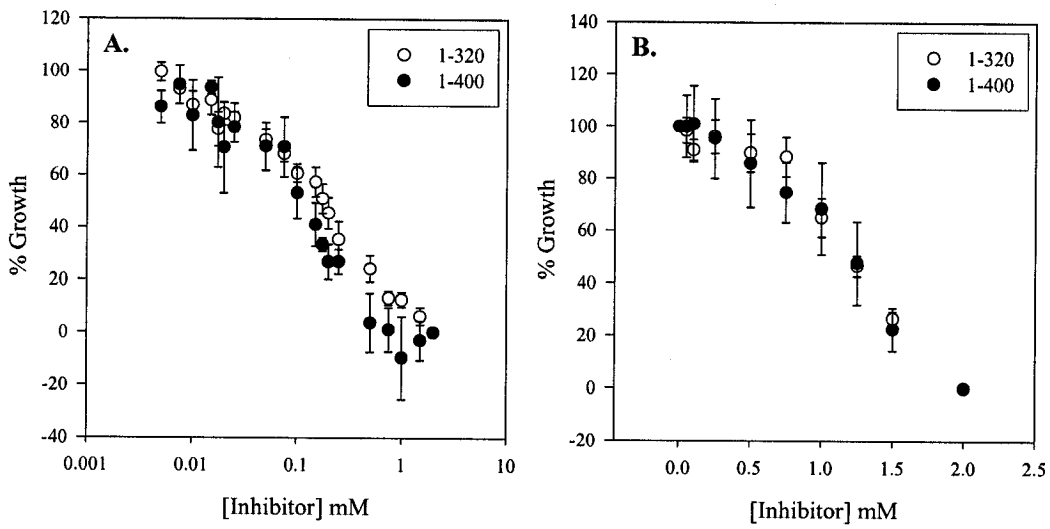

Figure 4.6: Including the 80 C-terminal amino acids to the catalytic domain does not affect the sensitivity of the PTP1B to inhibitors. The catalytic domain of PTP1B (amino acids 1-320) or the extended construct (1-400) was co-transformed in YPH499 yeast along with v-Src. % Growth refers to the absorbance at 600nm after 68 hours of growth normalized to 100% in the absence of inhibitor and 0% in the presence of 2mM inhibitor. Error bars are standard error n=5.

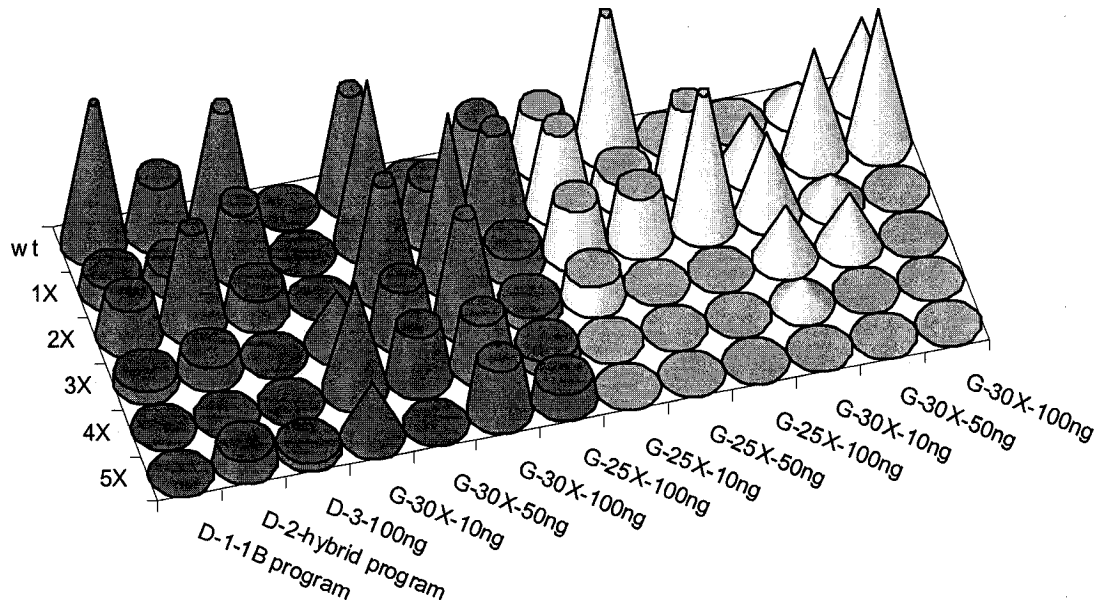

Figure 4.7: Degenerate PCR conditions yield a distribution of mutation rates from no mutations in product (wt) up to five mutations (5X). Different library-generation conditions using the Diversify (D) or the Genemoph (G) kits and with PTP1B-1-320 (grey series) or PTP1B 1-400 (white series) as templates are shown along with the number of amplification cycles (eg. -30X) and the quantity of template used (eg -50ng). For the diversify kit, the results from two amplification programs are shown: D-1 with a program optimized for PTP1B amplification, D-2 and D-3 with a program mixing the manufacturer-suggested and the PTP1B program. Cone height represents the number of clones with the specified mutation rate expressed as a percentage of total number of clones sequenced for that condition.

4.3.4. Growth Assays on Agar with Inhibitor L-O

When first used, growth assays on agar were found to be non-quantitative compared to liquid assays and did not respond to inhibition. However, since the BzN-EJJ-amide compound used in these initial trials was one later found to be ineffective in yeast (see Fig.34) it was thought that a read-out might now be obtained by using L-O. Although the yeast system was well characterized with liquid assays, transplanting the assay to agar would be extremely advantageous in terms of increased throughput for screening a

library: from the last screen the use of liquid assays limited the number of clones evaluated for resistance to 1% of the total transformants.

The growth assay shown in Figure 2.1 was reproduced in Figure 4.8 but using 2mM L-O and yeast co-transformed with PTP1B and/or v-Src with the addition of the appropriate empty vector to allow growth of all permutations on the same double dropout media. Treatment with 2mM of L-O was not toxic to the yeast as shown in Figure 4.8 when comparing the columns Glucose and Glucose + I. Expression of v-Src compromised yeast growth but co-expression of PTP1B did not show the obvious rescue previously observed in Figure 2.1. The same results were obtained with a drop-test (Table 4.3).

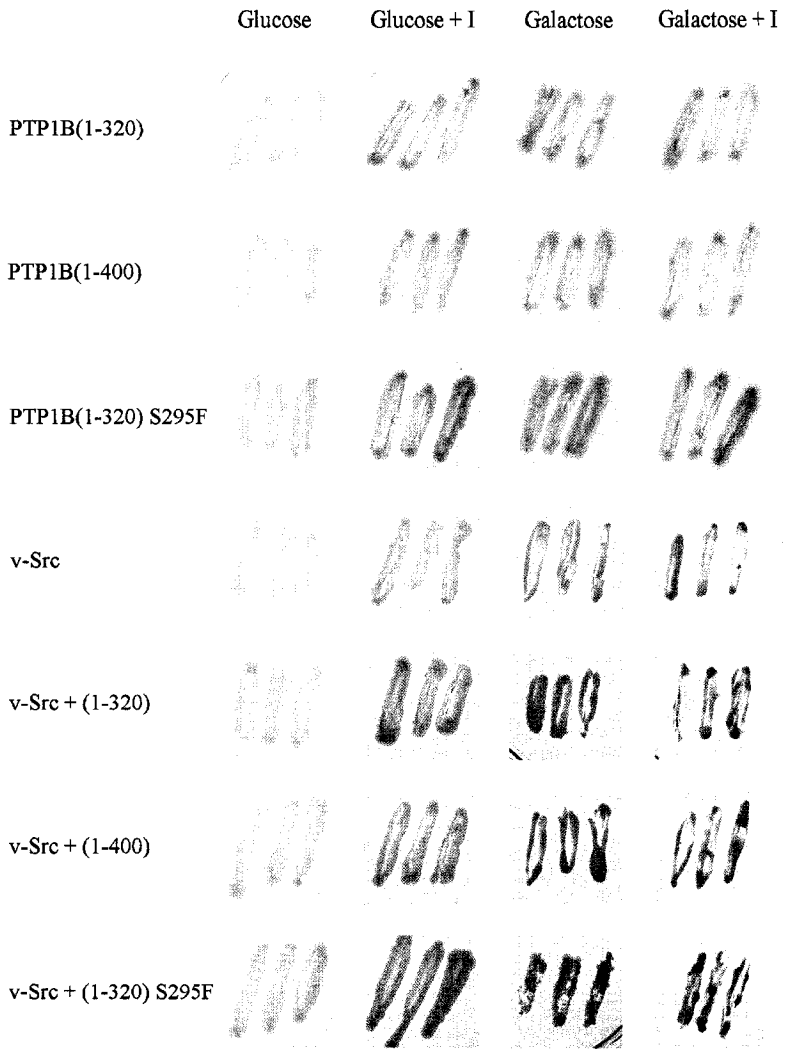

Figure 4.8: Measuring growth of yeast by streaking on agar plates allows the observation of GAL1-driven v-Src lethality but not of the rescue mediated by PTP1B. YPH499 yeast were co-transformed with p415GAL1 and p416GAL1-PTP1B-1-320 [PTP1B(1-320)] or p415GAL1 and p416GAL1-PTP1B-1-400 [PTP1B(1-400)] or p415GAL1 and p416GAL1-PTP1B-S295F [PTP1B(1-320) S295F] or p415GAL1-v-Src and p416GAL1 [v-Src] or p415GAL1-v-Src and p416GAL1-PTP1B-1-320 [v-Src + (1-320)] or p415GAL1-v-Src and p416GAL1-PTP1B-1-400 [v-Src + (1-400)] or p415GAL1-v-Src and p416GAL1-PTP1B-S295F [v-Src + (1-320)S295F], three colonies from each of the resulting transformations were picked and streaked in double drop out media containing glucose or galactose as carbon source with or without 2mM L-O (+I).

Table 4.3: The number of colonies obtained from the drop test on glucose or galactose media, with or without inhibitor, for yeast expressing wild-type PTP1B (1-320 or 1-400), mutant S295F PTP1B or v-Src, or co-expressing v-Src and wild-type PTP1B (1-320 or 1-400) or S295F PTP1B.

	Glucose	Galactose	Galactose + 2mM L-O
PTP1B(1-320)	7	15	17
PTP1B(1-400)	16	18	16
PTP1B(1-320) S295F	17	19	26
v-Src	21	0	0
v-Src + 1-320	20	0	0
v-Src + 1-400	22	0	0
v-Src + (1-320) S295F	13	0	0

To decrease v-Src expression thereby facilitating rescue, the experiment was repeated using v-Src driven under the GALL promoter. Lowering expression of v-Src resulted in growth of the streaks similar to the positive controls (Fig. 4.9A) thereby hiding a rescue effect by PTP1B. The corresponding drop-test did however show the lethality of v-Src, rescue by PTP1B and reversal with the inhibitor but the S295F resistant mutant failed to show resistance (Table 4.4). From these results, streaking was found to be inadequate in discriminating growth and the drop test unable to identify a known inhibitor resistant mutant.

Table 4.4: The number of colonies obtained from the drop test on galactose media, with or without inhibitor, for yeast expressing v-Src or co-expressing v-Src and wild-type PTP1B (1-320 or 1-400) or S295F PTP1B.

	Galactose	Galactose + 2mM L-O
v-Src	2	0
v-Src + 1-320	6	0
v-Src + 1-400	12	2
v-Src + (1-320) S295F	12	1

Instead of painting the yeast on the agar, the same yeast used for Figure 4.9A were replica plated on agar using filter-paper to lift the colonies from the transformation plate onto the assay plates. Although yeast expressing v-Src were able to form colonies, the shape of the colonies was irregular compared to the smoothness of the controls (Fig. 4.9B). Co-expression of PTP1B returned the colonies to the smoothness of the controls and treatment with 2mM L-O prevented the return thereby promoting irregular colonies. Although the phenotype of the deregulation of mitosis generated by expression of v-Src changed from lack of growth observed in liquid cultures to irregular colonies, this phenotype was reversed by co-expression of PTP1B and the reversal prevented by the inhibitor. The S295F mutant, which showed resistance in the liquid assay, was unable to revert the colonies to smoothness in the presence of the inhibitor. Although using this assay would have considerably streamlined the screen, the lack of a quantitative readout and the inability to identify a known resistant mutant made the replica plating ineffectual.

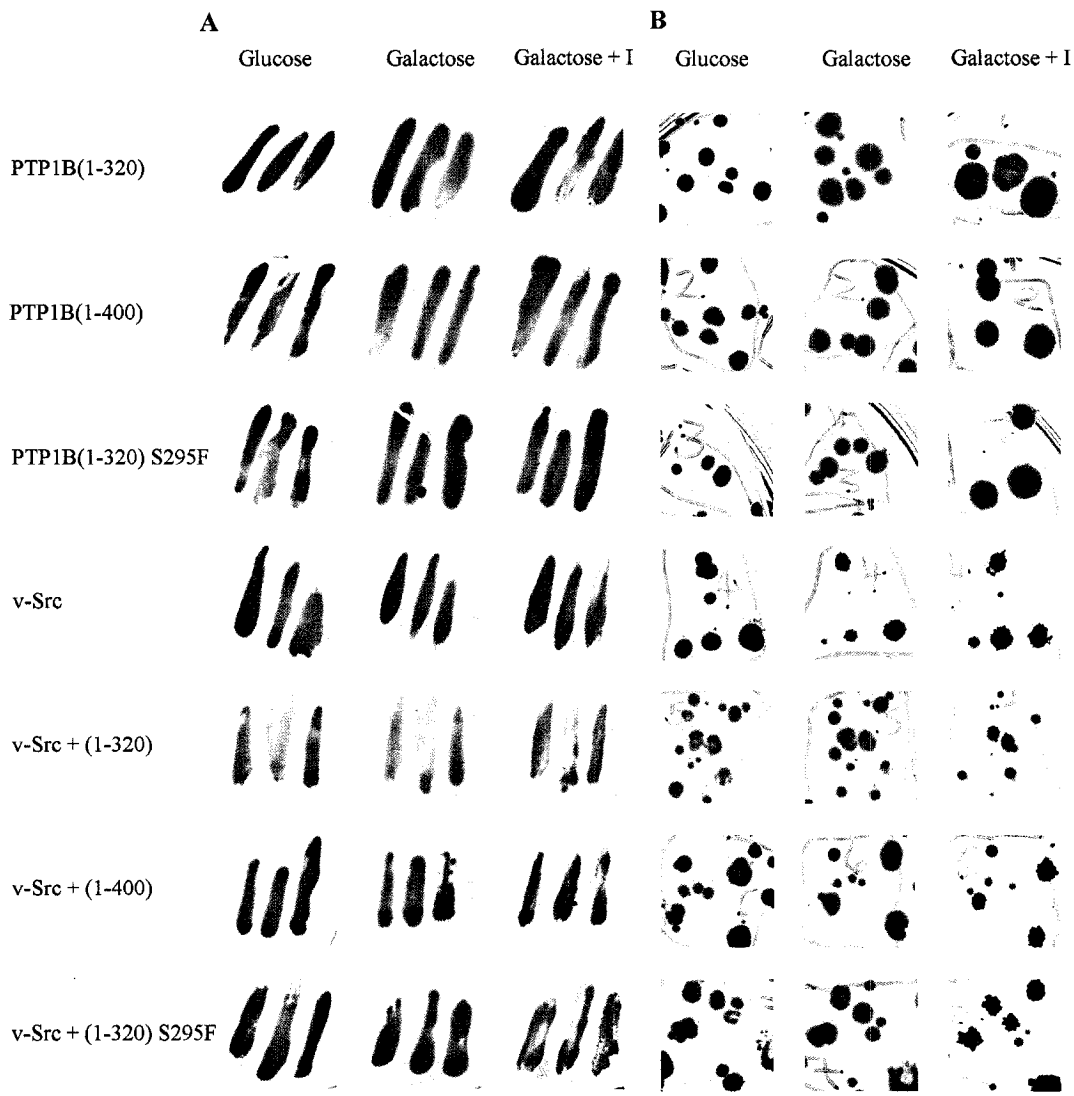

Figure 4.9: Although streaking the yeast does not reveal the lethality of GALL-driven v-Src expression, replica plating reveals aberrant colony morphology with v-Src expression, reversal with PTP1B co-expression and sensitivity to inhibitors. YPH499 yeast were transformed as in Figure 4.8 but using p415GALL instead of p415GAL1 to express v-Src and streaked as in Fig. 4.8 or replica plated.

4.3.5. Curves Direct from Plate

Whilst changing the inhibitor was thought to address the false positives in the last screen, it was suspected that the liquid assay protocol might also have contributed to the variability in the growth of the clones. Indeed, since the density of the start culture is not

well controlled in the library screen, it was found that inoculation of a well with a large amount of yeast lowers the apparent lethality of yeast expressing v-Src alone (Fig. 4.10).

As an aside, it was noticed that rescuing yeast had a characteristic shape to the curve they generated compared with control curve. When the yeast were dependent on PTP1B for growth they display a more pronounced sigmoidal-shaped curve (longer lag period) than the controls, both positive and negative, which showed a more rectangular hyperbola-shaped curve (Fig. 4.11); this behavior is also abrogated when too much start culture is used (red-filled symbols).

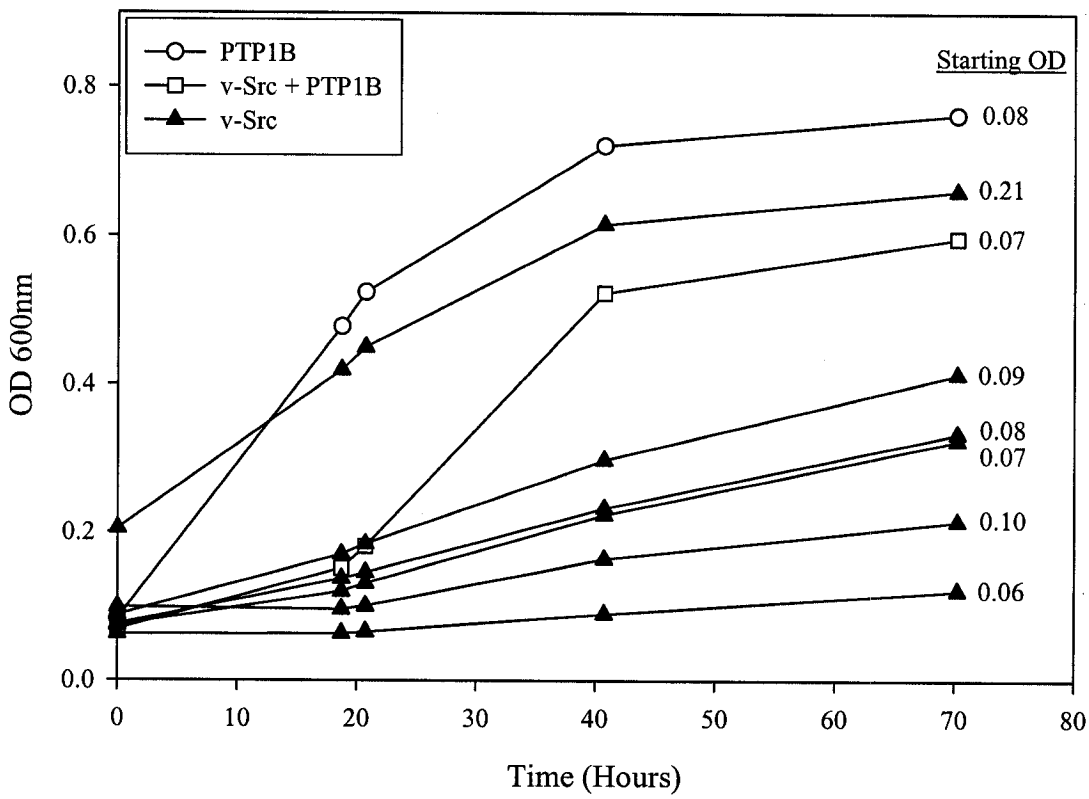

Figure 4.10: Increasing the density of the starting culture obscures the v-Src lethality. Yeast were co-transformed with p415GALL and p416GAL1-PTP1B (PTP1B) or p415GALL-v-Src and p416GAL1 (v-Src) or p415GALL-v-Src and p416GAL1-PTP1B (v-Src + PTP1B). The resulting clones were picked and resuspended in 40μL of 15% glycerol. Ten microliters of this suspension was used for growth curves. The variation in the starting OD results from variation of the amount of yeast material picked.

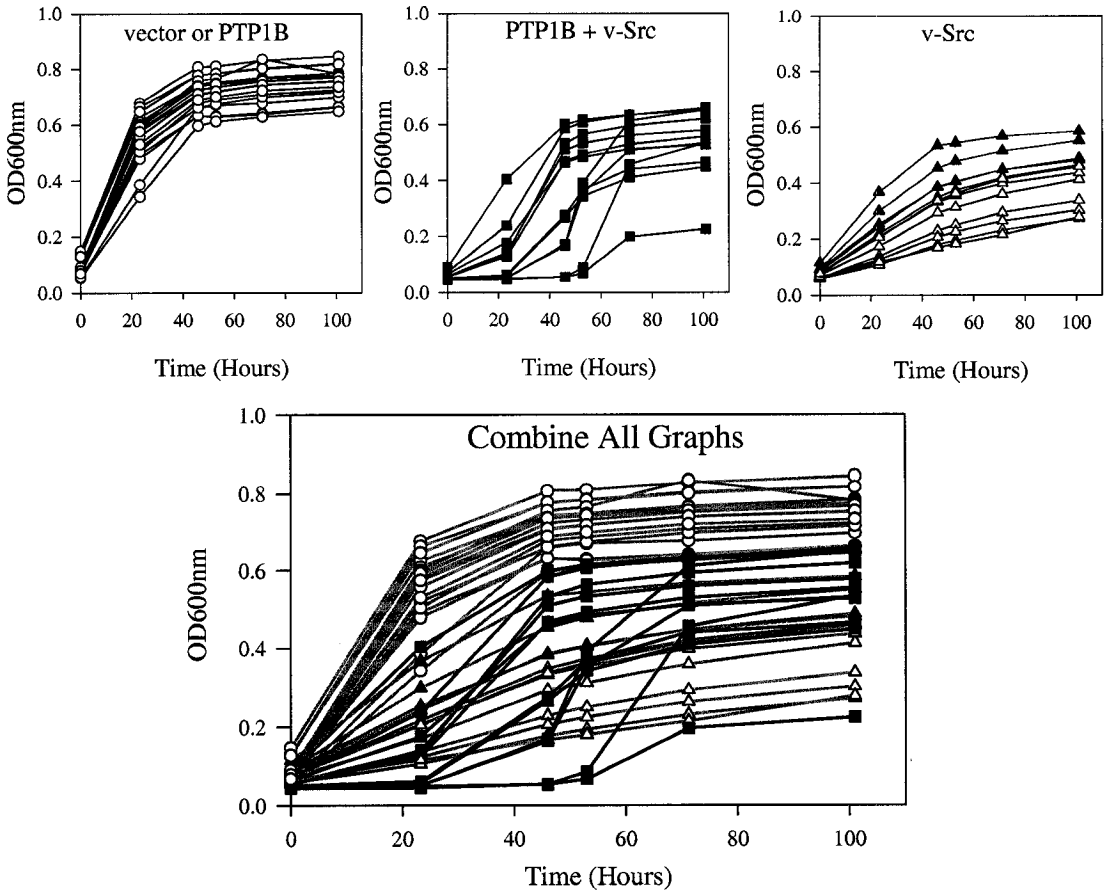

Figure 4.11: Yeast whose growth is dependent on PTP1B activity show more sigmoidal-shaped curves easily identified amongst other curves. YPH499 yeast were co-transformed with p415GALL and p416GAL1 (vector) or p415GALL and p416GAL1-PTP1B (PTP1B) or p415GALL-v-Src and p416GAL1-PTP1B (v-Src + PTP1B) or p415GALL-v-Src and p416GAL1 (v-Src). Around a dozen of the resulting colonies were resuspended in 15% glycerol and assayed for growth.

Figure 4.12 shows the range in the rescue growth of multiple colonies expressing the same PTP1B, either wild type 1-320 or 1-400 or the S295F resistant mutant in the presence of inhibitor (screening conditions). Even when the amount of yeast picked to inoculate the starting culture is closely monitored, there is still a slight variability inherent in the assay itself. However, resistant mutations are well identifiable and yeast expressing different length of PTP1B cluster individually.

Edge effects can occur when the outside rows and columns of the 96-well plate experience a different environment than the inside wells of the plate. In this assay, the outside wells may experience greater variation in temperature when they are taken out of the incubator to be read. To verify if these edge effects affected the growth of yeast, all the wells of a 96-well plate were inoculated with yeast expressing v-Src and PTP1B. Figure 4.13 shows the absorbance of the 96 wells after 95 hours of growth showing that yeast in the outside wells did indeed grow less than in the middle wells. To prevent these edge effects in the screen, the outside wells were filled with oil-covered water to provide a temperature buffer for the inside assay-wells.

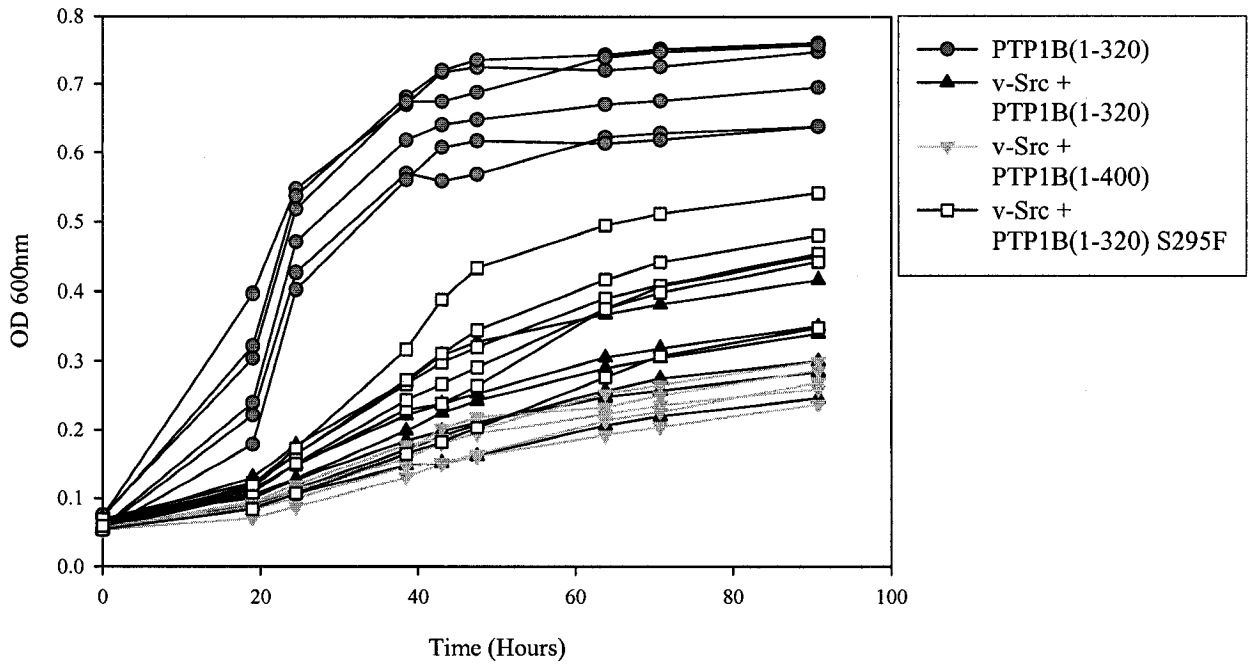

Figure 4.12: Even with well controlled starting densities, the growth of clones transformed with the same DNA varies within the assay yet the resistance of the S295F mutant is well distinguishable from the sensitivity of the wild-type PTP1B. YPH499 yeast were co-transformed with p415GALL and p416GAL1-PTP1B-1-320 [PTP1B(1-320)] or p415GALL-v-Src and p416GAL1-PTP1B-1-320 [v-Src + PTP1B(1-320)] or p415GALL-v-Src and p416GAL1-PTP1B-1-400 [v-Src + PTP1B(1-400)] or p415GALL-v-Src and p416GAL1-PTP1B-S295F [v-Src +PTP1B(1-320)S295F]. Six clones from each transformation were picked, resuspended in glycerol and grown in the presence of 0.5mM L-O.

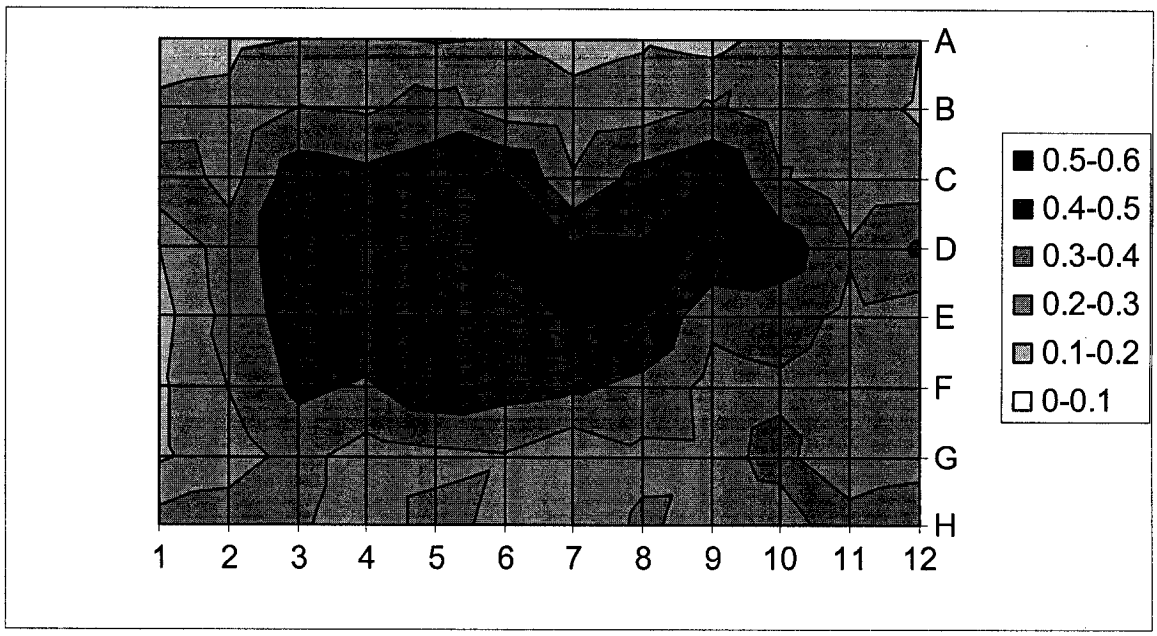

Figure 4.13: Edge effects lower the growth of yeast located in the outside wells of the 96-well plate. YPH499 yeast co-transformed with p415GALL-v-Src and p416GAL1-PTP1B were inoculated at the same starting density in all wells of a 96 well plate. The absorbance at 600nm obtained after 95 hours of growth was graphed as a grey-scale intensity on a matrix representing the columns (numbered one to twelve) and the rows (labelled A to H) of the 96-well plate.

4.3.6. New Transformation Protocol

The H2 strain was created to allow the library to be transformed in the yeast alone thereby bypassing the need to co-transform the v-Src plasmid. However, as described in Chapter 2, the response of PTP1B in that strain was not very robust. It was found that the H2 strain was not necessary for efficient transformation if a sequential transformation protocol was used to first transform v-Src and then transform the library in a separate step. In essence, the sequential transformation requires first transforming one plasmid, growing the yeast from the resulting stationary dropout culture to an exponential one in complete media and transforming the second plasmid. This technique would allow the

transformation of the two plasmids while avoiding the reduced efficiency of transforming both at once.

Although this technique ensures the first plasmid (here v-Src) is not lost while the yeast is being cultured for the second transformation, there was the possibility that v-Src expression might be leaky and would prevent adequate growth or would promote adaptation by the yeast resulting in loss of lethality once the promoters were turned on. It has been reported that spontaneous v-Src resistant colonies might arise from leaky expression that could desensitize the cells or promote the accumulation of resistant mutations in the culture[159]. Also, if the v-Src expression was leaky, v-Src protein would accumulate for three days before PTP1B introduction; the increased quantities of v-Src might diminish the window of PTP1B rescue. Yeast transformed using this technique were tested for effective v-Src lethality and PTP1B rescue by comparing with yeast co-transformed with v-Src and PTP1B or the appropriate empty vectors. Figure 4.14A shows a similar rescue is mediated by PTP1B whether it is co-transformed with v-Src or transformed sequentially first or second. Regardless of the transformation protocol, this rescue is equally sensitive to the inhibitor (Fig. 4.14B). The v-Src lethality is not affected by the transformation procedure. Using this sequential transformation protocol allowed the expression of v-Src and the PTP1B library in the wild-type YPH499 strain to replace the unpredictable H2 strain.

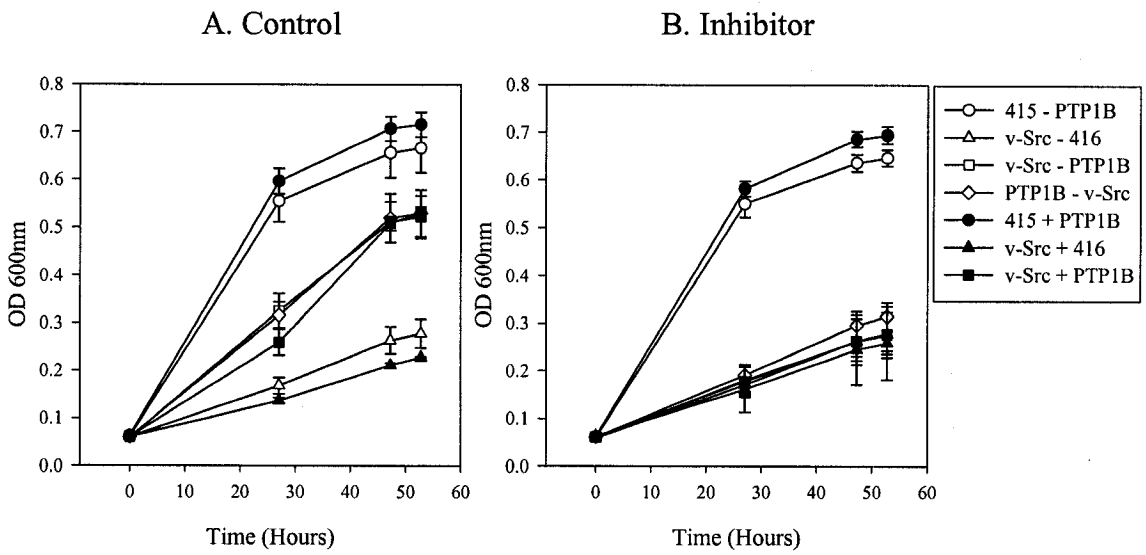

Figure 4.14: Yeast transformed sequentially express and rescue the v-Src phenotype as well as doubly transformed yeast and are equally sensitive to PTP1B inhibitors. YPH499 yeast were co-transformed with p415GALL and PTP1B (415 +/- PTP1B) or p415GALL-v-Src and p416GAL1 (v-Src +/- 416) or p415GALL-v-Src and p416GAL1-PTP1B (v-Src +/- PTP1B). "–" separating the keywords denotes the plasmid on the left was transformed first and the plasmid on the right was transformed second (sequential transformation); "+" denotes both plasmids were transformed in the yeast at the same time (double transformation).

4.3.7. Screen IV

PTP1B 1-400 was screened for inhibitor determinants in wild-type yeast sequentially transformed with v-Src and a library of PTP1B mutants. The library was generated with the same primers as previously used to allow homologous recombination. Although the yield of the library reaction was low (Fig. 4.15), the small amount of library obtained was transformed, along with 1μg of *Eco*R I and *Sal* I-digested de-phosphorylated p416GAL1, in YPH499 previously transformed with p415GALL-v-Src.

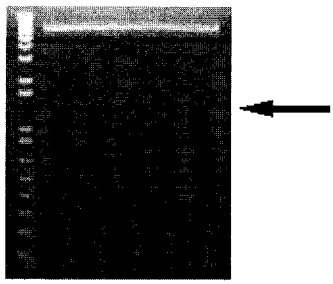

Figure 4.15: Yields of library were greatly reduced by using primers reconstituted in water and stored for 18 months at -20°C. TBE gel of the library generated for screen IV and gel cleaned before transformation.

A low copy vector was chosen to express the library in contrast to the high copy vector used in previous screens using the H2 strain. The high copy vector was used in the H2 strain because it generated a greater window of rescue, as opposed to the wild-type yeast strain which did not show any improvement in the rescue window generated by PTP1B on a high copy vector compare to the low copy vector. Since expression from the high copy vector can generate inhibitor resistance and is not necessary for an adequate rescue in the wild-type yeast, the use of a low copy vector could be useful to improve the quality of the screen.

The sequential transformation of the library resulted in 91 476 transformants, 2664 of which were carefully picked to control the density of the starting culture and inoculated in 50μL of 15% glycerol in the 60 inner wells of 96-well plates. Ten microliters of this suspension was transferred to assay wells with or without 0.75mM of inhibitor L-O. The concentration of inhibitor used was chosen to give the maximal abrogation of PTP1B-mediated rescue while low enough to permit identification of resistant mutants (Fig. 4.16).

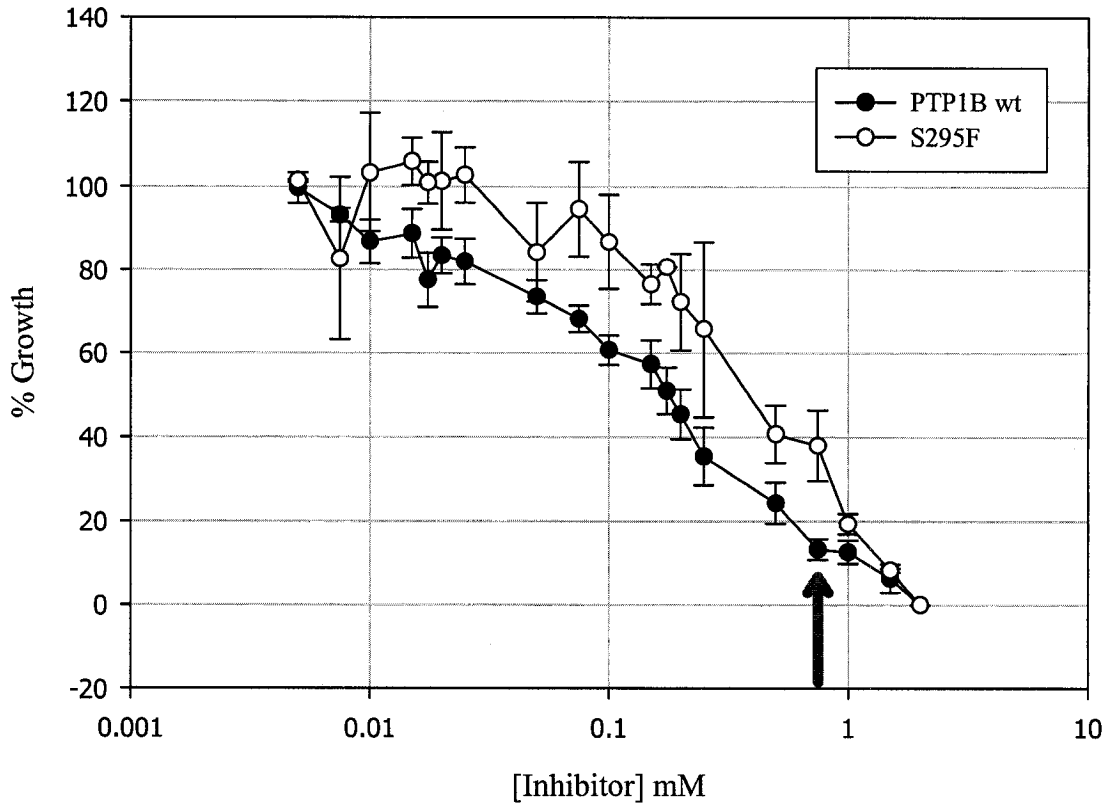

Figure 4.16: The S295F PTP1B mutant is dose-dependently resistant to the inhibitor L-O. YPH499 yeast were co-transformed with p415GALL-v-Src and p416GAL1-PTP1B wild-type or S295F mutant. % Growth refers to the absorbance at 600nm after 68 hours of growth normalized to 100% in the absence of inhibitor and 0% in the presence of 2mM inhibitor. Data for the wild-type enzyme transcribed from Figure 4.4 for comparison. Arrow highlights 0.75mM L-O. Error bars are standard error n=2.

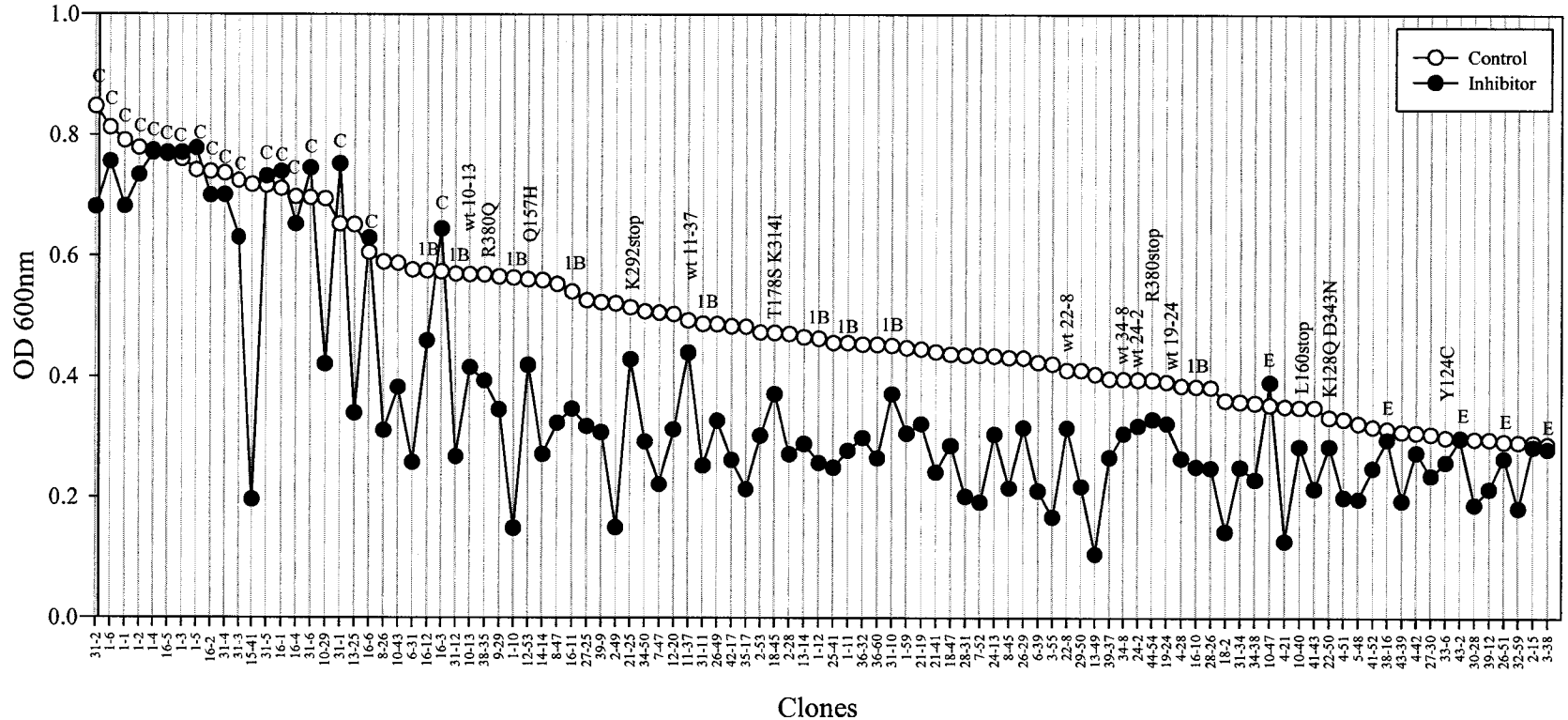

Figure 4.17: Sixty-eight library clones from screen IV were able to rescue the growth of yeast expressing v-Src. The absorbance at 600nm after 70 hours of growth in the presence or absence of 0.75mM L-O is shown for the top 98 growers in the screen: "C' indicates control yeast not expressing v-Src, "1B" indicates yeast co-transformed with p415GALL-v-Src and p416GAL1-PTP1B-1-400, "E" indicates empty clones that have not integrated a library fragment. The other labels correspond to the sequencing data shown in Table 4.5.

Table 4.5: Nucleotide mutations and associated amino acid change in 14 resistant clones identified in screen IV.

Clone	Nucleotide	Amino Acid	% of control growth
33-6	A371G	Y124C	86
22-50	A382C G1027A	K128Q D343N	85
12-53	G471T	Q157H	75
10-40	T479A	L160stop	81
18-45	A532T A941T	T178S K314I	79
21-25	A874T	K292stop	83
38-35	(G1005A) G1139A	R380Q	69
44-54	(C630T) C1138T	R380stop	83
34-8	(C486T)	WT	77
24-2	(A534G)	WT	81
11-37	(G15A)	WT	89
22-8		WT	77
19-24		WT	82
10-13		WT	73

% of control growth refers to absorbance at 600nm after 50 hours in the presence of inhibitor *versus* control growth. Nucleotide mutations in parentheses are non-coding, WT = wild type.

Twenty one clones were selected for sequencing (Table 4.5). Seven of them held a recirculized P416GAL1 plasmid that had not integrated a library fragment and identified the threshold of growth in the screen (0.3OD). From this threshold, it was realized that only 68 out of the 2664 clones picked showed rescue growth on galactose. Six of the clones contained silent or no mutations. Figure 4.17 shows the top 98 growers of the screen, annotated with the sequencing results, showing the start of the growth threshold (E) which is flatly propagated for the rest of the 2664 assayed clones.

The behavior of the controls included in the screen was plotted against the data obtained from the response of PTP1B to 0.75mM L-O measured in previous experiments (Fig. 4.18). This comparison revealed that the wild-type PTP1B seemed to be more resistant to inhibition in the screen than in the exploratory experiments.

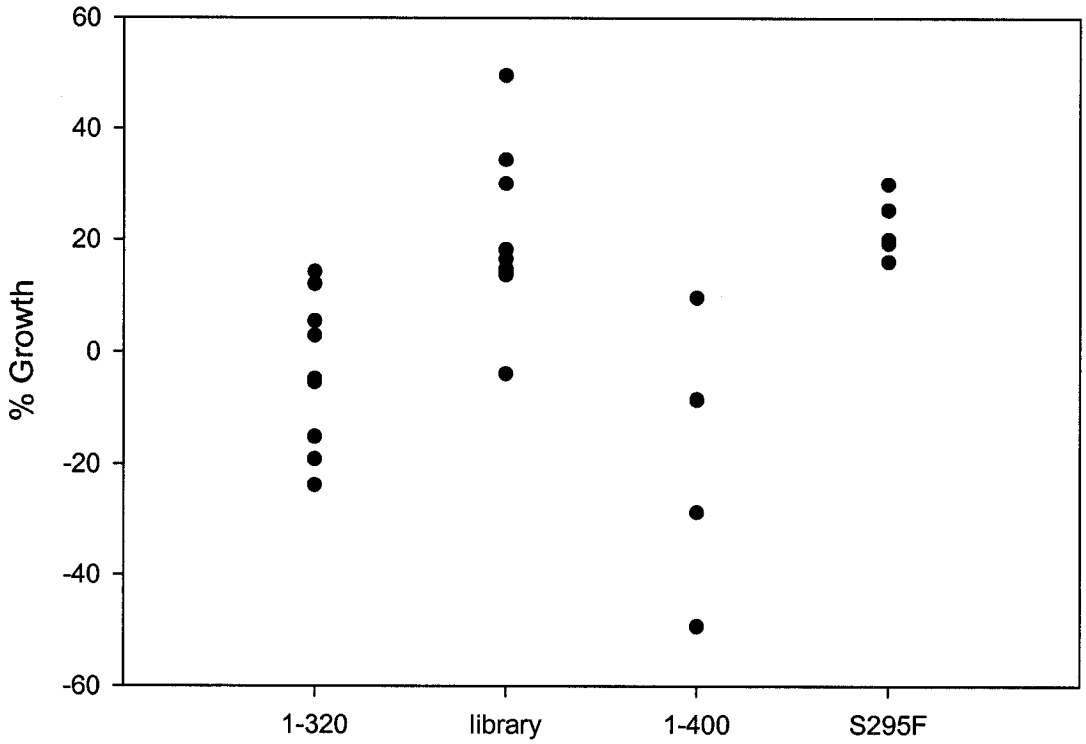

Figure 4.18: Spread and shift of the effect of 0.75mM L-O on the growth of yeast expressing v-Src and PTP1B in the context of a library screen or exploratory growth curves. The data for "1-320", "1-400" and "S295F" was calculated from previous experiments (Figure 4.4, 4.6, 4.16 and Table 4.2). "library" regroups the values collected over the three days of the library screen IV for the PTP1B-1-400 control. % growth is the absorbance at 600nm as a percentage of the absorbance of yeast not expressing v-Src (minus the background growth of yeast expressing v-Src).

All the clones showing mutations were reintroduced in YPH499 yeast but using growth curves started from an overnight culture of a mixture of clones obtained from the co-transformation of the rescued plasmid with v-Src. Table 4.6 shows the ability of the

clones to rescue the v-Src phenotype and Figure 4.19 shows the response of the clones to increasing amounts of L-O.

When Y124C and L160stop were reintroduced in yeast they could not rescue from the v-Src phenotype thereby confirming the threshold of rescue identified from the empty clones. These two clones were identified as resistant in the screen because of the way resistance was calculated: the inhibitor did not affect their growth compared to their control; in effect the control, yeast expressing the clone but not treated with inhibitor, did not grow at all. Their lack of activity was reassuring as residue 124 is strictly conserved amongst all vertebrate PTP and is thought to have a crucial role in maintaining the structure of the active site and the L160 truncation does not even contain the active site PTP loop. Clone 10-37 and 11-37, identified as wild-type, were also reintroduced in yeast to verify their resistance. They rescued the yeast but were as sensitive to the inhibitor as the control. Of all the clones tested, only K292stop showed clear resistance to the inhibitor.

Table 4.6: Catalytic activity of the selected clones from screen IV as measured by their ability to rescue the v-Src phenotype.

Clone	% of normal growth	% of wt rescue
Y124C	-13	-21
L160stop	7	11
11-37 (WT)	42	76
K128Q D343N	55	85
R380Q	56	102
Q157H	57	88
Wild-type control	60	100
T178S K314I	70	127
R380stop	71	129
10-13 (WT)	73	112
K292stop	74	123

Wt = Wild-type

% Normal Growth is absorbance at 600nm after 70 hours of growth setting growth of yeast expressing only PTP1B at 100% and yeast expressing only v-Src at 0%.

% Wild-Type Rescue is absorbance at 600nm after 70 hours of growth setting the growth of yeast co-expressing v-Src and wild-type PTP1B at 100% and yeast expressing v-Src alone at 0%.

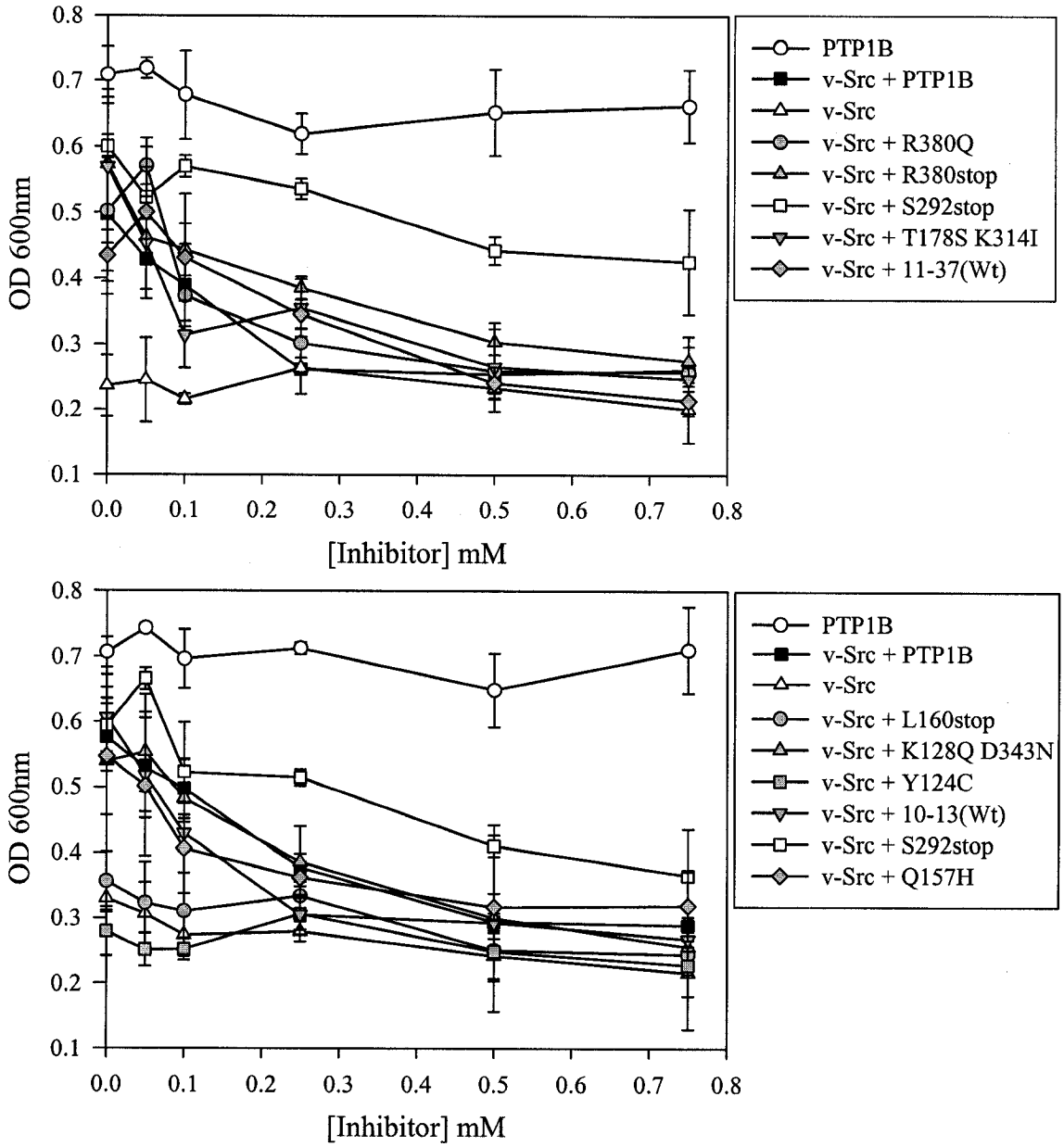

Figure 4.19: Reintroducing clones selected from screen IV in yeast and assaying for growth in the presence of inhibitor reveals the resistance of the S292stop mutant. YPH499 yeast were co-transformed with the plasmid rescued from the library clones and p415GALL-v-Src. For controls yeast were co-transformed with p415GALL and p416GAL1-PTP1B-1-400 (PTP1B), p415GALL-v-Src and p416GAL1-PTP1B-1-400 (v-Src + PTP1B) or p415GALL-v-Src and p416GAL1 (v-Src). A few of the resulting colonies were pooled for each transformation, grown overnight and the resulting suspension was used for growth curves in the presence of increasing concentrations of L-O and the absorbance at 600nm after 70 hours of growth was measured. Error bars are standard deviation n=3.

4.3.8. Screen V

Screen IV proved uninformative due to the very low proportion of clones that expressed PTP1B. This was probably due to a low library to vector ratio. The labor-intensive step in the screening process is transferring the colonies from the agar of the transformation to the wells of the liquid assay. To prevent the needless picking of clones that are not expressing PTP1B, it was thought that screening the clones for the presence of an active PTP1B prior to the resistance assay would be advantageous.

Plating the transformation directly on agar with galactose as sole carbon source yielded very little colonies. It was found in the literature[156] that this efficiency could be increased by adding trace amounts of glucose in the galactose-containing plates. However, the literature-suggested concentration of 0.005% glucose did not increase the efficiency (Table 4.7). A titration of glucose was made to find the right concentration which would be high enough to obtain a good efficiency and yet low enough to ensure that the expression from the GAL promoter was not inhibited. Table 4.8 shows that 0.025% to 0.075% glucose is necessary for efficient growth of the transformed yeast in the presence of galactose. Expression of v-Src starts to become repressed around 0.1% glucose as seen by the increase in the number of colonies. To get maximal transformation efficiency yet maintain adequate expression in the library screen, 0.075% glucose was added to the agar transformation plates containing 2% galactose.

Table 4.7: Adding 0.005% glucose did not increase the number of colonies obtained from the co-transformation of yeast plated on galactose-containing agar plates.

	Vector	PTP1B	v-Src	v-Src + PTP1B
0.005% Glucose / 2% Galactose	32	11	0	0
2% Glucose	724	355	181	73

Yeast were co-transformed with 2μg each p415GALL and p416GAL1 (vector), p415GALL and p416GAL1-PTP1B (PTP1B), p415GALL-v-Src and p416GAL1 (v-Src) or p415GALL-v-Src and p416GAL1-PTP1B (v-Src + PTP1B) and 500μL of the resulting reaction was plated on 100mm plates.

Table 4.8: Number of colonies obtained from the co-transformation of YPH499 yeast grown on galactose-containing plates spiked with trace amounts of glucose.

% glucose with 2% galactose	Vector	PTP1B	v-Src	v-Src + PTP1B
0.01	190	179	1	2
0.025	215	186	3	2
0.05	239	181	4	16
0.075	268	199	1	25
0.1	272	186	25	57
2	245	189	87	86
2 (no galactose)	263	139	95	70

YPH499 yeast were transformed as for Table 4.7 but 150μL of the resulting reaction was plated on 70mm plates.

About 8μg of library generated with freshly synthesized primers (Figure 4.20) and 1μg of linearized vector were transformed sequentially as for screen IV but plated on agar containing 2% galactose to induce expression of v-Src and PTP1B and 0.075% to maintain transformation efficiency. An aliquot of the transformation mix was plated on glucose-containing plates to monitor the total number of transformants obtained: 471 colonies grew from 300μL of the 19.8mL transformation mix to give a total of 31 086

colonies. This number is slightly low compare to screen III where 150 000 transformants were obtained or even screen IV where 91 476 transformants were obtained. Thirteen thousand seven hundred and ninety six clones grew on the galactose-containing plates, this number of rescuing clones is impressively higher than screen IV (68 active clones) or screen III (657 active clones) which is probably due to the method of evaluating activity in the screen. Twenty-one hundred and six of these rescued clones were picked on three consecutive days and assayed for resistance in the same way as the clones from screen IV; 149 of them displayed greater resistance to L-O than the S295F mutant control incorporated in the assay.

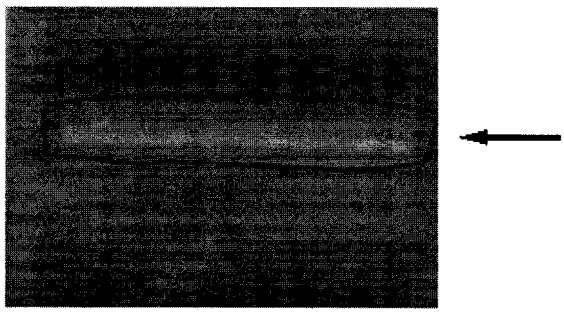

Figure 4.20: Amount of library used for screen V. TBE gel of the library generated for screen V and gel cleaned before transformation.

The controls included in the resistance assay were well inhibited or showed good resistance on all three days. Of note, as the colonies stayed on the plates longer, the ability of the inhibitor to abolish the growth of the wild-type yeast or the mutant was decreased. Nevertheless, when compared on the same day, the S295F mutant always showed good resistance compared to the wild-type controls (Fig. 4.21).

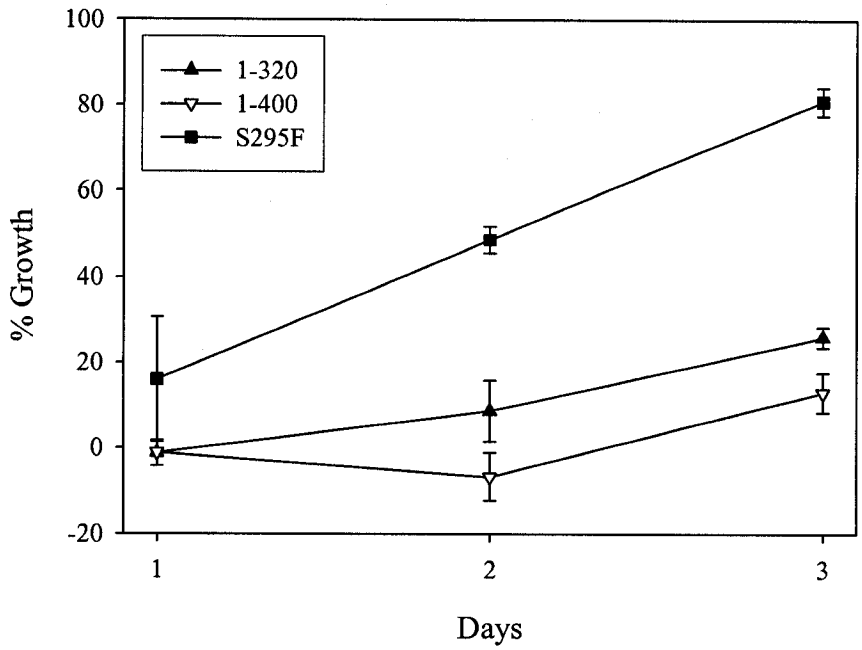

Figure 4.21: Although the S295F PTP1B mutant is always resistant to inhibitor compared to the wild-type PTP1B, lengthening the stay of the clones on agar plates before being assayed lowers inhibitor sensitivity. YPH499 yeast were co-transformed sequentially with p415GALL-v-Src and p416GAL1-PTP1B-1-320 or p416GAL1-PTP1B-1-400 or p416GAL1-PTP1B-S295F. The colonies obtained from the transformation were picked and assayed for growth in the presence of 0.75mM L-O on three consecutive days. % Growth is the absorbance at 600nm after 48 hours of growth as a percentage of the absorbance of yeast not expressing v-Src (minus the background absorbance of yeast expressing only v-Src). Error bars are standard deviation n=3.

Table 4.9: Nucleotide mutations and associated amino acid change in 52 resistant clones identified in screen V.

Clone	Nucleotide	Amino Acid	% growth	Day picked
46	C862T (A916G)	Q**288**Stop	66	1
262	(C21T) C868T (A1044T)	Q**290**Stop	93	1
1504	(G798A) C868T (C984T)	Q**290**Stop	97	3
235	G873A	W**291**Stop	66	1
670	G872A	W**291**Stop	61	1
404	A412T G873A (A1111T)	T*138*S W**291**Stop	63	1
979	T150A G872A	S50R W**291**Stop	65	2
742	C862DEL	Q**288**R then ISGRSFPTRTWSPHPSISPHLPGHPNE SWSHTMGNAGSSSQITSG	70	2
8	G850del	D**284**T then LPCRISGRSFPTRTWSPHPSISPHLPG HPNESWSHTMGNAGSSSQITSG	65	1
355	G846del	D**284**T then LPCRISGRSFPTRTWSPHPSISPHLPG HPNESWSHTMGNAGSSSQITSG	61	1
1117	C886del	H**296**T then RTWSPHPSISPHLPGHPNESWSHTM GNAGSSSQITSG	58	2
883	G22A	E8K	50	2
698	A74T (T+28G)	H25Y	76	1
658	G100T C994T	V34L Q332Stop	68	1
42	T198A (A387T) (C461T)	Y66STOP	84	1
135	A557C A1189DEL	E**186**A K397R then TRTRHWSTSSHVISYVTLTFTPSPHIR SNRKGRS	72	1
1204	G556A	E**186**K	58	2
1909	T559C (T855A)	S**187**P	88	3
722	C566T	A**189**V	68	2
18	A703G	M235V	99	1
838	A874G	K**292**E	72	2
1036	C884T	S**295**F	50	2
1422	C884A G1123A (C1185A)	S**295**Y V375M	79	3
2034	C833T G889A	A**278**V E**297**K	80	3

2039	A65C G889A	D22A E**297**K	79	3
754	(A756G) C857T C984A A988G C1163T A1199G	S**286**F F328L N330D A388V D400G	69	2
176	G9T G10A C624G (C672T) C857T (G1197A)	M3I E4K H208Q S**286**F	82	1
2067	A837C C895A	K**279**N L**299**M	85	3
1823	A449C C908A (C960T)	K**150**T P303H	87	3
2024	(C21T) A449G C854A G1112A	K**150**R S**285**Y	82	3
1363	(C276T) C560T A613G A836G	S**187**L S205G K**279**R	56	2
1012	C247G A557T T698C G889A	L83V E**186**V L233S E**297**K	51	2
804	C522G G1094A	F174L S365N	60	2
1753	G364A (C525T) C902A C1154T C1155T	A122T P301H A385V	83	3
784	C487T G619A G1021A	L*163*F E207K D341N	58	2
652	A455G (G471A) A497G G565T (C588T) G1031A A1114DEL (C+37T) (T+42C)	Y**152**C Q*166*R A**189**S C344Y S372V then GSWGEVFEVPRLPPQPKGSRHCPRR TRTRHWSTSSHVISYVTPTFTPSPHIR SNRKGRS	72	1
325	(T261A) C376A G847A G892A A1046T T1116A	P*126*T G**283**R D**298**N E349V S372R	86	1
460	G342A A400T A422C G556A C1117T	M114I I*134*F K*141*T E**186**K R373W	67	1
546	G108T A828T G847A G952T (A1019G)	K36N E**276**D G**283**R E318Stop	66	1
945	G965A	G322E	53	2
654 *	(G471A) G999A	W333Stop	105	1
286	(A384G) A1189DEL	K397R then TRTRHWSTSSHVISYVTLTFTPSPHIR SNRKGRS	73	1
414	T84A T274C C943T	S28R C102R R315Stop	60	1
1480	(C-35A) (C-29T) T180A A441C (T528C) C573A G1069A G1126T	H60Q E*147*D F**191**L A357T G376W	79	3
1791	(A336G) T454A G790A C994T	Y**152**N A264T Q332Stop	81	3
1181	(C949T) (C+13A)	WT	53	2
1213	(A+75T)	WT	54	2
1681	(A93G) (C138T)	WT	83	3
93*		WT	96	1
528*		WT	106	1

424	WT	58	1
1316	WT	50	2

% Growth is the absorbance at 600nm after 48 hours of growth as a percentage of the absorbance of yeast not expressing v-Src (minus the background absorbance of yeast expressing only v-Src). Nucleotide mutations in parentheses are non-coding, '-' denotes 5' of the start ATG, '+' denotes 3' after the end TAG, WT = wild type. Residue number are highlighted in bold when part of the α7 region and italicized when part of the exterior tip of the β-sheet.

Table 4.9 shows the sequence of the retrieved plasmids from the 52 clones that grew best in the presence of inhibitor (day one 105% to 58% of growth, day two 72% to 50% and day three 97% to 79%). A few variants were identified from the shape of their growth curve. Figure 4.22A shows the curves of the clones selected from day 1. Of interest is the shape and clustering of clones 93, 528 and 654 which have less lag and are similar to the control curve (Fig. 4.22B) whereas the rest of the clones cluster together and are similar to the S295F control curve. When sequenced, two of these variant clones were wild types and the third was a truncation beyond the catalytic domain.

The distribution of the mutants on the structure of PTP1B is shown in Figure 4.23. The mutations avoid the active site loops and concentrate on α7 and its surrounding region notably N-terminal α3, C-terminal α6 and β9-β10 loop (numbering as per [79]). There is also a concentration of mutants on the exterior tip of the β-sheet (β7 to β8 and β10 to β11) which has also been identified in the screen III (Figure 4.24).

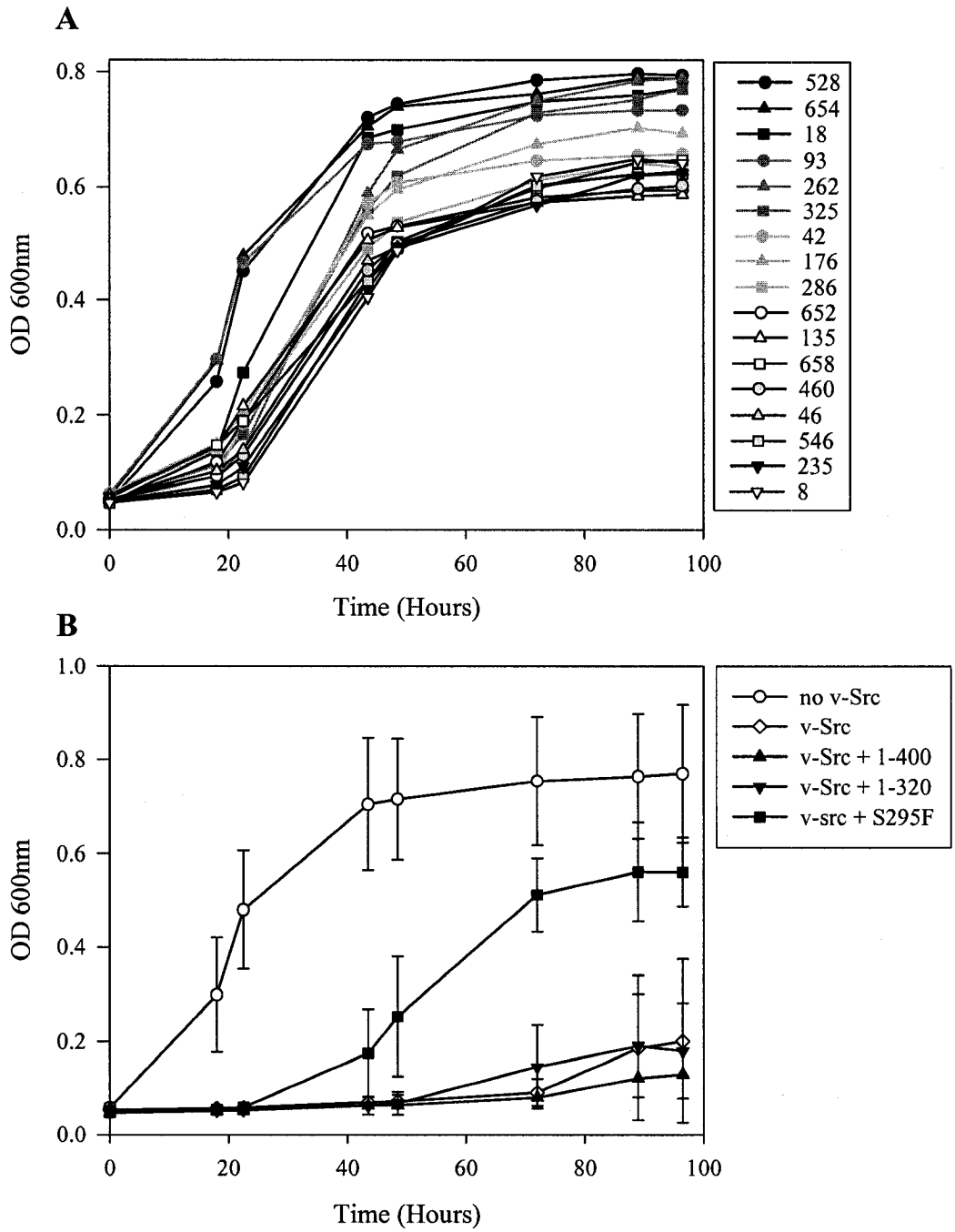

Figure 4.22: Variants in the screen can be identified by the shape of their growth curves. A) Growth curves of clones picked on day one of screen V. B) Growth curves of the controls included in screen V. Error bars are standard deviation n=3.

Figure 4.23: The clustering of inhibitor resistant mutations identified in screen V is highest around the α7 helix. The location of the resistant mutations were plotted on the structure of PTP1B co-crystallized with two phosphotyrosines (entry 1PTY from the RCSB Protein Data Bank) and coloured in blue for residues identified once and in red for residues identified two or more times. Only the side chains of the residues forming the resistant pocket around the α7 helix are shown.

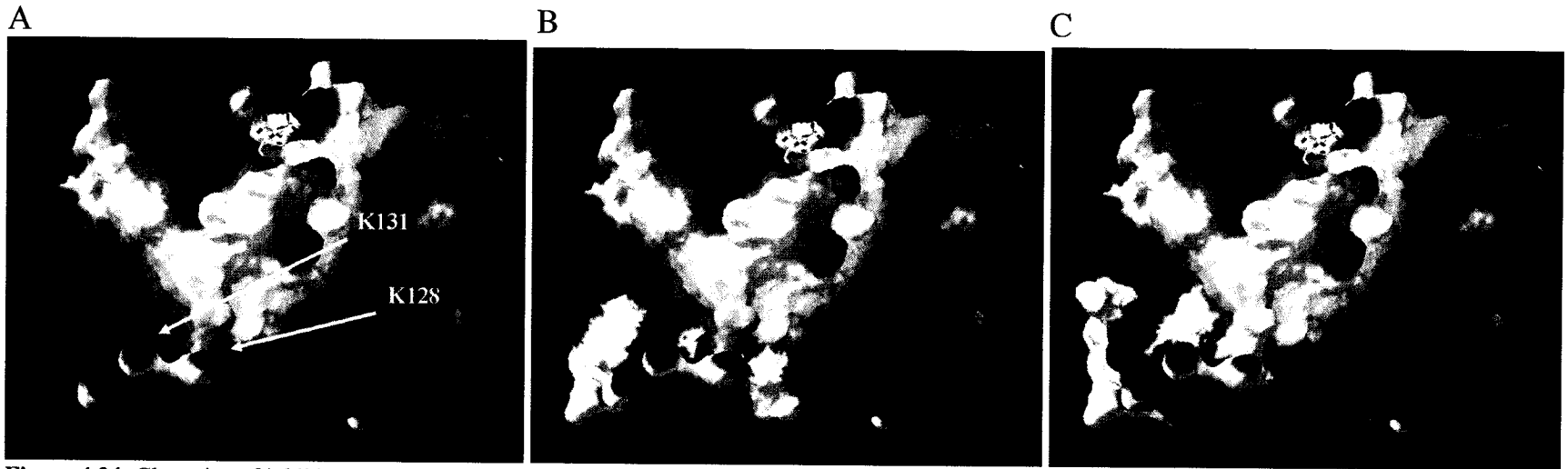

Figure 4.24: Clustering of inhibitor resistant mutations on the exterior tip of the β-sheet. Electrostatic map surface of PTP1B co-crystallized with two phosphotyrosines (entry 1PTY from the RCSB Protein Data Bank) with residues coloured according to their electrostatic potential (pH7 default protonation): red is negatively charged, blue is positively charged. Residues identified in the screens that locate to the exterior tip of the β-sheet are highlighted in yellow. A) Location of residues K128 and K131. B) Mutations identified from screen V using PTP1B-1-400 as template and inhibitor L-O. C) Mutations identified from screen III using PTP1B-1-320 as template and inhibitor L-B.

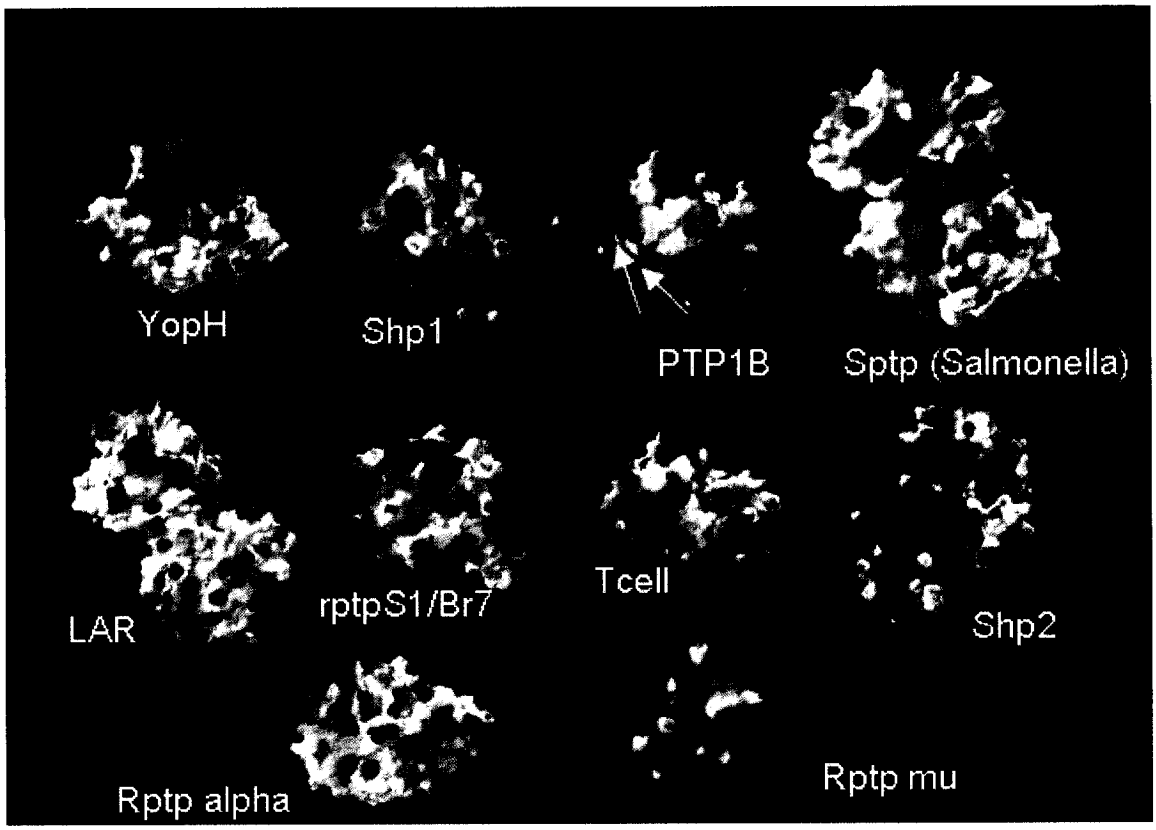

Figure 4.25: Comparing electrostatic surfaces of tyrosine phosphatases reveals the lack of equivalent positive prongs found on PTP1B. Available 3D structures for tyrosine phosphatases from the SCOP database were displayed as electrostatic surfaces and oriented to place the equivalent residues to PTP1B's K128 and K131 at the bottom left (arrows on PTP1B), the WPD loop is highlighted in green to locate the active site on the different phosphatases.

4.4. Conclusions

Changing the inhibitor was thought to be a necessary improvement to reduce the rate of false positives seen in screen III. The benefit of a more potent inhibitor could not be determined from screen IV because the insufficient quantity of library used led to very few clones that could rescue the v-Src phenotype. This wasted screen drove the development of a pre-selection for activity/rescue by plating the transformation directly on galactose. Further streamlining by including the inhibitor in the agar plate was however not successful. Along with the new inhibitor, these changes resulted in a very low rate of false positives in screen V.

Picking clones for the resistance assay from a pool already selected for activity enhanced the quality of the screen by increasing the number of potential candidates examined and removing the handling of uninteresting clones: although a similar restricted number of clones were picked, these did not contain inactive mutations or empty clones and the number of 96-well growth plates to be periodically read was halved.

The results from the screen were found to be bottlenecked first by the resistance assay and again, more severely, by the retrieval and sequencing of the mutants. The pre-selection eased the first restrictive step but still, the resistance assay was awkward for library screening. Easing the second bottleneck could be accomplished by modifying the sequencing PCR to use heat-released template DNA as for the colony PCR technique thereby bypassing the inefficient purification of plasmid DNA from yeast.

4.4.1. Yeast as an Inhibitor Screen

Testing of various inhibitors for efficiency in the yeast system revealed that potency depended on size and charge but not on the ability to inhibit purified PTP1B. For instance, the potent PTP1B peptide inhibitor BzN-EJJ-amide which has a M_r of 800 and contains five negative charges was shown to be inactive in this assay. This was also the fate of the other charged inhibitors with M_r ranging from 547 to 804. Likewise, the highly charged suramin with a M_r of 1429 was also minimally effective. The only compounds, besides vanadate, that had activity in the assay, contained two negative charges and had M_r <500. These compounds as well as vanadate all have similar potency on the purified PTP1B enzyme but L-O was significantly more potent at inhibiting yeast growth than the others. This is likely a reflection of the cell permeable properties of the compounds.

4.4.2. Inhibitor Determinants

The mutations identified in screen V avoided all loops associated with catalytic activity or substrate binding. This was expected and rewarding because of the first-pass selection to rescue the yeast from v-Src lethality which requires intact substrate binding and catalytic activity. However, some mutations did come close to the active site such as D22, H25 and S28 located on the α2' helix lining the secondary binding site but pointing towards the solvent; the same for M114 and A122 which are located right before and after the West loop and A264 located near the East loop and the catalytic residues Q262 and Q266.

In addition to avoiding critical loops, no mutations were found buried in the core of the enzyme except L83V. This mutation is conservative and occurs as part of a quadruple mutant including E186V and E297K indicating its low probability of being a resistance-causing mutation. This supports the ability of the screen to discard mutations that would disturb the overall structure of the enzyme.

Surface modeling of PTP1B reveals a mostly negative surface with a cluster of positively charged residues around the active site. Two positively charged residues (K128 and K131) strike out of the negatively charged surface of PTP1B (Fig. 4.24A). The clustering of mutation on the exterior of the β-sheet avoid these two residues and its immediate region but surround it (Fig. 4.24B and C). The electrostatic properties of this region are not conserved (Fig. 4.25) and might be part of a unique substrate recognition feature of PTP1B. In the same way mutations identified in the screens were absent from the active site because of the requirement for catalytic activity, the absence of mutations directly on this region indicate its potential importance for the rescue activity of PTP1B in yeast. However, this region may be modulated at a distance to confer inhibitor resistance, explaining how mutations identified in two separate screens surround it.

Although these residues are not part of the active site, they have been suggested to participate in macro-substrate recognition and their motions are coupled to occupation of the active site. The model of the PTP1B-IR complex[125] has identified residues 133-140 to form an important hydrophobic patch outside the active site responsible for binding the receptor. Dynamic modeling with peptide substrate[87] indicate a decrease in the mobility of residues 128-141 with binding.

S205, E207 and H208 are clustered on the loop linking the α3 helix and the β12-strand (201-210). These mutations are found in combination with mutations in the α7 region or the tip of the β-sheet. This would indicate that they may not be strong determinants of inhibitor binding but can be assumed to have little detrimental effect on catalytic activity. Modeling studies of the motions induced in PTP1B from substrate binding identified largest movements to occur in this loop (198-209) and to be associated with the motions of the WPD loop[87]. This loop hangs below the active site and is in close proximity to the FKVRESGS SH2-like phosphotyrosine recognition motif (residues 196-203). No mutations were found directly on this motif. Although this motif has not been identified in the literature as participating in phosphotyrosine binding by PTP1B, it has been observed to be coincidently similar to the FLVRESES motif of SH2 domains[97,102,119]. This motif is highly conserved in SH2 domains and the arginine and the two serines are critical for phosphotyrosine binding[241,242].

A large number of mutations identified in screen V coded for truncations: 11 mutants contained a stop codon or a change in frame occurring in the α7 helix or in the loop preceding it. Although very few clones were obtained in the first-pass selection of screen IV, it did identify one resistant mutation which was a truncation at K292. Truncation of the α7 helix was reported to decrease the activity of the phosphatase[74] but K292stop was as competent as the wild-type PTP1B to rescue the yeast from v-Src lethality. K292 is located at the extreme C-terminal end of the helix, leaving most of it intact such that the effect on catalytic activity may not be fully present compared to ablation of the entire helix. This truncation was however sufficient to make the enzyme resistant to the inhibitor. The other six truncations in screen V were located in the C-

terminal tail between residues 315 and 333 along with two more frame shifts at residue 372 and 397.

Inclusion of the last 80 residues of the C-terminal region did not affect the catalytic activity of PTP1B in yeast nor its susceptibility to inhibition. Since there are no models of the structure of these residues to guide the interpretations of results, the primary sequence was used to identify two regions where inhibitor-resistant mutants clustered. One region included mutants in proximity to the S378 phosphorylation site (S372R, R373W, V375M and G376W), while the other region included mutants in proximity to the S386 phosphorylation site and the 386-397 putative SH3-binding site (A385V and A388V). However, the participation of the C-terminal region of PTP1B in inhibitor binding was not clear because all mutations in that region occurred in combination with other mutations. This weak contribution might be due to an effect of C-terminal residue mutations on the efficiency of the enzyme, thereby failing first-pass selection, or simply their lack of participation in inhibitor binding.

The results from screen V showed a high mutation density clustering on the α7 helix, extending through the turn to the C-terminal region of the α6 helix and highlighting the β9-β10 loop. This emphasized the involvement of the entire helix in inhibitor binding but also suggested that modulation of its interactions with the core of the enzyme, through the β9-β10 loop, could mediate inhibitor resistance. The α6-α7 turn region which included some residues on the α6 helix was also highlighted indicating a possible role in the orientation of the helix.

The residues on the α3 helix involved in the hydrogen bond network with the α7 helix (N193, S190 and E200) were not identified in the screen. This omission might

result from the non-exhaustive sequencing of all resistant mutations or their involvement in enzymatic activity. The resistant positions identified on the α3 helix were located at the top of the helix which leads to the WPD loop and include E186, S187, A189 and F191. This region has been implicated in the lack of WPD loop closure with binding of an allosteric inhibitor[74].

5. Conclusions

5.1. The Advantage of Yeast to Screen for PTP1B inhibitors.

Although our goal was to identify inhibitor determinants of PTP1B, the yeast system was found to be equally useful to identify PTP1B inhibitors with enhanced permeabilities. The three active inhibitors (L-B, L-O, L-N) in the yeast system described here all have significant bioavailability[240] whereas the peptide inhibitor, BzN-EJJ-amide, is not bioavailable[243]. Although potent PTP1B inhibitors have been described, cell permeability and bioavailability of these compounds still remain an issue[73]. In addition to providing a cellular environment for PTP1B, thereby protecting it from oxidation and inactivation, the use of this yeast system requires the compounds to have a certain degree of cell permeability. Because of these features and the simple scoreable phenotype, the PTP1B yeast screen can be easily established for high throughput screening of sample collections or complex mixtures (*i.e.* natural products) to identify lead cell-permeable PTP1B inhibitors.

5.2. Putative Binding Determinants for the Inhibitors L-B and L-O.

There are no crystal structures resolved for the complex of PTP1B with either L-B or L-O. Binding determinants for these two inhibitors can however be deduced by analogy with other compounds for which determinants are known.

L-B, which was used in the first three screens, is obtained by replacing the war head- distal chlorine atom of L-H with bromine. The structure of PTP1B in complex

with L-H has been resolved by Dr. G. Scapin but not published. In crystal structures[83,129,130], this difluorophosphonomethyl group engages the phosphatase by extensive hydrogen bonding with the PTP-loop and R221. Two of the equatorial oxygen atoms are involved in hydrogen bonds with the main chain amino groups of S216, A217, G218, I219 and G220. The other oxygen atom engages the side chain of residue 215, which is mutated to a serine for crystallography, and the side chain and main chain amino groups of R221. The two fluorine atoms engage the phenyl side chain of F182 in Van der Waals interactions.

The distal phenyl ring lies in a hydrophobic pocket formed by residues V49, I219 and the aliphatic side chains of D48 and Q262. The distal bromine residue may be involved in hydrophobic interaction with the side chain of M258 as has been proposed for a different compound with an equivalent chlorine which penetrates the secondary binding site[244].

Occupation of the war head ortho position by a chlorine or bromine atom increases inhibitor potency 100-fold. The mechanism for this potentiation is unknown and the crystal structure does not reveal obvious interaction with the bromine atom. A buried water molecule is located within hydrogen bonding distance from the ortho bromine, from E115, which engages R221 in two hydrogen bonds, and from D181 which is hydrogen bonded to the main chain nitrogen of F182. This water molecule is absent from PTP1B-inhibitor complexes using the same war head without the ortho bromine.

L-O, used in screens IV and V, has not been crystallized with PTP1B. Binding determinants for this inhibitors can however be deduced by analogy with other compounds for which determinants are known. L-O belongs to a series of inhibitors

sharing a basic core consisting of a naphthalene ring with a difluorophosphonomethyl war head at position 6. This war head engages the phosphatase in the same set of interactions already described and the naphthalene ring is sandwiched between Y46 and F182 with additional Van der Waals interactions with A217, I219, K120 and V49 and a cation-pi interaction with the side chain nitrogen group of K120.

L-O has an additional bromine atom at an equivalent "ortho" position on carbon 7 similar to L-B and L-H which presumably engages in the same set of interactions. The contribution of the carbon-nitrile substituent on carbon 3 of the L-O inhibitor is speculative. A structure has been solved with a carboxylic acid as a substituent in the same position but was found to have no interaction with the enzyme[130]. Interestingly, moving this carboxylic acid to carbon two allows it to interact with R47 and D48 via a water molecule[83].

5.3. The α7 Helix as an Inhibitor Determinant Region.

L-B and L-O inhibitor determinants for PTP1B identified by the yeast screen avoided all active site loops and so did not coincide with known substrate or inhibitor determinants. A high density cluster was identified on the α7 helix along with the surface region of the protein against which it lays.

The α7 helix (to which we include the few C-terminal visible residues) stitches on to the rest of the enzyme through a series of hydrogen bonds with neighbouring α3 helix and β9-β10 loop. (See Figure 5.1)

N193, on the α3 helix, engages in three hydrogen bonds with S295 and E297, on the α7 helix, along with Y152 on the β9-β10 loop. Y152 also interacts with the backbone

carbonyl of S190 on the α3 helix. In addition to N193, E297 also hydrogen bonds with Y153 and its main-chain carbonyl interacts with main-chain nitrogen of S151. The hydroxyl side chain of S151 engages the main-chain carbonyl of H296.

Along with this five hydrogen bonds cluster involving the α3 helix and the β-sheet, the α7 helix is further anchored with another hydrogen bond between its Q288 and E200 (α3 helix) and burial of W291 in the hydrophobic pocket formed by the α3 and α6 helices. The turn between the α6 and α7 helices is maintained by interactions between the main-chain nitrogen and carbonyl of D284 and K279.

This network of interactions firmly places the α7 helix onto the core of the phosphatase. Replacement of serine 295 with a bulky phenylalanine, identified in screen I and again in screen V, would prevent the close association of this helix with the rest of the protein through steric hindrance and disruption of the hydrogen bond network which is especially rich in its vicinity.

5.3.1. Correlation between an Ordered α7 Helix and a Closed WPD loop.

The α7 helix was not ordered in the first crystal structure resolved for PTP1B[79]. There are now 62 available 3-dimensional structures for PTP1B as the apo-enzyme or in complex with synthetic substrates or with small molecule inhibitors. Although the sample size is small there seems to be a correlation between closure of the WPD loop and ordering of the helix. An ordered α7 helix was found in thirty of the 40 structures with a closed WPD loop while it was absent in the other ten structures. Amongst the 22 structures with an open WPD loop, 16 do not mention the helix but the remaining six structures show or describe a disordered helix.

Figure 5.1: Interactions stitching the α7 helix on the surface of the PTP domain of PTP1B. Residues participating in the association between the α7 helix and the rest of the protein are shown modeled on the three-dimensional structure of PTP1B (entry 1G1H in the RCSB Protein Data Bank). Active site loops are coloured as per Figure 1.1. Pink: PTP loop, Blue: North loop, Yellow: West loop, Green: WPD loop, Purple: East loop with the Arginine 24 also shown in purple as the far limit of the secondary site. Hydrogen bonds are shown in green dotted lines. A) Overview of the residues involved in the interaction, B) Enlargement of the region around the knot.

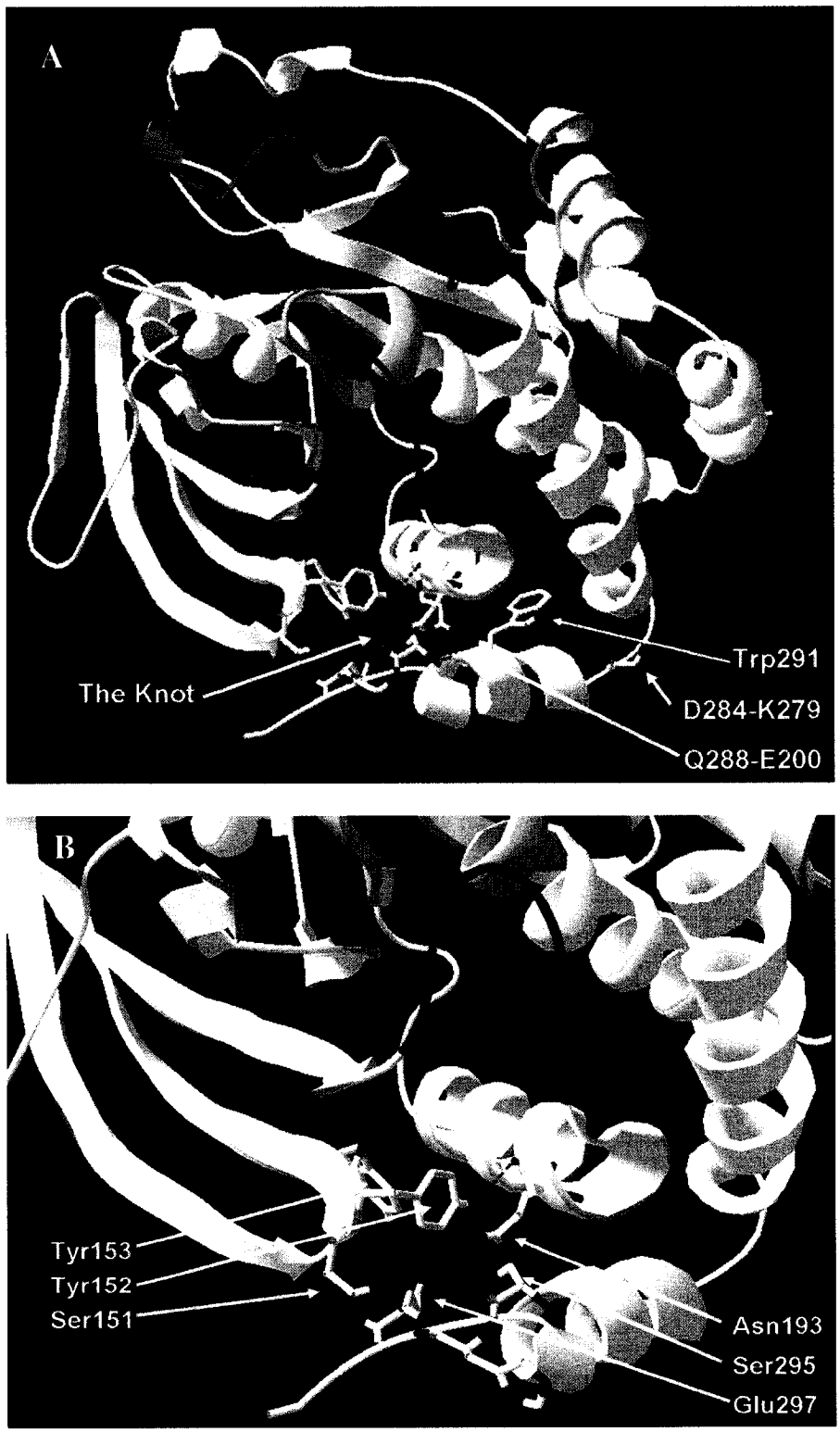

In addition, from discussions with Dr. G. Scapin, non-published Merck structures of PTP1B include twelve instances of a closed loop, seven with an ordered helix and the remaining five not showing those residues. The presence or absence of the helix was found to be dependent on the crystal packing and the space group of the protein. Although the structure of the C215D mutant is published (1PA1) showing the WPD loop in the closed conformation and the helix ordered, it was pointed out that the open WPD loop was modeled with 30% occupancy and in that position the α7 helix had increased B factors reflecting probable partial disordering. Preliminary data from crystallization of the S295F mutant apo-structure (G.Scapin) with an open WPD loop showed a displaced and slightly disordered helix

If the absence of the α7 helix residues in a structure is assumed to be due to its disorder it can be concluded that when the WPD loop is closed, the helix can be ordered or disordered but when the WPD loop is open, the helix is always disordered.

In structures where the WPD loop is open and the α7 helix is disordered (e.g. 1BZH), N193 rotates away from the β sheet towards the α6 helix. Y152 still hydrogen bonds with N193 and so is pulled along with the movement of N193 but the interactions with E297 and S295 are broken. In effect, all the interactions of E297 and H296 with the β-sheet are lost.

If the motion of the two structures is coordinated, disruption of the α7 helix by mutations such as the S295F could also disrupt binding at the active site through the same coordinating mechanism.

5.3.2. Allosteric Site Inhibitor

Although the WPD-α7 helix correlation amongst X-ray structures may be disputable, a link between the α7 helix and the motion of the WPD loop was proposed from studying the mechanism of an allosteric inhibitor binding in the cleft between the α6 and the α3 helix and disrupting the α7 helix[74].

When this inhibitor binds PTP1B, it engages N193 in a hydrogen bond, breaking the network of interactions seen between Y152-N193-S295/E297, and occupies the hydrophobic cleft used by W291. The clash between the inhibitor and W291 pushes the α7 helix away from the rest of the enzyme. Disruption of the interactions with the rest of the protein is proposed to cause the unravelling of the α7 helix[74].

The inhibitor was also found to interact with P188 and L192 to push F191 into the space normally occupied by W179 when the WPD loop is closed. The inability of W179 to change its conformation locked the WPD loop in an open conformation preventing D181 from entering the active site and effectively preventing substrate dephosphorylation.[74]

The dual effect of the inhibitor to disorder the α7 helix and prevent WPD loop closure prompted the authors to suggest that this last visible helix acted to stabilize the closure of the WPD loop. Interestingly, this non-competitive inhibitor was found to be threefold more potent when a full length, 1-403, PTP1B construct was used instead of 1-298 suggesting that residues beyond the α7 helix affected the core PTP domain.[74]

5.3.3. The Contribution of Tyrosines 152 and 153

Tyrosines 152 and 153, sandwiched between the β-sheet and the α3 helix, are critical for binding the IR and cadherin. The conservative mutation of these residues to phenylalanine did not affect catalytic activity but was enough to abolish this interaction[101,102]. These same residues are involved in maintaining the contact between the α7 helix and the rest of the phosphatase through hydrogen bonding between their hydroxyl groups and N193, S190, S295 and E297. Binding of the allosteric inhibitor abolished these interactions by disrupting the α7 helix and engaging N193. The convergence on these tyrosine residues could indicate that the complex formed with the IR or cadherin may also modulate the interaction between the α7 helix and the PTP1B catalytic domain.

Aromatic-aromatic interactions have been found to stabilize the protein's tertiary fold by linking secondary elements to result in greater thermal stability[245,246]. Eighty percent of aromatic pairs identified in proteins are involved in networks formed by groups of three or more tyrosine, phenylalanine and tryptophan residues located between 4.5 and 7Å apart and oriented in a near perpendicular fashion to each other with dihedral angles between 50° and 90°[245]. Tyrosines 152 and 153 are oriented in such a fashion and are in close orientation to the stacked F174, F194 and Y176, linking the β11 strand to the α3 helix, with Y176 located within 4Å of the WPD loop's W179.

These aromatic-aromatic networks are often located near the active site[246] and in the case of chymotrypsin participate in binding the inhibitor 6-chloro-2-pyrone by engaging its aromatic group with the active site's tyrosine 228[245]. In PTP1B, disturbing the N193-Y152-S295/E297 hydrogen bond-knot may disturb the orientation of the two

tyrosines 152 and 153 which might be communicated to the active site through the F174-F194-Y176 stacking.

5.3.4. Commonality with Receptor-Type Tyrosine Phosphatase Regulation

Regardless of their divergent primary sequence, tyrosine phosphatases share a common tertiary structure[81]. The SCOP database reviews and organizes available 3D structures from the PDB databank into protein folds and families. PTP1B is found under the "high-molecular phosphotyrosine protein phosphatases" along with structures from PTPμ, PTPα, SHP1, SHP2, PTP-sl/br7 (PCPTP), TCPTP, YopH, Sptp and LAR. Figure 4.25 shows representative structures for each of these phosphatases to highlight the lack of conservation of the two positive prongs created by K128 and K131 on an otherwise negative surface. In addition, none of these structures show the last helix observed in PTP1B, thereby precluding any comparison, except for the structure of the receptor-type phosphatase (RPTP) LAR which reveals interesting similarities.

Most RPTPs contain two tandem PTP domains. The membrane distal domain, D2, generally lacks efficient catalytic activity and is thought to play a role in substrate specificity or in regulating the activity of the D1 domain[247]. LAR is the only RPTP with both domains crystallized in tandem[248]. Inspection of the orientation of the two domains reveals that the α7 helix of D1 is essentially replaced with D2.

Both domains show the same tertiary fold with the only difference being a longer loop between the α1' and α2' helices in D2. The two domains are connected by a linker loop of four residues, G^{1585}HTE, which shows slight flexibility allowing a rotation of about 3.5° between the two domains. The glycine residue of this loop is critical to

mediate the sharp turn and to lock the orientation at the D1-end of the loop. This residue is stabilized by interactions with R1505, on the α3 helix, and A1581 on the α6 helix; this is similar to the D284-K279 interaction in PTP1B which mediates the turn between the α6 and α7 helices and the E200-Q288 hydrogen bond. The hydroxyl group of T1587 interacts with Q1843 and D1840 on the α5 helix on the D2 domain. This linker loop is highly conserved in RPTPs with both the glycine and the threonine being invariant.[248]

The two domains are also linked by contacts between the β9-β10 loop and the α3 helix of D1 and the β2-β3 loop and the α4 helix of D2. Y1462 (β9-β10 loop) and R1506 (α3 helix) are hydrogen bonded together and to E1836 (α4 helix) through a water molecule[248]. This is reminiscent of the Y152-N193-S295/E297 interactions seen in PTP1B between the same β loop and α3 helix and the α7 helix. In addition, the main chain nitrogen of A1460, which corresponds to the position of S151 in PTP1B, engages Y1677, on the β2 strand of the D2 domain in a hydrogen bond[248]. The importance of these residues and therefore their role in the association between the two domains is highlighted by their high degree of conservation amongst RPTPs containing two PTP domains[248].

In effect, hydrogen bonding and extensive Van der Waals interactions create a tight and complementary fit between the two domains and succeeds in burying 650Å of surface[248]. This large inter-domain contact and limited flexibility suggest that the function of one domain could not be independent of the other[248]. The contribution of the D2 domain to the activity of the D1 is speculative but since the D2 domain is highly conserved, more so than the D1 domain, this indicates it does have a necessary function which has not yet been determined[248]. The similarities found between the interactions

between the two domains of LAR and the ones between the α7 helix and the core of the PTP1B PTP domain may imply a common mechanism of action.

Modulation of the D1-D2 interface by small molecules has been observed to activate LAR and PTPα[249]. This activation was not universal for all RPTP because CD45, along with all non-transmembrane phosphatases tested, was found to be inhibited by these same compounds. Binding of the activator was dependent on the presence of both domains and led to a 4.5-fold increase in the activity of the phosphatase. Disruption of the conserved linker by a mutation of the critical glycine to a valine residue led to an increase in affinity to the activator resulting in 13.5-fold activation. Although increased flexibility between the two domains facilitated activation, a double mutation of the residues corresponding to R1505 and R1506, which are involved in maintaining the interaction between the two domains, decreased activator affinity and activation.

In the proposed model, the activator disrupted the D1-D2 contacts to cause D1 to adopt a higher-activity conformation. This activation was not due to a loss of inhibition by D2 but depended on the formation of new contacts with D2: D1 alone has the same kinetics as the D1-D2 complex and cannot be activated without the presence of D2.[249] It is possible that the α7 helix could modulate the activity or binding affinity of the PTP1B core through similar interactions as the D2 domain on D1.

5.4. Future Work

Sequencing of the resistant mutations from the last screen identified some positions two or more times suggesting that good coverage of the PTP1B amino acid sequence had been obtained. However, only the top 52 resistant clones have been sequenced from this screen leaving ~100 clones with more resistance than the S295F control unexplored and other clones which might show only modest resistance but might provide insight about resistance mechanisms.

Sequencing more clones might reveal interesting information about PTP1B inhibitor binding but the data already obtained has uncovered questions whose answers may be more enlightening than further resistance mapping. The foremost of these would be: how does the α7 region which is so distant from the active site affect competitive inhibitor binding?

Although the mechanism of resistance of the α7 helix mutants is not fully understood, this region displays interesting characteristics worthy of exploration. First the knot region showing extensive hydrogen bonding between the α7 helix, the α3 helix and the β-sheet is the source of broad inhibitor resistance, has been involved in LAR inter-domain contact and in binding the IR. To confirm the role of this knot in inhibitor binding, strategic site-directed mutagenesis of the participating residues need to be done: E297, N193, Y152 and S151. In addition, S295 has been found mutated to both phenylalanine and tyrosine in the screens. These replacements are very disruptive. Mutations of the position with less disruptive replacements such as alanine, valine and leucine to remove the hydroxyl group and slowly increase bulkyness, threonine to conserve the hydroxyl group but explore the sensitivity of the region for bulkier residues,

aspartate to explore an increase in charge and other amino acids might give insight into the role of S295 in the region.

Propagation of the disruption of this knot to the active site can also be studied by site directed mutagenesis following the path of the aromatic scaffolds created by the tyrosine 152 and 153 and the stacked F174, F194 and Y176. Tyrosines 152 and 153 could be replaced by phenylalanine to explore the control of the orientations of these residues by the knot through the tyrosyl hydroxyl group. Also, these positions could each be mutated to non-aromatic residues and evaluated for inhibitor resistance. A drawback of this strategy is the high likelihood that disruption of the buried aromatic stacking will disrupt the structure of the enzyme.

The mechanism of the α7 helix inhibitor resistance may also be mediated by residues on the other side of the α3 helix through the region occupied by the Sunesis allosteric inhibitor. The principle interaction in that region consists of burial of the α7 helix W291 between the α3 and the α6 helix. This burial can be disrupted by mutation of W291 to hydrophilic amino acids or introduction of bulkier residues on the α3 and the α6 helix in the appropriate position such as G277 or L192.

From the result of these mutations, further positions closer to the active site could be targeted to elucidate the network of interactions mediating the inhibitor resistance starting from the α7 helix and terminating at the active site.

Another cluster of resistant mutations surrounding lysines 128 and 131 has been identify on the exterior tip of the β-sheet. This region has been involved in binding the IR by contributing an important hydrophobic patch outside the active site. Synthetic substrates, such as DiFMUP or FDP, would not be adequate to study mutations in this

region since their size allows them only to interact with active site residues. Peptide substrates would also be inadequate since they have been shown to interact with residues on the north loop or in the secondary binding site only. Macromolecular substrates such as the phosphorylated IR or EGFR need to be used to study the effect of lysines 128 and 131 on substrate recognition and their surrounding residues on inhibitor binding.

The crystal structure of the S295F mutation has been partially resolved by Dr. G. Scapin showing no changes at the active site and a slightly disordered α7 helix. Resolution of a structure in complex with an inhibitor has not been successful using protocols adapted for the wild-type enzyme. A "soaking" protocol as the one used for the allosteric inhibitor has been proposed as an alternative. Resolution of this complex might give some indications as to the mechanism of the S295F broad spectrum inhibitor resistance.

The yeast system developed here has been used to screen inhibitors and PTP1B mutations but it could also be used to identify PTP1B regulatory proteins in a cDNA library by transforming it in yeast expressing PTP1B and v-Src and assaying for growth. Negative regulation could be identified by a reduction of growth whereas positive regulation would be identified as a potentiation of the rescue. The nature of these regulatory partners would provide insight into the function of PTP1B and might also provide additional targets for the treatment of diabetes.

5.5. Summary

The use of a yeast system to screen all amino acids of PTP1B for involvement in inhibitor binding proved useful in identifying a region not previously examined by traditional techniques.

The mechanism by which this active site-distal region mediates its effect on competitive inhibitor is not fully understood. A tight knot comprising of a group of hydrogen bonds between the α7 helix, the α3 helix and the β9-β10 loop could be the focus of regulation.

This knot is involved in the interaction with the IR, in LAR's D1-D2 domain modulation, in aromatic-aromatic networks and is also disturbed by allosteric inhibition. Mutation of a critical player in that interaction, S295F, preserves catalytic activity in the yeast but protects against inhibition by small-molecule inhibitors. This region could be exploited in the design of new inhibitors with better bioavailability properties than compounds directed against the active site.

6. Reference List

1. Rizvi,A.A. Type 2 diabetes: epidemiologic trends, evolving pathogenetic [corrected] concepts, and recent changes in therapeutic approach. *South. Med J* **97**, 1079-1087 (2004).

2. International Diabetes Federation. Diabetes Atlas 2003. International Diabetes Federation, Brussels (2003).

3. Saltiel,A.R. & Kahn,C.R. Insulin signalling and the regulation of glucose and lipid metabolism. *Nature* **414**, 799-806 (2001).

4. Asante-Appiah,E. & Kennedy,B.P. Protein tyrosine phosphatases: the quest for negative regulators of insulin action. *Am J Physiol Endocrinol. Metab* **284**, E663-E670 (2003).

5. Suzuki,T., Hiroki,A., Watanabe,T., Yamashita,T., Takei,I. & Umezawa,K. Potentiation of Insulin-related Signal Transduction by a Novel Protein-tyrosine Phosphatase Inhibitor, Et-3,4-dephostatin, on Cultured 3T3-L1 Adipocytes. *J. Biol. Chem.* **276**, 27511-27518 (2001).

6. Xie,L., Lee,S.Y., Andersen,J.N., Waters,S., Shen,K., Guo,X.L., Moller,N.P., Olefsky,J.M., Lawrence,D.S. & Zhang,Z.Y. Cellular effects of small molecule PTP1B inhibitors on insulin signaling. *Biochemistry* **42**, 12792-12804 (2003).

7. Tonks,N.K., Cicirelli,M.F., Diltz,C.D., Krebs,E.G. & Fischer,E.H. Effect of microinjection of a low-Mr human placenta protein tyrosine phosphatase on induction of meiotic cell division in Xenopus oocytes. *Mol Cell Biol* **10**, 458-463 (1990).

8. Liotta,A.S., Kole,H.K., Fales,H.M., Roth,J. & Bernier,M. A synthetic tris-sulfotyrosyl dodecapeptide analogue of the insulin receptor 1146-kinase domain inhibits tyrosine dephosphorylation of the insulin receptor in situ. *J. Biol. Chem.* **269**, 22996-23001 (1994).

9. Ahmad,F., Li,P.M., Meyerovitch,J. & Goldstein,B.J. Osmotic loading of neutralizing antibodies demonstrates a role for protein-tyrosine phosphatase 1B in negative regulation of the insulin action pathway. *J Biol Chem* **270**, 20503-20508 (1995).

10. Kenner,K.A., Anyanwu,E., Olefsky,J.M. & Kusari,J. Protein-tyrosine Phosphatase 1B Is a Negative Regulator of Insulin- and Insulin-like Growth Factor-I-stimulated Signaling. *J. Biol. Chem.* **271**, 19810-19816 (1996).

11. Venable,C.L., Frevert,E.U., Kim,Y.B., Fischer,B.M., Kamatkar,S., Neel,B.G. & Kahn,B.B. Overexpression of protein-tyrosine phosphatase-1B in adipocytes inhibits insulin-stimulated phosphoinositide 3-kinase activity without altering glucose transport or Akt/Protein kinase B activation. *J Biol Chem* **275**, 18318-18326 (2000).

12. Egawa,K., Maegawa,H., Shimizu,S., Morino,K., Nishio,Y., Bryer-Ash,M., Cheung,A.T., Kolls,J.K., Kikkawa,R. & Kashiwagi,A. Protein-tyrosine Phosphatase-1B Negatively Regulates Insulin Signaling in L6 Myocytes and Fao Hepatoma Cells. *J. Biol. Chem.* **276**, 10207-10211 (2001).

13. Clampit,J.E., Meuth,J.L., Smith,H.T., Reilly,R.M., Jirousek,M.R., Trevillyan,J.M. & Rondinone,C.M. Reduction of protein-tyrosine phosphatase-1B increases insulin signaling in FAO hepatoma cells. *Biochem. Biophys. Res. Commun.* **300**, 261-267 (2003).

14. Shi,K., Egawa,K., Maegawa,H., Nakamura,T., Ugi,S., Nishio,Y. & Kashiwagi,A. Protein-Tyrosine Phosphatase 1B Associates with Insulin Receptor and Negatively Regulates Insulin Signaling without Receptor Internalization. *J. Biochem.* **136**, 89-96 (2004).

15. Galic,S., Hauser,C., Kahn,B.B., Haj,F.G., Neel,B.G., Tonks,N.K. & Tiganis,T. Coordinated Regulation of Insulin Signaling by the Protein Tyrosine Phosphatases PTP1B and TCPTP. *Mol. Cell. Biol.* **25**, 819-829 (2005).

16. Shimizu,S., Maegawa,H., Egawa,K., Shi,K., Bryer-Ash,M. & Kashiwagi,A. Mechanism for Differential Effect of Protein-Tyrosine Phosphatase 1B on Akt Versus Mitogen-Activated Protein Kinase in 3T3-L1 Adipocytes. *Endocrinology* **143**, 4563-4569 (2002).

17. Romsicki,Y., Reece,M., Gauthier,J.Y., Asante-Appiah,E. & Kennedy,B.P. Protein Tyrosine Phosphatase-1B Dephosphorylation of the Insulin Receptor Occurs in a Perinuclear Endosome Compartment in Human Embryonic Kidney 293 Cells. *J. Biol. Chem.* **279**, 12868-12875 (2004).

18. Issad,T., Boute,N., Boubekeur,S. & Lacasa,D. Interaction of PTPB with the insulin receptor precursor during its biosynthesis in the endoplasmic reticulum. *Biochimie* **87**, 111-116 (2005).

19. Boute,N., Boubekeur,S., Lacasa,D. & Issad,T. Dynamics of the interaction between the insulin receptor and protein tyrosine-phosphatase 1B in living cells. *EMBO Rep.* **4**, 313-319 (2003).

20. Goldstein,B.J., Bittner-Kowalczyk,A., White,M.F. & Harbeck,M. Tyrosine dephosphorylation and deactivation of insulin receptor substrate-1 by protein-tyrosine phosphatase 1B. Possible facilitation by the formation of a ternary complex with the Grb2 adaptor protein. *J Biol Chem* **275**, 4283-4289 (2000).

21. Cell Signaling Technology. Cell Signaling Technology Product Pathways. Cell Signaling Technology. 2004. http://www.cellsignal.com/

22. Bleyle,L.A., Peng,Y., Ellis,C. & Mooney,R.A. Dissociation of PTPase Levels from Their Modulation of Insulin Receptor Signal Transduction. *Cell. Signal.* **11**, 719-725 (1999).

23. Elchebly,M., Payette,P., Michaliszyn,E., Cromlish,W., Collins,S., Loy,A.L., Normandin,D., Cheng,A., Himms-Hagen,J., Chan,C.C., Ramachandran,C., Gresser,M.J., Tremblay,M.L. & Kennedy,B.P. Increased insulin sensitivity and obesity resistance in mice lacking the protein tyrosine phosphatase-1B gene. *Science* **283**, 1544-1548 (1999).

24. Klaman,L.D., Boss,O., Peroni,O.D., Kim,J.K., Martino,J.L., Zabolotny,J.M., Moghal,N., Lubkin,M., Kim,Y.B., Sharpe,A.H., Stricker-Krongrad,A., Shulman,G.I., Neel,B.G. & Kahn,B.B. Increased energy expenditure, decreased adiposity, and tissue-specific insulin sensitivity in protein-tyrosine phosphatase 1B-deficient mice. *Mol. Cell. Biol.* **20**, 5479-5489 (2000).

25. Qiu,W., Avramoglu,R.K., Dube,N., Chong,T.M., Naples,M., Au,C., Sidiropoulos,K.G., Lewis,G.F., Cohn,J.S., Tremblay,M.L. & Adeli,K. Hepatic PTP-1B Expression Regulates the Assembly and Secretion of Apolipoprotein B-Containing Lipoproteins: Evidence From Protein Tyrosine Phosphatase-1B Overexpression, Knockout, and RNAi Studies. *Diabetes* **53**, 3057-3066 (2004).

26. Whitfield,A.J., Barrett,P.H., van Bockxmeer,F.M. & Burnett,J.R. Lipid Disorders and Mutations in the APOB Gene. *Clin. Chem.* **50**, 1725-1732 (2004).

27. Chan,D.C., Barrett,P.H. & Watts,G.F. Lipoprotein transport in the metabolic syndrome: methodological aspects of stable isotope kinetic studies. *Clin Sci (Lond)* **107**, 221-232 (2004).

28. Taghibiglou,C., Rashid-Kolvear,F., Van Iderstine,S.C., Le Tien,H., Fantus,I.G., Lewis,G.F. & Adeli,K. Hepatic Very Low Density Lipoprotein-ApoB Overproduction Is Associated with Attenuated Hepatic Insulin Signaling and Overexpression of Protein-tyrosine Phosphatase 1B in a Fructose-fed Hamster Model of Insulin Resistance. *J. Biol. Chem.* **277**, 793-803 (2002).

29. Bluher,M., Michael,M.D., Peroni,O.D., Ueki,K., Carter,N., Kahn,B.B. & Kahn,C.R. Adipose Tissue Selective Insulin Receptor Knockout Protects against Obesity and Obesity-Related Glucose Intolerance. *Dev. Cell* **3**, 25-38 (2002).

30. Kushner,J.A., Haj,F.G., Klaman,L.D., Dow,M.A., Kahn,B.B., Neel,B.G. & White,M.F. Islet-Sparing Effects of Protein Tyrosine Phosphatase-1b Deficiency Delays Onset of Diabetes in IRS2 Knockout Mice. *Diabetes* **53**, 61-66 (2004).

31. Haj,F.G., Markova,B., Klaman,L.D., Bohmer,F.D. & Neel,B.G. Regulation of Receptor Tyrosine Kinase Signaling by Protein Tyrosine Phosphatase-1B. *J. Biol. Chem.* **278**, 739-744 (2003).

32. Markova,B., Herrlich,P., Ronnstrand,L. & Bohmer,F.D. Identification of protein tyrosine phosphatases associating with the PDGF receptor. *Biochemistry* **42**, 2691-2699 (2003).

33. Dadke,S. & Chernoff,J. Interaction of protein tyrosine phosphatase (PTP) 1B with its substrates is influenced by two distinct binding domains. *Biochem J* **364**, 377-383 (2002).

34. Bjorge,J.D., Pang,A. & Fujita,D.J. Identification of Protein-tyrosine Phosphatase 1B as the Major Tyrosine Phosphatase Activity Capable of Dephosphorylating and Activating c-Src in Several Human Breast Cancer Cell Lines. *J. Biol. Chem.* **275**, 41439-41446 (2000).

35. Ramachandran,C. & Kennedy,B.P. Protein tyrosine phosphatase 1B: a novel target for type 2 diabetes and obesity. *Curr. Top. Med. Chem.* **3**, 749-757 (2003).

36. Cheng,A., Uetani,N., Simoncic,P.D., Chaubey,V.P., Lee-Loy,A., McGlade,C.J., Kennedy,B.P. & Tremblay,M.L. Attenuation of leptin action and regulation of obesity by protein tyrosine phosphatase 1B. *Dev. Cell* **2**, 497-503 (2002).

37. Spiegelman,B.M. & Flier,J.S. Obesity and the Regulation of Energy Balance. *Cell* **104**, 531-543 (2001).

38. Unger,R.H. LIPOTOXIC DISEASES. *Annu. Rev. Med.* **53**, 319-336 (2002).

39. Zabolotny,J.M., Bence-Hanulec,K.K., Stricker-Krongrad,A., Haj,F., Wang,Y., Minokoshi,Y., Kim,Y.B., Elmquist,J.K., Tartaglia,L.A., Kahn,B.B. & Neel,B.G. PTP1B Regulates Leptin Signal Transduction In Vivo. *Dev. Cell* **2**, 489-495 (2002).

40. Lam,N.T., Lewis,J.T., Cheung,A.T., Luk,C.T., Tse,J., Wang,J., Bryer-Ash,M., Kolls,J.K. & Kieffer,T.J. Leptin Increases Hepatic Insulin Sensitivity and Protein Tyrosine Phosphatase 1B Expression. *Mol. Endocrinol.* **18**, 1333-1345 (2004).

41. Zinker,B.A., Rondinone,C.M., Trevillyan,J.M., Gum,R.J., Clampit,J.E., Waring,J.F., Xie,N., Wilcox,D., Jacobson,P., Frost,L., Kroeger,P.E., Reilly,R.M., Koterski,S., Opgenorth,T.J., Ulrich,R.G., Crosby,S., Butler,M., Murray,S.F., McKay,R.A., Bhanot,S., Monia,B.P. & Jirousek,M.R. PTP1B antisense oligonucleotide lowers PTP1B protein, normalizes blood glucose, and improves insulin sensitivity in diabetic mice. *Proc. Natl. Acad. Sci. U. S. A.* **99**, 11357-11362 (2002).

42. Rondinone,C.M., Trevillyan,J.M., Clampit,J., Gum,R.J., Berg,C., Kroeger,P., Frost,L., Zinker,B.A., Reilly,R., Ulrich,R., Butler,M., Monia,B.P., Jirousek,M.R. & Waring,J.F. Protein tyrosine phosphatase 1B reduction regulates adiposity and expression of genes involved in lipogenesis. *Diabetes* **51**, 2405-2411 (2002).

43. Haj,F.G., Zabolotny,J.M., Kim,Y.B., Kahn,B.B. & Neel,B.G. Liver specific protein-tyrosine phosphatase 1B (PTP1B) Re-expression alters glucose homeostasis of PTP1B-/-mice. *J. Biol. Chem.* M413240200 (2005).

44. Zabolotny,J.M., Haj,F.G., Kim,Y.B., Kim,H.J., Shulman,G.I., Kim,J.K., Neel,B.G. & Kahn,B.B. Transgenic Overexpression of Protein-tyrosine Phosphatase 1B in Muscle Causes Insulin Resistance, but Overexpression with Leukocyte Antigen-related Phosphatase Does Not Additively Impair Insulin Action. *J. Biol. Chem.* **279**, 24844-24851 (2004).

45. Forsell,P., Boie,Y., Montalibet,J., Collins,S. & Kennedy,B.P. Genomic characterization of the human and mouse protein tyrosine phosphatase-1B genes. *Gene* **260**, 145-153 (2000).

46. Bento,J.L., Palmer,N.D., Mychaleckyj,J.C., Lange,L.A., Langefeld,C.D., Rich,S.S., Freedman,B.I. & Bowden,D.W. Association of Protein Tyrosine Phosphatase 1B Gene Polymorphisms With Type 2 Diabetes. *Diabetes* **53**, 3007-3012 (2004).

47. Palmer,N.D., Bento,J.L., Mychaleckyj,J.C., Langefeld,C.D., Campbell,J.K., Norris,J.M., Haffner,S.M., Bergman,R.N. & Bowden,D.W. Association of Protein Tyrosine Phosphatase 1B Gene Polymorphisms With Measures of Glucose Homeostasis in Hispanic Americans: The Insulin Resistance Atherosclerosis Study (IRAS) Family Study. *Diabetes* **53**, 3013-3019 (2004).

48. Mok,A., Cao,H., Zinman,B., Hanley,A.J.G., Harris,S.B., Kennedy,B.P. & Hegele,R.A. A Single Nucleotide Polymorphism in Protein Tyrosine Phosphatase PTP-1B Is Associated with Protection from Diabetes or Impaired Glucose Tolerance in Oji-Cree. *J Clin Endocrinol Metab* **87**, 724-727 (2002).

49. Echwald,S.M., Bach,H., Vestergaard,H., Richelsen,B., Kristensen,K., Drivsholm,T., Borch-Johnsen,K., Hansen,T. & Pedersen,O. A P387L variant in protein tyrosine phosphatase-1B (PTP-1B) is associated with type 2 diabetes and impaired serine phosphorylation of PTP-1B in vitro. *Diabetes* **51**, 1-6 (2002).

50. Di Paola,R., Frittitta,L., Miscio,G., Bozzali,M., Baratta,R., Centra,M., Spampinato,D., Santagati,M.G., Ercolino,T., Cisternino,C., Soccio,T., Mastroianno,S., Tassi,V., Almgren,P., Pizzuti,A., Vigneri,R. & Trischitta,V. A variation in 3' UTR of hPTP1B increases specific gene expression and associates with insulin resistance. *Am J Hum. Genet.* **70**, 806-812 (2002).

51. De Cosmo,S., Marucci,A., Ciociola,E., Di Paola,R., Pucci,L., Penno,G., Del Prato,S., Piras,G.P., Trevisan,R., Giunti,S., Viberti,G.C. & Trischitta,V. Lack of evidence for the 1484insG variant at the 3'-UTR of the protein tyrosine phosphatase 1B (PTP1B) gene as a genetic determinant of diabetic nephropathy development in type 1 diabetic patients. *Nephrol. Dial. Transplant.* **19**, 2419-2420 (2004).

52. Santaniemi,M., Ukkola,O. & Kesaniemi,A. Tyrosine phosphatase 1B and leptin receptor genes and their interaction in type 2 diabetes. *J. Intern. Med.* **256**, 48-55 (2004).

53. McGuire,M.C., Fields,R.M., Nyomba,B.L., Raz,I., Bogardus,C., Tonks,N.K. & Sommercorn,J. Abnormal regulation of protein tyrosine phosphatase activities in skeletal muscle of insulin-resistant humans. *Diabetes* **40**, 939-942 (1991).

54. Kusari,J., Kenner,K.A., Suh,K.I., Hill,D.E. & Henry,R.R. Skeletal muscle protein tyrosine phosphatase activity and tyrosine phosphatase 1B protein content are associated with insulin action and resistance. *J Clin Invest* **93**, 1156-1162 (1994).

55. Ahmad,F., Azevedo,J.L., Cortright,R., Dohm,G.L. & Goldstein,B.J. Alterations in skeletal muscle protein-tyrosine phosphatase activity and expression in insulin-resistant human obesity and diabetes. *J Clin Invest* **100**, 449-458 (1997).

56. Wu,X., Hardy,V.E., Joseph,J.I., Jabbour,S., Mahadev,K., Zhu,L. & Goldstein,B.J. Protein-tyrosine phosphatase activity in human adipocytes is strongly correlated with insulin-stimulated glucose uptake and is a target of insulin-induced oxidative inhibition. *Metabolism* **52**, 705-712 (2003).

57. Ahmad,F., Considine,R.V., Bauer,T.L., Ohannesian,J.P., Marco,C.C. & Goldstein,B.J. Improved sensitivity to insulin in obese subjects following weight loss is accompanied by reduced protein-tyrosine phosphatases in adipose tissue. *Metabolism* **46**, 1140-1145 (1997).

58. Cheung,A., Kusari,J., Jansen,D., Bandyopadhyay,D., Kusari,A. & Bryer-Ash,M. Marked impairment of protein tyrosine phosphatase 1B activity in adipose tissue of obese subjects with and without type 2 diabetes mellitus. *J Lab Clin Med* **134**, 115-123 (1999).

59. Worm,D., Vinten,J. & Beck-Nielsen,H. The significance of phosphotyrosine phosphatase (PTPase) 1B in insulin signalling. *Diabetologia* **42**, 1146-1149 (1999).

60. Dadke,S.S., Li,H.C., Kusari,A.B., Begum,N. & Kusari,J. Elevated Expression and Activity of Protein-Tyrosine Phosphatase 1B in Skeletal Muscle of Insulin-Resistant Type II Diabetic Goto-Kakizaki Rats. *Biochem. Biophys. Res. Commun.* **274**, 583-589 (2000).

61. Hirata,A.E., Alvarez-Rojas,F., Campello Carvalheira,J.B., de Oliveira Carvalho,C.R., Dolnikoff,M.S. & Abdalla Saad,M.J. Modulation of IR/PTP1B interaction and downstream signaling in insulin sensitive tissues of MSG-rats. *Life Sci.* **73**, 1369-1381 (2003).

62. Lee,S.R., Kwon,K.S., Kim,S.R. & Rhee,S.G. Reversible Inactivation of Protein-tyrosine Phosphatase 1B in A431 Cells Stimulated with Epidermal Growth Factor. *J. Biol. Chem.* **273**, 15366-15372 (1998).

63. Mahadev,K., Zilbering,A., Zhu,L. & Goldstein,B.J. Insulin-stimulated Hydrogen Peroxide Reversibly Inhibits Protein-tyrosine Phosphatase 1B in Vivo and Enhances the Early Insulin Action Cascade. *J. Biol. Chem.* **276**, 21938-21942 (2001).

64. Salmeen,A., Andersen,J.N., Myers,M.P., Meng,T.C., Hinks,J.A., Tonks,N.K. & Barford,D. Redox regulation of protein tyrosine phosphatase 1B involves a sulphenyl-amide intermediate. *Nature* **423**, 769-773 (2003).

65. van Montfort,R.L., Congreve,M., Tisi,D., Carr,R. & Jhoti,H. Oxidation state of the active-site cysteine in protein tyrosine phosphatase 1B. *Nature* **423**, 773-777 (2003).

66. Taylor,S.D. Inhibitors of protein tyrosine phosphatase 1B (PTP1B). *Curr. Top. Med Chem* **3**, 759-782 (2003).

67. Pei,Z., Liu,G., Lubben,T.H. & Szczepankiewicz,B.G. Inhibition of protein tyrosine phosphatase 1B as a potential treatment of diabetes and obesity. *Curr. Pharm. Des* **10**, 3481-3504 (2004).

68. Huyer,G., Kelly,J., Moffat,J., Zamboni,R., Jia,Z., Gresser,M.J. & Ramachandran,C. Affinity selection from peptide libraries to determine substrate specificity of protein tyrosine phosphatases. *Anal. Biochem.* **258**, 19-30 (1998).

69. Vetter,S.W., Keng,Y.F., Lawrence,D.S. & Zhang,Z.Y. Assessment of protein-tyrosine phosphatase 1B substrate specificity using "inverse alanine scanning". *J. Biol. Chem.* **275**, 2265-2268 (2000).

70. You,T., Muise,E.S., Itie,A., Michaliszyn,E., Wagner,J., Jothy,S., Lapp,W.S. & Tremblay,M.L. Impaired bone marrow microenvironment and immune function in T cell protein tyrosine phosphatase-deficient mice. *J Exp Med* **186**, 683-693 (1997).

71. Johnson,T.O., Ermolieff,J. & Jirousek,M.R. PROTEIN TYROSINE PHOSPHATASE 1B INHIBITORS FOR DIABETES. *Nat Rev Drug Discov* **1**, 696-709 (2002).

72. Liu,G. & Trevillyan,J.M. Protein tyrosine phosphatase 1B as a target for the treatment of impaired glucose tolerance and type II diabetes. *Curr. Opin. Investig. Drugs* **3**, 1608-1616 (2002).

73. Taylor,S.D. & Hill,B. Recent advances in protein tyrosine phosphatase 1B inhibitors. *Expert Opin. Investig. Drugs* **13**, 199-214 (2004).

74. Wiesmann,C., Barr,K.J., Kung,J., Zhu,J., Erlanson,D.A., Shen,W., Fahr,B.J., Zhong,M., Taylor,L., Randal,M., McDowell,R.S. & Hansen,S.K. Allosteric inhibition of protein tyrosine phosphatase 1B. *Nat Struct. Mol Biol.* **11**, 730-737 (2004).

75. ISIS Pharmaceuticals. ISIS Phamaceuticals Antisense Pipeline. ISIS Pharmaceuticals. 2005. http://www.isispharm.com/product_pipeline.html

76. Frangioni,J.V., Beahm,P.H., Shifrin,V., Jost,C.A. & Neel,B.G. The nontransmembrane tyrosine phosphatase PTP-1B localizes to the endoplasmic reticulum via its 35 amino acid C-terminal sequence. *Cell* **68**, 545-560 (1992).

77. Sell,S.M. & Reese,D. Insulin-inducible changes in the relative ratio of PTP1B splice variants. *Mol Genet. Metab* **66**, 189-192 (1999).

78. Shifrin,V.I. & Neel,B.G. Growth factor-inducible alternative splicing of nontransmembrane phosphotyrosine phosphatase PTP-1B pre-mRNA. *J Biol. Chem.* **268**, 25376-25384 (1993).

79. Barford,D., Flint,A.J. & Tonks,N.K. Crystal structure of human protein tyrosine phosphatase 1B. *Science* **263**, 1397-1404 (1994).

80. Jia,Z., Barford,D., Flint,A.J. & Tonks,N.K. Structural basis for phosphotyrosine peptide recognition by protein tyrosine phosphatase 1B. *Science* **268**, 1754-1758 (1995).

81. Andersen,J.N., Mortensen,O.H., Peters,G.H., Drake,P.G., Iversen,L.F., Olsen,O.H., Jansen,P.G., Andersen,H.S., Tonks,N.K. & Moller,N.P. Structural and evolutionary relationships among protein tyrosine phosphatase domains. *Mol Cell Biol.* **21**, 7117-7136 (2001).

82. Scapin,G., Patel,S., Patel,V., Kennedy,B. & Asante-Appiah,E. The structure of apo protein-tyrosine phosphatase 1B C215S mutant: more than just an S --> O change. *Protein Sci* **10**, 1596-1605 (2001).

83. Groves,M.R., Yao,Z.J., Roller,P.P., Burke,T.R., Jr. & Barford,D. Structural basis for inhibition of the protein tyrosine phosphatase 1B by phosphotyrosine peptide mimetics. *Biochemistry* **37**, 17773-17783 (1998).

84. Peters,G.H., Frimurer,T.M., Andersen,J.N. & Olsen,O.H. Molecular dynamics simulations of protein-tyrosine phosphatase 1B. II. substrate-enzyme interactions and dynamics. *Biophys J* **78**, 2191-2200 (2000).

85. Juszczak,L.J., Zhang,Z.Y., Wu,L., Gottfried,D.S. & Eads,D.D. Rapid loop dynamics of Yersinia protein tyrosine phosphatases. *Biochemistry* **36**, 2227-2236 (1997).

86. Romsicki,Y., Scapin,G., Beaulieu-Audy,V., Patel,S., Becker,J.W., Kennedy,B.P. & Asante-Appiah,E. Functional characterization and crystal structure of the C215D mutant of protein-tyrosine phosphatase-1B. *J Biol. Chem.* **278**, 29009-29015 (2003).

87. Peters,G.H., Frimurer,T.M., Andersen,J.N. & Olsen,O.H. Molecular dynamics simulations of protein-tyrosine phosphatase 1B. I. ligand-induced changes in the protein motions. *Biophys J* **77**, 505-515 (1999).

88. Puius,Y.A., Zhao,Y., Sullivan,M., Lawrence,D.S., Almo,S.C. & Zhang,Z.Y. Identification of a second aryl phosphate-binding site in protein-tyrosine phosphatase 1B: a paradigm for inhibitor design. *Proc. Natl. Acad. Sci. U. S. A.* **94**, 13420-13425 (1997).

89. Peters,G.H., Iversen,L.F., Branner,S., Andersen,H.S., Mortensen,S.B., Olsen,O.H., Moller,K.B. & Moller,N.P. Residue 259 is a key determinant of substrate specificity of protein-tyrosine phosphatases 1B and alpha. *J Biol. Chem.* **275**, 18201-18209 (2000).

90. Brautigan,D.L. & Pinault,F.M. Serine phosphorylation of protein tyrosine phosphatase (PTP1B) in HeLa cells in response to analogues of cAMP or diacylglycerol plus okadaic acid. *Mol Cell Biochem* **127-128**, 121-129 (1993).

91. Schievella,A.R., Paige,L.A., Johnson,K.A., Hill,D.E. & Erikson,R.L. Protein tyrosine phosphatase 1B undergoes mitosis-specific phosphorylation on serine. *Cell Growth Differ.* **4**, 239-246 (1993).

92. Flint,A.J., Gebbink,M.F., Franza,B.R., Jr., Hill,D.E. & Tonks,N.K. Multi-site phosphorylation of the protein tyrosine phosphatase, PTP1B: identification of cell cycle regulated and phorbol ester stimulated sites of phosphorylation. *EMBO J.* **12**, 1937-1946 (1993).

93. Shifrin,V.I., Davis,R.J. & Neel,B.G. Phosphorylation of protein-tyrosine phosphatase PTP-1B on identical sites suggests activation of a common signaling pathway during mitosis and stress response in mammalian cells. *J. Biol. Chem.* **272**, 2957-2962 (1997).

94. Ravichandran,L.V., Chen,H., Li,Y. & Quon,M.J. Phosphorylation of PTP1B at Ser(50) by Akt impairs its ability to dephosphorylate the insulin receptor. *Mol. Endocrinol.* **15**, 1768-1780 (2001).

95. Moeslein,F.M., Myers,M.P. & Landreth,G.E. The CLK family kinases, CLK1 and CLK2, phosphorylate and activate the tyrosine phosphatase, PTP-1B. *J. Biol. Chem.* **274**, 26697-26704 (1999).

96. Seely,B.L., Staubs,P.A., Reichart,D.R., Berhanu,P., Milarski,K.L., Saltiel,A.R., Kusari,J. & Olefsky,J.M. Protein tyrosine phosphatase 1B interacts with the activated insulin receptor. *Diabetes* **45**, 1379-1385 (1996).

97. Liu,F. & Chernoff,J. Protein tyrosine phosphatase 1B interacts with and is tyrosine phosphorylated by the epidermal growth factor receptor. *Biochem J* **327 (Pt 1)**, 139-145 (1997).

98. Charbonneau,H., Tonks,N.K., Kumar,S., Diltz,C.D., Harrylock,M., Cool,D.E., Krebs,E.G., Fischer,E.H. & Walsh,K.A. Human placenta protein-tyrosine-phosphatase: amino acid sequence and relationship to a family of receptor-like proteins. *Proc. Natl. Acad. Sci U. S. A* **86**, 5252-5256 (1989).

99. Dadke,S., Kusari,A. & Kusari,J. Phosphorylation and activation of protein tyrosine phosphatase (PTP) 1B by insulin receptor. *Mol. Cell. Biochem.* **221**, 147-154 (2001).

100. Tao,J., Malbon,C.C. & Wang,H.Y. Insulin stimulates tyrosine phosphorylation and inactivation of protein-tyrosine phosphatase 1B in vivo. *J. Biol. Chem.* **276**, 29520-29525 (2001).

101. Rhee,J., Lilien,J. & Balsamo,J. Essential tyrosine residues for interaction of the non-receptor protein-tyrosine phosphatase PTP1B with N-cadherin. *J Biol. Chem.* **276**, 6640-6644 (2001).

102. Bandyopadhyay,D., Kusari,A., Kenner,K.A., Liu,F., Chernoff,J., Gustafson,T.A. & Kusari,J. Protein-tyrosine phosphatase 1B complexes with the insulin receptor in vivo and is tyrosine-phosphorylated in the presence of insulin. *J. Biol. Chem.* **272**, 1639-1645 (1997).

103. Balsamo,J., Leung,T., Ernst,H., Zanin,M.K., Hoffman,S. & Lilien,J. Regulated binding of PTP1B-like phosphatase to N-cadherin: control of cadherin-mediated adhesion by dephosphorylation of beta-catenin. *J Cell Biol.* **134**, 801-813 (1996).

104. Liu,F., Hill,D.E. & Chernoff,J. Direct binding of the proline-rich region of protein tyrosine phosphatase 1B to the Src homology 3 domain of p130(Cas). *J Biol. Chem.* **271**, 31290-31295 (1996).

105. Frangioni,J.V., Oda,A., Smith,M., Salzman,E.W. & Neel,B.G. Calpain-catalyzed cleavage and subcellular relocation of protein phosphotyrosine phosphatase 1B (PTP-1B) in human platelets. *EMBO J.* **12**, 4843-4856 (1993).

106. Zhang,Z.Y., Maclean,D., McNamara,D.J., Sawyer,T.K. & Dixon,J.E. Protein tyrosine phosphatase substrate specificity: size and phosphotyrosine positioning requirements in peptide substrates. *Biochemistry* **33**, 2285-2290 (1994).

107. Zhang,Z.Y. Protein-tyrosine phosphatases: biological function, structural characteristics, and mechanism of catalysis. *Crit. Rev. Biochem. Mol. Biol.* **33**, 1-52 (1998).

108. Tonks,N.K. PTP1B: from the sidelines to the front lines! *FEBS Lett.* **546**, 140-148 (2003).

109. Denu,J.M. & Dixon,J.E. Protein tyrosine phosphatases: mechanisms of catalysis and regulation. *Curr. Opin. Chem. Biol.* **2**, 633-641 (1998).

110. Flint,A.J., Tiganis,T., Barford,D. & Tonks,N.K. Development of "substrate-trapping" mutants to identify physiological substrates of protein tyrosine phosphatases. *Proc. Natl. Acad. Sci. U. S. A.* **94**, 1680-1685 (1997).

111. Zhang,Y.L., Yao,Z.J., Sarmiento,M., Wu,L., Burke,T.R., Jr. & Zhang,Z.Y. Thermodynamic study of ligand binding to protein-tyrosine phosphatase 1B and its substrate-trapping mutants. *J Biol. Chem.* **275**, 34205-34212 (2000).

112. Kolmodin,K. & Aqvist,J. The catalytic mechanism of protein tyrosine phosphatases revisited. *FEBS Lett.* **498**, 208-213 (2001).

113. Peters,G.H., Frimurer,T.M. & Olsen,O.H. Electrostatic evaluation of the signature motif (H/V)CX5R(S/T) in protein-tyrosine phosphatases. *Biochemistry* **37**, 5383-5393 (1998).

114. Pannifer,A.D., Flint,A.J., Tonks,N.K. & Barford,D. Visualization of the cysteinyl-phosphate intermediate of a protein-tyrosine phosphatase by x-ray crystallography. *J Biol. Chem.* **273**, 10454-10462 (1998).

115. Pedersen,A.K., Guo,X.L., Moller,K.B., Peters,G.H., Andersen,H.S., Kastrup,J.S., Mortensen,S.B., Iversen,L.F., Zhang,Z.Y. & Moller,N.P. Residue 182 influences the second step of protein-tyrosine phosphatase-mediated catalysis. *Biochem J* **378**, 421-433 (2004).

116. Hoff,R.H., Wu,L., Zhou,B., Zhang,Z.Y. & Hengge,A.C. Does Positive Charge at the Active Sites of Phosphatases Cause a Change in Mechanism? The Effect of the Conserved Arginine on the Transition State for Phosphoryl Transfer in the Protein-Tyrosine Phosphatase from *Yersinia* . *J. Am. Chem. Soc.* **121**, 9514-9521 (1999).

117. Vetter,S.W., Keng,Y.F., Lawrence,D.S. & Zhang,Z.Y. Assessment of protein-tyrosine phosphatase 1B substrate specificity using "inverse alanine scanning". *J Biol. Chem.* **275**, 2265-2268 (2000).

118. Zhang,Z.Y., Thieme-Sefler,A.M., Maclean,D., McNamara,D.J., Dobrusin,E.M., Sawyer,T.K. & Dixon,J.E. Substrate specificity of the protein tyrosine phosphatases. *Proc. Natl. Acad. Sci U. S. A* **90**, 4446-4450 (1993).

119. Milarski,K.L., Zhu,G., Pearl,C.G., McNamara,D.J., Dobrusin,E.M., Maclean,D., Thieme-Sefler,A., Zhang,Z.Y., Sawyer,T., Decker,S.J. & . Sequence specificity in recognition of the epidermal growth factor receptor by protein tyrosine phosphatase 1B. *J Biol. Chem.* **268**, 23634-23639 (1993).

120. Agostinis,P., Donella-Deana,A., Van Hoof,C., Cesaro,L., Brunati,A.M., Ruzzene,M., Merlevede,W., Pinna,L.A. & Goris,J. A comparative study of the phosphotyrosyl phosphatase specificity of protein phosphatase type 2A and phosphotyrosyl phosphatase type 1B using phosphopeptides and the phosphoproteins p50/HS1, c-Fgr and Lyn. *Eur J Biochem* **236**, 548-557 (1996).

121. Huyer,G., Kelly,J., Moffat,J., Zamboni,R., Jia,Z., Gresser,M.J. & Ramachandran,C. Affinity selection from peptide libraries to determine substrate specificity of protein tyrosine phosphatases. *Anal. Biochem* **258**, 19-30 (1998).

122. Glover,N.R. & Tracey,A.S. Nuclear magnetic resonance and restrained molecular dynamics studies of the interaction of an epidermal growth factor-derived peptide with protein tyrosine phosphatase 1B. *Biochemistry* **38**, 5256-5271 (1999).

123. Sarmiento,M., Puius,Y.A., Vetter,S.W., Keng,Y.F., Wu,L., Zhao,Y., Lawrence,D.S., Almo,S.C. & Zhang,Z.Y. Structural basis of plasticity in protein tyrosine phosphatase 1B substrate recognition. *Biochemistry* **39**, 8171-8179 (2000).

124. Wang,X.Y., Bergdahl,K., Heijbel,A., Liljebris,C. & Bleasdale,J.E. Analysis of in vitro interactions of protein tyrosine phosphatase 1B with insulin receptors. *Mol. Cell. Endocrinol.* **173**, 109-120 (2001).

125. Glover,N.R. & Tracey,A.S. Modeling studies of the interactions between the insulin receptor kinase domain and protein tyrosine phosphatase 1B. *J. Am. Chem. Soc.* **121**, 3579-3589 (1999).

126. Salmeen,A., Andersen,J.N., Myers,M.P., Tonks,N.K. & Barford,D. Molecular basis for the dephosphorylation of the activation segment of the insulin receptor by protein tyrosine phosphatase 1B. *Mol Cell* **6**, 1401-1412 (2000).

127. Dadke,S., Kusari,J. & Chernoff,J. Down-regulation of insulin signaling by protein-tyrosine phosphatase 1B is mediated by an N-terminal binding region. *J. Biol. Chem.* **275**, 23642-23647 (2000).

128. Bleasdale,J.E., Ogg,D., Palazuk,B.J., Jacob,C.S., Swanson,M.L., Wang,X.Y., Thompson,D.P., Conradi,R.A., Mathews,W.R., Laborde,A.L., Stuchly,C.W., Heijbel,A., Bergdahl,K., Bannow,C.A., Smith,C.W., Svensson,C., Liljebris,C., Schostarez,H.J., May,P.D., Stevens,F.C. & Larsen,S.D. Small molecule peptidomimetics containing a novel phosphotyrosine bioisostere inhibit protein tyrosine phosphatase 1B and augment insulin action. *Biochemistry* **40**, 5642-5654 (2001).

129. Burke,T.R., Jr., Ye,B., Yan,X., Wang,S., Jia,Z., Chen,L., Zhang,Z.Y. & Barford,D. Small molecule interactions with protein-tyrosine phosphatase PTP1B and their use in inhibitor design. *Biochemistry* **35**, 15989-15996 (1996).

130. Yao,Z.J., Ye,B., Wu,X.W., Wang,S., Wu,L., Zhang,Z.Y. & Burke,T.R., Jr. Structure-based design and synthesis of small molecule protein-tyrosine phosphatase 1B inhibitors. *Bioorg. Med. Chem.* **6**, 1799-1810 (1998).

131. Iversen,L.F., Andersen,H.S., Branner,S., Mortensen,S.B., Peters,G.H., Norris,K., Olsen,O.H., Jeppesen,C.B., Lundt,B.F., Ripka,W., Moller,K.B. & Moller,N.P. Structure-based design of a low molecular weight, nonphosphorus, nonpeptide, and highly selective inhibitor of protein-tyrosine phosphatase 1B. *J Biol. Chem.* **275**, 10300-10307 (2000).

132. Sarmiento,M., Wu,L., Keng,Y.F., Song,L., Luo,Z., Huang,Z., Wu,G.Z., Yuan,A.K. & Zhang,Z.Y. Structure-based discovery of small molecule inhibitors targeted to protein tyrosine phosphatase 1B. *J Med. Chem.* **43**, 146-155 (2000).

133. Murthy,V.S. & Kulkarni,V.M. Molecular modeling of protein tyrosine phosphatase 1B (PTP 1B) inhibitors. *Bioorg. Med. Chem.* **10**, 897-906 (2002).

134. Scapin,G., Patel,S.B., Becker,J.W., Wang,Q., Desponts,C., Waddleton,D., Skorey,K., Cromlish,W., Bayly,C., Therien,M., Gauthier,J.Y., Li,C.S., Lau,C.K., Ramachandran,C.,

Kennedy,B.P. & Asante-Appiah,E. The structural basis for the selectivity of benzotriazole inhibitors of PTP1B. *Biochemistry* **42**, 11451-11459 (2003).

135. Jia,Z., Ye,Q., Dinaut,A.N., Wang,Q., Waddleton,D., Payette,P., Ramachandran,C., Kennedy,B., Hum,G. & Taylor,S.D. Structure of protein tyrosine phosphatase 1B in complex with inhibitors bearing two phosphotyrosine mimetics. *J Med. Chem.* **44**, 4584-4594 (2001).

136. Asante-Appiah,E., Patel,S., Dufresne,C., Roy,P., Wang,Q., Patel,V., Friesen,R.W., Ramachandran,C., Becker,J.W., Leblanc,Y., Kennedy,B.P. & Scapin,G. The structure of PTP-1B in complex with a peptide inhibitor reveals an alternative binding mode for bisphosphonates. *Biochemistry* **41**, 9043-9051 (2002).

137. Gao,Y., Voigt,J., Zhao,H., Pais,G.C., Zhang,X., Wu,L., Zhang,Z.Y. & Burke,T.R., Jr. Utilization of a peptide lead for the discovery of a novel PTP1B-binding motif. *J Med. Chem.* **44**, 2869-2878 (2001).

138. Pei,Z., Li,X., Liu,G., Abad-Zapatero,C., Lubben,T., Zhang,T., Ballaron,S.J., Hutchins,C.W., Trevillyan,J.M. & Jirousek,M.R. Discovery and SAR of novel, potent and selective protein tyrosine phosphatase 1B inhibitors. *Bioorg. Med. Chem. Lett.* **13**, 3129-3132 (2003).

139. Xin,Z., Oost,T.K., Abad-Zapatero,C., Hajduk,P.J., Pei,Z., Szczepankiewicz,B.G., Hutchins,C.W., Ballaron,S.J., Stashko,M.A., Lubben,T., Trevillyan,J.M., Jirousek,M.R. & Liu,G. Potent, selective inhibitors of protein tyrosine phosphatase 1B. *Bioorg. Med. Chem. Lett.* **13**, 1887-1890 (2003).

140. Liu,G., Xin,Z., Pei,Z., Hajduk,P.J., Abad-Zapatero,C., Hutchins,C.W., Zhao,H., Lubben,T.H., Ballaron,S.J., Haasch,D.L., Kaszubska,W., Rondinone,C.M., Trevillyan,J.M. & Jirousek,M.R. Fragment screening and assembly: a highly efficient approach to a selective and cell active protein tyrosine phosphatase 1B inhibitor. *J Med. Chem.* **46**, 4232-4235 (2003).

141. Zhao,H., Liu,G., Xin,Z., Serby,M.D., Pei,Z., Szczepankiewicz,B.G., Hajduk,P.J., Abad-Zapatero,C., Hutchins,C.W., Lubben,T.H., Ballaron,S.J., Haasch,D.L., Kaszubska,W., Rondinone,C.M., Trevillyan,J.M. & Jirousek,M.R. Isoxazole carboxylic acids as protein tyrosine phosphatase 1B (PTP1B) inhibitors. *Bioorg. Med. Chem. Lett.* **14**, 5543-5546 (2004).

142. Liu,D.G., Gao,Y., Voigt,J.H., Lee,K., Nicklaus,M.C., Wu,L., Zhang,Z.Y. & Burke,T.R., Jr. Acylsulfonamide-containing PTP1B inhibitors designed to mimic an enzyme-bound water of hydration. *Bioorg. Med. Chem. Lett.* **13**, 3005-3007 (2003).

143. Andersen,H.S., Olsen,O.H., Iversen,L.F., Sorensen,A.L., Mortensen,S.B., Christensen,M.S., Branner,S., Hansen,T.K., Lau,J.F., Jeppesen,L., Moran,E.J., Su,J., Bakir,F., Judge,L., Shahbaz,M., Collins,T., Vo,T., Newman,M.J., Ripka,W.C. & Moller,N.P. Discovery and SAR of a novel selective and orally bioavailable nonpeptide classical competitive inhibitor class of protein-tyrosine phosphatase 1B. *J Med. Chem.* **45**, 4443-4459 (2002).

144. Andersen,H.S., Iversen,L.F., Jeppesen,C.B., Branner,S., Norris,K., Rasmussen,H.B., Moller,K.B. & Moller,N.P. 2-(oxalylamino)-benzoic acid is a general, competitive inhibitor of protein-tyrosine phosphatases. *J Biol. Chem.* **275**, 7101-7108 (2000).

145. Iversen,L.F., Andersen,H.S., Moller,K.B., Olsen,O.H., Peters,G.H., Branner,S., Mortensen,S.B., Hansen,T.K., Lau,J., Ge,Y., Holsworth,D.D., Newman,M.J. & Hundahl Moller,N.P. Steric hindrance as a basis for structure-based design of selective inhibitors of protein-tyrosine phosphatases. *Biochemistry* **40**, 14812-14820 (2001).

146. Guo,X.L., Shen,K., Wang,F., Lawrence,D.S. & Zhang,Z.Y. Probing the molecular basis for potent and selective protein-tyrosine phosphatase 1B inhibition. *J Biol. Chem.* **277**, 41014-41022 (2002).

147. Sun,J.P., Fedorov,A.A., Lee,S.Y., Guo,X.L., Shen,K., Lawrence,D.S., Almo,S.C. & Zhang,Z.Y. Crystal structure of PTP1B complexed with a potent and selective bidentate inhibitor. *J Biol. Chem.* **278**, 12406-12414 (2003).

148. Glover,N.R. & Tracey,A.S. Structure, modelling, and molecular dynamics studies of the inhibition of protein tyrosine phosphatase 1B by sulfotyrosine peptides. *Biochem Cell Biol.* **77**, 469-486 (1999).

149. Pillai,R., Kytle,K., Reyes,A. & Colicelli,J. Use of a yeast expression system for the isolation and analysis of drug-resistant mutants of a mammalian phosphodiesterase. *Proc. Natl. Acad. Sci. U. S. A.* **90**, 11970-11974 (1993).

150. Atienza,J.M. & Colicelli,J. Yeast model system for study of mammalian phosphodiesterases. *Methods* **14**, 35-42 (1998).

151. Sibley,C.H., Brophy,V.H., Cheesman,S., Hamilton,K.L., Hankins,E.G., Wooden,J.M. & Kilbey,B. Yeast as a model system to study drugs effective against apicomplexan proteins. *Methods* **13**, 190-207 (1997).

152. Atienza,J.M., Susanto,D., Huang,C., McCarty,A.S. & Colicelli,J. Identification of inhibitor specificity determinants in a mammalian phosphodiesterase. *J. Biol. Chem.* **274**, 4839-4847 (1999).

153. Brophy,V.H., Vasquez,J., Nelson,R.G., Forney,J.R., Rosowsky,A. & Sibley,C.H. Identification of Cryptosporidium parvum dihydrofolate reductase inhibitors by complementation in Saccharomyces cerevisiae. *Antimicrob. Agents Chemother.* **44**, 1019-1028 (2000).

154. Broach,J.R. & Thorner,J. High-throughput screening for drug discovery. *Nature* **384**, 14-16 (1996).

155. Hammonds,T.R., Maxwell,A. & Jenkins,J.R. Use of a rapid throughput in vivo screen to investigate inhibitors of eukaryotic topoisomerase II enzymes. *Antimicrob. Agents Chemother.* **42**, 889-894 (1998).

156. Tugendreich,S., Perkins,E., Couto,J., Barthmaier,P., Sun,D., Tang,S., Tulac,S., Nguyen,A., Yeh,E., Mays,A., Wallace,E., Lila,T., Shivak,D., Prichard,M., Andrejka,L., Kim,R. & Melese,T. A streamlined process to phenotypically profile heterologous cDNAs in parallel using yeast cell-based assays. *Genome Res.* **11**, 1899-1912 (2001).

157. Potvin,J., Fonchy,E., Conway,J. & Champagne,C.P. An automatic turbidimetric method to screen yeast extracts as fermentation nutrient ingredients. *J. Microbiol. Methods* **29**, 153-160 (1997).

158. Martin,G.S. The hunting of the Src. *Nat Rev. Mol Cell Biol* **2**, 467-475 (2001).

159. Brugge,J.S., Jarosik,G., Andersen,J., Queral-Lustig,A., Fedor-Chaiken,M. & Broach,J.R. Expression of Rous sarcoma virus transforming protein pp60v-src in Saccharomyces cerevisiae cells. *Mol. Cell. Biol.* **7**, 2180-2187 (1987).

160. Kornbluth,S., Jove,R. & Hanafusa,H. Characterization of avian and viral p60src proteins expressed in yeast. *Proc. Natl. Acad. Sci. U. S. A.* **84**, 4455-4459 (1987).

161. Liebl,E.C., England,L.J., DeClue,J.E. & Martin,G.S. Host range mutants of v-src: alterations in kinase activity and substrate interactions. *J Virol.* **66**, 4315-4324 (1992).

162. Xu,Y. & Lindquist,S. Heat-shock protein hsp90 governs the activity of pp60v-src kinase. *Proc. Natl. Acad. Sci U. S. A* **90**, 7074-7078 (1993).

163. Boschelli,F. Expression of p60v-src in Saccharomyces cerevisiae results in elevation of p34CDC28 kinase activity and release of the dependence of DNA replication on mitosis. *Mol. Cell. Biol.* **13**, 5112-5121 (1993).

164. Florio,M., Wilson,L.K., Trager,J.B., Thorner,J. & Martin,G.S. Aberrant protein phosphorylation at tyrosine is responsible for the growth-inhibitory action of pp60v-src expressed in the yeast Saccharomyces cerevisiae. *Mol. Biol. Cell* **5**, 283-296 (1994).

165. Dey,B., Caplan,A.J. & Boschelli,F. The Ydj1 molecular chaperone facilitates formation of active p60v-src in yeast. *Mol Biol Cell* **7**, 91-100 (1996).

166. Trager,J.B. & Martin,G.S. The role of the Src homology-2 domain in the lethal effect of Src expression in the yeast Saccharomyces cerevisiae. *Int. J. Biochem. Cell Biol.* **29**, 635-648 (1997).

167. Cross,F.R., Garber,E.A., Pellman,D. & Hanafusa,H. A short sequence in the p60src N terminus is required for p60src myristylation and membrane association and for cell transformation. *Mol Cell Biol* **4**, 1834-1842 (1984).

168. Schultz,A.M., Henderson,L.E., Oroszlan,S., Garber,E.A. & Hanafusa,H. Amino terminal myristylation of the protein kinase p60src, a retroviral transforming protein. *Science* **227**, 427-429 (1985).

169. Tian,M. & Martin,G.S. Reduced phosphotyrosine binding by the v-Src SH2 domain is compatible with wild-type transformation. *Oncogene* **12**, 727-734 (1996).

170. Garber,E.A., Cross,F.R. & Hanafusa,H. Processing of p60v-src to its myristylated membrane-bound form. *Mol Cell Biol* **5**, 2781-2788 (1985).

171. Murphy,S.M., Bergman,M. & Morgan,D.O. Suppression of c-Src activity by C-terminal Src kinase involves the c-Src SH2 and SH3 domains: analysis with Saccharomyces cerevisiae. *Mol Cell Biol* **13**, 5290-5300 (1993).

172. Superti-Furga,G., Fumagalli,S., Koegl,M., Courtneidge,S.A. & Draetta,G. Csk inhibition of c-Src activity requires both the SH2 and SH3 domains of Src. *EMBO J* **12**, 2625-2634 (1993).

173. Koegl,M., Courtneidge,S.A. & Superti-Furga,G. Structural requirements for the efficient regulation of the Src protein tyrosine kinase by Csk. *Oncogene* **11**, 2317-2329 (1995).

174. Keegan,K. & Cooper,J.A. Use of the two hybrid system to detect the association of the protein-tyrosine-phosphatase, SHPTP2, with another SH2-containing protein, Grb7. *Oncogene* **12**, 1537-1544 (1996).

175. Mousseau,D.D., Banville,D., L'Abbe,D., Bouchard,P. & Shen,S.H. PILRalpha, a novel immunoreceptor tyrosine-based inhibitory motif-bearing protein, recruits SHP-1 upon tyrosine phosphorylation and is paired with the truncated counterpart PILRbeta. *J Biol Chem.* **275**, 4467-4474 (2000).

176. Kawachi,H., Fujikawa,A., Maeda,N. & Noda,M. Identification of GIT1/Cat-1 as a substrate molecule of protein tyrosine phosphatase zeta /beta by the yeast substrate-trapping system. *Proc. Natl. Acad. Sci U. S. A* **98**, 6593-6598 (2001).

177. Kimura,Y., Yahara,I. & Lindquist,S. Role of the protein chaperone YDJ1 in establishing Hsp90-mediated signal transduction pathways. *Science* **268**, 1362-1365 (1995).

178. Woodford-Thomas,T.A., Rhodes,J.D. & Dixon,J.E. Expression of a protein tyrosine phosphatase in normal and v-src-transformed mouse 3T3 fibroblasts. *J Cell Biol* **117**, 401-414 (1992).

179. Xing,Z., Chen,H.C., Nowlen,J.K., Taylor,S.J., Shalloway,D. & Guan,J.L. Direct interaction of v-Src with the focal adhesion kinase mediated by the Src SH2 domain. *Mol Biol Cell* **5**, 413-421 (1994).

180. Superti-Furga,G., Jonsson,K. & Courtneidge,S.A. A functional screen in yeast for regulators and antagonizers of heterologous protein tyrosine kinases. *Nat Biotechnol.* **14**, 600-605 (1996).

181. Prejdova,J., Soucek,M. & Konvalinka,J. Determining and overcoming resistance to HIV protease inhibitors. *Curr. Drug Targets Infect. Disord.* **4**, 137-152 (2004).

182. Velazquez-Campoy,A., Muzammil,S., Ohtaka,H., Schon,A., Vega,S. & Freire,E. Structural and thermodynamic basis of resistance to HIV-1 protease inhibition: implications for inhibitor design. *Curr. Drug Targets Infect. Disord.* **3**, 311-328 (2003).

183. Cabib,E., Bowers,B., Sburlati,A. & Silverman,S.J. Fungal cell wall synthesis: the construction of a biological structure. *Microbiol. Sci* **5**, 370-375 (1988).

184. De Nobel,J.G. & Barnett,J.A. Passage of molecules through yeast cell walls: a brief essay-review. *Yeast* **7**, 313-323 (1991).

185. Stolz,J. & Munro,S. The components of the Saccharomyces cerevisiae mannosyltransferase complex M-Pol I have distinct functions in mannan synthesis. *J Biol. Chem.* **277**, 44801-44808 (2002).

186. Yip,C.L., Welch,S.K., Klebl,F., Gilbert,T., Seidel,P., Grant,F.J., O'Hara,P.J. & MacKay,V.L. Cloning and analysis of the Saccharomyces cerevisiae MNN9 and MNN1 genes required for complex glycosylation of secreted proteins. *Proc. Natl. Acad. Sci U. S. A* **91**, 2723-2727 (1994).

187. De Nobel,J.G., Klis,F.M., Priem,J., Munnik,T. & van den,E.H. The glucanase-soluble mannoproteins limit cell wall porosity in Saccharomyces cerevisiae. *Yeast* **6**, 491-499 (1990).

188. Zlotnik,H., Fernandez,M.P., Bowers,B. & Cabib,E. Saccharomyces cerevisiae mannoproteins form an external cell wall layer that determines wall porosity. *J Bacteriol.* **159**, 1018-1026 (1984).

189. Emter,R., Heese-Peck,A. & Kralli,A. ERG6 and PDR5 regulate small lipophilic drug accumulation in yeast cells via distinct mechanisms. *FEBS Lett.* **521**, 57-61 (2002).

190. Gaber,R.F., Copple,D.M., Kennedy,B.K., Vidal,M. & Bard,M. The yeast gene ERG6 is required for normal membrane function but is not essential for biosynthesis of the cell-cycle-sparking sterol. *Mol. Cell. Biol.* **9**, 3447-3456 (1989).

191. Jensen-Pergakes,K.L., Kennedy,M.A., Lees,N.D., Barbuch,R., Koegel,C. & Bard,M. Sequencing, disruption, and characterization of the Candida albicans sterol methyltransferase (ERG6) gene: drug susceptibility studies in erg6 mutants. *Antimicrob. Agents Chemother.* **42**, 1160-1167 (1998).

192. Bard,M., Lees,N.D., Burrows,L.S. & Kleinhans,F.W. Differences in crystal violet uptake and cation-induced death among yeast sterol mutants. *J. Bacteriol.* **135**, 1146-1148 (1978).

193. Kleinhans,F.W., Lees,N.D., Bard,M., Haak,R.A. & Woods,R.A. ESR determinations of membrane permeability in a yeast sterol mutant. *Chem. Phys. Lipids* **23**, 143-154 (1979).

194. Paunola,E., Qiao,M., Shmelev,A. & Makarow,M. Inhibition of translocation of beta -lactamase into the yeast endoplasmic reticulum by covalently bound benzylpenicillin. *J Biol. Chem.* **276**, 34553-34559 (2001).

195. Vogel,J.P., Lee,J.N., Kirsch,D.R., Rose,M.D. & Sztul,E.S. Brefeldin A causes a defect in secretion in Saccharomyces cerevisiae. *J Biol. Chem.* **268**, 3040-3043 (1993).

196. Jackson,C.L. & Kepes,F. BFR1, a multicopy suppressor of brefeldin A-induced lethality, is implicated in secretion and nuclear segregation in Saccharomyces cerevisiae. *Genetics* **137**, 423-437 (1994).

197. Johnston,M. & Carlson,M. The Molecular an Cellular Biology of the Yeast Saccharomyces. Jones,E.W., Pringle,J.R. & Broach,J.R. (eds.), pp. 193-281 (Cold Spring Harbor Laboratory Press,1992).

198. Mumberg,D., Muller,R. & Funk,M. Regulatable promoters of Saccharomyces cerevisiae: comparison of transcriptional activity and their use for heterologous expression. *Nucleic Acids Res.* **22**, 5767-5768 (1994).

199. Szostak,J.W., Orr-Weaver,T.L., Rothstein,R.J. & Stahl,F.W. The double-strand-break repair model for recombination. *Cell* **33**, 25-35 (1983).

200. Orr-Weaver,T.L., Szostak,J.W. & Rothstein,R.J. Yeast transformation: a model system for the study of recombination. *Proc. Natl. Acad. Sci U. S. A* **78**, 6354-6358 (1981).

201. Mezard,C. & Nicolas,A. Homologous, homeologous, and illegitimate repair of double-strand breaks during transformation of a wild-type strain and a rad52 mutant strain of Saccharomyces cerevisiae. *Mol Cell Biol.* **14**, 1278-1292 (1994).

202. Brachmann,C.B., Davies,A., Cost,G.J., Caputo,E., Li,J., Hieter,P. & Boeke,J.D. Designer deletion strains derived from Saccharomyces cerevisiae S288C: a useful set of strains and plasmids for PCR-mediated gene disruption and other applications. *Yeast* **14**, 115-132 (1998).

203. Muhlrad,D., Hunter,R. & Parker,R. A rapid method for localized mutagenesis of yeast genes. *Yeast* **8**, 79-82 (1992).

204. Orr-Weaver,T.L., Szostak,J.W. & Rothstein,R.J. Methods in Enzymology, Recombinant DNA. Wu,R., Grossman,L. & Moldave,K. (eds.), pp. 228-245 (Academic Press, Inc., New York,1983).

205. Sikorski,R.S. & Hieter,P. A system of shuttle vectors and yeast host strains designed for efficient manipulation of DNA in Saccharomyces cerevisiae. *Genetics* **122**, 19-27 (1989).

206. Bruschi,C.V. & Howe,G.A. High frequency FLP-independent homologous DNA recombination of 2 mu plasmid in the yeast Saccharomyces cerevisiae. *Curr. Genet.* **14**, 191-199 (1988).

207. Cost,G.J. & Boeke,J.D. A useful colony colour phenotype associated with the yeast selectable/counter-selectable marker MET15. *Yeast* **12**, 939-941 (1996).

208. Myers,T.A. & Nickoloff,J.A. Nonselective colony-color assays for HIS3, LEU2, LYS2, TRP1 and URA3 in ade2 yeast strains using media with limiting nutrients. *Biotechniques* **26**, 850-854 (1999).

209. Swarup,G., Cohen,S. & Garbers,D.L. Inhibition of membrane phosphotyrosyl-protein phosphatase activity by vanadate. *Biochem. Biophys. Res. Commun.* **107**, 1104-1109 (1982).

210. Van Etten,R.L., Waymack,P.P. & Rehkop,D.M. Transition Metal Ion Inhiition of Enzyme-Catalyzed Phosphate Ester Displacement Reactions. *J. Amer. Chem. Soc.* **96**, 6782-6785 (1974).

211. Kovach,J.S., Svingen,P.A. & Schaid,D.J. Levamisole potentiation of fluorouracil antiproliferative activity mimicked by orthovanadate, an inhibitor of tyrosine phosphatase. *J. Natl. Cancer Inst.* **84**, 515-519 (1992).

212. Heo,Y.S., Ryu,J.M., Park,S.M., Park,J.H., Lee,H.C., Hwang,K.Y. & Kim,J. Structural basis for inhibition of protein tyrosine phosphatases by Keggin compounds phosphomolybdate and phosphotungstate. *Exp. Mol. Med.* **34**, 211-223 (2002).

213. Peters,K.G., Davis,M.G., Howard,B.W., Pokross,M., Rastogi,V., Diven,C., Greis,K.D., Eby-Wilkens,E., Maier,M., Evdokimov,A., Soper,S. & Genbauffe,F. Mechanism of insulin sensitization by BMOV (bis maltolato oxo vanadium); unliganded vanadium (VO4) as the active component. *J Inorg. Biochem* **96**, 321-330 (2003).

214. Desmarais,S., Friesen,R.W., Zamboni,R. & Ramachandran,C. [Difluro(phosphono)methyl]phenylalanine-containing peptide inhibitors of protein tyrosine phosphatases. *Biochem. J.* **337 (Pt 2)**, 219-223 (1999).

215. Skorey,K.I., Kennedy,B.P., Friesen,R.W. & Ramachandran,C. Development of a robust scintillation proximity assay for protein tyrosine phosphatase 1B using the catalytically inactive (C215S) mutant. *Anal. Biochem.* **291**, 269-278 (2001).

216. Huyer,G., Liu,S., Kelly,J., Moffat,J., Payette,P., Kennedy,B., Tsaprailis,G., Gresser,M.J. & Ramachandran,C. Mechanism of inhibition of protein-tyrosine phosphatases by vanadate and pervanadate. *J. Biol. Chem.* **272**, 843-851 (1997).

217. Agatep, R, Kirkpatrick, RD, Parchaliuk, DL, Woods, RA, and Gietz, RD. Transformation of Saccharomyces cerevisiae by the lithium acetate/single-stranded carrier DNA/polyethylene glycol (LiAc/ss-DNA/PEG) protocol. Technical Tips Online. 1998. http://tto.trends.com

218. Nelson, Z. **Electroporation**. Fred Hutchinson Cancer Research Center. 4-11-2004. http://www.fhcrc.org/labs/gottschling/yeast/ytrans.html

219. Burke,D., Dawson,D. & Stearns,T. METHODS IN YEAST GENETICS. A Cold Spring Harbor Laboratory Course Manual. Cold Spring Harbor Laboratory Press, (2000).

220. Hughes,W.E., Pocklington,M.J., Orr,E. & Paddon,C.J. Mutations in the Saccharomyces cerevisiae gene SAC1 cause multiple drug sensitivity. *Yeast* **15**, 1111-1124 (1999).

221. Thompson,J.R., Register,E., Curotto,J., Kurtz,M. & Kelly,R. An improved protocol for the preparation of yeast cells for transformation by electroporation. *Yeast* **14**, 565-571 (1998).

222. Melese,T. & Hieter,P. From genetics and genomics to drug discovery: yeast rises to the challenge. *Trends Pharmacol. Sci.* **23**, 544-547 (2002).

223. Kolaczkowski,M., Kolaczowska,A., Luczynski,J., Witek,S. & Goffeau,A. In vivo characterization of the drug resistance profile of the major ABC transporters and other components of the yeast pleiotropic drug resistance network. *Microb. Drug Resist.* **4**, 143-158 (1998).

224. Kaur,R. & Bachhawat,A.K. The yeast multidrug resistance pump, Pdr5p, confers reduced drug resistance in erg mutants of Saccharomyces cerevisiae. *Microbiology* **145 (Pt 4)**, 809-818 (1999).

225. Gulnik,S.V., Suvorov,L.I., Liu,B., Yu,B., Anderson,B., Mitsuya,H. & Erickson,J.W. Kinetic characterization and cross-resistance patterns of HIV-1 protease mutants selected under drug pressure. *Biochemistry* **34**, 9282-9287 (1995).

226. Gulnik,S.V., Erickson,J.W. & Xie,D. Vitamins and Hormones. Litwack,G. (ed.), pp. 213-256 (Academic Press, New York,1999).

227. Asante-Appiah,E., Ball,K., Bateman,K., Skorey,K., Friesen,R., Desponts,C., Payette,P., Bayly,C., Zamboni,R., Scapin,G., Ramachandran,C. & Kennedy,B.P. The YRD motif is a major determinant of substrate and inhibitor specificity in T-cell protein-tyrosine phosphatase. *J. Biol. Chem.* **276**, 26036-26043 (2001).

228. Montalibet,J., Skorey,K.I. & Kennedy,B.P. Protein tyrosine phosphatase: enzymatic assays. *Methods* **35**, 2-8 (2005).

229. Zhang,Y.L., Keng,Y.F., Zhao,Y., Wu,L. & Zhang,Z.Y. Suramin is an active site-directed, reversible, and tight-binding inhibitor of protein-tyrosine phosphatases. *J. Biol. Chem.* **273**, 12281-12287 (1998).

230. Bernier,M., Laird,D.M. & Lane,M.D. Insulin-activated tyrosine phosphorylation of a 15-kilodalton protein in intact 3T3-L1 adipocytes. *Proc. Natl. Acad. Sci U. S. A* **84**, 1844-1848 (1987).

231. Bernier,M., Laird,D.M. & Lane,M.D. Effect of vanadate on the cellular accumulation of pp15, an apparent product of insulin receptor tyrosine kinase action. *J Biol. Chem.* **263**, 13626-13634 (1988).

232. Frost,S.C. & Lane,M.D. Evidence for the involvement of vicinal sulfhydryl groups in insulin-activated hexose transport by 3T3-L1 adipocytes. *J Biol. Chem.* **260**, 2646-2652 (1985).

233. Frost,S.C., Kohanski,R.A. & Lane,M.D. Effect of phenylarsine oxide on insulin-dependent protein phosphorylation and glucose transport in 3T3-L1 adipocytes. *J Biol. Chem.* **262**, 9872-9876 (1987).

234. Garcia-Morales,P., Minami,Y., Luong,E., Klausner,R.D. & Samelson,L.E. Tyrosine phosphorylation in T cells is regulated by phosphatase activity: studies with phenylarsine oxide. *Proc. Natl. Acad. Sci U. S. A* **87**, 9255-9259 (1990).

235. Knutson,V.P., Ronnett,G.V. & Lane,M.D. Rapid, reversible internalization of cell surface insulin receptors. Correlation with insulin-induced down-regulation. *J Biol. Chem.* **258**, 12139-12142 (1983).

236. Levenson,R.M. & Blackshear,P.J. Insulin-stimulated protein tyrosine phosphorylation in intact cells evaluated by giant two-dimensional gel electrophoresis. *J Biol. Chem.* **264**, 19984-19993 (1989).

237. Li,J., Elberg,G. & Shechter,Y. Phenylarsine oxide and vanadate: apparent paradox of inhibition of protein phosphotyrosine phosphatases in rat adipocytes. *Biochim. Biophys Acta* **1312**, 223-230 (1996).

238. Liao,K., Hoffman,R.D. & Lane,M.D. Phosphotyrosyl turnover in insulin signaling. Characterization of two membrane-bound pp15 protein tyrosine phosphatases from 3T3-L1 adipocytes. *J Biol. Chem.* **266**, 6544-6553 (1991).

239. Zhang,Z.Y. & Van Etten,R.L. Purification and characterization of a low-molecular-weight acid phosphatase--a phosphotyrosyl-protein phosphatase from bovine heart. *Arch. Biochem. Biophys.* **282**, 39-49 (1990).

240. Montalibet,J. & Kennedy,B.P. Using yeast to screen for inhibitors of protein tyrosine phosphatase 1B. *Biochem Pharmacol* **68**, 1807-1814 (2004).

241. Zhu,G., Decker,S.J., Mayer,B.J. & Saltiel,A.R. Direct analysis of the binding of the abl Src homology 2 domain to the activated epidermal growth factor receptor. *J Biol. Chem.* **268**, 1775-1779 (1993).

242. Mayer,B.J., Jackson,P.K., Van Etten,R.A. & Baltimore,D. Point mutations in the abl SH2 domain coordinately impair phosphotyrosine binding in vitro and transforming activity in vivo. *Mol Cell Biol.* **12**, 609-618 (1992).

243. Dufresne,C., Roy,P., Wang,Z., Asante-Appiah,E., Cromlish,W., Boie,Y., Forghani,F., Desmarais,S., Wang,Q., Skorey,K., Waddleton,D., Ramachandran,C., Kennedy,B.P., Xu,L., Gordon,R., Chan,C.C. & Leblanc,Y. The development of potent non-peptidic PTP-1B inhibitors. *Bioorg. Med. Chem. Lett.* **14**, 1039-1042 (2004).

244. Liu,G., Xin,Z., Liang,H., Abad-Zapatero,C., Hajduk,P.J., Janowick,D.A., Szczepankiewicz,B.G., Pei,Z., Hutchins,C.W., Ballaron,S.J., Stashko,M.A., Lubben,T.H., Berg,C.E., Rondinone,C.M., Trevillyan,J.M. & Jirousek,M.R. Selective protein tyrosine phosphatase 1B inhibitors: targeting the second phosphotyrosine binding site with non-carboxylic acid-containing ligands. *J Med Chem* **46**, 3437-3440 (2003).

245. Burley,S.K. & Petsko,G.A. Aromatic-aromatic interaction: a mechanism of protein structure stabilization. *Science* **229**, 23-28 (1985).

246. Kannan,N. & Vishveshwara,S. Aromatic clusters: a determinant of thermal stability of thermophilic proteins. *Protein Eng.* **13**, 753-761 (2000).

247. Zhang,Z.Y. & Dixon,J.E. Protein tyrosine phosphatases: mechanism of catalysis and substrate specificity. *Adv. Enzymol. Relat Areas Mol Biol.* **68**, 1-36 (1994).

248. Nam,H.J., Poy,F., Krueger,N.X., Saito,H. & Frederick,C.A. Crystal structure of the tandem phosphatase domains of RPTP LAR. *Cell* **97**, 449-457 (1999).

249. McCain,D.F., Wu,L., Nickel,P., Kassack,M.U., Kreimeyer,A., Gagliardi,A., Collins,D.C. & Zhang,Z.Y. Suramin derivatives as inhibitors and activators of protein-tyrosine phosphatases. *J Biol. Chem.* **279**, 14713-14725 (2004).

Appendix 1:

Inhibitor Structures

Abbreviations used in the thesis	Full Name	Structure
BzN-EJJ-amide	N-benzoyl-L-glutamyl- [4-phosphono(difluoromethyl)]-L-phenylalanyl- [4-phosphono(difluoromethyl)]-L-phenylalanineamide	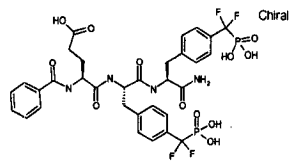
L-A	N-benzoyl-[4-phosphono(difluoromethyl)]-L-phenylalanyl- [4-phosphono(difluoromethyl)]-L-phenylalanineamide	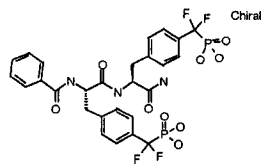
L-B	1-{*m*-bromo-*p*-[phosphono(difluoromethyl)]phenyl}-3-[*p*-chlorophenyl]- 2-thiapropane	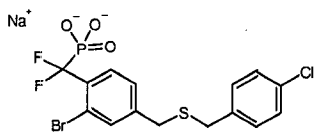
L-C	2-(1*H*-benzotriazyl)- 2,7-diphenyl-1- *p*-[phosphono(difluoromethyl)]phenylhepta-4,6-dien-3-one	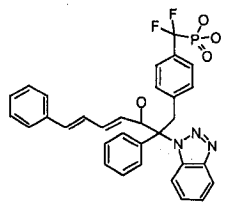
L-D	1,2-biphenyl-2,2-di{*m*-bromo-*p*-[phosphono(difluoromethyl)]-phenylmethyl}ethanone	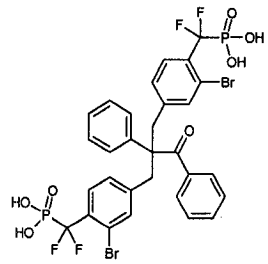
L-E	1,2-diphenyl-2,2-di{*p*-[phosphono(difluoromethyl)]phenylmethyl}ethanone	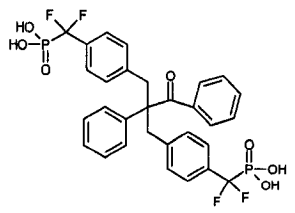

L-F	2-*p*-benzonitrile-3-*p*-fluorophenyl-1-(2-phenylcyclopropane)-2- *p*-[phosphono(difluoromethyl)]phenylmethylpropan-3-one	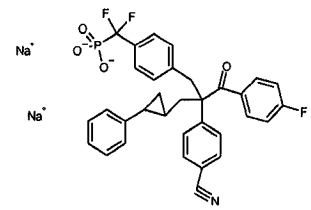
L-G	2-(1*H*-benzotriazyl)- 2- *p*-carboxyphenyl-5-phenyl-1-*p*-[phosphono(difluoromethyl)]phenylpent-4-ene	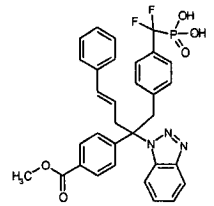
L-H	1-{*m*-bromo-*p*-[phosphono(difluoromethyl)]phenyl}-3-[*p*-bromophenyl]- 2-thiapropane	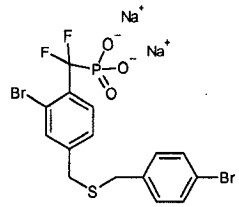
L-I	1-*m*-bromo-*p*-[phosphono(difluoromethyl)]phenyl-3,4-diphenyl-2-thiabutane	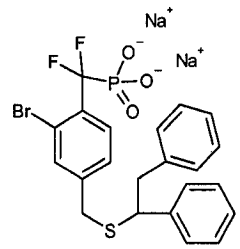
L-J	3-4'*H*-(N-ethanonebiphenyl-3-sulfonamide)-1-{*m*-bromo-*p*-[phosphono(difluoromethyl)]phenyl}-2-thiapropane	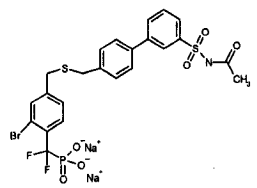
L-K	1-*m*-bromo-*p*-(phosphono(difluoromethyl)phenyl)-3-4'*H*-(-3-phosphonobiphenyl)-2-thiapropane	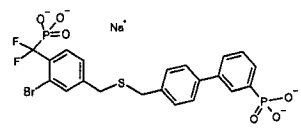
L-L	2-(1*H*-benzotriazyl)-2-phenyl-1-*p*-(phosphono(difluoremethyl)phenyl)-3-4'*H*-(-3-phosphonophenyl)propane	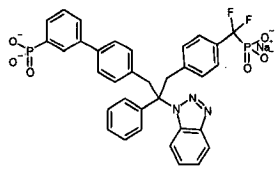

L-M	1-*m*-bromo-*p*-(phosphono(difluoremethyl)phenyl)-5-*m*-phosphonophenyl-2-thiapentane	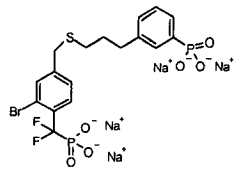
L-N	3- *m*-bromo-*p*-(phosphono(difluoremethyl)phenyl)-1,2-diphenylpropan-1-one	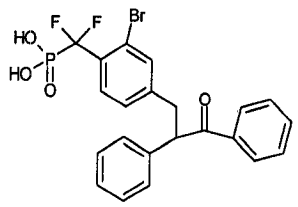
L-O	7-bromo-6-difluoromethylphosphonate-3-napthalenonitrile	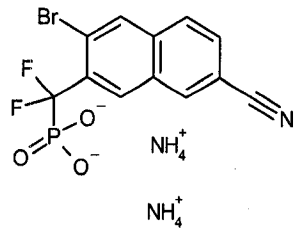
L-P	1-*m*-bromo-*p*-(phosphono(difluoremethyl)phenyl)-5-*m*-phenylsulfonamide-2-thiapent-4-yne	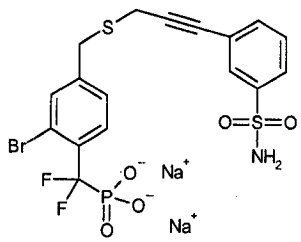
L-Q	1-*m*-bromo-*p*-(phosphono(difluoremethyl)phenyl)-3-*m*-phenoxyphenyl-2-oxapropane	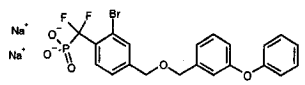
L-R	3-*p*-bromophenyl-1-*m*-bromo-*p*-(phosphono(difluoremethyl)phenyl)-2-thiapropane	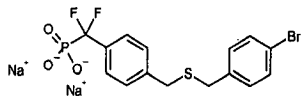
L-S	1-*m*-bromo-*p*-(phosphono(difluoremethyl)phenyl)-2-phenylmethylbenzotriazol	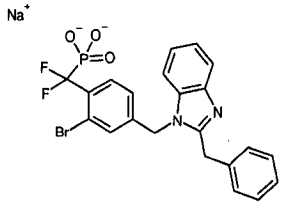

Appendix 2:

Primer Sequences

Primer Name	Sequence
298fwd	GGTCGACTGGGGGCTACAGGTCCTCGTGG
298rvrs	GACTACAAGGACGACGATGACAAG
400fwd (*Eco*R I)	GAATTCATGGAGATGGAAAAGGAG
400rvrs (*Sal* I)	GTCGACCAGTGCCTAGTCCTCGTCCTTC
fwdhom	AGGAGAAAAAACCCCGGATTCTAGAACTAGTGGATCCCCCGGGC TGCAGGAATTCATG
gammafwd	CTCGTGCAGGGGCGAATTGGGTACC
gammarvrs	TAAAGGGAACAAAAGCTGCACCTCTA
libfout	GTTAATATACCTCTATACTTTAAC
librout	CTTCCTTTTCGGTTAGAGCGGATG
Mutfwd (*Eco*R I)	TCCCCCGGGCTGCAGGAATTCATG
Mutrvrs (*Sal* I)	CGTCGACTCAAGAGAATTAATTCTCA
PA	TTTTTATCAAACTAGCGTTG
PB2	GAAGACACAAATTGAAATTAAC
PC	AATGTAAGATCTCTCGAGTT
PC2	GAAAGTTCAAGAATGAGGCTGGT
PD	CCTTCTTCCGTTGATATCAA
Ptp10	CAGGATCAGTGGAAGGAGCTTTCC
Ptp6	AAAAGCAGGGGTGTCGTCATG
Ptp7	GTCTTCAAAGATCATCTC
Ptp8	CTTTTCAAAGTCCGAGAG
Ptp9	TATCAGCCAGACAGAAGG
ptpin1	GGGCGGGCCTCGGGGCTAAGAG

ptpin2	ACGGAAGAGTCCCCCATGATGAA
rvrshom	GGGGGAGGGCGTGAATGTAAGCGTGACATAACTAATTACATGAC TCGAGGTCGAC
S8	GTACCTGCAGGCCCAGCTGCTCCCT
seq303	GCTATGACCATGATTACGCCAAGCTC
srcfwd (*Xba* I)	CGTCTAGAATGGGGAGTAGCAAGAGCAAGCC
srcrvrs (*Sal* I)	GTCGACCTACTCAGCGACCTCCAACACACAAGC
v1	CGTCTAGAATGGGGAGTAGCAAGAGCAAGCC
v2	GTCGACCTACTCAGCGACCTCCAACACACAAGC
v3	CTGGTGGCTGGCTCATTCCGTGA
v4	CTGATGGCTTGTGCCACCGCCTG
v5	GGTGGTGCCGTTCCAGGTTCCCCA
v6	GCCCAAAGTCAGCCACCTTGCA
v7	GCCGGCGCTGGCTGGGGTCCTTA
v8	GTACCTGCAGGCCCAGCTGCTCCCT
Y2	TAAACTCCATCAAATGGTCAGGTC
Y3	TATAGAATTGTGTAGAATTGCAGA
Y4	TACGTCGTAAGGCCGTTTCTGACA

Parentheses indicate consensus site for restriction digest included in the primer.

Appendix 3:

Analysis of the PTP1B Promoter

Abstract

Analysis of the PTP1B Promoter

Inhibition of Protein Tyrosine Phosphatase 1B (PTP1B) has been proposed as a novel therapy to treat type 2 diabetes by sensitising the patients to the effect of insulin while protecting them against diet-induced obesity. Regulation of the levels of PTP1B protein in the cell has been observed in response to insulin and the insulin-sensitizing thiazolidinediones. The 5' untranslated region of the PTP1B gene was explored to define transcriptional elements forming the promoter. Deletion constructs of the 8kb region upstream from the start ATG codon were inserted in the pSEAP vector system to drive the expression of secreted alkaline phosphates. Basal expression was measured in 3 cell lines representing insulin-responsive tissues: HepG2 hepatocytes, L6 myotubes and 3T3 L1 adipocytes. The pattern of regulation was similar in all 3 cell lines with maximal expression obtained using 432 base pairs of the sequence immediately upstream from the ATG codon. Further truncation resulted in a gradual loss of transcriptional activity. The promoter sequence was evaluated for regulation by insulin and rosiglitazone: insulin did not alter the transcriptional activity of the PTP1B promoter and rosiglitazone reduced promoter activity in a non-specific fashion.

Table of Contents

Table of Figures

List of Abbreviations

ATCC: American Tissue Culture Collection

CAT: Chloramphenicol Acetyl Transferase

IR: Insulin Receptor

GFP: Green Fluorescent Protein

OLETF: Otsuka Long-Evans Tokushima Fatty

PBS: Phosphate Buffered Saline

PPARγ: Peroxisome Proliferative Activated Receptor γ

PPRE: PPARγ Response Element

PTP1B: Protein Tyrosine Phosphatase 1B

PRS: p210 Bcr-Abl Responsive Sequence

RXR: Retinoid X Receptor

SEAP: Secreted Alkaline Phosphatase

SNP: Single nucleotide Polymorphism

YB-1: Y-box binding protein 1

A.1. Introduction

Insulin has been observed to modulate the expression levels of Protein Tyrosine Phosphatase 1B (PTP1B) in cell culture. Increase in PTP1B mRNA, protein and activity has been observed in L6 cells treated with insulin or IGF1[1]. This insulin-induced mRNA increase has also been seen in Fao hepatocytes[2].

Thiazolidinediones are used as insulin sensitization agents in the clinic. They act as agonists for the nuclear receptor Peroxisome Proliferative Activated Receptor γ (PPARγ) which dimerizes with Retinoid X Receptor (RXR) and has been involved in transcriptional events leading to adipocytes differentiation and proliferation[3,4]. Rosiglitazone[5] treatment, which results in insulin sensitization, may downregulate PTP1B expression at the promoter level through PPARγ activation.

Treatment of Rat 1 fibroblasts with high levels of glucose (27mM glucose) resulted in a decrease in insulin-mediated auto-phosphorylation of the Insulin Receptor (IR) and increased total tyrosine phosphatase activity along with an increase in PTP1B protein levels. Treatment with pioglitazone, a thiazolidine derivative, normalized both the IR phosphorylation and the PTP1B protein and activities levels[6]. Treatment of the insulin-resistant Otsuka Long-Evans Tokushima Fatty (OLETF) rats with troglitazone reduced circulating triglyceride levels and tended to also reduce insulin and glucose levels. This treatment also resulted in a normalization of the increased total tyrosine phosphatase activity in the visceral and epididymal fat pads along with normalizing the increased PTP1B protein content[7].

Basal expression from the PTP1B promoter was measured in three cell lines representing insulin responsive tissue: HepG2 hepatocytes, L6 myotubes and 3T3L1 adipocytes, using Secreted Alkaline Phosphatase (SEAP) as the reporter system. In this system, alkaline phosphatase is secreted in the media facilitating activity assays which require simply removing an aliquot from the media in which the cells grow and assaying for activity with p-nitrophenylphosphate. This system is convenient to measure activity of the promoter over time and treatments. In addition to basal activity, the effect of insulin or of the thiazolidinedione rosiglitazone on the PTP1B promoter was also measured.

A.2. Material and Methods

A.2.1. Plasmid Constructs

PTP1B promoter construct were clone in the Great Escape SEAP Reporter System 2 from Clontech.

Promoter deletion 8kb to 2kb cloned in pSEAP2 were constructed by Y. Boie. Fragments of the PTP1B promoter were generated by polymerase chain reaction using the pSAEP2-2kb plasmid as template. The primer used to generate the sense strand for construct #1 (bases -1 to –183) was CTCGAGGGCGTGATGCGTAGTTCC, construct #2 (bases –1 to –206) CTCGAGCTTCAGGGGCGGAGCC-3', construct #3 (bases -1 to –233) CTCGAGATTCTCGATCGCTGATT-3', construct #4 (bases –1 to –337) CTCGAGGCCCCAAAGCGGAGGA-3', construct #4AA was CTCGAGCCCCGGAGCGGAGGA (polymorphism underlined) and for construct #5 (bases –1 to –432) CTCGAGCTCAATGCCCTCCCGGGC-3'. These primers introduce a *Xho* I site at the 5' end. The antisense strand was generated with CTGCTCGAACTCCTTTTCCATAAGCTTGACGGGCC3' for all five constructs introducing a *Hind* III site at the 3' end. The PCR product was cloned into pSEAP2-Basic.

The #5AA construct was generated using stitch up PCR with the primer CGAGCCCAGAGCCCCAAAGCGGAGGAGGGAAC and the common antisense primer and separately with the sense primer used to clone construct #5 and GTTCCCTCCTCCGCTTTGGGGCTCTGGGCTCG both using pSEAP2-2kb as template (polymorphism underlined). The program used was 95°C 2min, 55°C 30sec, 72°C 45sec, 28

cycles of 95°C 45sec, 55°C 30sec, 72°C 45sec and finally 95°C 45 sec, 56°C 30sec and 72°C 5min. The two resulting PCR products were gel cleaned eluted in 30μL water, 0.5 and 1μL of which were used in another PCR reaction with the sense primer for construct #5 and the common antisense primer. The resulting PCR product was cloned in pSEAP2-Basic.

Both sense and antisense strands of the PPARγ Response Element (PPRE) sequence[8] were synthesized as 32mer oligonucleotides, phosphorylated with T7 kinase and annealed. 53ng of the duplex was ligated with the 33ng of the pSEAP-promoter previously digested with XhoI, filled in with Klenow and dephosphorylated with alkaline phosphatase.

PPARγ was amplified by PCR using CGGAATTCATGGGTGAAACTCTGG previously phosphorylated on the 5' end and CTAGTACAAGTCCTTGTAGATCTC as primers and pSG-PPARγ2 as template (Courtesy Merck Rahway) with the program 94°C 4min, 25 cycles of 94°C 15sec, 55°C 15sec, 72°C 1.5min, and finishing with 72°C 7min. The resulting PCR product was ligated into pCR 3.1-Uni. RXR courtesy W. Cromlish .

To transfer the system into the Chloramphenicol Acetyl Transferase (CAT) reporter system (Promega), constructs #3 and #5 were cut out from their pSEAP location with *Bst*B I and *Xho* I and ligated with pCAT-Basic previously digested with *Sal* I and *Acc* I.
All plasmids were sequenced.

A.2.2. Cell Culture and Transfection

All cell culture media, fetal bovine serum and media supplements from Gibco BRL.

Human hepatocellular carcinoma cell line HepG2 (American Tissue Culture Collection (ATCC)) was cultured in minimum essential medium supplemented with 10% FBS, 1% Na pyruvate, 1% nonessential amino acids and 1% penicillin/streptomycin. Cells (5

x 10^5) were seeded on 6-well plates 24 hours before transfection with Lipofectamine Plus (Gibco BRL) as per manufacturer protocol. The promoter constructs (2μg) along with 2μg of pCH110 (Pharmacia), expressing β-galactosidase, were transfected for five hours in minimum essential medium. The transfected cells were then cultured in complete medium for 40 hours at which point the media was collected for SEAP assay and the cells were harvested for gal assay (Mammalian β-Gal Assay Pierce).

L6 rat myoblast cells were cultured in D-MEM with 10% FBS, 1% Na pyruvate and 1% penicillin/streptomycin. Cells (4 x 10^5) were seeded on 6-well plates three days before transfection with Lipofectamine Plus (Gibco BRL) as per manufacturer protocol. The promoter constructs (1μg) along with 1μg of phRL-TK(Int$^-$) (Promega), expressing luciferase, were transfected for five hours in D-MEM.. The transfected cells were then cultured in complete medium for 24 hours and induced to differentiate in 2% FBS-containing media. After eight days most of the cells were differentiated to myotubes, media was collected for SEAP assay and the cells were harvested for luciferase assay (Renilla Luciferase Assay System Promega).

3T3 L1 preadipocytes were cultured in D-MEM with 10% NBCS and 1% penicillin/streptomycin. Cells (1.5 x 10^6) were seeded in 600cm^2 flasks, grown to confluence for four days. The media was replaced with D-MEM with 10% FBS, 500uM IBMX, 1μM dexamethasone, 10mM HEPES and 1μg/mL insulin. After two days, the media was replaced with D-MEM supplemented with 10% FBS and 1μg/mL insulin and two days later DMEM supplemented with 10% FBS only. The media was refreshed after three days of growth and the differentiated cells were electroporated two days later. The adipocytes were trypsinized using 0.05% trypsin in D-MEM, resuspended in 12mL D-MEM containing 10% FBS and

spun down at 3500RPM for four minutes. The cells were washed with 20mL phosphate buffered saline (PBS), pelleted at 3500RPM for four minutes and reconstituted in 7mL PBS, counted and diluted to 1 x 10^6 cells/ml. 0.5mL aliquots were transferred to a 0.4cm-gap electroporation cuvette along with 100μg of the promoter constructs and 25μg of phRL-TK(Int$^-$) and electroporated with 0.16kV and 960μF. The cells were transferred to the well of a 24-well collagen-treated plate with 1mL of D-MEM with 10% FBS. The media was refreshed the next day, collected 48 hours later for SEAP assay and the cells were harvested for luciferase assay.

A.2.3. SEAP assay

In a 96-well plate, 100μL of media in which transfected cells were cultured was added to 100μL of 20mM para-nitrophenylphoshate dissolved in SEAP buffer (1M diethanolamine pH 9.8, 10mM homoarginine, 2mM $MgCl_2$). Absorbance at 405nm was read after a 10 to 20 minutes incubation at room temperature.

A.2.4. CAT Assay

Cells were washed 3x with PBS, scraped into 400μL of 0.25M Tris pH 8.0 and lysed with three freeze-thaw cycles. 120μL of the extract was combined with 5μL of ^{14}C-Chloramphenicol at 0.025mCi/mL and 5μL of n-Butryl CoA at 5mg/mL in 0.25M tris pH 8.0. The reaction was left to proceed for 4hours at 37°C, stopped with 300μL mixed xylenes and vortex. The upper organic phase was removed and re-extracted using 100μL of 0.25M tris pH8.0 twice. 190μL of the organic phase was reacted with 3.5mL of Econofluor II reagent and activity was counted with a scintillation counter.

A.2.5. Western Blotting

Cells were harvested in MPER reagent (Pierce) containing 100mM vanadate, 0.18μL of 30% peroxide and a mini EDTA-free protease inhibitor tablet (Boehringer Mannheim). Protein content was measured with Coomassie Plus Reagent (Pierce) and 30μg of protein were separated on 4-12% gradient SDS-PAGE (NuPAGE), transferred to a PVDF or nitrocellulose membrane, blocked with 5% milk in TTBS, probed with anti-PTP1B antibody (Courtesy Dr. E. Asante-Apiah) or anti-IR antibody (Transduction laboratories 138430), washed, developed with chemiluminescence and visualized using a CCD camera.

A.3. *Results*

A.3.1. Basal Expression Levels

Eight kilobases of the genomic sequence upstream from the ATG start codon of the PTP1B gene were sequentially deleted to identify elements that would control PTP1B expression in the cell. The region was first grossly truncated from 8kb, to 5kb, to 3kb and finally to 2kb of sequence (work of Y. Boie). Further truncations were strategically placed to remove recognizable elements 500 base pairs upstream from the start ATG. These include GC rich regions, an inverted CCAAT box and a putative transcription start site identified by 5' RACE (Work of Y. Boie). Figure A.1 shows the placement of these last deletions.

In addition, a discrepancy between our sequence and the one submitted in Genbank, replacing GG at -327 and -326 with AA, was identified and constructs with either the AA or the GG sequence were generated for truncation #5 and #4. Screening databanks of transcription factors revealed that the GG sequence created a recognition site for AdH1-US2 while the AA sequence picked up TCSF_CF.

In HepG2 cells, maximal expression was obtained using construct #5 with little effect of the polymorphism on expression (Figure A.2). Progressive truncation of this construct resulted in a gradual loss of activity. Inclusion of only the putative transcription start site was not sufficient to induce expression from the promoter. Longer constructs than #5 showed progressive decrease in transcriptional activity. This pattern was very similar for L6 myotubes (Figure A.3) but somewhat altered for 3T3 L1 adipocytes which showed greater activity from the longer construct (Figure A.4).

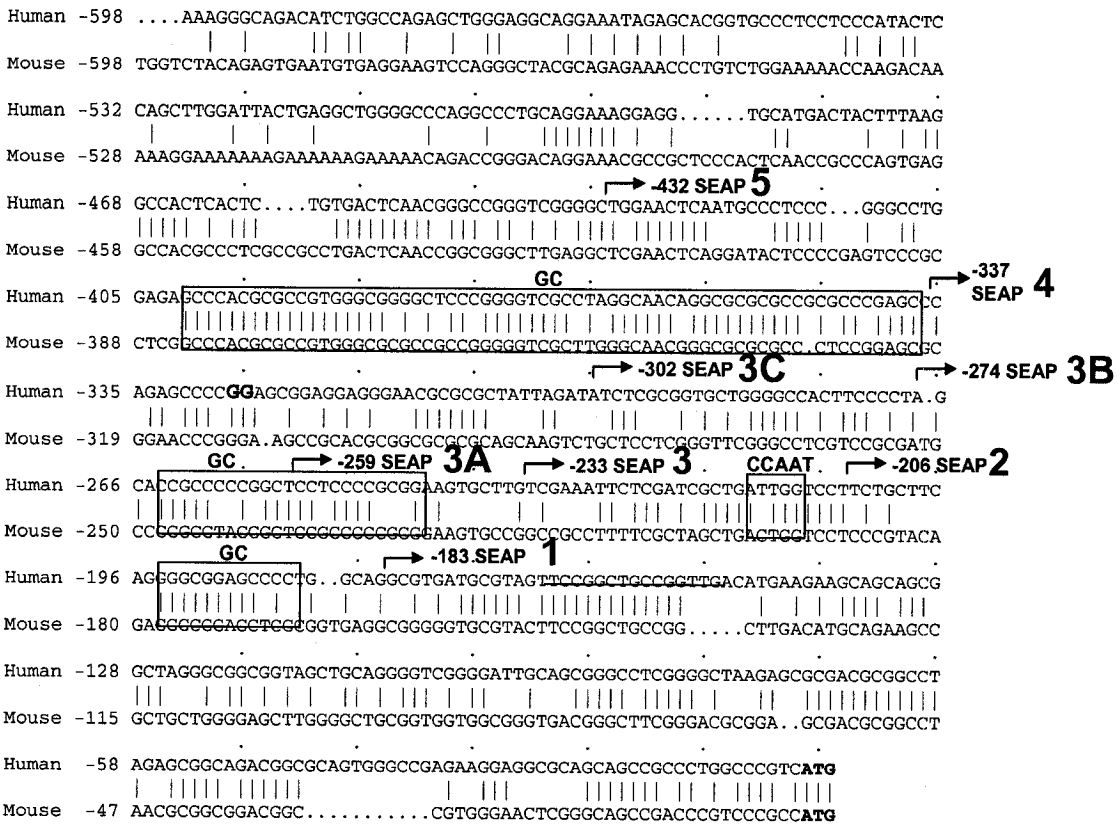

Figure A.1: Genomic sequence aligning the mouse and human sequence upstream from the ATG of the PTP1B gene. Arrows indicate the start sites for constructs #1 to #5, boxes highlight GC-rich regions, the transcriptional start site is underlined, bold GG indicates location of possible polymorphism.

Transfection efficiencies in the differentiated L6 and 3T3 1 cells were verified by visualization of Green Fluorescent Protein (GFP) expression. Figure A.5 and 6 shows expression of the exogenous protein in the characteristic elongated myotubes of the differentiated L6 cells and in the lipid droplet-containing 3T3 L1 adipocytes.

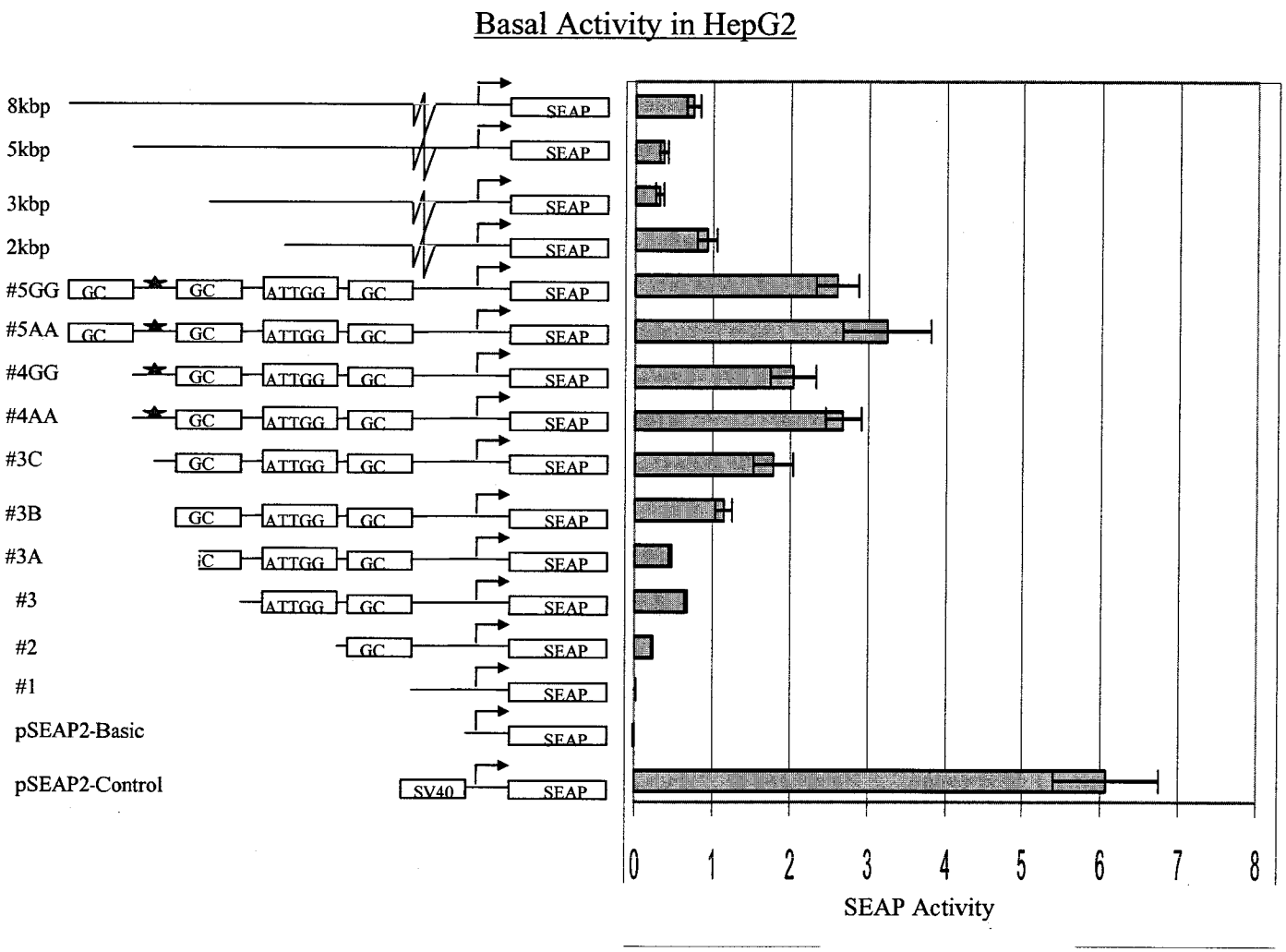

Figure A.2: Basal activity of deletion constructs of the PTP1B promoter in HepG2 hepatocytes. SEAP activity represents the mean SEAP activity normalized for transfection efficiency on β-galactosidase. Error bars are standard deviation n = 3.

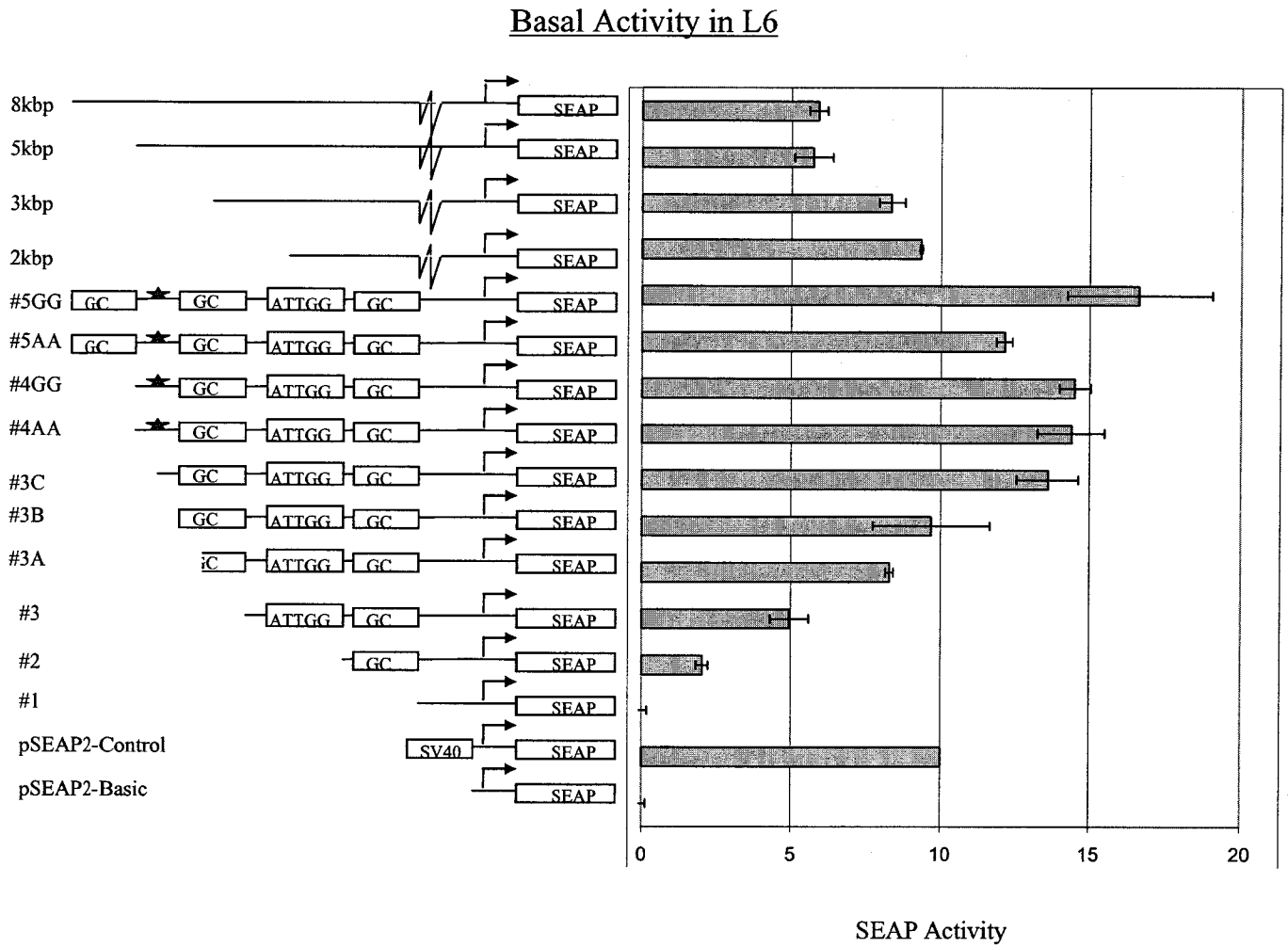

Figure A.3: Basal activity of deletion constructs of the PTP1B promoter in differentiated L6 myotubes. SEAP Activity represents the mean SEAP activity for two separate experiments done. Error bars are standard error n =2.

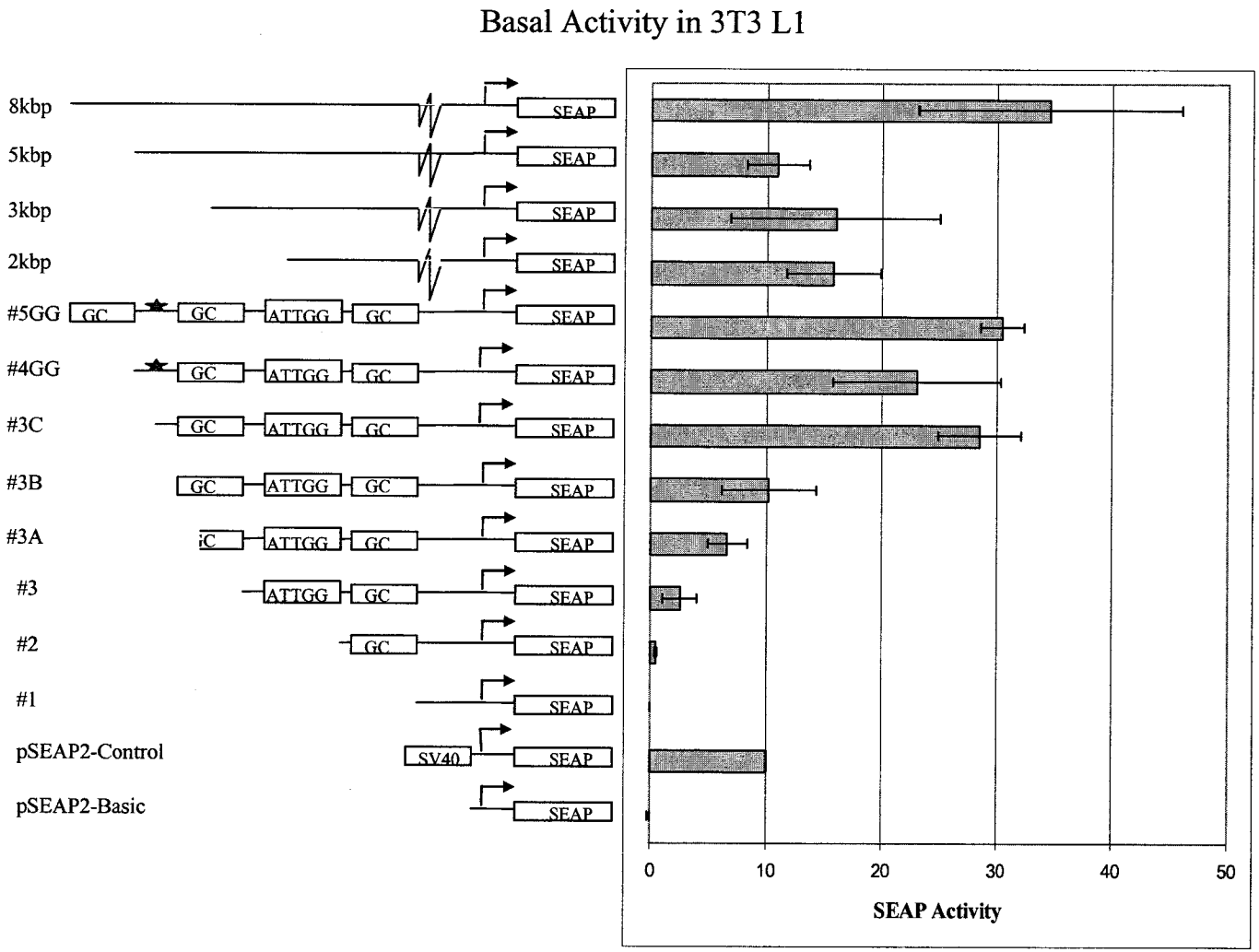

Figure A.4: Basal activity of deletion constructs of the PTP1B promoter in differentiated 3T3L1 adipocytes. SEAP Activity represents the mean SEAP activity normalized for transfection efficiency on luciferease. Error bars are standard error n = 2.

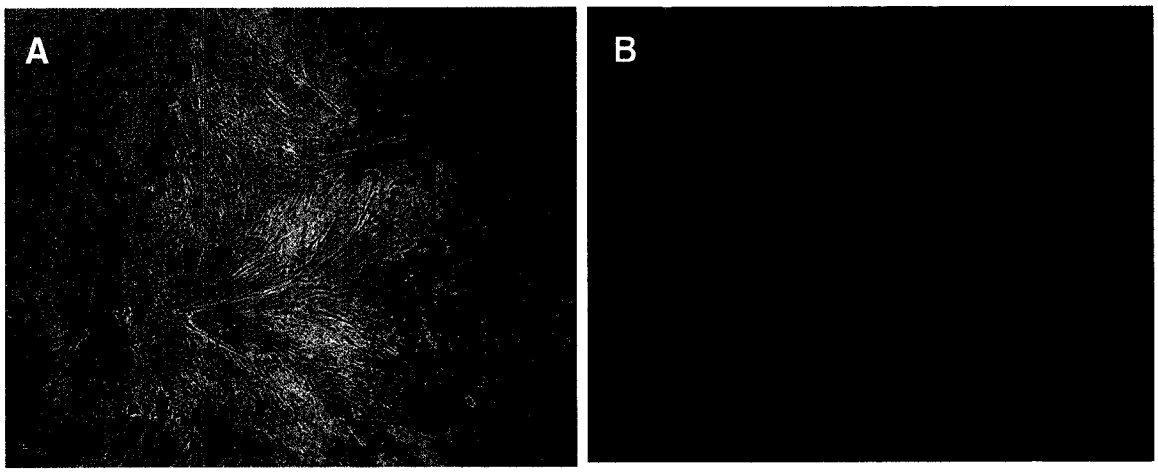

Figure A.5: Differentiated L6 myotubes expressing GFP. L6 cells were transfected with 1μg of GFP-expressing plasmid and differentiated for eight days. A) Phase contrast microscopy, fivefold magnification. B) Same field as A) excited under fluorescent light.

Figure A.6: Differentiated 3T3L1 adipocytes expressing GFP. 3T3L1 were differentiated and electroporated with 100μg of GFP-expressing plasmid. A) Phase contrast microscopy, 40-fold magnification. B) Same field as A) under normal light and fluorescent light. C) Same field as A) excited under fluorescent light.

A.3.2. Effect of Insulin on Expression Levels

Treatment with insulin had very little effect on expression from the PTP1B promoter in HepG2 cells (Figure A.7). Overexpression of the IR in the HepG2 cells to increase insulin signalling did not increase this response (Figure A.8).

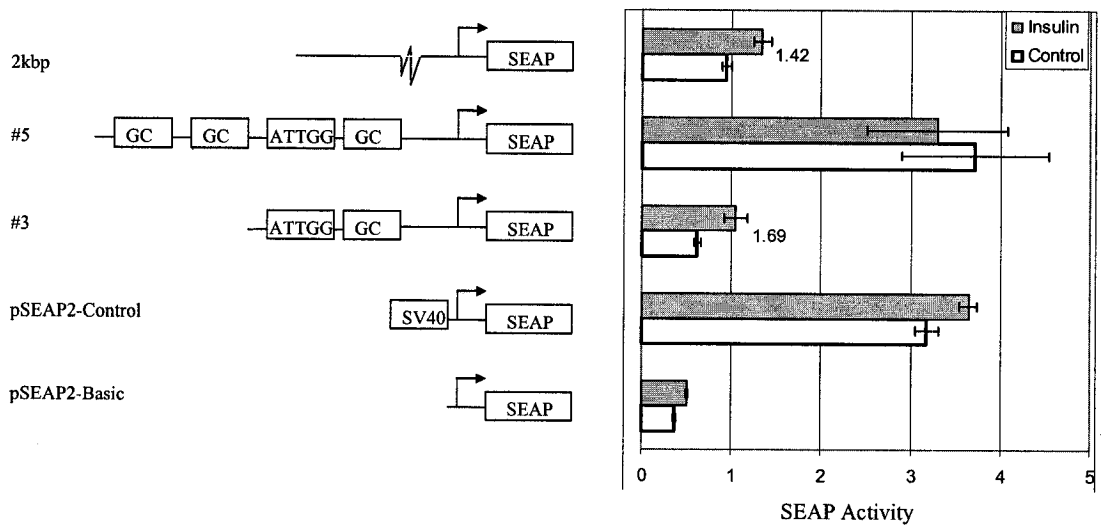

Figure A.7: Effect of insulin on the expression from the PTP1B promoter in HepG2 cells. HepG2 cells were transfected with the different promoter constructs, and treated with 10μM insulin for 24hours. SEAP activity represents the mean SEAP activity normalized for transfection efficiency on β-galactosidase. Numbers indicated at the end of the bars indicate fold difference with treatment. Error bars are standard deviation n=3.

A similar negative result was obtained for L6 myotubes. However, normalization of the L6 data proved non-trivial as the promoter driving luciferase expression was affected by insulin preventing normalization on transfection efficiency as was the protein content, from the mitogenic effects of insulin, preventing normalization by cell numbers. Nonetheless, comparison of raw expression levels before and after insulin treatment show a small response in construct #5 which is lost in construct #3 (Figure A.9). This response was however not very robust.

Expression levels of the transfected IR were measured by western blotting revealing clear increase in IR precursor and β-subunit for the HepG2 cells but a more modest increase in the L6 myotubes (Figure A.10). Treatment with insulin clearly reduced the levels of the IR β-subunit in the HepG2 cells (Figure A.10) but did not affect PTP1B levels (Figure A.11).

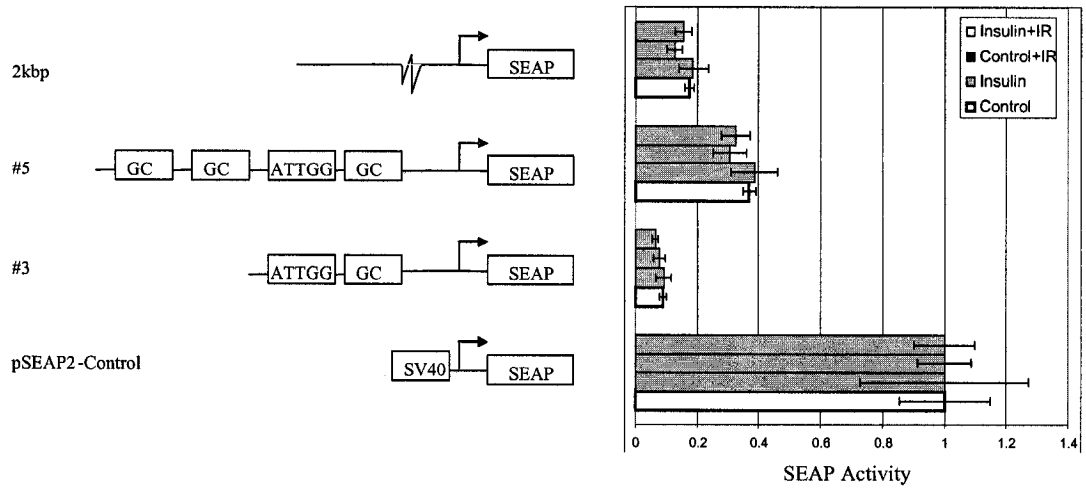

Figure A.8: Overexpression of the IR in HepG2 cells does not sensitize the promoter activity to the actions of insulin. HepG2 cells were transfected with the different promoter constructs along with 1μg of the human IR (Courtesy B. Zhang) or 1μg of GFP-expressing plasmid and treated with 100nM insulin for 18hours. SEAP activity represents the mean SEAP activity normalized for transfection efficiency on β-galactosidase. Error bars are standard error n=2.

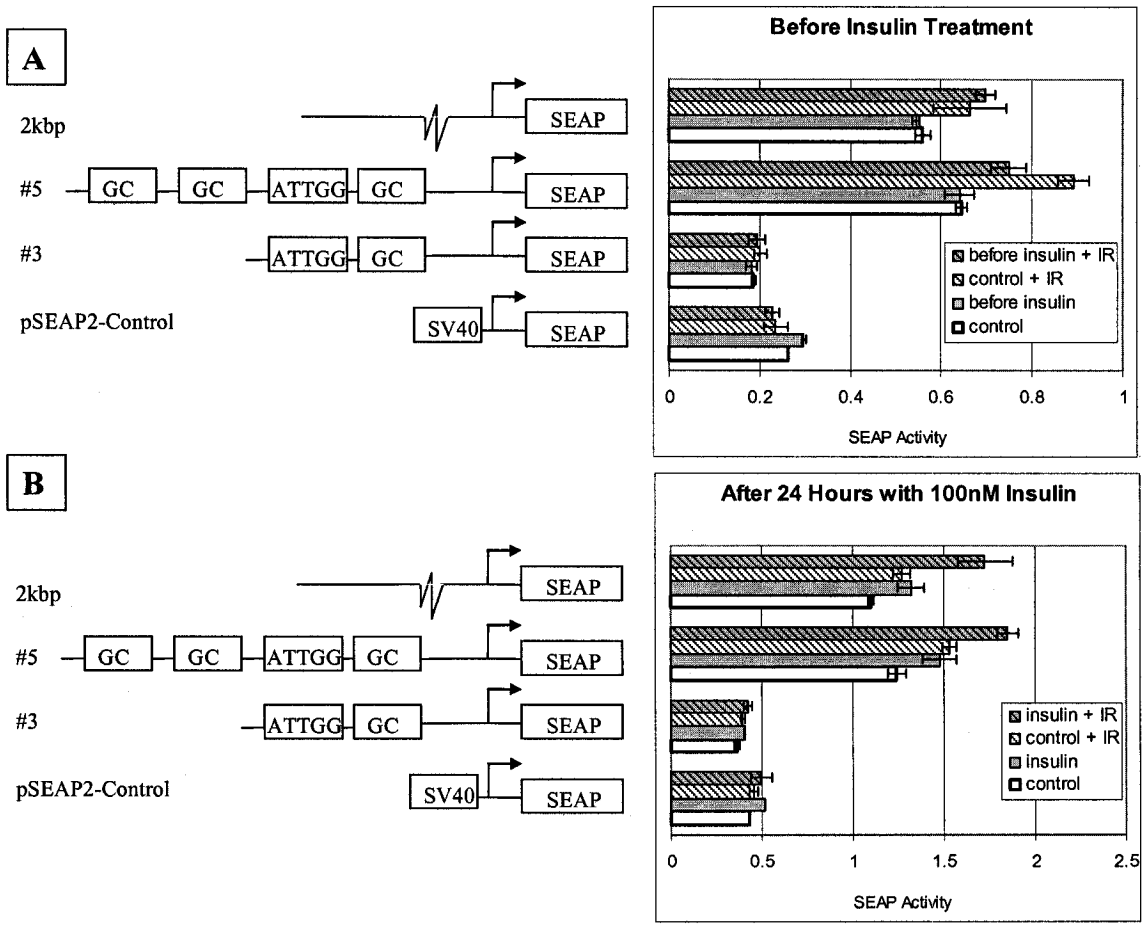

Figure A.9: Insulin treatment does not result in a robust modulation of the PTP1B promoter in L6 myotubes overexpressing (or not) the IR. L6 myocytes were transfected with the different promoter constructs along with 1μg of the human IR or 1μg of GFP-expressing plasmid, left untreated for 24 hours and then treated with or without 100nM insulin for 24hours. A) SEAP activity collected 24 hours after transfection. B) SEAP activity collected 24 hours after insulin treatment. Error bars are standard deviation n=3.

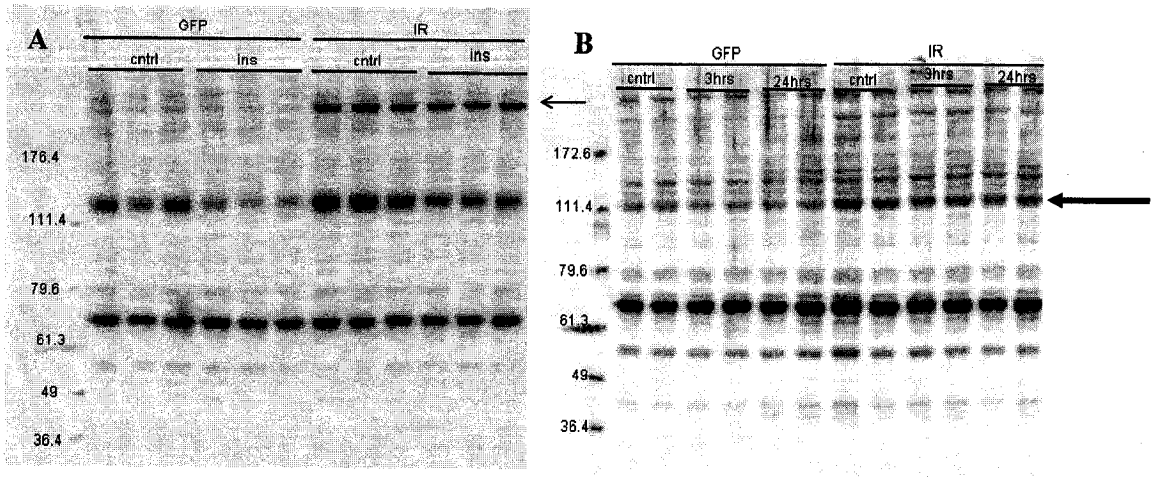

Figure A.10: Western blot of the IR in HepG2 and L6 cells. A) HepG2 cells were transfected with the IR or GFP and treated with or without 100nM insulin for 24hours. B) L6 cells were transfected with the IR or GFP, differentiated to myotubes and treated with 100nM insulin for three or 24 hours. Large arrow indicates the β-subunit of the IR, smaller arrow indicate the IR precursor.

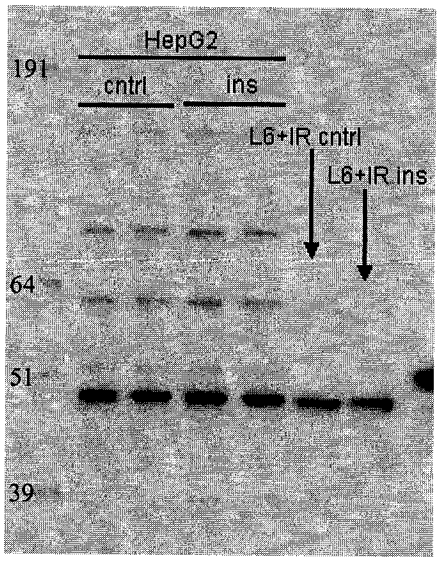

Figure A.11: Western blot of PTP1B in HepG2 or L6 cells treated with insulin. Duplicate wells of HepG2 cells treated with or without 100nM insulin for 18 hours and L6 cells transfected with the IR and treated with 100nM insulin for 24 hours.

A.3.3. Effect of Rosiglitazone on Expression Levels

Treatment with rosiglitazone activates the PPARγ nuclear receptor which dimerizes with RXR and binds DNA at the PPRE (Figure A.12). Rosiglitazone treatment of HepG2 cells transfected with the PTP1B promoter constructs did not alter transcriptional activity of any of the promoter constructs (Figure A.13). It did, however, increase expression of the construct containing the multimerized tandem sequences of PPRE.

Overexpression of PPARγ and RXR in HepG2 cells did confer the promoter constructs sensitivity to rosiglitazone (Figure A.14). The reduced activity of the promoter was however non-specific, equally affecting all truncations in addition to the control vector containing the SV40 promoter.

In case the Great Escape SEAP vector system contained a PPRE element somewhere else in the sequence, a few constructs were transferred to a different vector system driving expression of chloramphenicol acetyltransferase. Although this transfer abolished the response of construct #3, the SV40 control plasmid still responded to the treatment (Figure A.15). The response of construct #5 and the control required the overexpression of both PPARγ and RXR. Overexpressing PPAR γ alone did not sensitize the system to rosiglitazone.

PPARγ Response Element

ACGCGTCAAATATAGGCCATAGGTCAAGATCT

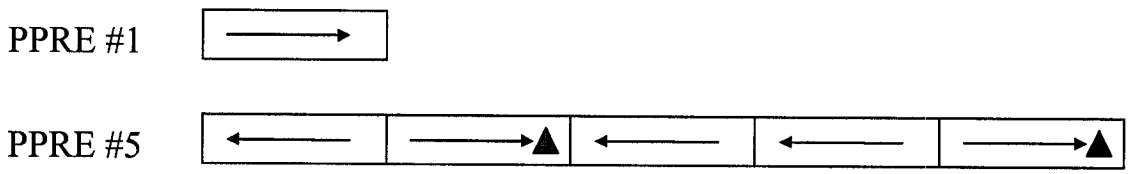

Figure A.12: Sequence of the PPRE and schematic of constructs cloned in pSEAP-promoter. The sequence of the PPRE is shown underlined with the bold adenosine base sometimes mutated to a thymidine. Overhanging bases were added as *Mlu* I and *Bgl* II restriction sites. The PPRE #1 construct contains only one copy of the PPRE oriented as shown in the boxed sequence. The PPRE #5 construct contains five repeats, in either forward or reverse orientation with the A/T mutation indicated by a triangle.

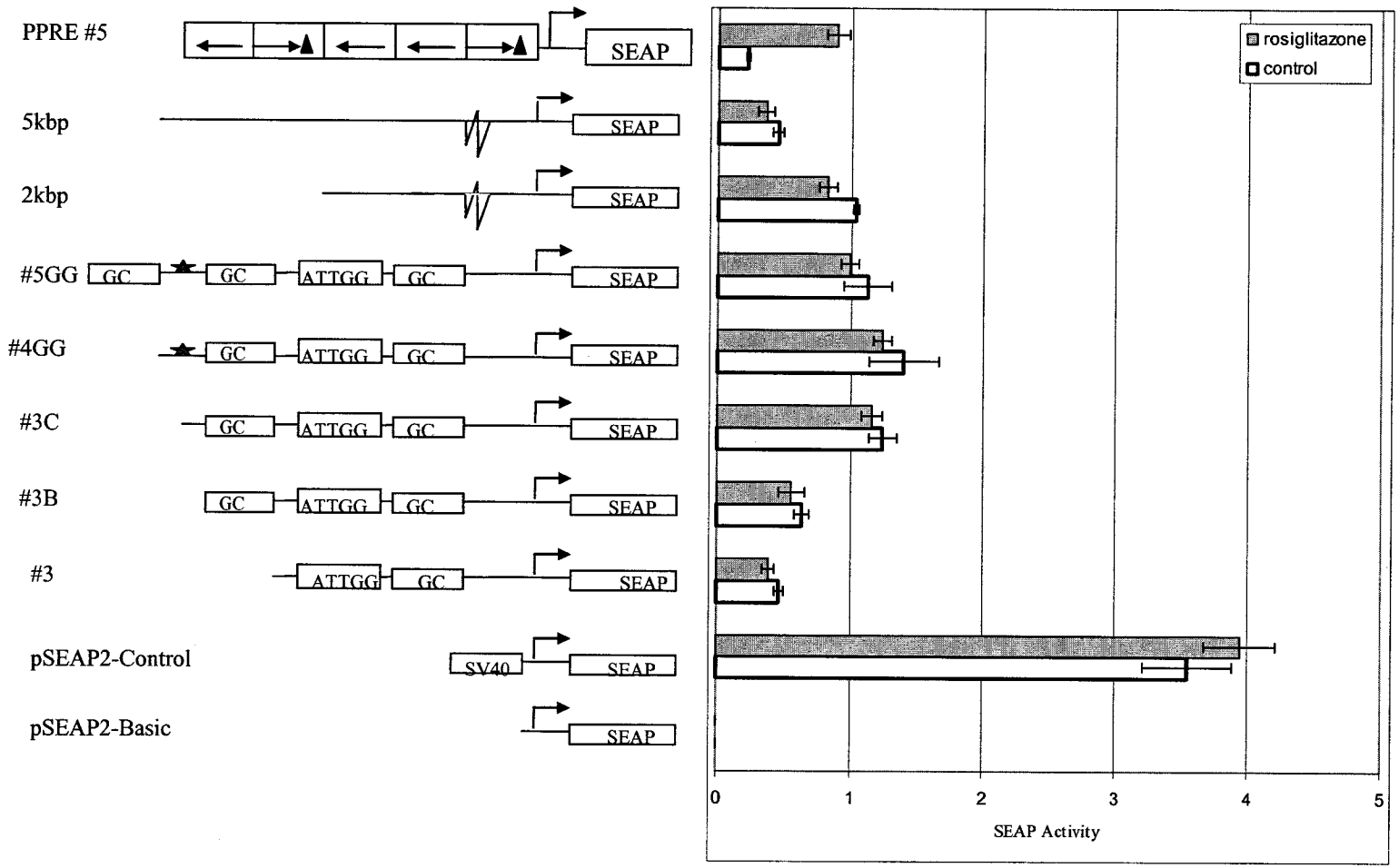

Figure A.13: Effect of rosiglitazone on the activity of the PTP1B promoter in HepG2 cells. HepG2 cells were transfected with the different promoter constructs, and treated with 20μM rosiglitazone for 48hours. SEAP activity represents the mean SEAP activity normalized for transfection efficiency on β-galactosidase. Error bars are standard deviation n=3.

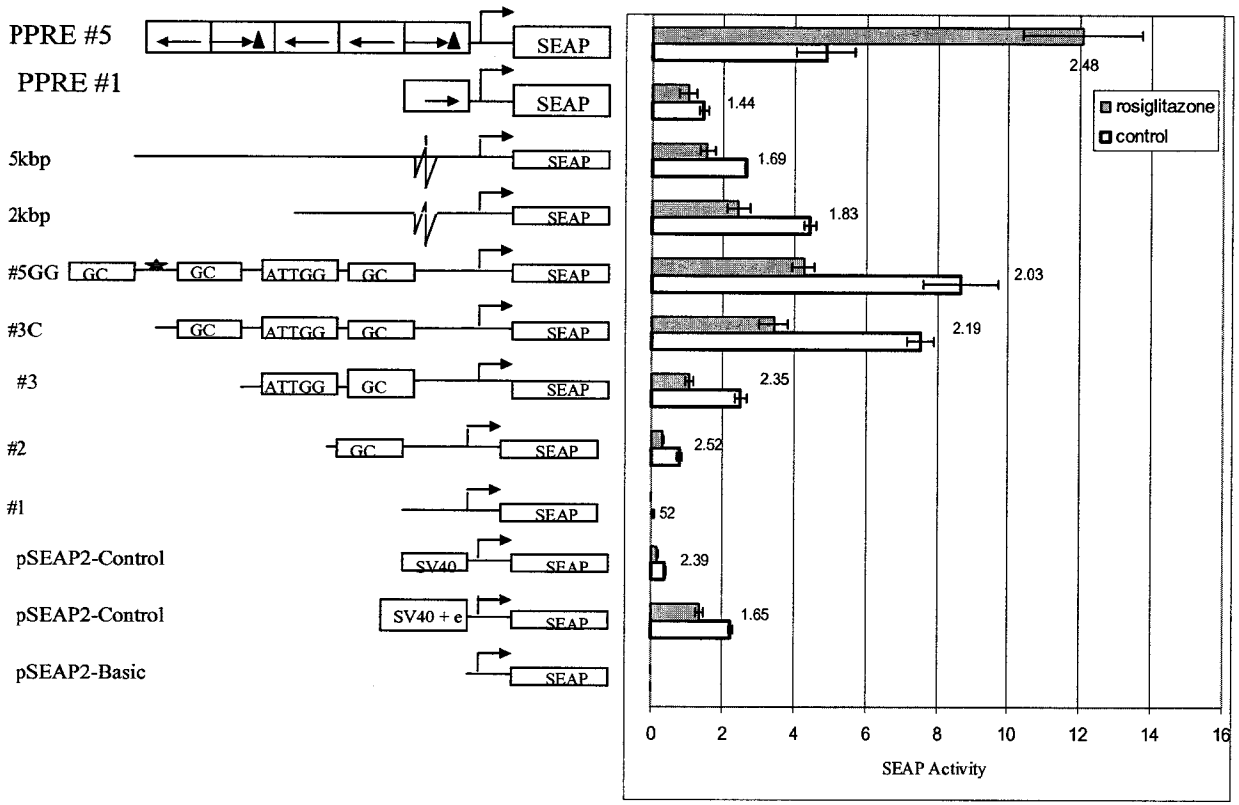

Figure A.14: Effect of rosiglitazone on the activity of the PTP1B promoter in HepG2 cells overexpressing PPARγ and RXR. HepG2 cells were transfected with 1μg of the different promoter constructs, 1μg of PPARγ-expressing plasmid and 1μg of RXR expressing plasmid and treated with 20μM rosiglitazone for 48hours. SEAP activity represents the mean SEAP activity normalized for transfection efficiency on β-galactosidase. Numbers indicated at the end of the bars indicate fold difference with treatment. Error bars are standard deviation n=3.

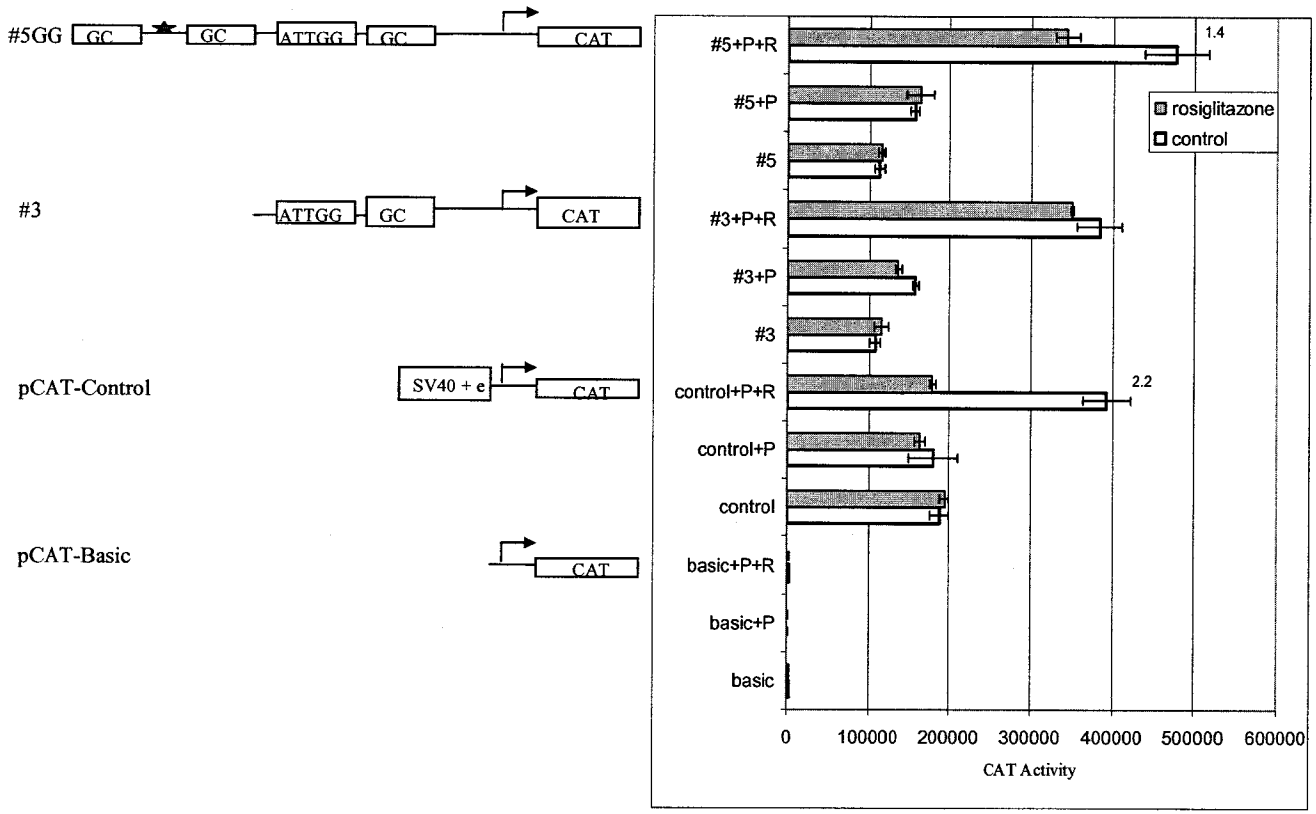

Figure A.15: Effect of rosiglitazone on the activity of the PTP1B promoter in HepG2 cells overexpressing PPARγ and RXR using chloroamphenicol acetyltransferase as reporter gene. HepG2 cells were transfected with 1μg of the different promoter constructs with or without 1μg of PPARγ-expressing plasmid (+P) and with or without 1μg of RXR expressing plasmid (+R) and treated with 20μM rosiglitazone for 48hours. CAT activity represents the mean CAT activity normalized for transfection efficiency on β-galactosidase. Numbers indicated at the end of the bars indicate fold difference with treatment. Error bars are standard deviation n=3.

A.4. Conclusions

Maximal expression from the 5' region of the PTP1B gene was obtained within the proximal 432 base pairs. This sequence included three GC-rich regions as well as an inverted CCAAT box. Expression patterns did not strongly differ between cell lines representing insulin responsive tissues: liver, muscle and adipose tissue.

Studies on the PTP1B promoter have since been published revealing regulation by Bcr-Abl and Y-box binding protein 1 (YB-1). In the first study[9], basal expression of the PTP1B promoter in Rat1 fibroblasts was dependent on a consensus sequence recognized by GATA-binding protein located between -311 and -295 (our numbering system). Truncation of this sequence resulted in decreased basal promoter activity. In our system this region is truncated right after the GATA sequence by construct #3C. They did not see any modulation of the promoter activity with longer constructs extending up to 2kb but identified the same transcriptional start site.

They also identified a p210 Bcr-Abl responsive sequence (PRS) located between -193 and -181 which corresponds to our proximal GC box truncated from construct #2 to obtain construct #1. This PRS recruited Sp1 and Sp3, stimulating transcriptional activity, and Egr-1 repressing Sp3-mediated activity. Bcr-Abl suppressed the expression of Egr-1 and resulted in a fourfold activation of the PTP1B promoter.

The second study[10] focused on the enhancer sequence identified in the region -311 and -295. Further deletion studies identified a sequence spanning the region -299 to -288 which recruits YB-1. Although the PTP1B promoter does not contain a Y-box

(CTGATTGG(C/T)(C/T)AA), overexpression of YB-1 in rat1 fibroblasts resulted in increased PTP1B levels while depletion of YB-1 with anti-sense resulted in 70% decrease in the transcriptional activity of the PTP1B promoter. Deletion of the -299 to -288 region abolished the response of the promoter to YB-1 in both Rat1 fibroblasts and HepG2 cells.

As opposed to expected results, insulin did not have any effect on the transcriptional activity of the PTP1B promoter. Since the levels of PTP1B protein measured by western blotting did not confirm previous published observations, it is possible that the cell culture conditions used here were not optimized to observe that regulation of PTP1B promoter activity. However, overexpression of the IR to ensure insulin signalling even in potentially unfavourable conditions did not sensitize the promoter.

The effect on the levels of PTP1B seen in previous studies may also have been mediated by another mechanism than transcriptional control. Treatment of human fibroblasts with insulin was seen to affect the ratio of PTP1B mRNA splice variants increasing by 37% the amounts of the longer mRNA transcript. Increase in the proportion of the longer mRNA transcript has been identified to be correlated with increase percent body fat and fasting insulin levels in non-diabetic Pima Indians[11].

The longer mRNA transcript translates to a truncated enzyme replacing the C-terminal sequences FLFNSNT for VCFH. This truncation may affect localization of the PTP1B enzyme to the endoplastic reticulum thereby affecting its regulation and activity.

Rosiglitazone treatment did have an effect on the PTP1B promoter but deletion constructs were not able to identify the region recognized by PPARγ and RXR. Interestingly, the control vector using the SV40 promoter also responded to rosiglitazone indicating a potential response from the vector used and not the promoters. Transfer into a different

vector system did not abolish this response. Examination of the SV40 promoter sequence revealed the presence of a putative PPRE sequence (TCTCAATTAGTCA) which might mediate this response.

Finally, a comprehensive study[12,13] of the prevalence of PTP1B Single Nucleotide Polymorphisms (SNP) in a large population (811 subjects) did not identify the AA/GG polymorphism at -327. Although this polymorphism could theoretically recruit different transcriptional factors, it did not modulate basal PTP1B promoter activity in either of the cell type studied.

The genomic region examined here is limited to the 5' untranslated region of the PTP1B gene. Transcriptional regulation may be dictated by sequences located downstream from the start ATG codon. SNP analysis revealed an association between SNP located in intronic non-coding region of PTP1B with protection against or sensitivity for type 2 diabetes. These SNPs located downstream from the region examined here could regulate PTP1B transcription.

A.5. Reference List

1. Kenner,K.A., Hill,D.E., Olefsky,J.M. & Kusari,J. Regulation of protein tyrosine phosphatases by insulin and insulin-like growth factor I. *J. Biol. Chem.* **268**, 25455-25462 (1993).

2. Hashimoto,N. & Goldstein,B.J. Differential regulation of mRNAs encoding three protein-tyrosine phosphatases by insulin and activation of protein kinase C. *Biochem Biophys Res Commun.* **188**, 1305-1311 (1992).

3. Spiegelman,B.M. PPAR-gamma: adipogenic regulator and thiazolidinedione receptor. *Diabetes* **47**, 507-514 (1998).

4. Auwerx,J. PPAR+|, the ultimate thrifty gene. *Diabetologia* **42**, 1033-1049 (1999).

5. Balfour,J.A. & Plosker,G.L. Rosiglitazone. *Drugs* **57**, 921-930 (1999).

6. Maegawa,H., Ide,R., Hasegawa,M., Ugi,S., Egawa,K., Iwanishi,M., Kikkawa,R., Shigeta,Y. & Kashiwagi,A. Thiazolidine Derivatives Ameliorate High Glucose-induced Insulin Resistance via the Normalization of Protein-tyrosine Phosphatase Activities. *J. Biol. Chem.* **270**, 7724-7730 (1995).

7. Tagami,S., Honda,T., Yoshimura,H., Homma,H., Ohno,K., Ide,H., Sakaue,S. & Kawakami,Y. Troglitazone ameliorates abnormal activity of protein tyrosine phosphatase in adipose tissues of Otsuka Long-Evans Tokushima Fatty rats. *Tohoku J Exp Med* **197**, 169-181 (2002).

8. Juge-Aubry,C., Pernin,A., Favez,T., Burger,A.G., Wahli,W., Meier,C.A. & Desvergne,B. DNA Binding Properties of Peroxisome Proliferator-activated Receptor Subtypes on Various Natural Peroxisome Proliferator Response Elements. IMPORTANCE OF THE 5'-FLANKING REGION. *J. Biol. Chem.* **272**, 25252-25259 (1997).

9. Fukada,T. & Tonks,N.K. The Reciprocal Role of Egr-1 and Sp Family Proteins in Regulation of the PTP1B Promoter in Response to the p210 Bcr-Abl Oncoprotein-tyrosine Kinase. *J. Biol. Chem.* **276**, 25512-25519 (2001).

10. Fukada,T. & Tonks,N.K. Identification of YB-1 as a regulator of PTP1B expression: implications for regulation of insulin and cytokine signaling. *EMBO J* **22**, 479-493 (2003).

11. Sell,S.M. & Reese,D. Insulin-inducible changes in the relative ratio of PTP1B splice variants. *Mol Genet. Metab* **66**, 189-192 (1999).

12. Bento,J.L., Palmer,N.D., Mychaleckyj,J.C., Lange,L.A., Langefeld,C.D., Rich,S.S., Freedman,B.I. & Bowden,D.W. Association of Protein Tyrosine Phosphatase 1B Gene Polymorphisms With Type 2 Diabetes. *Diabetes* **53**, 3007-3012 (2004).

13. Palmer,N.D., Bento,J.L., Mychaleckyj,J.C., Langefeld,C.D., Campbell,J.K., Norris,J.M., Haffner,S.M., Bergman,R.N. & Bowden,D.W. Association of Protein Tyrosine Phosphatase 1B Gene Polymorphisms With Measures of Glucose Homeostasis in Hispanic Americans: The Insulin Resistance Atherosclerosis Study (IRAS) Family Study. *Diabetes* **53**, 3013-3019 (2004).